

Kumulative Dissertation

Quantum Entanglement in fundamental Tests of Physics

*Dem Fachbereich Physik und Elektrotechnik der Universität Bremen
zur Erlangung des akademischen Grades
Doktor der Naturwissenschaften (Dr. rer. nat.)
vorgelegte Dissertation*

von

Roy Barzel

1. Gutachter: Prof. Dr. Claus Lämmerzahl
2. Gutachter: Prof. Dr. Meike List



Universität Bremen

Danksagung

Meinen ersten Dank möchte ich an den Erstgutachter der vorliegenden Dissertation, *Claus Lämmerzahl*, richten. Ich kann allen, die mit Dir zusammenarbeiten und Dich näher kennen, nur voll und ganz zustimmen, dass auch ich niemanden in meinem persönlichen Umfeld kenne, der sein Leben derartig bedingungslos der Wissenschaft widmet - um nicht zu sagen aufopfert - wie Du. Ich habe von Dir vieles gelernt.

Ebenfalls bedanken möchte ich mich an dieser Stelle bei *Meike List*, welche sich dankenswert erweise dazu bereiterklärt hat, die Zweitbegutachtung der Arbeit zu übernehmen.

Meinen nächsten Dank möchte ich an David Edward Bruschi und Andreas Wolfgang Schell richten. Als "Newcomer im Geschäft" hat mich Euer Interesse an und die Wertschätzung meiner Arbeit sehr bestärkt und motiviert.

Einen besonderen Dank möchte ich an Dennis Rätsel aussprechen: Du bist Dir für keine Rechnung zu schade, penibel und detailverliebt. Ein echter Wissenschaftler, mit dem Herzen am rechten Fleck. So wie auch bei Claus, frage ich mich allzu oft, wo Du die Muße und die Zeit hernimmst, so aktiv in allen Bereichen Deiner Tätigkeit zu sein. Du rechnest dem Ergebnis entgegen und nicht der nächsten Veröffentlichung. Ich schaue mit Stolz zu Dir auf und es ist mir eine Ehre, mit Dir zusammenzuarbeiten.

Natürlich möchte ich auch meinen Doktoranden-Kollegen *Sandro Gödtel, Florian Seemann* und *Felix Willenborg* für die Unterstützung und die gegenseitige Motivation den Schritt der Promotion zu gehen, danken. Insbesondere möchte ich an dieser Stelle *Marian Cepok* danken, mit dem ich seit Beginn unseres ersten Studentages das wortwörtliche Vergnügen hatte, einen, über ein halbes Jahrzehnt andauernden, Konkurrenzkampf zu bestreiten. Es war mir eine Ehre und ich hoffe, dass wir uns eines Tages auf ein Patt einigen können.

Ebenfalls bedanken möchte ich mich auch bei allen anderen Mitgliedern unserer Arbeitsgruppe, vor allem aber bei *Eva Hackmann* und *Christian Pfeifer*. Eva, dein Wirken in der Gruppe hat mir von Beginn an Sicherheit und Stabilität vermittelt. Darüber hinaus habe ich den größten Respekt vor Deiner Leistung.

Christian, Dir danke ich für die zahlreichen, sehr interessanten, Gespräche über nicht-lineare Algebra. In diesem Zusammenhang möchte ich mich auch bei *Domenico Gulini* bedanken. Der großen Anerkennung, die Du -so wie auch Claus- in Wissenschaftlicher-Kreisen genießt, sowie Deinem bewundernswerten Wissensschatz, eifere ich nach.

Einen höchst persönlichen Dank möchte ich an meine *Familie* richten, an meine Eltern, *Elisabeth* und *Paul*, meine *Schwester, Vanessa*, an *Imke* und an meinen *Sohn, Maxi*.

An meine Eltern: Ihr habt mir immer alles, was ich wollte, gegeben. Viel mehr als ich brauchte. Ohne Euch wäre ich niemals dahin gekommen, wo ich heute stehe.

Meiner kleinen Schwester möchte ich für unsere tolle Kindheit und Jugend danken. Du bist ein unfassbar toller Mensch und hast Dich in einer bemerkenswerten Art und Weise zu einer Erwachsenen Frau entwickelt.

Imke, ich danke Dir für den selbstlosen und bedingungslosen Beistand in den letzten Jahren und für unseren wundervollen Sohn, den Du mir geschenkt hast.

Auch möchte ich meinen Freunden –*Nastasia Deininger, Nathalie Waßner, Eric Wil- lenberg, Nikolai Iliew, Dirk Emmrich, Michelle Tenkhoff, Tim Benedikt Schwarz* und *Daniël Demir*– meinen herzlichsten Dank aussprechen. Ich habe in den letzten Jahren unglaublich viel von Euch gelernt.

Wahre Freunde erkennt man im Schatten der Nacht und nicht im Schein der Sonne.

Darstellung des Eigenanteils an den Publikationen

An der Abfassung sämtlicher für die vorliegende kumulative Dissertation verwendeten Publikationen waren neben dem Kandidaten selbst weitere Autoren beteiligt. Im Folgenden werden der Eigenanteil des Kandidaten sowie die Beiträge der Koautoren dargestellt.

Publikation I

Reference: [BL23]

Die Idee der Arbeit entspringt dem Kandidaten. Der Kandidat hat sämtliche numerische und analytische Rechnungen durchgeführt. Der Kandidat hat den gesamten Text der Publikation verfasst, welcher von seinem Betreuer, Claus Lämmerzahl, korrekturgelesen worden ist, sich dadurch jedoch im Wesentlichen nicht verändert hat. Der Kandidat hat alle Abbildungen der Publikation erstellt. Die Interpretation der Ergebnisse ist–wie auch die Auswahl der zitierten Literatur–vollständig dem Kandidaten zuzurechnen.

Publikation II

Reference: [BBSL22]

Die Idee der Arbeit entspringt dem Kandidaten. Der Kandidat hat sämtliche numerische und analytische Rechnungen durchgeführt. Der Kandidat hat den gesamten Text der Publikation verfasst, welcher von seinem Betreuer, Claus Lämmerzahl, David Edward und Andreas Wolfgang Schell korrekturgelesen worden ist, sich dadurch jedoch im Wesentlichen nicht verändert hat. Der Kandidat hat alle Abbildungen der Publikation erstellt. Die Interpretation der Ergebnisse ist–wie auch die Auswahl der zitierten Literatur, abgesehen von einer Referenz–vollständig dem Kandidaten zuzurechnen.

Publikation III

Reference: [BGK⁺24]

Die Idee der Arbeit entspringt dem Kandidaten. Der Kandidat hat sämtliche numerische und analytische Rechnungen durchgeführt, die in ihrer Gesamtheit von Dennis Rätzel nachvollzogen und gegengerechnet worden sind. Die Einbeziehung von Referenz [52], auf welche das Mode-Swapper-Model der in der Arbeit modellierten Quantenspeicher zurückzuführen ist, wurde durch Dennis

Rätzel eingebracht. Die entsprechende Dokumentation zu den Quantenspeichern im Anhang B wurde durch Dennis Rätzel vorgenommen, wobei die Ausarbeitung der Ergebnisse in Zusammenarbeit mit dem Kandidaten erfolgte. Der erste Entwurf des gesamten Textes, abgesehen von Kapitel 4 und Anhang B, wurde durch den Kandidaten getätigten. Im weiteren Verlauf der Arbeit wurde der Text von allen Autoren in gemeinschaftlicher Zusammenarbeit überarbeitet.

Dennis Rätzel hat –durch seine langjährigen Kontakte und gesammelte Expertise auf dem Feld– die Zusammenarbeit mit den Berliner Experimentatoren, Mustafa Gündoğan und Markus Krutzik, ermöglicht, auf welche die experimentelle Machbarkeits-Studie –dokumentiert in Kapitel 4– zurückzuführen ist. Darunter zählt auch die Literaturauswahl der in diesem Kapitel aufgeführten Referenzen zu den entsprechenden Experimenten, welche zum Großteil auf die Experimentatoren, Mustafa Gündoğan und Markus Krutzik, zurückzuführen ist.

Alle Abbildungen der Arbeit wurden durch den Kandidaten erstellt.

Die diversen Maße der Verschränkung im Formalismus der zweiten Quantisierung wurden bereits im ersten Entwurf der Arbeit des Kandidaten verfasst, wobei die zusätzlich und nachträglich eingeführte Deklaration und Definition der Struktur des Hilbertraums auf Seite 18 im Anhang C der Veröffentlichung von Dennis Rätzel stammt.

Die zentrale Interpretation der Arbeit hinsichtlich der Verschränkungsdynamik zwischen den internen und externen Freiheitsgraden einzelner Quantenteilchen und deren Aufbau auf Kosten der Verschränkung zwischen den Quantenteilchen untereinander geht auf den Kandidaten zurück. Die Betrachtung der verschränkten Uhrenzustände in der Einleitung und im Anhang A geht auf den Kandidaten zurück, sowohl als auch die Betrachtung des Mach-Zehnder und HOM-Experimentes mit optischen "Delay Lines" samt der entsprechenden Berechnungen in Anhang C. Die dazu mathematisch analoge Idee zur Betrachtung der Quantenspeicher stammt von Dennis Rätzel und wurde in Gemeinschaft mit dem Kandidaten im Detail ausgearbeitet.

Selbstständigkeitserklärung

Hiermit erkläre ich an Eides statt, dass ich die hier vorliegende Dissertation selbstständig und ohne fremde Hilfe verfasst habe, bis auf die in der Bibliographie angegebenen Quellen keine weiteren Quellen benutzt habe und die den Quellen wörtlich oder inhaltlich entnommenen Stellen als solche kenntlich gemacht habe.

Roy Barzel, January 16, 2025

Abstract

This cumulative dissertation explores the intersection of quantum mechanics and general relativity, focusing on the effects of *post-Newtonian gravity* on the *genuine quantum properties of quantum entanglement* (QE) and *quantum indistinguishability* (QI).

In other words, the thesis' core lies in the consideration of physics that cannot be explained without considering both, general relativity and quantum mechanics; respectively including phenomena that are genuine to the respective theory, i.e., phenomena that entirely elude the explanatory potential of any Newtonian theory of gravity and any classical theory of physics in general.

At the very heart of this investigation lies the *Hong-Ou-Mandel (HOM) interference experiment*, which serves as a tool for examining the interplay between *genuine quantum properties*—such as QE & QI—and *genuine relativistic effects*—such as the gravitational redshift.

The research demonstrates how gravitational influences, particularly the gravitational redshift, can alter the detection statistics of photons, leading to a transition from *photon bunching* to *photon anti-bunching* –a genuine quantum phenomenon– which is particularly pronounced for *frequency-entangled* photons.

This underlines the potential of using *spectral* quantum entanglement as a probe for relativistic phenomena within *multi-particle interference experiments*, such as HOM-interference.

Additionally, the thesis investigates the role of *quantum memories* in a *relativistic context*, emphasizing their importance for *long-distance, space-based quantum communication* and *fundamental tests of physics*. The integration of quantum memories with HOM interference in a gravitational field provides a novel avenue for understanding quantum resources under relativistic conditions. The findings suggest that even in *terrestrial environments*, such as within the *Drop Tower of the University of Bremen* in the vicinity of the Earth's weak gravitational field, relativistic effects can have a significant impact on quantum entanglement and indistinguishability, leading to observable genuine quantum phenomena that could be tested with *current or near-future quantum memory technology*.

Moreover, experiments performed by an independent group that tested the influence of the classical Doppler shift on frequency entangled photons led to results that are in perfect alignment with our theoretical predictions. This alignment strengthens the expectation that our predictions will hold true when considering more fundamental scenarios in a general relativistic context, where the associated genuine quantum phenomenology ultimately originates due to gravitational effects.

Through theoretical modeling and experimental proposals, this work contributes to the broader goal of reconciling quantum mechanics with general relativity, offering new insights into the behavior of quantum systems in curved spacetime. The implications of this research extend to the development of space-based quantum technologies, where the effects of gravity on quantum resources must be carefully considered. Ultimately, this dissertation provides both a theoretical framework and practical guidelines for future experiments aimed at testing the fundamental principles of quantum mechanics and general relativity in their union.

Abbreviation	Meaning
QE	Quantum Entanglement
QI	Quantum Indistinguishability
HOM	Hong-Ou-Mandel
QMem	Quantum Memory
FEP	Frequency-Entangled Photons
ED	Entanglement Dynamics
MZ	Mach-Zehnder
SQF	Second Quantization Formalism
FQF	First Quantization Formalism
DOF	Degree of Freedom
BIV	Bell Inequality Violation
P_c	HOM Bunching Anti-bunching Probability Difference
$\sigma = U, L, E$	Observer Frame
h_1, h_2	Interfering Beamsplitter spatial input modes
U, L, \oplus, \ominus	Interfering Beamsplitter spatial output modes
$\mathcal{S}_{xy}, \mathcal{A}_{xy}$	Symmetrization and anti-symmetrization operators w.r.t. x and y
U_σ	Gravitational Potential of Frame σ
$\Theta_{\sigma\sigma'}$	Redshift Factor between Frames σ and σ'
$z_{\sigma\sigma'}$	Redshift between Frames σ and σ'
$\Delta_{\Theta^{-1}}$	Differential Redshift Factor
$\tau_{\sigma s}$	Local Storage Time at Frame σ
$\tau_{\sigma d}$	Local Delay Time at Frame σ
μ	Frequency Separation of FEP
ξ	Frequency Bandwidth of FEP

Table 1: List of abbreviations used in the thesis.

Contents

Danksagung	3
Darstellung des Eigenanteils an den Publikationen	5
Publikation I	5
Publikation II	5
Publikation III	5
Selbstständigkeitserklärung	6
Abstract	7
1 Introduction	13
1.1 Introduction	13
1.2 Outline	14
1.3 Topical positioning of the work	15
1.4 Literary classification	18
1.4.1 Frequency entangled photons	18
1.4.2 Quantum memories	19
1.4.3 Relativistic redshift in a quantum mechanical framework	21
1.4.4 HOM-interference as genuine quantum phenomenon	21
1.4.5 Gravitationally driven entanglement dynamics	22
2 Two photon interference	25
2.1 Introduction	25
2.2 HOM-experiment	25
2.2.1 Mathematical basics	26
2.2.1.1 First and second quantization	26
2.2.1.2 HOM-detection statistics	29
2.2.1.3 Photon bunching	29
2.3 Major achievements	31
2.3.1 Systematic formalism	31
2.3.1.1 Pure and mixed quantum states	31
2.3.1.2 Symmetries of quantum states	32
2.3.1.3 Hilbert (dual) vector and operator space	32
2.3.1.4 Orthogonality and completeness relations	33
2.3.1.5 Basis-representation of quantum states and linear operators	33
2.3.1.6 Expectation values	34
2.3.1.7 Detection Statistics & Glauber's Theory of Quantum Coherence	34

2.3.1.8	Interferometer Propagation Superoperator	35
2.3.1.9	Specialization to standard result	35
2.3.2	Entanglement monogamy and indistinguishability	37
2.3.3	Interferogramm for frequency-entangled photons	38
2.3.3.1	Spectrum of frequency entangled photons	38
2.3.3.2	Interferogram and deviation to existing literature	38
2.3.3.3	Identifying contra indicative detection statistics	39
2.3.3.4	Erroneous prediction of quantum supremacy	40
2.3.3.4.1	Erroneous fraction of anti-bunching prediction	43
3	Observer dependance in two photon interference	57
3.1	Introduction	57
3.2	Observer dependence of interference	58
3.2.1	Redshift	58
3.2.2	Redshifted photon states	58
3.2.3	Redshifted Interferogram	59
3.2.4	Unitary dilation	61
3.2.4.1	Pair dilation operators	61
3.3	Summary of Central Results	62
4	Gravitationally driven entanglement dynamics	77
4.1	Introduction	77
4.2	Theory model for relativistic effects on quantum resources	78
4.2.1	Existing literature's approaches	78
4.2.1.1	Heuristic models	78
4.2.1.2	Models from first principles	78
4.2.2	Outline of possible approach	78
4.2.3	Relativistic description of spacetime	79
4.2.3.1	First and second order ppN-metric	79
4.2.4	Quantum description	80
4.2.4.1	Klein-Gordon equation in ppN approximation	80
4.3	Modeling quantum memories	82
4.3.1	Mode swapper	84
4.4	Quantum memory assisted HOM-interference in a gravitational field	85
4.4.1	Single particle evolution	85
4.4.2	Two-particle considerations	89
4.5	HOM-interferogram	89
4.5.1	Interpretation in terms of entanglement	90
4.6	Experimental observability and interpretation	91
5	Conclusion	115
5.1	Summary of the methodological approach	115
6	Outlook	117
6.1	Quantum Memories in Space	117
6.1.1	Introduction	117
6.1.2	Incorporating Relativistic Effects	117
6.1.3	Developing Advanced Theoretical Models	118
6.1.4	Spatio-Temporal Continuum Description	118
6.1.5	Including Decoherence and Environmental Effects	118

CONTENTS

11

6.1.6	Matter-Assisted Quantum Optics on Curved Spacetime	118
6.1.7	Investigating Relativistic Effects and Decoherence	118
6.1.8	Balancing Accuracy and Computational Efficiency	119
6.1.9	Future Collaborations and Applications	119
6.2	Mathematical Characterization of Quantum Mechanics	120
6.2.1	The Separability Problem in Quantum Mechanics	120

Chapter 1

Introduction

1.1 Introduction

It is a broadly held consensus within the physics community that one of the grand challenges in advancing our understanding of nature lies in reconciling *quantum theory* with the *theory of general relativity*. Although both theories have demonstrated extraordinary predictive accuracy within their respective domains, their integration into a common joint framework exposes fundamental theoretical conflicts at a simultaneous paucity of experimental tests. This juxtaposition of deep theoretical insight against practical experimental challenges forms the core inquiry of this thesis.

Both quantum mechanics and general relativity are based on distinct mathematical structures and conceptual frameworks. While experimental physics has traditionally resolved theoretical disputes through empirical tests, the extreme conditions required to probe the interactions between quantum and relativistic effects mean that such experiments are still nascent. They generally confirm only the most fundamental predictions of each theory.

Among the notable experiments at this interface are the Pound and Rebka experiment [1], which demonstrated gravitational redshift on photons, and the COW experiment [2], which measured gravitational phase shifts in neutron interferometry. These experiments, along with the Hafele and Keating experiment [3], that proved the time dilation effect on atomic clocks, are pivotal in that they provide empirical data at the intersection of quantum mechanics and general relativity, affirming the need for a unified theory that can accommodate both frameworks.

This work aims to explore this interface further by focusing on phenomena that do not have classical analogs, such as quantum entanglement (QE) and quantum indistinguishability (QI). These quantum resources challenge the deterministic and continuous nature of classical theories, including general relativity, through principles like Born's rule and the measurement postulate, which introduce inherent probabilism and discontinuity into the quantum framework; issues that are either directly addressed by QI and QE.

The fundamental challenge—and the focus of this thesis—is to identify experimental conditions within the capabilities of current or near-future technology that can test these quantum resources under relativistic conditions.

1.2 Outline

We begin with a *topical positioning* of the work in Section 1.3, where we provide a concise overview of the covered topics and their place within the broader scientific landscape of physics. Following this, Section 1.4 offers a *literary classification*, summarizing the key research fields explored in this thesis in more detail. Here, we also reference the most significant scientific works that inspired and contributed to the foundational ideas and methods presented.

The main chapters of this thesis follow, each corresponding to the scientific articles on which this work is based. These chapters, while partially interdependent, can be viewed as building upon one another.

Chapter 2 introduces the foundational experiment under investigation: the *HOM-interference experiment*. Section 2.2 briefly discusses the origins of HOM-interference, and introduces the necessary *mathematical preliminaries* that lead to the theoretical prediction and explanation of the counterintuitive phenomenon of photon bunching.

Within the same chapter, Section 2.3 highlights our *major achievements* from the work [BL23]. These include the *systematic theoretical description* that intuitively identifies detection statistics with the squared modulus of the photonic wave function (documented in Subsection 2.3.1), our insight that indistinguishability is ultimately linked to entanglement through the *theorem of entanglement monogamy* (Section 2.3.2), and the solution of the *HOM-interferogram for frequency-entangled photons* (Section 2.3.3).

Chapter 3 recapitulates the results from our publication [BL23]. Utilizing the formalism developed in the previous section, we consider, in an abstract manner —i.e., without assuming an underlying theoretical model—the alteration of the photonic wave function due to redshift as a *spectral dilation operation*.

Building on this foundation, Chapter 4 documents the results from Ref. [BGK⁺24]. Section 4.2 revisits relevant literature and presents a derivation of our model for coherently incorporating the redshift into a quantum mechanical framework, leading to the dilation model discussed in Chapter 3.

In Section 4.3, we describe how we model the devices—*quantum memories*—required to observe qualitative alterations in the detection statistics of frequency-entangled photons in terrestrial scenarios requiring coherent interrogation durations of photons *on the order of seconds* under gravitational influence.

Section 4.4 then synthesizes these elements to formulate a theory for *quantum memory-assisted HOM-interference in a gravitational field*. We compute the corresponding interferogram under relativistic influence in Section 4.5, and finally, discuss the potential for experimental observability in Section 4.6.

1.3 Topical positioning of the work

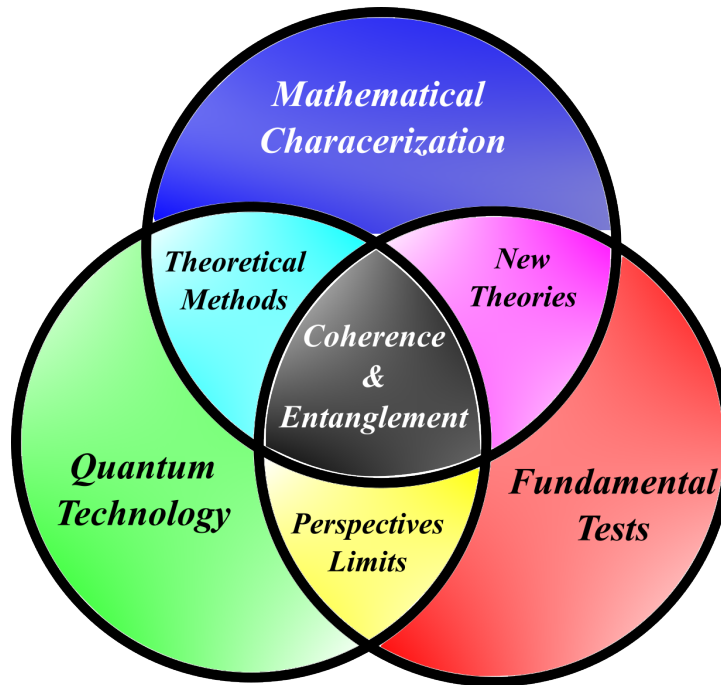


Figure 1.1: Scope of research around Coherence and Entanglement

Key-Words

1. Fundamental test of physics:
 - 1.1. Quantum coherence, entanglement, and indistinguishability
 - 1.2. Gravitational redshift, post Newtonian metric gravity
 - 1.3. Genuine quantum test of general relativity
2. Quantum optics:
 - 2.1. HOM-interference
 - 2.2. Photon bunching, photon anti-bunching, quantum supremacy
 - 2.3. Frequency entangled photons, quantum beating
 - 2.4. Light-matter interaction, Jannes Cumming model
3. Quantum technologies:
 - 3.1. Long distance quantum communication
 - 3.2. Quantum memories

This thesis is positioned within the field of *theoretical physics*, specifically at the intersection of quantum mechanics and general relativity, with a focus on *fundamental tests of physics* that explore the integration of these foundational theories.

As illustrated in Fig. 1.1, while the broader research that led to this work encompasses a wide range of topics surrounding *quantum coherence and entanglement*, the scope of this documentation is narrowed to investigate *fundamental tests of physics*. These tests have significant implications for quantum memory-assisted long-distance and extended-duration quantum information processing, particularly in the context of optical entanglement-based, space-borne quantum communication.

Frequency-entangled photons (FEPs) are selected as the central focus of investigation due to their empirical potential in demonstrating multi-particle quantum phenomena under gravitational influences. These photons offer *superior sensitivity and applicability* compared to single-particle or massive quantum systems.

Hong-Ou-Mandel interference (HOM-interference) is the primary context for our investigation of FEPs. The characteristic prediction of FEPs in HOM-interference—specifically, the phenomenon of *quantum beating*¹—along with the precision of contemporary experimental techniques, makes these resources particularly promising for *tests of relativity*. This phenomenon could be used to detect the *Earth's gravitational redshift* in scenarios involving highly detuned and entangled photon frequencies.

Genuine quantum phenomena are those that entirely defy explanation by any classical physical theory, with relativity being one such. Understanding these phenomena within a relativistic framework is of particular theoretical interest, as *classical wave mechanics* can often account for "ordinary coherence" in optics, which is not the case for entanglement, i.e., coherent correlations. In this thesis, we examine two genuine quantum properties—quantum entanglement and quantum indistinguishability—in their foundational interplay [BL23]. As a result, this thesis addresses key aspects of the *foundations of quantum mechanics*.

By focusing on the influence of metric (i.e., post-Newtonian) gravity on these genuine quantum resources [BBSL22, BGK⁺24], this work also situates itself within the specific context of *genuine quantum tests of post-Newtonian metric gravity*.

Quantum optics is one of the primary research areas intersecting with this work. Within this framework, we characterize not only entangled photons in HOM-interference but also quantum memories—devices that are critical for the near- and mid-term advancement of quantum communication and quantum information processing.

A key aspect of this thesis is the exploration of quantum memories in relativistic settings, an area that has previously remained largely unexplored.

Quantum memories (QMems), which can preserve quantum information over macroscopic periods and under extreme conditions, are essential for advancing our understanding of quantum coherence and entanglement in a relativistic context, where the Earth's *weak* gravitational interaction requires for macroscopically large interrogation durations to render the effects as observable. Integrating QMems into experimental setups designed for relativistic conditions could revolutionize the storage, manipulation, and retrieval of quantum information, thereby enhancing the potential for robust quantum communication networks in space.

The theoretical modeling of these memories in this thesis is conducted within a quantum optical framework, specifically using the Jaynes-Cummings model, which captures the essential properties of light-matter interaction in a fully quantum mechanical theory.

In summary, through theoretical frameworks and experimental proposals, this work aims to

¹A periodic transition between photon bunching and photon anti-bunching in the delay

pioneer approaches for near-future fundamental physics tests. It leverages FEPs and QMems within quantum optical frameworks to push the boundaries of our understanding of quantum resources—and, more broadly, the performance of quantum technologies—in gravitational fields.

1.4 Literary classification

The *cumulative PhD-thesis* on hand is based on three *peer-reviewed* publications, which were published in scientific journals, and are referred to in this work as

Author's publications

1. [BL23]: Barzel, R., Lämmerzahl, C. (2023). Role of indistinguishability and entanglement in Hong-Ou-Mandel interference and finite-bandwidth effects of frequency-entangled photons. *Physical Review A*, *107*(3), 032205.
2. [BBSL22]: Barzel, R., Bruschi, D. E., Schell, A. W., Lämmerzahl, C. (2022). Observer dependence of photon bunching: The influence of the relativistic redshift on Hong-Ou-Mandel interference. *Physical Review D*, *105*(10), 105016.
3. [BGK⁺24]: Barzel, R., Gündoğan, M., Krutzik, M., Rätzel, D., Lämmerzahl, C. (2024). Entanglement dynamics of photon pairs and quantum memories in the gravitational field of the earth. *Quantum*, *8*, 1273.

In the following, we will briefly outline the content of our work, explaining why the topics covered are relevant to current scientific discussions in physics—at least from our perspective. We will also provide relevant scientific references that either intersect with or have inspired our research.

1.4.1 Frequency entangled photons

All works have in common that they investigate FEP. From our perspective, FEP are indeed some of the most important resources (and certainly will gain even more interest in future) for

- genuine quantum tests of gravity and
- entanglement based quantum communication.

The strongest post-Newtonian gravitational effect – the hallmark prediction of general relativity – is the *gravitational redshift*, which primarily couples to the spectral degree of freedom (DOF). The ever-increasing *frequency separations/detunings*

$$\text{today: } \mu \approx (100 - 1,000) \text{ THz},$$

(see for instance [4]), achievable due to continuous progress in experimental photon control, lead to a decrease in the required interrogation time for photons to be coherently influenced by gravity, specifically by the redshift effect.

In a terrestrial scenario, such as the *Drop Tower Bremen*, the redshift between the gravitational potential levels of the Tower's tip w.r.t. its bottom is approximately

$$z \approx 0.9 \cdot 10^{-14},$$

where *qualitative changes* in the genuine quantum properties of photons in an entangled and indistinguishable pair are expected to occur in the *regime of seconds* [BBSL22, BGK⁺24]

$$\tau \gtrsim \frac{\pi}{2\mu z} \approx \text{seconds.} \tag{1.1}$$

The *fundamental limit on the attenuation of light in fiber cables*,

$$\alpha \gtrsim 0.16 \text{ dB/km},$$

unfortunately makes coherent detection impossible over distances greater than a few hundred kilometers, with new records becoming less frequent over time [5, 6]. This is a major problem not only for *long-distance quantum communication*, but also for fiber-based quantum tests of general relativity, which require a cable length at a refractive index of

$$n \approx 1.5 \text{ of approximately } d = \frac{c}{n} \cdot 1 \text{ second} \approx 200,000 \text{ km.}$$

Conversely, cable lengths capable of reconstructing the transmission of genuine quantum properties [5] allow for light confinement in the range of

$$\delta\tau \lesssim \frac{n}{c} \cdot 100 \text{ km} \approx 750 \text{ microseconds,}$$

just enough to achieve milliradians of the required quantum phases that reveal a significant impact of gravity on photons [7]. This is a serious problem, especially since there is no foreseeable solution for significantly improving fiber-based light transmission.

1.4.2 Quantum memories

Currently, there is a strong desire in physics—both for fundamental research and technological advancement—to push the development of quantum memories to their limits [8–16]. The most compelling reason for this is their status as a key technology in quantum computing, specifically for quantum information processors, and in quantum communication for *quantum repeaters*. These repeaters are essential for enabling intercontinental quantum key distribution by storing *pre-distributed entanglement*.

The first entity to achieve reliable quantum coherent storage and long-duration control of quantum entanglement is expected to gain a significant and presently inestimable advantage in the global race of the second quantum revolution. This entails these devices and their development out-reaching relevance that widely encompasses beyond the concerns of academic physics, ranging into economy, society and geostrategic politics; for better or *worse*.

In each case, the durations of quantum coherent information processing targeted by quantum memories lie in the macroscopic regime. Long-distance quantum communication, aims at the distribution of entanglement storing quantum repeaters over hundreds to thousands of kilometers and height distances in the inhomogeneous gravitational field of the earth.

This places constraints on the resources and protocol implementation of quantum applications. In the case of aiming to pre-distribute, store, and process spectral entanglement in quantum memories, frequency detunings in any form (including those arising from uncertainties) are limited by the storage duration τ and the mutual redshift z between the communicators, as detunings of

$$\mu \lesssim \frac{\pi}{2\tau z} \tag{1.2}$$

will lead to a qualitative alteration of the entanglement expected to be processed. In such cases, it is necessary to account for and compensate for these effects.

Compensation is indeed possible in the case of *coherent* gravitational influence on the quantum resources, as the unitary action of gravity could be reversed. This is, of course, different in the case of incoherent uncertainties, such as those arising from a "lack of knowledge" about, for instance, the redshift.

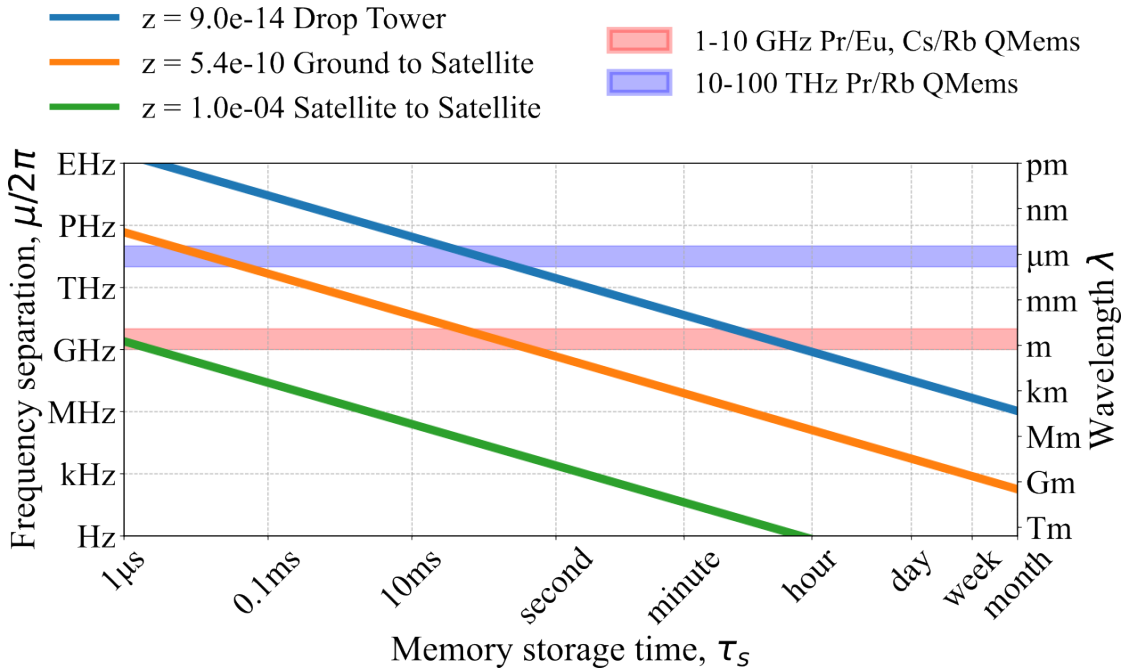


Figure 1.2: Allowed frequency detunings—from estimation formula (1.1)—of entangled quantum memories (QMems) in the case of entanglement-based quantum communication between the ground and the tip of Bremen’s Drop Tower ($z = 0.9 \cdot 10^{-14}$), ground to satellite communication (geosynchronous orbit, $z = 5.4 \cdot 10^{-4}$), and two counter-propagating satellites featuring a mutual *Doppler shift* of $z = 10^{-4}$. The shaded areas correspond to already tested QMem architectures operating at frequencies between (1 – 10) GHz [10–14] and (10 – 100) THz [15, 16].

Figure 1.2 shows the maximally allowed frequency detuning—the phase oscillation frequency of spectral entanglement correlations—depending on the desired storage time, along with already tested quantum memory architectures operating in the radio and optical frequency regimes of GHz and THz.

The necessity to account for and compensate for relativistic effects in space-based and quantum memory-assisted pre-distribution of entanglement is clearly seen here. The quantum memory system operating at GHz frequencies (red-shaded area) [15, 16] is capable of reliable storage up to microseconds in a communication task between two satellites (green line). Longer detection times would lead to a qualitative change in the joint detection behavior of the photons in pair measurements, possibly implemented in a communication task.

Of course, for the pre-distribution of entanglement, one would like to have initialization times for the communication protocol that are much larger, such as in the regime of minutes or hours. Here, one can see that a protocol requiring such storage times and employing state-of-the-art memories operating at radio frequencies would already break down—if not corrected—for height differences of a hundred meters, as in the Bremen Drop Tower.

However, while these effects pose challenges that must be carefully considered in quantum technologies to ensure their accurate and undistorted functioning, these same effects offer advantages for fundamental tests, where they are deliberately induced and observed. For example, GHz-

QMEMS (highlighted in the blue-shaded area of Fig. 1.2) could make the gravitational influence on particle statistics observable within a time frame of seconds, such as in Drop Tower experiments (represented by the blue line in Fig. 1.2) according to our estimate (1.1).

1.4.3 Relativistic redshift in a quantum mechanical framework

The quantitative estimates for the required duration of coherent gravitational interaction on optical entanglement of FEP (1.1), and the limiting operation frequency of QMEMS (1.2), are derived from a theoretical framework that accounts for the coherent alteration of quantum resources under the influence of gravitational redshift, and potentially higher-order gravitational effects.

These theories are not novel and do not originate from this thesis; they are largely based on earlier pioneering work in this field [17–20]. However, our contribution [BBSL22] distinguishes itself by focusing on experimental scenarios that are feasible with current or near-future technology, and by extending the analysis to a multi-particle framework, whereas earlier literature primarily focused on single particles affected by gravitational forces.

In essence, modeling spectral shifts in energies and frequencies requires a mathematically consistent translation of the classical redshift from general relativity [21] into the quantum mechanical framework. This involves reconciling quantum coherence with relativistic spacetime, a task typically approached through quantum field theory in curved spacetime contexts [19].

Regarding the theoretic modeling in Ref [BBSL22] it is promising that an already successfully conducted proof-of-principle experiment—considering the classical Doppler shift in a rotating table experiment—could validate our predictions [22]; grounded on a theoretical framework [23], that is aligned with ours [BBSL22].

1.4.4 HOM-interference as genuine quantum phenomenon

HOM interference [24] is central to this work, largely because it represents a straightforward, well-studied quantum optical experiment. This experiment is more stable, routine, well-understood, and cost-effective compared to setups in solid-state physics, for example. More importantly, it directly addresses the genuinely quantum properties of *entanglement and indistinguishability*.

The reason this experiment highlights quantum indistinguishability is clear: it *emerged* from theoretical considerations of multi-particle indistinguishable quantum particles exhibiting quantum statistics that were expected to lead to notable correlation effects, such as photon bunching [24] and anti-bunching [25].

It is less widely known—yet central to our publication [BGK⁺24]—that these effects correspond to quantum entanglement, at least in the absence of decoherence. As any correlated two-particle measurement is a consequence of the coherent correlation of several particles in an entirely *pure state* in HOM-interference, this mathematically implies that the state *must* contain multi-particle entanglement.

In this case, the photons exhibit *spatial mode entanglement*. Remarkably, this entanglement between initially independent particles arises not from physical interactions mediated by natural forces, as is typically the case, but from the quantum statistical properties of fundamentally indistinguishable particles when they interfere.

Beyond these considerations, HOM interference allows for the exploration of entanglement beyond the scenario of initially independent particles becoming correlated through interference.

In this context, photon bunching—aligned with the bosonic nature of photonic quantum statistics—is observed.

Operating HOM interferometers with initially entangled photons —entangled in degrees of freedom (DOFs) such as polarization, orbital angular momentum, frequency, and/or time—reveals intriguing phenomena, including photon *anti-bunching*—a coherent spatial mode anti-correlation—which is more naturally associated with fermionic quantum statistics.

However, this exotic statistical behavior in photons is the result of a "fermionic spatial *substate*," where the wave function exhibits anti-symmetry with respect to particle exchange. To maintain an entirely symmetric, bosonic multi-photon wave function, the remaining DOFs of the photons must feature in their entirety a residual substate whose wave function carries the fermionic signature of particle-exchange anti-symmetry.

Notably, an anti-symmetric multi-particle wave function of bosons cannot be factorized into single-particle bosonic sub-wave functions [26]. Therefore, the only possible origin of photon anti-bunching must be the entanglement of other DOFs besides the spatial one. This elevates the observation of photon anti-bunching to the status of a *Bell inequality violation* (BIV) [27, 28], which serves as sufficient evidence of entanglement *between* the interfering photons. This, in turn, makes these experiments appealing for entanglement-based quantum key distribution, where the privacy of a communication channel could be verified through BIV.

1.4.5 Gravitationally driven entanglement dynamics

Furthermore, HOM interference —recognized from its inception as primarily dependent on the *spectral* properties of the resources used—makes its study in a relativistic context particularly compelling when conducted with FEP. This combines all the key aspects of this thesis into a single experiment that, as previously mentioned, can be carried out cost-effectively with state-of-the-art QMems in a terrestrial environment such as the Drop Tower in Bremen.

In other words, we can observe genuine multi-particle entanglement in a highly precise and measurable degree of freedom, which is crucially desired for encoding quantum information efficiently, and which moreover also couples to the relativistic redshift, with significant implications for entanglement-based quantum communication.

Indeed, one of the central insights from our work [BBSL22] and [BGK⁺24] is that gravity, when considered from the theoretical level of metric gravity onwards—starting with first-order effects—leads to non-trivial alterations of quantum entanglement within the photons used. This results in the fundamental and technologically relevant phenomenon of altering the detection statistics of frequency-entangled photons from bunching, which is bosonic in nature, to anti-bunching, which is fermionic, and vice versa.

In particular, during the *continuous* transition from photon bunching to photon anti-bunching, the spatial correlation between the photons is lost at the point of equal probability between these two phenomena. This can be interpreted—both formally and physically [BGK⁺24]—as a loss of entanglement due to the creation of entanglement, not shared between the particles themselves, but between distinct DOFs of the same particle. According to the *theorem of entanglement monogamy*, this can only occur at the cost of reducing the entanglement shared between the spatial DOFs of *distinct* particles.

These considerations have gained recognition in the literature [7, 29–36], often discussed under the term "entanglement between internal and external DOFs due to gravity," and have attracted

significant attention as a potential explanation for fundamental issues such as macroscopic decoherence² [29].

In our publication [BGK⁺24], this is precisely the perspective we take on HOM interference. We argue that the phase evolution of interfering photons, conditioned by their spatial propagation path, leads to their spatial mode becoming entangled with their spectral DOF, which is itself already entangled. This entanglement, in turn, dilutes and finally erases the initially monogam inter-particle frequency and spatial entanglement, as evidenced by the loss of correlated interference behavior in the detection statistics.

²i.e., the decoherence of quantum systems as they scale up to macroscopic spatial extensions and numbers of particles.

Chapter 2

Two photon interference

2.1 Introduction

Quantum entanglement (QE) and quantum indistinguishability (QI) are one of the defining features that contrast the physical phenomenology of quantum mechanics from the one of classical physics, as both these phenomena elude any classical explanation. This is also the case as both these phenomena are multi-particle effects, and it was already recognized from the early days of quantum mechanics on, that it is precisely this counterintuitive behavior of composite quantum systems that finds no explanation in terms of the behavior of its individual constituent parts, that marks the entire departure of quantum mechanics from classical physics [37].

One experiment which highlights these two multi-particle phenomena in a particular way in its simplest facility is the *HOM¹-experiment*, which was first conducted 1987 by the experiment's name sakes Hong, Ou and Mandel, with photons within their seminal work [24]. The essence of this experiment lies in the investigation of *two-photon interference*, i.e., the interference of two photons when simultaneously impacting a common beam splitter as seen in Fig. 2.1.

2.2 HOM-experiment

The HOM-experiment (see 2.2) aims at the observation of the genuine quantum effect, commonly termed *photon bunching*, which finds its theoretical explanation solely in terms of purely quantum mechanical considerations without classical analog. More concretely, the phenomenon's explanation requires the consideration of the *particle nature* of light within an *entirely* quantum mechanical theory of electromagnetism, thereby going beyond the wave mechanics of Maxwell's classical theory of electromagnetism. Above this particle-interpretation of light, the occurrence of this effect moreover demands for a further genuine quantum property, that is the *fundamental* indistinguishability of quantum objects, either not possessing any classical pendant. Practically, photon bunching manifests itself through a correlated exit of two photons throughout of a similar exit port when simultaneously interfering on a common beam-splitter, experimentally reflected by suppression of the complementary event, that is, the coincident detection at distinct detectors; called *photon anti-bunching*. This suppression is show in Fig. 2.3, and is commonly termed the *HOM-dip*.

¹Hong, Ou and Mandel

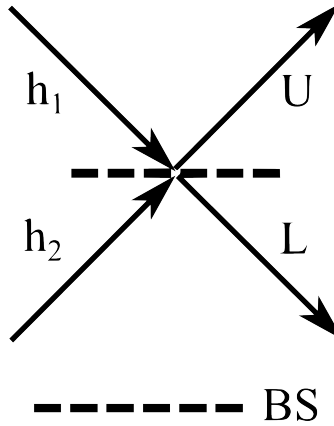


Figure 2.1: Two-photon interference. BS: Beam splitter. Input modes: h_1 and h_2 . Output modes: U and L .

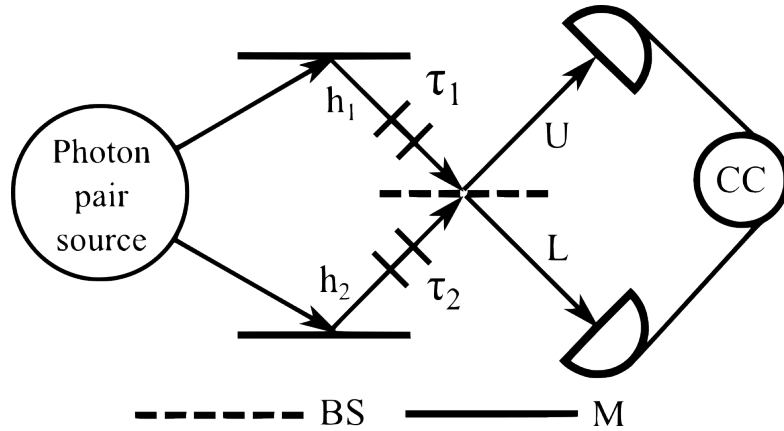


Figure 2.2: Hong-Ou-Mandel (HOM) experiment. BS: Beam splitter; M: Mirror; CC: Coincidence count logic.

In the following, we want to briefly revise the mathematical basics of HOM-interference. The reader that is familiar with HOM-interference may skip these, and might continue reading from Sec. 2.3 onwards.

2.2.1 Mathematical basics

2.2.1.1 First and second quantization

The theoretical framework that accounts for both of the aforementioned concepts (namely the particle nature of photons and their fundamental indistinguishability) by construction is the *second quantization formalism* (SQF), which we want to contrast against the *first quantization formalism* (FQF), the quantum mechanical framework of distinguishable particles.

We consider a two-particle quantum state of two photons in modes that are associated to the input ports h_1 and h_2 of the beam splitter from Fig. 2.1. The associated single-particle Hilbert

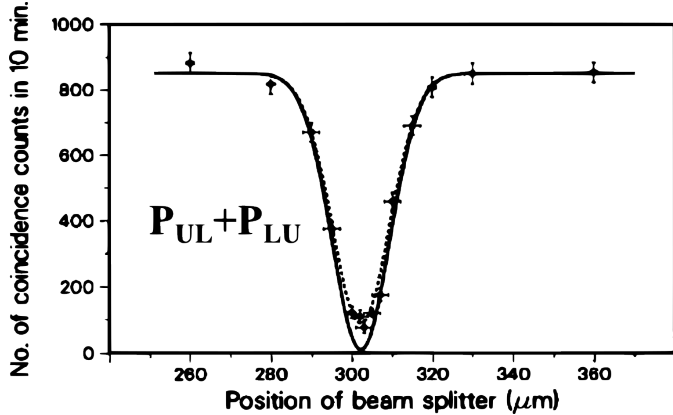


Figure 2.3: HOM-dip. Original measurement results from Ref. [24]. The coincidence counts are a measure of the photon anti-bunching probability $P_{UL} + P_{LU}$.

space

$$\mathcal{H} = \text{span}\{|h_1\rangle, |h_2\rangle\}, \quad (2.1)$$

is two-dimensional. In first quantization the associated quantum state reads

$$|\psi\rangle = |h_1\rangle \otimes |h_2\rangle = |h_1 h_2\rangle \quad (2.2)$$

and in second quantization

$$|\psi\rangle = \hat{a}_{h_1}^\dagger \hat{a}_{h_2}^\dagger |0\rangle = \frac{1}{\sqrt{2}}(|h_1 h_2\rangle + |h_2 h_1\rangle), \quad (2.3)$$

where $|0\rangle$ is the vacuum state and $\hat{a}_{h_i}^\dagger$ and \hat{a}_{h_i} with $i = 1, 2$ are photonic creation and annihilation operators that satisfy the bosonic commutation relation

$$[\hat{a}_{h_i}, \hat{a}_{h_j}^\dagger] = \delta_{ij}, \quad (2.4a)$$

$$[\hat{a}_{h_i}^{(\dagger)}, \hat{a}_{h_j}^{(\dagger)}] = 0, \quad (2.4b)$$

where other commutators vanish and $i, j = 1, 2$.

One can see the difference between first and second quantized quantum states (2.2) and (2.3) in their symmetry. Where the second quantized state (2.3) is symmetric in the mode-labels h_1 and h_2 , the first quantized state (2.2) accounts for the distinguishability of the two considered photons implicitly by their position in the tensor product state. Therefore, note that $|h_1 h_2\rangle \neq |h_2 h_1\rangle$, but however $\hat{a}_{h_1}^\dagger \hat{a}_{h_2}^\dagger |0\rangle = \hat{a}_{h_2}^\dagger \hat{a}_{h_1}^\dagger |0\rangle$.

When impinging on the beam splitter the two photons interfere and are emitted into the light-field modes that are associated with the beam splitter's output ports U and L , either spanning a two-dimensional Hilbert space

$$\mathcal{H} = \text{span}\{|U\rangle, |L\rangle\}. \quad (2.5)$$

The corresponding linear map/operator \hat{U}_{BS} between the single-particle Hilbert spaces (2.1) and (2.5) of the beam splitter is a unitary transformation, which we characterize through the matrix

$$\hat{U}_{BS} = \begin{pmatrix} \sqrt{r} & -e^{-i\theta}\sqrt{t} \\ e^{i\theta}\sqrt{t} & \sqrt{r} \end{pmatrix}, \quad (2.6)$$

and which is conventionally given in first quantization through the unitary mapping between the basis states² [38]

$$\begin{pmatrix} |h_1\rangle \\ |h_2\rangle \end{pmatrix} \mapsto \hat{U}_{BS} \begin{pmatrix} |U\rangle \\ |L\rangle \end{pmatrix}. \quad (2.7)$$

and in second quantization in terms of the mapping of the creation operators [38]

$$\begin{pmatrix} \hat{a}_{h_1}^\dagger \\ \hat{a}_{h_2}^\dagger \end{pmatrix} \mapsto \hat{U}_{BS} \begin{pmatrix} \hat{a}_U^\dagger \\ \hat{a}_L^\dagger \end{pmatrix}, \quad (2.8)$$

where r and t are the reflection- and transmission-coefficient of the beam splitter and θ is the beam-splitter's phase. Further, \hat{a}_σ^\dagger and \hat{a}_σ with $\sigma = U, L$ are photonic creation and annihilation operators that satisfy the bosonic commutation relation

$$[\hat{a}_\sigma, \hat{a}_{\sigma'}^\dagger] = \delta_{\sigma\sigma'}, \quad (2.9a)$$

$$[\hat{a}_\sigma^{(\dagger)}, \hat{a}_{\sigma'}^{(\dagger)}] = 0, \quad (2.9b)$$

where other commutators vanish and $\sigma, \sigma' = U, L$.

In the following we set $r = t = 1/2$, as common with HOM-interference, i.e., we consider a 50:50 beam splitter

$$\hat{U}_{BS} = \frac{1}{\sqrt{2}} \begin{pmatrix} 1 & -e^{-i\theta} \\ e^{i\theta} & 1 \end{pmatrix} \quad (2.10)$$

that transforms the spatial modes through mapping them as

$$|h_1\rangle \mapsto \frac{1}{\sqrt{2}}(|U\rangle - e^{-i\theta}|L\rangle), \quad (2.11a)$$

$$|h_2\rangle \mapsto \frac{1}{\sqrt{2}}(e^{i\theta}|U\rangle + |L\rangle), \quad (2.11b)$$

and

$$\hat{a}_{h_1}^\dagger \mapsto \hat{b}_{h_1}^\dagger := \frac{1}{\sqrt{2}}(\hat{a}_U^\dagger - e^{-i\theta}\hat{a}_L^\dagger), \quad (2.12a)$$

$$\hat{a}_{h_2}^\dagger \mapsto \hat{b}_{h_2}^\dagger := \frac{1}{\sqrt{2}}(e^{i\theta}\hat{a}_U^\dagger + \hat{a}_L^\dagger), \quad (2.12b)$$

which can be equivalently obtained from the action

$$\hat{b}_{h_i}^\dagger = \hat{U}_{MS}\hat{a}_{h_i}^\dagger\hat{U}_{MS}^\dagger \quad (2.13)$$

with the unitary *mode swapper operator*,

$$\hat{U}_{MS} = \exp\left(\frac{\pi}{2} \sum_{i=1}^2 [\hat{b}_{h_i}^\dagger \hat{a}_{h_i} - \hat{b}_{h_i} \hat{a}_{h_i}^\dagger]\right), \quad (2.14)$$

which will become of importance several times in this thesis.

²of course it would be also possible to describe the beam splitter's action in terms of how it acts on the components of vectors of the respective Hilbert spaces. However, here we choose to show its action on the basis states for the sake of transparency.

2.2.1.2 HOM-detection statistics

In the following, we call U and L the detector modes. The probability to detect one photon in detector mode σ and the other photon in detector mode σ' is denoted as

$$P_{\sigma\sigma'}, \quad \text{with } \sigma, \sigma' = U, L, \quad (2.15)$$

and called the *joint detection statistics*, which in the here considered case consists of four events, namely

1. both photons are detected at the detector behind the output port U (P_{UU}),
2. one photon is detected at the detector U and the other at detector L (P_{UL}),
3. one photon is detected at the detector L and the other at detector U (P_{LU}),
4. both photons are detected at the detector behind the output port L (P_{LL}).

If operated with only one photon, we call the probability to detect this photon in mode σ

$$P_\sigma, \quad \text{with } \sigma = U, L, \quad (2.16)$$

the *single-particle detection statistics*.

2.2.1.3 Photon bunching

After the 50:50 BS then the first quantized two-photon state (2.2) when applied to (2.11b) renders the form

$$\begin{aligned} |\psi\rangle &= \frac{1}{2}(|U\rangle - e^{-i\theta}|L\rangle) \otimes (e^{i\theta}|U\rangle + |L\rangle) \\ &= \frac{1}{2}(e^{i\theta}|UU\rangle + |UL\rangle - |LU\rangle - e^{-i\theta}|LL\rangle), \end{aligned} \quad (2.17)$$

while the second quantized one (2.3) when applied to (2.12) does,

$$\begin{aligned} |\psi\rangle &= (\hat{a}_U^\dagger - e^{-i\theta}\hat{a}_L^\dagger)(e^{i\theta}\hat{a}_U^\dagger + \hat{a}_L^\dagger)|0\rangle \\ &= (e^{i\theta}\hat{a}_U^\dagger\hat{a}_U^\dagger + \hat{a}_U^\dagger\hat{a}_L^\dagger - \hat{a}_L^\dagger\hat{a}_U^\dagger - e^{-i\theta}\hat{a}_L^\dagger\hat{a}_L^\dagger)|0\rangle \\ &\stackrel{\text{Eq.(2.9b)}}{=} (e^{i\theta}\hat{a}_U^\dagger\hat{a}_U^\dagger - e^{-i\theta}\hat{a}_L^\dagger\hat{a}_L^\dagger)|0\rangle \\ &= \frac{1}{\sqrt{2}}(e^{i\theta}|UU\rangle - e^{-i\theta}|LL\rangle), \end{aligned} \quad (2.18)$$

where we for simplicity denoted the quantum state before and after the BS as $|\psi\rangle$, and expressed the final result of the second quantized calculation in first quantization to read off the detection statistics easily—which we do immediately.

In case of the simple example-state shown here, one can simply read off the associated detection statistics by Born's rule

$$P_{\sigma\sigma'} = |\langle\sigma\sigma'|\psi\rangle|^2, \quad (2.19)$$

with $\sigma, \sigma' = U, L$ from the first quantized state (2.17) as being uniformly distributed

$$\begin{aligned} P_{UU} &= P_{LL} = 1/4, \\ P_{UL} &= P_{LU} = 1/4. \end{aligned} \quad (2.20)$$

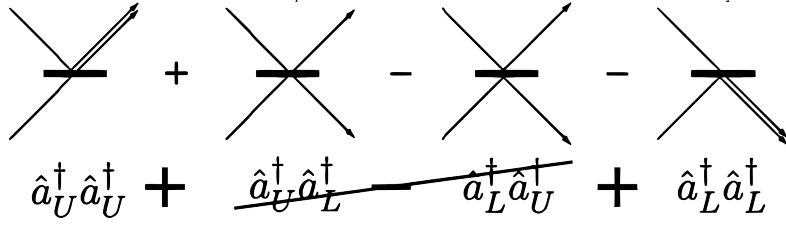


Figure 2.4: HOM-detection statistics. For indistinguishable particles the middle-terms cancel out each other; interestingly in a coherent way as probability *amplitudes*, and not just incoherently as probabilities, thereby serving to rule out a multi-particle quantum theory that exclusively is built up on the theoretical foundations of single-particle quantum mechanics.

and the second quantized one (given in first quantization in the last line of (2.18)) as being correlated showcasing photon bunching

$$\begin{aligned} P_{UU} &= P_{LL} = 1/2, \\ P_{UL} &= P_{LU} = 0. \end{aligned} \quad (2.21)$$

In any case the single-particle detection statistics arises as in standard probability-theory from the joint statistics as

$$P_\sigma = \sum_{\sigma'} P_{\sigma\sigma'}. \quad (2.22)$$

resulting from the computation in *both* FQF and SQF in

$$P_U = P_L = 1/2 \quad (2.23)$$

Since we assumed the photons (despite being indistinguishable) as independent of each other, the intuitive result of the joint detection statistics would suffice *statistical independence*, i.e.,

$$P_{\sigma\sigma'} = P_\sigma P_{\sigma'}, \quad (2.24)$$

which is aligned with the result from FQF and stands in contradiction with the result from SQF (as in this case there *exist no* P_σ from which (2.21) arises). In other words, there is no single-particle theory that explains photon bunching.

Thus, the experimental verification of photon bunching (see Fig 2.3) is one more of these examples that showcases that however counter-intuitive the predictions of the strict application of indecipherable quantum theoretical concepts seem to be, they nevertheless find their validity in the behavior of nature; certified by physical observation.

2.3 Mayor achievements

2.3.1 Systematic formalism

A notable achievement of our work [BL23] is the development of a general approach to characterize multi-photon quantum states within a quantum field theoretical framework. This approach employs SQF, which is intrinsic to many-particle quantum physics, enabling us to systematically derive the joint detection statistics for general multi-photon interference experiments. The strength of our method lies in its natural extensibility to arbitrarily complex experimental setups, rendering their analysis a matter of computational complexity alone.

Our ultimate goal is to derive the joint measurement statistics of two photons, specifically the probability that a detector, configured for a particular measurement setting, detects one photon with parameters σ_1 and another with parameters σ_2 . This probability is given by

$$P_{\sigma_1 \sigma_2} = \frac{\tilde{P}_{\sigma_1 \sigma_2}}{\int d\sigma_1 d\sigma_2 \tilde{P}_{\sigma_1 \sigma_2}} \quad (2.25)$$

where $\tilde{P}_{\sigma_1 \sigma_2}$ represents the unnormalized joint detection probability.

Since the nominator and denominator of the RHS of (2.25) are of the same order in the considered quantum states, we are able to neglect *normalization constants* or other constant³ pre-factors of the states that might arise during some of our calculations.

We here present an alternative, more general, derivation of our results in [BL23], where we solely considered pure states.

2.3.1.1 Pure and mixed quantum states

We apply the SQF and describe *unnormalized*⁴ pure two-photon states, where the i -th photon is characterized by its entire DOFs (denoted with the bold-font ω_i) as

$$|\psi\rangle = \int d\omega_1 d\omega_2 \Phi(\omega_1, \omega_2) a_{\omega_1}^\dagger a_{\omega_2}^\dagger |0\rangle, \quad (2.26)$$

and –beyond our documentation in [BL23]– we characterize *unnormalized*⁵ mixed states by the density operator

$$\rho = \int d\omega_1 d\omega_2 d\omega'_1 d\omega'_2 \Phi(\omega_1, \omega_2, \omega'_1, \omega'_2) a_{\omega_1}^\dagger a_{\omega_2}^\dagger |0\rangle \langle 0| a_{\omega'_1} a_{\omega'_2}, \quad (2.27)$$

where the state is entirely characterized by the photonic *wave function* $\Phi(\omega_1, \omega_2)$ in case of pure states and the photonic *density function* $\Phi(\omega_1, \omega_2, \omega'_1, \omega'_2)$ in case of mixed states. For both, we use the symbol Φ , where it should be clear from the context and the function arguments, which one is meant.

The hermiticity requirement on density operators, $\rho = \rho^\dagger$, translates to the condition on the density function

$$\Phi(\omega_1, \omega_2, \omega'_1, \omega'_2) = \Phi^*(\omega'_1, \omega'_2, \omega_1, \omega_2). \quad (2.28)$$

³i.e., state-independent

⁴i.e. possibly violating $|\langle \psi | \psi \rangle|^2 = 1$

⁵i.e. possibly violating $\text{Tr}\{\rho\} = 1$

In the special case of pure states the corresponding density operator $\rho = |\psi\rangle\langle\psi|$ is associated to the density function

$$\Phi(\omega_1, \omega_2, \omega'_1, \omega'_2) = \Phi(\omega_1, \omega_2)\Phi(\omega'_1, \omega'_2). \quad (2.29)$$

Both, pure and mixed states, neither need to be normalized, as in the very end we consider probability distributions that might be normalized through division by their own integrals over the entire domain of considered DOFs by means of Eq. (2.25).

The commutator relations are as usual

$$[\hat{a}_{\omega_i}, \hat{a}_{\omega_j}^\dagger] = \delta_{\omega_i \omega_j}, \quad (2.30a)$$

$$[\hat{a}_{\omega_i}^{(\dagger)}, \hat{a}_{\omega_j}^{(\dagger)}] = 0, \quad (2.30b)$$

where $\delta_{\omega_i \omega_j}$ is the multivariate delta function that is a product of Kronecker-deltas and Dirac-delta functions for each discrete and continuous DOF respectively. Likewise, each integral within the multidimensional integrals $\int d\omega_i$ has to be evaluated as a sum in case of each discrete DOF.

2.3.1.2 Symmetries of quantum states

The commutator relations (2.30b) allow us to rewrite the considered quantum states without changing the physics by means of symmetrized wave and density functions

$$|\psi\rangle = \int d\omega_1 d\omega_2 \mathcal{S}_{\omega_1 \omega_2} [\Phi(\omega_1, \omega_2)] a_{\omega_1}^\dagger a_{\omega_2}^\dagger |0\rangle, \quad (2.31)$$

and

$$\rho = \int d\omega_1 d\omega_2 d\omega'_1 d\omega'_2 \mathcal{S}_{\omega_1 \omega_2} [\mathcal{S}_{\omega'_1 \omega'_2} [\Phi(\omega_1, \omega_2, \omega'_1, \omega'_2)]] a_{\omega_1}^\dagger a_{\omega_2}^\dagger |0\rangle \langle 0| a_{\omega'_1} a_{\omega'_2}, \quad (2.32)$$

where

$$\mathcal{S}_{\omega_1 \omega_2} [f(\omega_1, \omega_2)] = f(\omega_1, \omega_2) + f(\omega_2, \omega_1) \quad (2.33)$$

is the symmetrization operator that symmetrizes arbitrary functions $f(\omega_1, \omega_2)$. Also, here we need not consider a normalized symmetrization, i.e.,

$$\mathcal{S}_{\omega_1 \omega_2} [f(\omega_1, \omega_2)] = [f(\omega_1, \omega_2) + f(\omega_2, \omega_1)] / 2,$$

due to (2.25) either. We define the normalized symmetrization with the bold font \mathbf{S}

2.3.1.3 Hilbert (dual) vector and operator space

The considered 2-particle Hilbert space

$$\mathcal{H} = \text{span}\{\mathfrak{B}\}, \quad (2.34)$$

in which we work, is spanned by the basis states

$$\mathfrak{B} = \{a_{\omega_1}^\dagger a_{\omega_2}^\dagger |0\rangle\}, \quad (2.35)$$

The dual-space is

$$\mathcal{H}^* = \text{span}\{\mathfrak{B}^*\} \quad (2.36)$$

with the dual-basis being spaned by

$$\mathfrak{B}^* = \{\langle 0 | a_{\omega_1} a_{\omega_2}\}.$$
 (2.37)

From the basis and dual-basis we can construct the space of linear operators on \mathcal{H} as

$$\mathcal{L}(\mathcal{H}) = \mathcal{H}^* \otimes \mathcal{H} \cong \text{Hom}(\mathcal{H}, \mathcal{H}) \cong \text{Hom}(\mathcal{L}(\mathcal{H}), \mathbb{C}),$$
 (2.38)

which we equipped directly with *cannonical isomorphisms*.

2.3.1.4 Orthogonality and completeness relations

For the rest of this section, 2.3.1 let

$$|\varphi_{\omega_1 \omega_2}\rangle := a_{\omega_1}^\dagger a_{\omega_2}^\dagger |0\rangle,$$
 (2.39)

$$\langle \varphi_{\omega_1 \omega_2}| := \langle 0| a_{\omega_1} a_{\omega_2},$$
 (2.40)

The *unnormalized orthogonality relation* reads

$$\langle \varphi_{\omega_1 \omega_2} | \varphi_{\omega'_1 \omega'_2} \rangle = \mathcal{S}_{\omega_1 \omega_2} [\delta_{\omega_1 \omega'_1} \delta_{\omega_2 \omega'_2}] = \delta_{\omega_1 \omega'_1} \delta_{\omega_2 \omega'_2} + \delta_{\omega_1 \omega'_2} \delta_{\omega_2 \omega'_1}$$
 (2.41)

The *unnormalized completeness relation* is characterized by the *unnormalized unit operator* on \mathcal{H}

$$\mathbb{1}_{\mathcal{H}} = \sum_{|\varphi\rangle \in \mathfrak{B}} |\varphi\rangle \langle \varphi| = \int d\omega_1 d\omega_2 a_{\omega_1}^\dagger a_{\omega_2}^\dagger |0\rangle \langle 0| a_{\omega_1} a_{\omega_2}.$$
 (2.42)

Again, as stated before, since we are only interested in the derivation of probabilities, we are allowed to work with unnormalized orthogonality relations and unnormalized unit operators, as the constant⁶ factors drop out in the normalization of the finally resulting probability distribution.

2.3.1.5 Basis-representation of quantum states and linear operators

Given this, we can easily expand the considered states (2.26) and (2.27) in this basis as

$$\langle \varphi_{\omega_1 \omega_2} | \psi \rangle = \mathcal{S}_{\omega_1 \omega_2} [\Phi(\omega_1, \omega_2)],$$
 (2.43a)

$$\langle \varphi_{\omega_1 \omega_2} | \rho | \varphi_{\omega'_1 \omega'_2} \rangle = \mathcal{S}_{\omega_1 \omega_2} [\mathcal{S}_{\omega'_1 \omega'_2} [\Phi(\omega_1, \omega_2, \omega'_1, \omega'_2)]].$$
 (2.43b)

Not only the density operator, but any linear operator $A \in \mathcal{L}(\mathcal{H})$ from the space of linear operators (2.38) on \mathcal{H} can be written as (2.32) like

$$A = \int d\omega_1 d\omega_2 d\omega'_1 d\omega'_2 \mathcal{S}_{\omega_1 \omega_2} \mathcal{S}_{\omega'_1 \omega'_2} [A(\omega_1, \omega_2, \omega'_1, \omega'_2)] a_{\omega_1}^\dagger a_{\omega_2}^\dagger |0\rangle \langle 0| a_{\omega'_1} a_{\omega'_2},$$
 (2.44)

and similarly represented with the basis states trough

$$\langle \varphi_{\omega_1 \omega_2} | A | \varphi_{\omega'_1 \omega'_2} \rangle = \mathcal{S}_{\omega_1 \omega_2} \mathcal{S}_{\omega'_1 \omega'_2} [A(\omega_1, \omega_2, \omega'_1, \omega'_2)],$$
 (2.45)

where we call $A(\omega_1, \omega_2, \omega'_1, \omega'_2)$ the density function of operator A .

⁶constant over the domain of DOFs.

2.3.1.6 Expectation values

Now, we want to give the *trace operation*, that, due to the canonical isomorphism (2.38) maps any (hermitian) operator to a (real) scalar given through

$$\begin{aligned}\text{Tr}\{\cdot\} : \mathcal{L}(\mathcal{H}) &\rightarrow \mathbb{C} \\ A &\mapsto \text{Tr}\{A\}\end{aligned}\tag{2.46}$$

with

$$\text{Tr}\{A\} = \sum_{|\varphi\rangle \in \mathfrak{B}} \langle \varphi | A | \varphi \rangle = \int d\omega_1 d\omega_2 \mathcal{S}_{\omega_1 \omega_2} [A(\omega_1, \omega_2, \omega_1, \omega_2)].\tag{2.47}$$

In particular we call the trace of the operator specified by the respective quantum state under consideration

$$\begin{aligned}\text{Tr}\{\rho A\} &= \langle A \rangle \\ &= \int d\omega_1 d\omega_2 d\omega'_1 d\omega'_2 \mathcal{S}_{\omega_1 \omega_2} \mathcal{S}_{\omega'_1 \omega'_2} [\Phi(\omega_1, \omega_2, \omega'_1, \omega'_2) A(\omega'_1, \omega'_2, \omega_1, \omega_2)]\end{aligned}\tag{2.48}$$

the *expectation value* of the operator A .

The generalization of our ansatz naturally extends to more than two particles by simply increasing the number of creation operators (and annihilation operators too, in case of mixed states and other linear operators on \mathcal{H}) and the function arguments of the wave and density functions. Furthermore, by building linear (convex) combinations of distinct variate wave (density) functions in (2.26) ((2.27)) one can coherently (incoherently) superimpose particle states of distinct particle number.

2.3.1.7 Detection Statistics & Glauber's Theory of Quantum Coherence

Building on the analysis presented in Ref. [BL23], we compute the detection statistics, specifically the probability of detecting one photon characterized by ω_1 and another by ω_2 in an interference experiment. By applying *Glauber's theory of optical quantum coherence* [39] to the standard time-dependent initial states in HOM interference (Eq. (1) in Ref. [BL23]), we demonstrated that the detection statistics are given by the squared modulus of the time-dependent wave function, integrated over the degrees of freedom (DOFs) to which the detectors are insensitive (see Eq. (9) in Ref. [BL23]).

In this section, we extend our previous results, where we initially assumed detectors sensitive only to the spatial DOF σ , with frequency ω as the sole remaining DOF. Here, the complete set of DOFs was denoted by $\omega = \{\sigma, \omega\}$.

We now generalize to the case where $\omega = \{\sigma, \bar{\sigma}\}$, where σ represents the set of DOFs to which the detectors are sensitive, and $\bar{\sigma}$ represents those to which they are insensitive. The unnormalized probability of detecting one photon at σ_1 and another at σ_2 is given by

$$\tilde{P}_{\sigma_1 \sigma_2} = \int d\bar{\sigma}_1 d\bar{\sigma}_2 \tilde{P}_{\omega_1 \omega_2},\tag{2.49}$$

where the unnormalized probability $\tilde{P}_{\omega_1 \omega_2}$ of finding one photon in state ω_1 and another in state ω_2 , according to Glauber's theory, is

$$\tilde{P}_{\omega_1 \omega_2} = \langle a_{\omega_1}^\dagger a_{\omega_2}^\dagger a_{\omega_2} a_{\omega_1} \rangle.\tag{2.50}$$

Within the framework presented here, this expression can be rewritten as

$$\tilde{P}_{\omega_1\omega_2} = |\langle \varphi_{\omega_1\omega_2} | \psi \rangle|^2 = |\mathcal{S}_{\omega_1\omega_2} [\Phi(\omega_1, \omega_2)]|^2. \quad (2.51)$$

In the case of mixed states ρ (as detailed in Eq. (2.27)), this generalizes to

$$\tilde{P}_{\omega_1\omega_2} = \langle \varphi_{\omega_1\omega_2} | \rho | \varphi_{\omega_1\omega_2} \rangle = \mathcal{S}_{\omega_1\omega_2} [\Phi(\omega_1, \omega_2, \omega_1, \omega_2)]. \quad (2.52)$$

Furthermore, this approach can be extended to the detection statistics of more than two particles by appropriately increasing the number of indices and function arguments in Equations (2.51) and (2.52).

2.3.1.8 Interferometer Propagation Superoperator

Finally, it is essential to emphasize that detection statistics must be evaluated at the detector modes, i.e., one has to "propagate" the initial state through the interferometer, thereby manipulating it appropriately. In the context of linear interferometry, where detection results are linearly dependent on the density operator (i.e., $P_{\sigma_1\sigma_2} \propto \rho$), each experiment is characterized by an interferometer-specific *propagation superoperator*:

$$\Lambda_{\tau} \in \mathcal{L}(\mathcal{L}(\mathcal{H})) = \mathcal{L}^*(\mathcal{H}) \otimes \mathcal{L}(\mathcal{H})$$

This superoperator is parameterized by experimental degrees of freedom (DOFs) τ , which the experimenter can adjust to initialize the resource quantum states, manipulate them during the experiment, and set the measurement parameters for readout.

In its most general form, Λ_{τ} is restricted to being a *positive map*, meaning it maps positive semidefinite density operators to positive semidefinite density operators. This allows it to account for phenomena such as particle loss, decoherence, and more. In its simplest form, Λ_{τ} acts as a unitary conjugation operator on the density operator ρ :

$$\Lambda_{\tau}(\rho) = U_{\tau} \rho U_{\tau}^{\dagger}$$

For pure input states, it acts as a unitary operation $U_{\tau} |\psi\rangle$.

In the specific case of standard HOM interference,

$$U_{\tau} = U_{\theta} U_{\tau_1\tau_2} \quad (2.53)$$

decomposes into the sequential application of optical delays $U_{\tau_1\tau_2}$ and a beam splitter U_{θ} (with beam splitter phase θ). Both operations can be modeled as mode swappers (2.14). The beam splitter is described by (2.12), incorporating spectral indices, while the optical delays are represented as:

$$\hat{a}_{h_j\omega_j}^{\dagger} \mapsto \hat{b}_{h_j\omega_j}^{\dagger} := \hat{a}_{h_j\omega_j}^{\dagger} e^{i\omega_j\tau_j} \quad (2.54)$$

for $j = 1, 2$.

2.3.1.9 Specialization to standard result

The standard case in HOM-interference (see Fig. 2.2) is the consideration of photon pairs rendering the initial state

$$|\psi\rangle = \int d\omega_1 d\omega_2 \Phi(\omega_1, \omega_2) \hat{a}_{h_1\omega_1}^{\dagger} \hat{a}_{h_2\omega_2}^{\dagger} |0\rangle, \quad (2.55)$$

which is often given (and also in Ref. [BL23]) after the application of optical delays

$$U_{\tau_1 \tau_2} |\psi\rangle = \int d\omega_1 d\omega_2 \Phi(\omega_1, \omega_2) e^{i\omega_1 \tau_1} e^{i\omega_2 \tau_2} \hat{a}_{h_1 \omega_1}^\dagger \hat{a}_{h_2 \omega_2}^\dagger |0\rangle \quad (2.56)$$

where in the following we denote with

$$\Phi^{\tau_1 \tau_2}(\omega_1, \omega_2) = \Phi(\omega_1, \omega_2) e^{i\omega_1 \tau_1} e^{i\omega_2 \tau_2} \quad (2.57)$$

the *time dependent spectral wave function*. After the BS, we then have

$$\begin{aligned} U_\theta U_{\tau_1 \tau_2} |\psi\rangle &= \int d\omega_1 d\omega_2 \left\{ \Phi^{\tau_1 \tau_2}(\omega_1, \omega_2) \left[e^{i\theta} \hat{a}_{U \omega_1}^\dagger \hat{a}_{U \omega_2}^\dagger - e^{-i\theta} \hat{a}_{L \omega_1}^\dagger \hat{a}_{L \omega_2}^\dagger \right] \right. \\ &\quad \left. + \Phi^{\tau_1 \tau_2}(\omega_1, \omega_2) \left[\hat{a}_{U \omega_1}^\dagger \hat{a}_{L \omega_2}^\dagger - \hat{a}_{L \omega_1}^\dagger \hat{a}_{U \omega_2}^\dagger \right] \right\} |0\rangle, \end{aligned} \quad (2.58)$$

which features spectral symmetry within the first rectangular bracket, and spectral anti-symmetry within the second rectangular bracket, and thus can be rewritten as

$$\begin{aligned} U_\theta U_{\tau_1 \tau_2} |\psi\rangle &= \int d\omega_1 d\omega_2 \left\{ \Phi_S^{\tau_1 \tau_2}(\omega_1, \omega_2) \left[e^{i\theta} \hat{a}_{U \omega_1}^\dagger \hat{a}_{U \omega_2}^\dagger - e^{-i\theta} \hat{a}_{L \omega_1}^\dagger \hat{a}_{L \omega_2}^\dagger \right] \right. \\ &\quad \left. + 2\Phi_A^{\tau_1 \tau_2}(\omega_1, \omega_2) \hat{a}_{U \omega_1}^\dagger \hat{a}_{L \omega_2}^\dagger \right\} |0\rangle, \end{aligned} \quad (2.59)$$

with

$$\Phi_S^{\tau_1 \tau_2}(\omega_1, \omega_2) = \frac{1}{2} (\Phi^{\tau_1 \tau_2}(\omega_1, \omega_2) + \Phi^{\tau_1 \tau_2}(\omega_2, \omega_1)) \quad (2.60a)$$

$$\Phi_A^{\tau_1 \tau_2}(\omega_1, \omega_2) = \frac{1}{2} (\Phi^{\tau_1 \tau_2}(\omega_1, \omega_2) - \Phi^{\tau_1 \tau_2}(\omega_2, \omega_1)) \quad (2.60b)$$

being the spectral symmetric and anti-symmetric part of the wave function.

From Eq. (2.59) it can be seen that the photon bunching probability $P_B = P_{UU} + P_{LL}$ and the photon anti-bunching probability $P_{\bar{B}} = P_{UL} + P_{LU}$ are respectively proportional to

$$P_B(\tau_1, \tau_2) \propto \int d\omega_1 d\omega_2 |\Phi_S^{\tau_1 \tau_2}(\omega_1, \omega_2)|^2, \quad (2.61a)$$

$$P_{\bar{B}}(\tau_1, \tau_2) \propto \int d\omega_1 d\omega_2 |\Phi_A^{\tau_1 \tau_2}(\omega_1, \omega_2)|^2, \quad (2.61b)$$

which gives us the central figure of merit in HOM-interference discussed in this thesis, that is, the difference probability, the *correlation measure* $P_c = P_B - P_{\bar{B}}$ that is

$$P_c(\tau_1, \tau_2) = \int d\omega_1 d\omega_2 \left(|\Phi_S^{\tau_1 \tau_2}(\omega_1, \omega_2)|^2 - |\Phi_A^{\tau_1 \tau_2}(\omega_1, \omega_2)|^2 \right), \quad (2.62)$$

where we replaced the proportionality relation through an equality by assuming the normalization condition

$$\int d\omega_1 d\omega_2 |\Phi^{\tau_1 \tau_2}(\omega_1, \omega_2)|^2 = 1 \quad (2.63)$$

to hold.

Here one can see—after the immediate step—that the measurement of photon anti-bunching corresponds to a sufficient proof of the presence of inter-particle⁷ entanglement, which by itself corresponds to the factorization of the investigated state (2.55) into a product of single particle states $|\psi\rangle = A_1^\dagger A_2^\dagger |0\rangle$ with the single-particle modes being

$$A_i^\dagger = \int d\omega_i \phi(\omega_i) \hat{a}_{h_i \omega_i}^\dagger \quad (2.64)$$

with $i = 1, 2$. In other words, the spectral wave function must factorize as

$$\Phi(\omega_1, \omega_2) = \phi_1(\omega_1) \phi_2(\omega_2). \quad (2.65)$$

In this case Eq. (2.62) simplifies to

$$P_c(\tau_1, \tau_2) = \int d\omega_1 d\omega_2 \phi_1(\omega_1) \phi_2^*(\omega_1) \cos(\tau(\omega_1 - \omega_2)) \phi_1^*(\omega_2) \phi_2(\omega_2) \quad (2.66)$$

with $\tau = \tau_1 - \tau_2$. In this context it is already known, that the cosine function in Eq. (2.66) is a *positive semidefinite kernel function*, which guarantees the positivity of (2.66). However, this can be also be seen by employing the trigonometric identity

$$\cos(\tau(\omega_1 - \omega_2)) = \cos(\tau\omega_1) \cos(\tau\omega_2) + \sin(\tau\omega_1) \sin(\tau\omega_2) \quad (2.67)$$

to obtain from (2.66) the result

$$P_c(\tau) = \left| \int d\omega \phi_1(\omega) \cos(\tau\omega) \phi_2^*(\omega) \right|^2 + \left| \int d\omega \phi_1^*(\omega) \sin(\tau\omega) \phi_2(\omega) \right|^2 \geq 0, \quad (2.68)$$

whose interpretation is the *exclusive* occurrence of photon bunching in the absence of inter-particle entanglement.

2.3.2 Entanglement monogamy and indistinguishability

In this section, we would like to discuss how (in)distinguishability and entanglement are related to each other.

Indeed, *intra-particle entanglement*—i.e., entanglement shared between distinct DOFs of the same particle—is, in some sense, proportional to the *distinguishability* between several particles. This distinguishability, in turn, constitutes a limit on their *inter-particle entanglement*—i.e., entanglement shared between distinct particles—by means of the *theorem of entanglement monogamy*. Simply spoken, intra-particle entanglement serves as an *experimenter's resource to contrast particles* against each other.

Imagine a photon of a certain frequency ω_1 , which is always found in some certain mode h_1 , while another photon of a different frequency ω_2 is always found in another mode h_2 . One can contrast them by saying: "*The one photon of frequency ω_1 is there, and the other photon is somewhere else.*"

This requires a strict correlation between the frequency and the spatial mode of each photon, i.e., entanglement between the frequency and mode of each photon. Then, if the photon can be ideally (i.e., with certainty) addressed in an experiment through their distinguishability, their internal DOFs must be maximally entangled, which in turn makes it impossible to further entangle these DOFs with others, for instance with DOFs of other particles to yield inter-particle entanglement.

⁷i.e., entanglement between distinct particles

2.3.3 Interferogramm for frequency-entangled photons

In the following, we provide the solution for the *interferogramm of frequency-entangled photons*, that was not mentioned before [40–42] in its whole generality in the literature.

2.3.3.1 Spectrum of frequency entangled photons

The standard source of these photonic resources is a periodically poled spontaneously down converting KTiOPO₄ crystal (ppKTP-crystal) rendering the emission of photon-pairs featuring a joint spectral wave function of

$$\phi_{\text{f.e.}}^{\varphi}(\omega_1, \omega_2) = \phi_{\text{f.d.}}(\omega_1, \omega_2) + e^{i\varphi} \phi_{\text{f.d.}}(\omega_2, \omega_1), \quad (2.69)$$

which by itself is composed of the joint spectrum of frequency detuned photons

$$\phi_{\text{f.d.}}(\omega_1, \omega_2) = \delta(\omega_p - \omega_1 - \omega_2) \operatorname{sinc}\left(\frac{\omega_1 - \omega_2 - \mu}{\xi}\right) \quad (2.70)$$

where ω_p is the pump-frequency, μ is the *spectral separation* between the carrier frequencies of the frequency-detuned photons, ξ is the *spectral single-photon bandwidth* and φ tunes the *spectral symmetry* against particle exchange (symmetric for $\varphi = 0$, anti-symmetric for $\varphi = \pi$).

In essence, (2.69) characterizes two frequency peaks each of bandwidth ξ with a mutual spectral distance to each other of μ .

2.3.3.2 Interferogram and deviation to existing literature

For these resources, the standardly employed solution in the literature was provided by Ramelow et al. [41], with his result to the associated interferogramm, which he originally formulated for the photon anti-bunching probability. From this follows the difference between photon bunching and photon anti-bunching probability $P_c = P_B - P_{\bar{B}}$, and their result is equivalent to

$$P_c(\tau) = R_{\mu\xi}^{\varphi\tau} := Z_{\mu\xi}^{\varphi\tau}, \quad (2.71)$$

where by contrast we derived

$$P_c(\tau) = \frac{R_{\mu\xi}^{\varphi\tau} + S_{\mu\xi}^{\varphi\tau}}{1 + R_{\mu\xi}^{\varphi 0} S_{\mu\xi}^{\varphi 0}} := B_{\mu\xi}^{\varphi\tau}, \quad (2.72)$$

with

$$R_{\mu\xi}^{\varphi\tau} = \cos(\mu\tau - \varphi) \operatorname{tri}\left(\frac{\xi\tau}{2}\right), \quad (2.73a)$$

$$S_{\mu\xi}^{\varphi\tau} = \operatorname{sinc}\left(\frac{2\mu}{\xi} \operatorname{tri}\left(\frac{\xi\tau}{2}\right)\right) \operatorname{tri}\left(\frac{\xi\tau}{2}\right), \quad (2.73b)$$

and $\tau = \tau_1 - \tau_2$ being the differential optical delay typically employed prior to the BS in HOM-interference (see Fig. 2.2), and

$$\operatorname{tri}(x) = \Theta(1 - |x|)(1 - |x|) \quad (2.74)$$

is the triangular function, where Θ denotes the Heaviside step function.

From Eqs. (2.73) it can be seen that both, Ramelow's and our interferogramms feature compact support in the differential optical delay within the open interval

$$\tau \in (-2/\xi, +2/\xi). \quad (2.75)$$

Indeed, both interferogramms are effectively scaled by the *spectral distance to bandwidth ratio*

$$\mu_\xi = \frac{2\mu}{\xi} \quad (2.76)$$

since we can rewrite (2.73) as

$$R_{\mu_\xi}^{\varphi\tau_\xi} = \cos(\mu_\xi\tau_\xi - \varphi)\text{tri}(\tau_\xi), \quad (2.77a)$$

$$S_{\mu_\xi}^{\varphi\tau_\xi} = \text{sinc}(\mu_\xi\text{tri}(\tau_\xi))\text{tri}(\tau_\xi), \quad (2.77b)$$

which are functions of the rescaled dimensionless delay

$$\tau_\xi = \frac{\tau\xi}{2} \in (-1, +1). \quad (2.78)$$

In the author's Ref. [BL23], several arguments are presented that exclude (2.71) as a general solution corresponding to the spectrum (2.69). However, here we rather want to highlight the technologically relevant aspect of the discrepancy between the existing literature and our result. Specifically, the occurrence of photon anti-bunching is of special interest, as it –in its role of a BIV– serves as a certificate for spectral entanglement, which could be used, through its observation, as a resource for authentication in entanglement-based quantum cryptography.

Our additional term $S_{\mu_\xi}^{\varphi\tau_\xi}$ in the interferogramm has a concrete physical meaning as it is arising from the *spectral indistinguishability related to finite-bandwidth effects* (i.e. spectral overlap) of the photons. This contribution *cannot* be associated to spectral anti-symmetry and thus not to photon anti-bunching [26]. This is why this term is of particular interest for the exact *performance-quantification* of entanglement-based quantum technologies as it can be seen as a distortion effect that impedes ideal photon anti-bunching.

2.3.3.3 Identifying contra indicative detection statistics

This is why the function

$$\Delta_{\mu_\xi}^{\varphi\tau_\xi} = R_{\mu_\xi}^{\varphi\tau} = -Z_{\mu_\xi}^{\varphi\tau_\xi} \cdot B_{\mu_\xi}^{\varphi\tau_\xi} \quad (2.79)$$

is of particular interest to us, as it is positive *if and only if* Ramelow's and our results have different signs. In other words, one result predicts photon bunching, while the other predicts contra indicative photon anti-bunching, or vice versa.

Indeed, the former solution $Z_{\mu_\xi}^{\varphi\tau_\xi}$ from Eq. (2.71) is the *small-bandwidth limit*, or equivalently in the limit of large-spectral separation of the author's general result $B_{\mu_\xi}^{\varphi\tau_\xi}$ from Eq. (2.72). In other words,

$$Z_{\mu_\xi}^{\varphi\tau_\xi} = \lim_{\mu_\xi \rightarrow \infty} B_{\mu_\xi}^{\varphi\tau_\xi}. \quad (2.80)$$

As ideal photon anti-bunching *necessitates perfect spectral anti-symmetry* of otherwise indistinguishable photons [26], any possible spectral overlap between the two spectral peaks (2.70) related

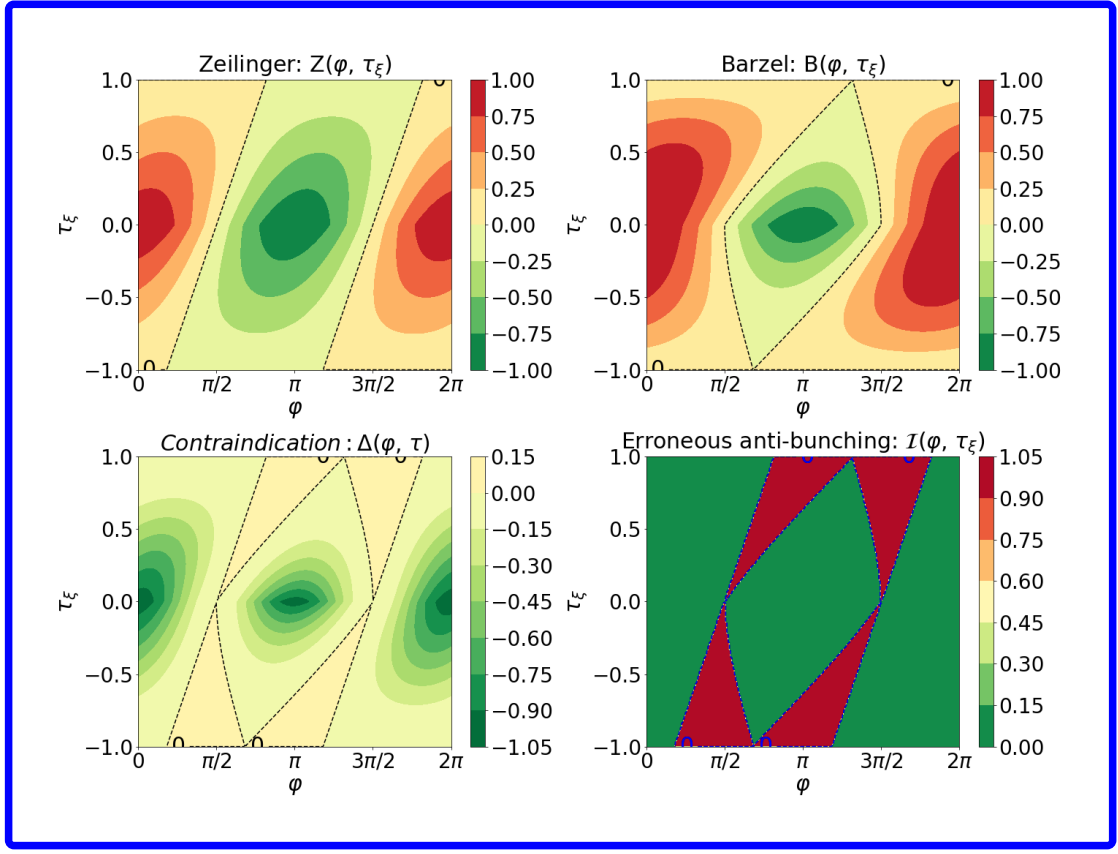


Figure 2.5: Visualization of Ramelow's result $Z_{\mu\xi}^{\varphi\tau\xi}$, which we refer to as "Zeilinger" (top-left), $B_{\mu\xi}^{\varphi\tau\xi}$ (top-right), $\Delta_{\mu\xi}^{\varphi\tau\xi}$ (bottom-left) and $I_{\mu\xi}^{\varphi\tau\xi}$ (bottom-right) in $\tau\varphi$ -configuration space. The value of the bandwidth-normalized spectral distance is $\mu\xi = 1/2$.

to *finite-bandwidth effects*—as the associated overlap corresponds to spectral symmetry—will lead to impede photon anti-bunching.

It is therefore not surprising that our result predicts "less" photon anti-bunching particularly for large-bandwidths, or equivalently for small spectral separations, i.e., in summary $\mu\xi \rightarrow 0$. This can be indeed seen from the comparison of the two topmost graphics of Fig. 2.5 that shows that the occurrence of photon anti-bunching of our result (top-right graphic) is restricted to a smaller—diamond shaped—region in the $\tau\varphi$ -configuration space w.r.t. Zeillinger's result (parallelogram-shaped region in the top-left graphic).

The qualitative *contra indicative* prediction of photon bunching and photon anti-bunching between Zeilinger's and our result, $\Delta_{\mu\xi}^{\varphi\tau\xi}$, is shown in the bottom-left graphic of Fig. 2.5.

2.3.3.4 Erroneous prediction of quantum supremacy

Moreover, we want to stress the danger of a *false prediction of photon anti-bunching* in a physical realm of photon bunching. Such a result could mislead the applicators into believing they can thwart adversarial attacks in a quantum-cryptographic authentication task, while in reality, they

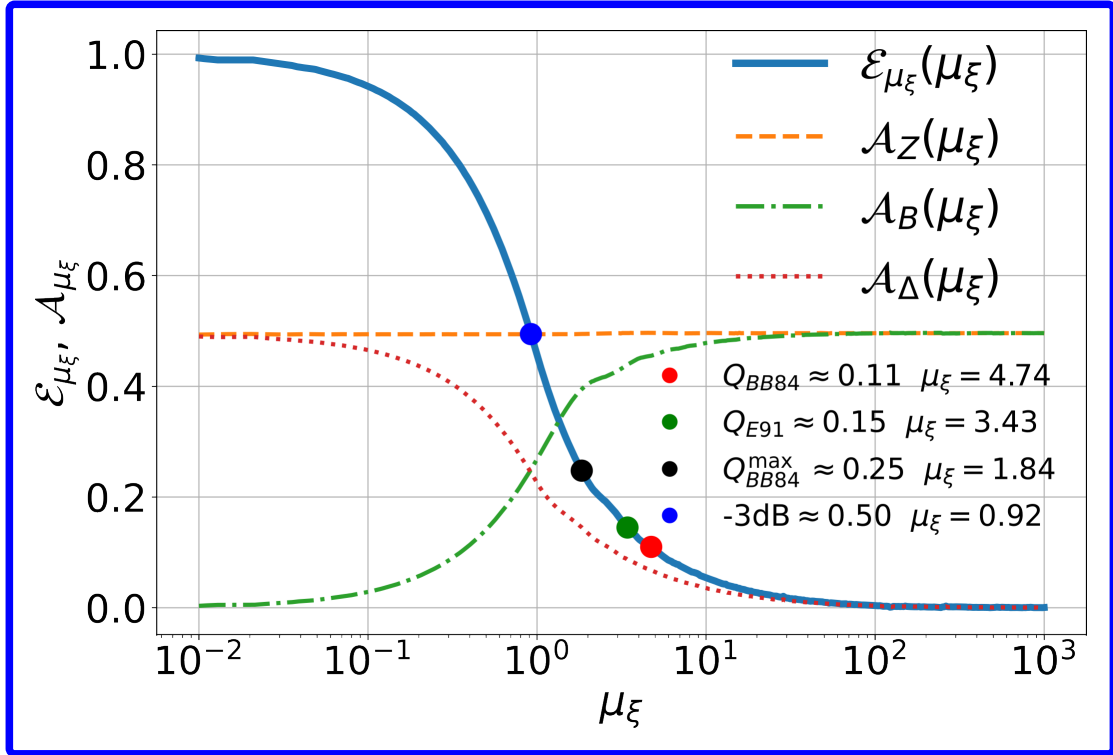


Figure 2.6: Visualization of Eqs. (2.82) and (2.87) (lines). The points on the blue curve of the error-rate can be found in their meaning in the list on page 43.

cannot. One function that indicates the fallacy of an erroneous interferogramm $Z_{\mu_\xi}^{\varphi\tau\xi}$ is the *indicator function*

$$\mathcal{I}_{\mu_\xi}^{\varphi\tau\xi}(Z_{\mu_\xi}^{\varphi\tau\xi}) = \Theta(-Z_{\mu_\xi}^{\varphi\tau\xi})\Theta(\Delta_{\mu_\xi}^{\varphi\tau\xi}), \quad (2.81)$$

as it is of value one *in the case and only in the case* of false-prediction of photon anti-bunching, and zero otherwise, and Θ denotes the Heaviside step function. In so far, the unity of (2.81), (i.e., $\mathcal{I}_{\mu_\xi}^{\varphi\tau\xi} = 1$) indicates an *erroneous assumption of quantum supremacy*, which we visualized for Ramelow's approximation in the bottom-right graphic of Fig. 2.5.

There, the red-colored area marks the region of erroneous quantum supremacy in the $\tau\varphi$ -configuration space, which by itself could hold as the parameter space of a possible quantum communication protocol, in which the sender encodes the quantum information to be transmitted in the phase φ and the receiver's readout is carried out by measurement of some observables parametrized by the optical delay τ .

In what follows, we do not want to address by no means any specific quantum protocol, but rather want to give a rough guide to estimate how the *overestimation of photon anti-bunching* of can be quantified with relevance to these technologies.

Despite, of many distinct protocols to imagine, the size of the average error would be a monotone to the fraction of the configuration space where photon anti-bunching is not predicted by the *actual* interferogram ($\mathcal{B}_{\mu_\xi}^{\varphi\tau\xi}$) *relative* to the *domain (or area) of interest*, \mathcal{A}_{μ_ξ} where our erroneous

interferogramm ($Z_{\mu_\xi}^{\varphi\tau_\xi}$) predicts photon anti-bunching. Expressed in a pictographic sense, this corresponds to the red-shaded fraction within the red parallelogram of the bottom right graphic of Fig. 2.5.

This quantity equals the integral of the indicator function, which we term the *error-rate*,

$$\mathcal{E}_{\mu_\xi} = \frac{1}{\mathcal{A}_{\mu_\xi}} \int_0^{2\pi} d\varphi \int_{-1}^{+1} d\tau_\xi \mathcal{I}_{\mu_\xi}^{\varphi\tau_\xi}, \quad (2.82)$$

The Domain, where our erroneous interferogramm predicts photon anti-bunching is

$$\mathcal{A}_{\mu_\xi}(-Z_{\mu_\xi}^{\varphi\tau_\xi}) = \frac{1}{\mathcal{A}} \int_0^{2\pi} d\varphi \int_{-1}^{+1} d\tau_\xi \Theta(-Z_{\mu_\xi}^{\varphi\tau_\xi}), \quad (2.83)$$

normalized to the parameter space

$$\mathcal{A} = 4\pi = \int_0^{2\pi} \int_{-1}^{+1} d\varphi d\tau_\xi. \quad (2.84)$$

Note that the negative sign in (2.83) arises from the interest of anti-bunching ($Z_{\mu_\xi}^{\varphi\tau_\xi} < 0$) and not bunching ($Z_{\mu_\xi}^{\varphi\tau_\xi} > 0$).

Another domain of interest is of course the domain of *actual* occurrence of photon-anti-bunching, that is,

$$\mathcal{A}_{\mu_\xi}(-B_{\mu_\xi}^{\varphi\tau_\xi}), \quad (2.85)$$

and moreover the area of contra indicative photon statistics in general

$$\mathcal{A}_{\mu_\xi}(\Delta_{\mu_\xi}^{\varphi\tau_\xi}), \quad (2.86)$$

which we displayed in Fig. 2.6, where we adopted the notation

$$\mathcal{A}_Z := \mathcal{A}_{\mu_\xi}(-Z_{\mu_\xi}^{\varphi\tau_\xi}), \quad (2.87a)$$

$$\mathcal{A}_B := \mathcal{A}_{\mu_\xi}(-B_{\mu_\xi}^{\varphi\tau_\xi}), \quad (2.87b)$$

$$\mathcal{A}_\Delta := \mathcal{A}_{\mu_\xi}(\Delta_{\mu_\xi}^{\varphi\tau_\xi}). \quad (2.87c)$$

There interestingly, it is seen from the orange line, that the fraction of the domain, where the interferogramm $Z_{\mu_\xi}^{\varphi\tau_\xi}$ predicts photon anti-bunching relative to the entire domain is equal to $\mathcal{A}_Z = 1/2$, and in particular not dependent on μ_ξ , which cannot be physically correct.

This is due to the reason that in the infinite bandwidth limit $\mu_\xi \rightarrow 0$ the two spectral peaks of the spectrum (2.70) due to their infinite extension in the spectral domain must coincide, which makes the spectrum (2.69) invariant under particle exchange, and indeed in this limit one finds that the loss of spectral antisymmetry

$$\phi_{\text{f.d.}}(\omega_1, \omega_2) = \phi_{\text{f.d.}}(\omega_2, \omega_1), \quad (2.88)$$

prohibits any occurrence of photon-anti bunching [26], which is precisely the prediction of our result \mathcal{A}_B as seen from the green line in Fig. 2.6. However, the two results converge again in the zero-bandwidth limit as $\lim_{\mu_\xi \rightarrow \infty} \mathcal{A}_{\mu_\xi}(B_{\mu_\xi}^{\varphi\tau_\xi}) = 1/2$.

With all of this information in accordance, it is however interesting to see that the red line in (2.6) envisages that in the small-bandwidth limit we find in half of the cases a qualitative contradiction

in the photon statistics of our result compared to former literature as $\lim_{\mu_\xi \rightarrow 0} \mathcal{A}_\Delta = 1/2$, which decreases towards larger bandwidths until it entirely erases in the infinite-bandwidth limit, where the results coincide.

Finally, it is intuitive that Ramelows's result, serving as the small-bandwidth approximation of frequency-entangled photons, significantly deviates from the general result, from the threshold $\mu_\xi = 1$ downwards, i.e., when $2\mu < \xi$. This threshold represents the point where two peaks, each with a width ξ , are separated by a distance of twice that width, effectively begin to overlap to impede photon anti-bunching.

2.3.3.4.1 Erroneous fraction of anti-bunching prediction

It is further shown in Fig. 2.6 that the error-rate (blue curve) can indeed take all values from $\lim_{\mu_\xi \rightarrow \infty} \mathcal{E}_{\mu_\xi} = 0$ up to $\lim_{\mu_\xi \rightarrow 0} \mathcal{E}_{\mu_\xi} = 1$ and thus can largely exceed typical values of tolerable *quantum-bit error-rates* (QBER) of various Quantum-key-distribution protocols for decreasing values of μ_ξ from certain threshold values on downwards. For instance

- The minimum QBER in the BB84 protocol [43] from which eavesdropping is possible $Q_{BB84} = 11\%$ of the BB84 protocol (from $\mu_\xi \leq 4.74$ on, see Figs. 2.6 and 2.10).
- The minimum QBER in the E91 protocol [44] from which eavesdropping is possible $QBER_{E91} = 14.6\%$ of the E91 protocol (from $\mu_\xi \leq 3.43$ on, see Figs. 2.6 and 2.11).
- The QBER in the BB84 protocol from which the entire protocol might be eavesdropped $Q_{BB84}^{\max} = 25\%$ of the BB84 protocol (from $\mu_\xi \leq 2.98365$ on, see Figs. 2.6 and 2.10).
- The -3dB limit, which for many protocols is the tolerable error due to *signal loss*.

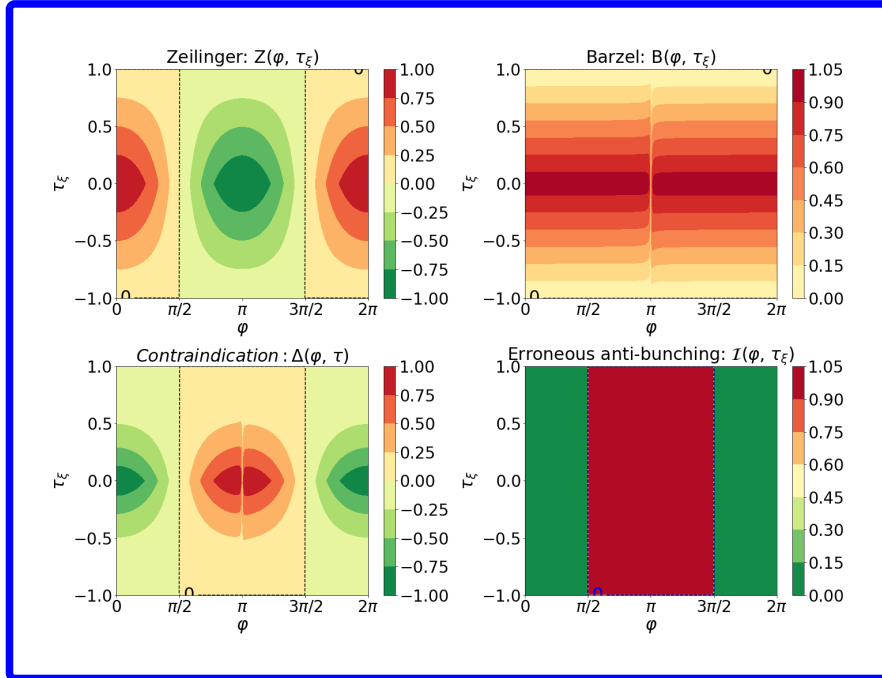


Figure 2.7: Same as Fig. 2.5, but with $\mu_\xi = 0.01$.

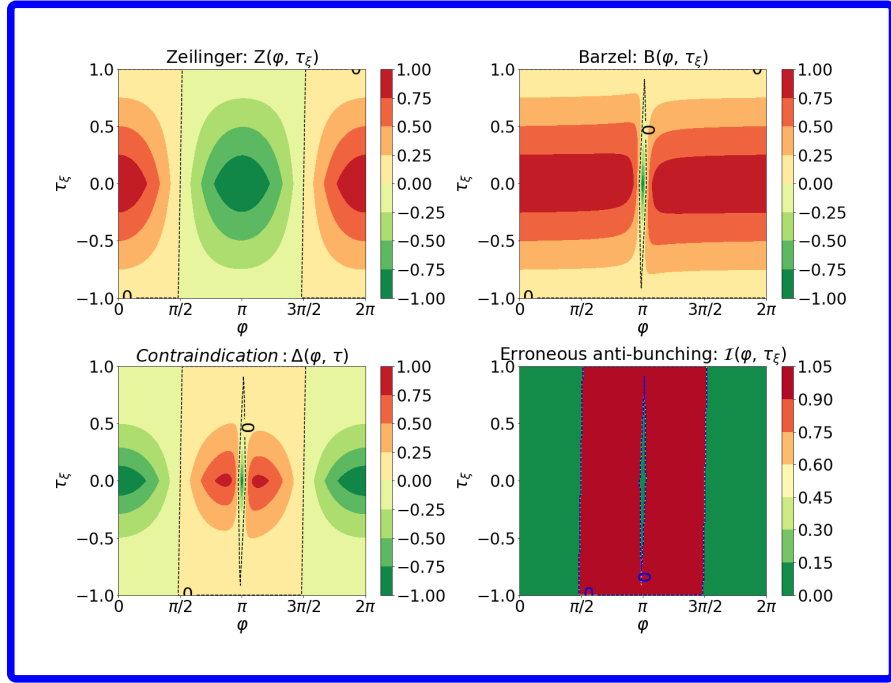


Figure 2.8: Same as Fig. 2.5, but with $\mu_\xi = 0.1$.

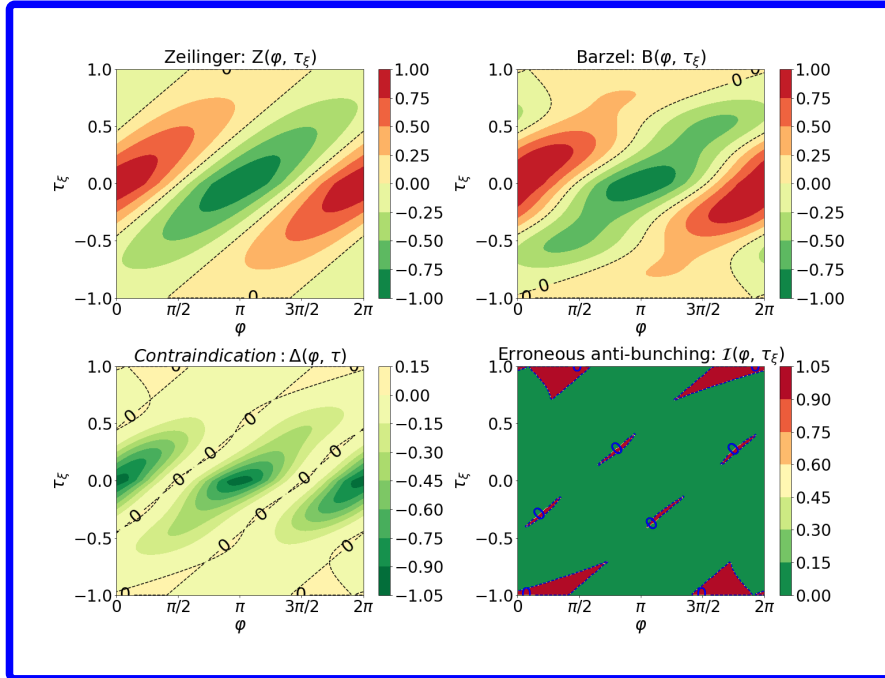


Figure 2.9: Same as Fig. 2.5, but with $\mu_\xi = 3.43$ associated to the E91 protocol with $\mathcal{A}_{\mu_\xi=3.43} = QBER_{E91} = 0.25$ (see list on page 43).

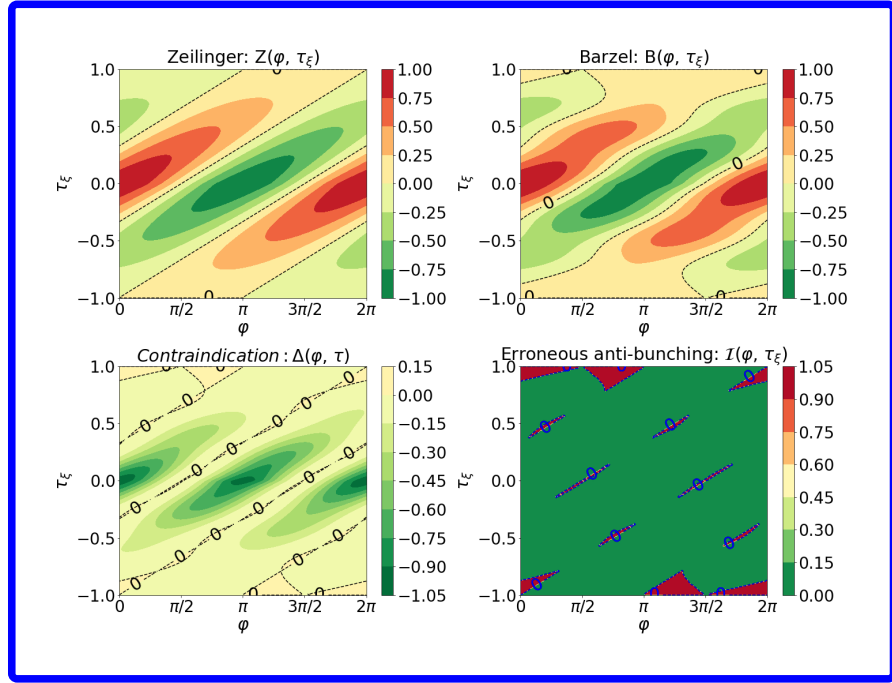
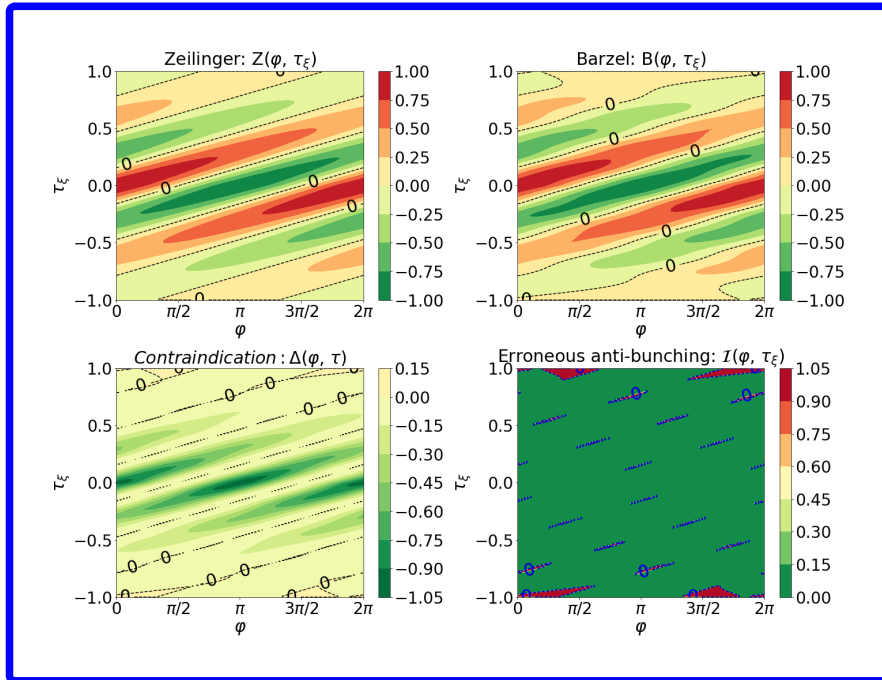
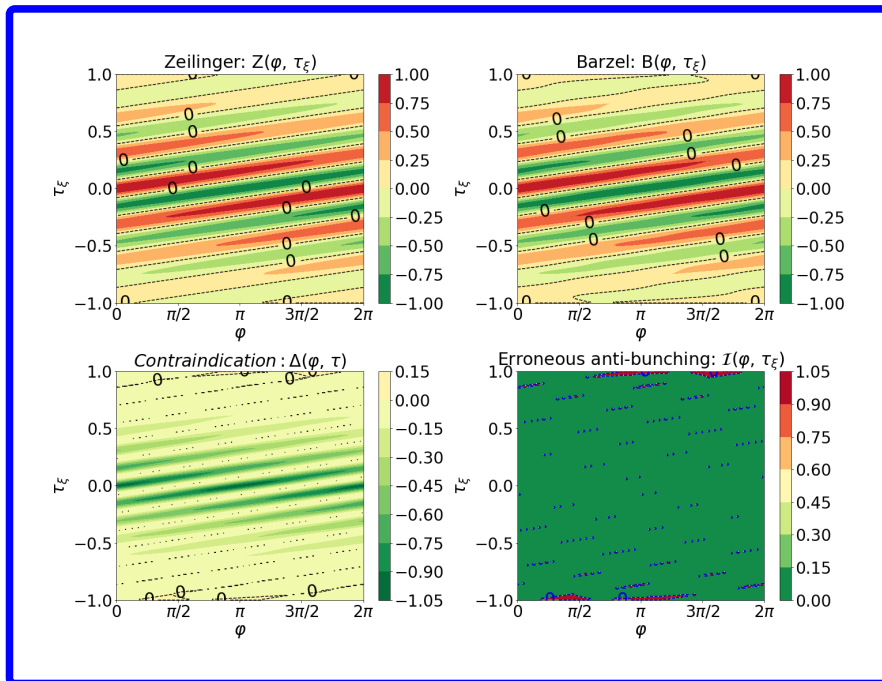


Figure 2.10: Same as Fig. 2.5, but with $\mu_\xi = 4.74$ associated to the BB84 protocol with $\mathcal{A}_{\mu_\xi=4.74} = Q_{BB84} = 0.146$ (see list on page 43).

Figure 2.11: Same as Fig. 2.5, but with $\mu_\xi = 10$.Figure 2.12: Same as Fig. 2.5, but with $\mu_\xi = 20$.

Role of indistinguishability and entanglement in Hong-Ou-Mandel interference and finite-bandwidth effects of frequency-entangled photons

Roy Barzel^{1,*} and Claus Lämmerzahl^{1,2,3}

¹ZARM, University of Bremen, 28359 Bremen, Germany

²DLR-Institute for Satellite Geodesy and Inertial Sensing, c/o University of Bremen, 28359 Bremen, Germany

³Institute of Physics, Carl von Ossietzky University Oldenburg, 26111 Oldenburg, Germany



(Received 22 February 2022; accepted 10 February 2023; published 9 March 2023)

We investigate the relation between indistinguishability and quantum entanglement in Hong-Ou-Mandel interference experiments theoretically and relate these quantum mechanical principles to the theorem of entanglement monogamy. Employing Glauber's theory of quantum coherence we compute the detection statistics in HOM interference of frequency-entangled photons and find an additional term in the coincidence detection probability, which is related to the spectral indistinguishability of the considered photons that arises from finite-bandwidth effects and therefore is relevant in the limit of low-frequency separations or large single-photon bandwidths. Compared to previous work in that context we treat all photonic degrees of freedom on equal footing.

DOI: [10.1103/PhysRevA.107.032205](https://doi.org/10.1103/PhysRevA.107.032205)

I. INTRODUCTION

Indistinguishability of physical systems is one of the important defining features of quantum systems without classical analogs. For example, the exchange interaction in metals, which arises as a consequence of the indistinguishability between the electrons in the conduction band, can change the magnetic properties of the system completely [1]. In the case of bosons in particular, indistinguishability leads to intriguing phenomena, such as Bose-Einstein condensation or *photon bunching* within interference experiments. The latter was witnessed in the pioneering Hong-Ou-Mandel (HOM) experiment [2], and today it is one of the celebrated results of quantum optics that the phenomenon of photon bunching can be used to measure time intervals in a sub-picosecond regime. This accuracy can even be enhanced in the presence of spectral entanglement [3], giving rise to the yet more counterintuitive and interesting phenomenon of *photon antibunching*, which is very uncharacteristic for photons as these naturally follow bosonic statistics. Needless to say, quantum entanglement is one of the most important physical phenomena which cannot be explained by means of a classical theory, and moreover, its existence has wide consequences in our interpretation of the nonlocal behavior of matter and the probabilistic character of nature. Since neither photon bunching nor photon antibunching can be explained without considering the particle character of photons, and since their occurrence is ultimately related to nonclassical features such as indistinguishability and entanglement, which are heralded in a particular way in HOM interference, these experiments today constitute one of the most important methods to test and study quantum mechanical principles. It is, therefore, of fundamental interest to precisely understand the role of indistinguishability and entanglement on the detection statistics

of HOM experiments, and the reader is referred to Ref. [4] and references therein for an extensive overview on recent progress and advances in the field and to Refs. [5,6] for a modern mathematical formulation of the phenomenon in the broader context of multiparticle interference.

In addition, the opportunity to provide highly accurate time measurements with HOM interference adds to the practical appeal of these experiments. Only recently it was demonstrated that HOM interference can be used to enhance the accuracy of clock synchronization [7,8], a feature that was already predicted theoretically [9]. Therefore, HOM-like schemes are also candidates for space-based implementations, such as the Global Positioning System (GPS), the installation of a global time standard, or, in a broader context, high-precision metrology in general.

Recently, the possibility to resolve time intervals below $(100 \text{ THz})^{-1}$ (i.e., in the inverse optical regime) with HOM interference of frequency-entangled photons was recognized to bare the potential of conducting fundamental tests of physics by addressing the interplay between gravity and quantum mechanics [10–12].

In the present paper we employ Glauber's theory of optical coherence [13] and extend previous work on multiphoton quantum interference [14] to incorporate all photonic degrees of freedom on equal footing. As a result, we obtain a convenient formalism, which on the one hand enables us to compute the detection statistics of multiphoton interference experiments from a general wave function and on the other hand heralds the role of quantum mechanical principles such as indistinguishability and quantum entanglement in a particular way.

We apply our formalism to compute the detection statistics of HOM interference with frequency-entangled photons [15], and we find an additional term in the corresponding interference pattern of coincidence detection compared to established results [3,15,16] and provide a physical interpretation for this term.

*Corresponding author: roy.barzel@zarm.uni-bremen.de

By contrasting the interference behavior of spectrally indistinguishable frequency-entangled photons with the one of spectrally distinguishable frequency-detuned photons, we draw conclusions on the relation between entanglement and indistinguishability in HOM interference and relate these concepts via the theorem of *entanglement monogamy*.

This work is organized as follows. In Sec. II we revise the basics of HOM interference, and we present our formalism and apply it to frequency-entangled photons. In Sec. III we relate the previously obtained results to former work and provide physical interpretation. Sections V and IV are dedicated to concluding our work and providing an outlook.

II. HONG-OU-MANDEL INTERFERENCE

Sections IIA and IIB of this paper are dedicated to developing the theoretical formalism to characterize HOM interference based on Glauber's theory of coherence. In Sec. IIC we show one of the main results of the present paper that is the HOM interference pattern of frequency-entangled photons, where we find an additional term related to the finite bandwidth of the employed photons, which was not mentioned in the literature [3,15,16] before.

A. Two-photon states

The theory for describing N -photon states has been extensively developed [17], and we leave details to the interested reader. A general two-photon state in the context of HOM interference is given by [14]

$$|\psi(\tau_1, \tau_2)\rangle = \mathcal{N}_\psi \int d\omega_1 d\omega_2 \Phi(\omega_1, \omega_2) e^{i\omega_1 \tau_1} e^{i\omega_2 \tau_2} \hat{a}_{\omega_1}^\dagger \hat{a}_{\omega_2}^\dagger |0\rangle, \quad (1)$$

where the bold ω denotes the set of parameters that characterize all degrees of freedom (DOFs) of a single photon, e.g., its frequency, orbital momentum, polarization, spatial mode, and so forth. In the case that a discrete DOF is considered (for instance, the polarization DOF) the integral in Eq. (1) has to be evaluated as a sum. We call $\Phi(\omega_1, \omega_2)$ the two-photon wave function. The slim ω denotes the photon frequency, which we treat separately from the other photonic DOFs σ . Thus, we can write all photonic DOFs as $\omega = \{\omega, \sigma\}$. Depending on the context we alternatively denote the photonic wave function as $\Phi(\omega_1, \omega_2) = \Phi(\omega_1, \sigma_1, \omega_2, \sigma_2) = \Phi_{\sigma_1 \sigma_2}(\omega_1, \omega_2)$.

The operators \hat{a}_ω and \hat{a}_ω^\dagger are bosonic annihilation and creation operators, respectively, which satisfy the canonical commutator relations $[\hat{a}_\omega, \hat{a}_{\omega'}^\dagger] = \delta_{\omega\omega'} \hat{a}_\omega^\dagger$, while all other commutators vanish. Here $\delta_{\omega\omega'}$ is the multidimensional delta function of the considered photonic DOFs. For each continuous DOF (for instance, the frequency) $\delta_{\omega\omega'}$ contains a Dirac δ distribution and for each discrete DOF it contains a Kronecker symbol as a factor. For instance, if we consider only the photon's polarization $P = H$ and V [horizontal (H) and vertical (V) polarization] and the photon's frequency ω (i.e., $\omega = \{\omega, P\}$), the delta function reads $\delta_{\omega\omega'} = \delta(\omega - \omega') \delta_{PP'}$.

Expression (1) depends on two times, τ_1 and τ_2 , that describe optical delays that can be applied independently to wave packets in HOM interferometry [14] (see Fig. 1). From an experimental point of view, these delays are typically

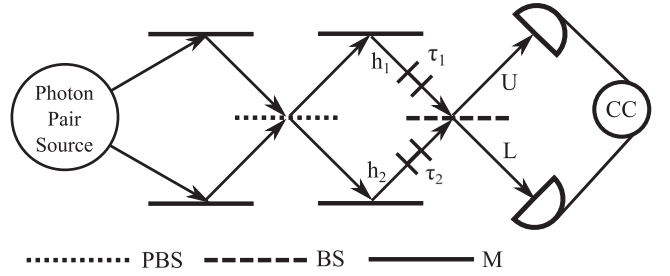


FIG. 1. Hong-Ou-Mandel (HOM) experiment with frequency-entangled photons. PBS, polarizing beam splitter; BS, beam splitter; M, mirror; CC, coincidence count logic.

realized via a variation of the optical path of the respective photons. In practice, this can be achieved, for instance, by a variation of the refractive index of the respective transmission path. The normalization constant \mathcal{N}_ψ has to be chosen in order to fulfill $\langle \psi | \psi \rangle = 1$. However, the procedure that is described in the following to compute the detection statistics of HOM interference is independent of the normalization constant as we show further below. For this reason, we omit it for the rest of this work.

B. Photon detection

Photon detection is described within Glauber's quantum theory of coherence [13]. The electric field operators are defined as

$$\hat{E}_\sigma^{(+)}(t) = i \int d\omega \mathcal{E}_\omega e^{-i\omega t} \hat{a}_\omega, \quad (2a)$$

$$\hat{E}_\sigma^{(-)}(t) = [\hat{E}_\sigma^{(+)}(t)]^\dagger, \quad (2b)$$

where $\mathcal{E}_\omega = \sqrt{[\hbar\omega/(4\pi\epsilon_0 c)]}$ is the frequency-dependent electric field per photon. The electric field operators are characterized by the parameter set σ .

Analogously we may define creation (annihilation) operators, which create (annihilate) a photon at time t , which are characterized by a parameter set σ as

$$\hat{a}_\sigma(t) = \int d\omega e^{-i\omega t} \hat{a}_\omega, \quad (3a)$$

$$\hat{a}_\sigma^\dagger(t) = \int d\omega e^{+i\omega t} \hat{a}_\omega^\dagger. \quad (3b)$$

The temporal creation (annihilation) operators (3) are basically Fourier transforms with respect to the frequency DOF of the spectral creation (annihilation) operators $\hat{a}_{\omega\sigma}^\dagger$ ($\hat{a}_{\omega\sigma}$). Note that for the remaining DOFs, σ are not integrated out in Eq. (3).

In Glauber's theory of optical coherence [13], the expectation value of a joint detection of two electric field quanta characterized by σ_1 and σ_2 at times t_1 and t_2 in the quantum state (1) reads

$$\Gamma_{\sigma_1 \sigma_2}(t_1, t_2) = \langle \psi | \hat{E}_{\sigma_1}^{(-)}(t_1) \hat{E}_{\sigma_2}^{(-)}(t_2) \hat{E}_{\sigma_2}^{(+)}(t_2) \hat{E}_{\sigma_1}^{(+)}(t_1) | \psi \rangle, \quad (4)$$

and the probability $p_{\sigma_1 \sigma_2}(t_1, t_2, \tau_1, \tau_2)$ of a joint detection of two photons characterized by σ_1 and σ_2 at times t_1 and t_2 is proportional to $\langle \psi(t_1, t_2) | \hat{a}_{\sigma_1}^\dagger(t_1) \hat{a}_{\sigma_2}^\dagger(t_2) \hat{a}_{\sigma_2}(t_2) \hat{a}_{\sigma_1}(t_1) | \psi(t_1, t_2) \rangle \equiv \langle \varphi | \varphi \rangle$,

where $|\varphi\rangle := \hat{a}_{\sigma_1}(t_2)\hat{a}_{\sigma_1}(t_1)|\psi(\tau_1, \tau_2)\rangle$. Using Eqs. (1) and (3), together with some algebra, we find that the detection probability $p_{\sigma_1\sigma_2}(t_1, t_2, \tau_1, \tau_2) \propto \langle\varphi|\varphi\rangle$ reads

$$\begin{aligned} p_{\sigma_1\sigma_2}(t_1, t_2, \tau_1, \tau_2) &\propto |\tilde{\Phi}_{\sigma_1\sigma_2}(t_1 - \tau_1, t_2 - \tau_2) \\ &\quad + \tilde{\Phi}_{\sigma_2\sigma_1}(t_2 - \tau_1, t_1 - \tau_2)|^2, \end{aligned} \quad (5)$$

where we have introduced the Fourier transform of the photonic wave function

$$\tilde{\Phi}_{\sigma_1\sigma_2}(T_1, T_2) = \int d\omega_1 d\omega_2 \Phi_{\sigma_1\sigma_2}(\omega_1, \omega_2) e^{-i\omega_1 T_1} e^{-i\omega_2 T_2}. \quad (6)$$

The probability $P_{\sigma_1\sigma_2}(\tau_1, \tau_2)$ to detect two photons irrespectively of the instance of time, when they are detected, is proportional to

$$\tilde{P}_{\sigma_1\sigma_2}(\tau_1, \tau_2) := \int dt_1 dt_2 p_{\sigma_1\sigma_2}(t_1, t_2, \tau_1, \tau_2). \quad (7)$$

We employ the convolution theorem from Fourier analysis and obtain

$$\begin{aligned} \tilde{P}_{\sigma_1\sigma_2}(\tau_1, \tau_2) &= \int d\omega_1 d\omega_2 [|\Phi_{\sigma_1\sigma_2}(\omega_1, \omega_2)|^2 \\ &\quad + |\Phi_{\sigma_2\sigma_1}(\omega_2, \omega_1)|^2] \\ &\quad + 2\text{Re} \left\{ \int d\omega_1 d\omega_2 \Phi_{\sigma_1\sigma_2}(\omega_1, \omega_2) \right. \\ &\quad \times \left. \Phi_{\sigma_2\sigma_1}^*(\omega_2, \omega_1) e^{-i(\omega_1 - \omega_2)(\tau_1 - \tau_2)} \right\}, \end{aligned} \quad (8)$$

which can be further simplified to the compact form

$$\tilde{P}_{\sigma_1\sigma_2}(\tau_1, \tau_2) = \int d\omega_1 d\omega_2 |\mathcal{S}[\Phi_{\sigma_1\sigma_2}^{(\tau_1, \tau_2)}(\omega_1, \omega_2)]|^2, \quad (9)$$

where $\Phi_{\sigma_1\sigma_2}^{(\tau_1, \tau_2)}(\omega_1, \omega_2) = \Phi_{\sigma_1\sigma_2}(\omega_1, \omega_2)e^{i\omega_1\tau_1}e^{i\omega_2\tau_2}$ is the time-dependent photonic wave function, which depends on the optical delays $\tau_{1,2}$, and \mathcal{S} is the symmetrization operator, which acts as $\mathcal{S}[\Phi_{\sigma_1\sigma_2}^{(\tau_1, \tau_2)}(\omega_1, \omega_2)] = \Phi_{\sigma_1\sigma_2}^{(\tau_1, \tau_2)}(\omega_1, \omega_2) + \Phi_{\sigma_2\sigma_1}^{(\tau_1, \tau_2)}(\omega_2, \omega_1)$. Finally, to obtain the normalized probabilities to detect one photon characterized by σ_1 and another characterized by σ_2 , we have to compute

$$P_{\sigma_1\sigma_2}(\tau_1, \tau_2) = \frac{\tilde{P}_{\sigma_1\sigma_2}(\tau_1, \tau_2)}{\int d\sigma_1 d\sigma_2 \tilde{P}_{\sigma_1\sigma_2}(\tau_1, \tau_2)}. \quad (10)$$

From the last expression it is seen that the normalization constant \mathcal{N}_ψ from Eq. (1) cancels out in the calculation because its square appears in the nominator and the denominator of Eq. (10).

Note the symmetries of the probabilities $P_{\sigma_1\sigma_2}(\tau_1, \tau_2) = P_{\sigma_2\sigma_1}(\tau_1, \tau_2) = P_{\sigma_1\sigma_2}(\tau_2, \tau_1)$ and that the probabilities are always a function of the difference $\Delta\tau := \tau_1 - \tau_2$ as can be seen from Eq. (8).

Equation (9) is a central result of the paper as we can use it to easily compute the joint detection statistics of HOM interference for any given two-photon wave function $\Phi_{\sigma_1\sigma_2}(\omega_1, \omega_2)$, and it moreover highlights the interpretation of the absolute square value of the (time-dependent) photonic wave function as being the probability for certain detection

events. Moreover, Eq. (9) clearly shows that only the symmetrized part of the photonic wave function is of physical relevance, which can be already inferred from Eq. (1), since it can be written solely in terms of the symmetrized time-dependent photonic wave function by use of the canonical commutator relations.

Apart from that, Eq. (8) emphasizes the role of indistinguishability between the two involved photons in HOM interference. The first two terms of Eq. (8) do not depend on the delays, in contrast to the last third term, the interference term. This term can be interpreted as the overlap of the joint photonic wave function at the interfering beam splitter (BS) with itself under an exchange of the function arguments, i.e., $\omega_1 \leftrightarrow \omega_2$, i.e., under particle exchange, and thus can serve as a measure of indistinguishability. If this overlap vanishes, the particles are considered as entirely distinguishable and HOM interference does not occur, and we show this in some concrete examples in the later sections.

Moreover, in the absence of entanglement, which is distinguished by the factorization of the two-photon wave function into two single-photon wave functions [18] [i.e., $\Phi_{\sigma_1\sigma_2}(\omega_1, \omega_2) = \Phi_{\sigma_1}(\omega_1)\Phi_{\sigma_2}(\omega_2)$], the interference term of Eq. (8) results in a positive value for $\sigma_1 = \sigma_2$. This increased detection probability for equally behaved ($\sigma_1 = \sigma_2$) photons implies that the factorization of the joint photonic wave function leads to the exclusive occurrence of photon bunching and thus certifies the occurrence of photon antibunching as a sufficient validation for the presence of entanglement, which was already recognized before in Ref. [19] and was also used in Ref. [20].

Furthermore, we want to add that using the same techniques as in the derivation of Eq. (9) we obtain for the single-particle detection statistics which is characterized by the probability $P_\sigma(\tau_1, \tau_2) = \int dt \langle\psi(\tau_1, \tau_2)|\hat{a}_\sigma^\dagger(t)\hat{a}_\sigma(t)|\psi(\tau_1, \tau_2)\rangle$ to detect a single photon in state σ the intuitive result

$$P_\sigma = \sum_{\bar{\sigma}} \frac{1}{2} (P_{\sigma\bar{\sigma}} + P_{\bar{\sigma}\sigma}) = \sum_{\bar{\sigma}} P_{\sigma\bar{\sigma}} \quad (11)$$

for all τ_1 and τ_2 , which we omitted as function arguments in Eq. (11).

Finally, we want to remark that the presented formalism here naturally extends to multiphoton interference experiments, where more than two photons are involved (see, for instance, Ref. [21]). In these cases an analog result to Eq. (9) is obtained for the multiphoton detection statistics where one has to symmetrize over the various DOFs of the involved photons. This also includes the special case of single-photon interference experiments like the Mach-Zehnder interferometer. Furthermore, also extending our formalism to mixed states is straightforward. However, we leave the concrete documentation of the extension of our formalism to mixed states for future work.

C. Frequency-entangled photons

The generation of frequency-entangled photons and their subsequent measurement within a HOM interference experiment is shown in Fig. 1; this was first demonstrated in Ref. [3] and was recently analyzed in more detail in Ref. [15]. For this, one first generates two polarization-entangled and

frequency-detuned photons which originate from a spontaneously down-converting periodically poled KTiOPO₄ crystal (ppKTP crystal). These photons render (up to normalization) the state

$$|\psi_{\text{f.d.}}\rangle = \int d\omega_1 d\omega_2 \phi_{\text{f.d.}}(\omega_1, \omega_2) e^{i\omega_1 \tau_1} e^{i\omega_2 \tau_2} \times (\hat{a}_{H_{h_1\omega_1}}^\dagger \hat{a}_{H_{h_2\omega_2}}^\dagger + \hat{a}_{V_{h_1\omega_1}}^\dagger \hat{a}_{V_{h_2\omega_2}}^\dagger) |0\rangle, \quad (12)$$

where the spectral wave function in this case reads

$$\phi_{\text{f.d.}}(\omega_1, \omega_2) = \delta(\omega_p - \omega_1 - \omega_2) \text{sinc}\left(\frac{\omega_1 - \omega_2 - \mu}{\xi}\right). \quad (13)$$

The subscript f.d. means frequency detuned, ω_p is the pump frequency of the down-converting process, μ is the frequency separation or detuning of the photons (which can be adjusted by tuning the ppKTP crystal's temperature), and ξ is the single-photon bandwidth.

The spectral wave function (13) is not square integrable due to the occurrence of the delta distribution $\delta(\omega_p - \omega_1 - \omega_2)$. This constitutes a problem in the evaluation of Eq. (8) [or rather Eq. (9)] due to the occurrence of squared delta functions $\delta^2(\omega_p - \omega_1 - \omega_2)$ under the integrals to evaluate. One approach to treat this problem stems from scattering theory. There, one uses the identity $\delta(\omega) = \lim_{T \rightarrow \infty} \int_{-T}^T dt \exp(i\omega t)$ to rewrite squares of delta distributions as $\delta^2(\omega) = T\delta(\omega)$, where T is the time over which the various detection events in an experiment are integrated. To obtain particle fluxes instead of particle numbers one has to divide expectation values by T . Thus, particle fluxes remain finite, also in the limit $T \rightarrow \infty$. The probability of a certain detection event is then recovered through division of the corresponding particle flux of the respective detection event by the sum of particle fluxes of all possible detection events.

After generation, the two polarization-entangled frequency-detuned photons interfere on a polarizing beam splitter (PBS), a process that transfers polarization entanglement onto the frequency DOF. The resulting (un-normalized) state after the PBS therefore reads

$$|\psi_{\text{f.e.}}\rangle = \int d\omega_1 d\omega_2 \phi_{\text{f.d.}}(\omega_1, \omega_2) \times (\hat{a}_{D_{h_1\omega_1}}^\dagger \hat{a}_{D_{h_2\omega_2}}^\dagger e^{i\omega_1 \tau_1} e^{i\omega_2 \tau_2} + e^{i\varphi} \hat{a}_{D_{h_1\omega_2}}^\dagger \hat{a}_{D_{h_2\omega_1}}^\dagger e^{i\omega_2 \tau_1} e^{i\omega_1 \tau_2}) |0\rangle, \quad (14)$$

where the subscript f.e. means frequency entangled and the operator $\hat{a}_{Ds\omega}^\dagger = (\hat{a}_{Hs\omega}^\dagger + \hat{a}_{Vs\omega}^\dagger)/\sqrt{2}$ creates a photon in the diagonal polarization state with frequency ω in the spatial mode s . Diagonal polarization of both photons has been achieved by a postselective measurement in Ref. [15] (not shown in Fig. 1). The polarization state of the photons is neither manipulated nor filtered or measured after the generation of the frequency-entangled photons in the experiment [15]. This is why we may discard it from here on, i.e., apart from the frequency we have only the spatial mode as the only left photonic DOF. Thus, we have $\sigma = s \in \{U, L\}$.

We also included the additional parameter φ in the state (14). This parameter controls the symmetry of the photonic

wave function in the frequency DOF. The value $\varphi = 0$ corresponds to a symmetric spectral wave function, while $\varphi = \pi$ corresponds to an antisymmetric spectral wave function as can be seen in Eq. (16).

We can rewrite the state (14) as

$$|\psi_{\text{f.e.}}\rangle = \int d\omega_1 d\omega_2 \phi_{\text{f.e.}}^\varphi(\omega_1, \omega_2) e^{i\omega_1 \tau_1} e^{i\omega_2 \tau_2} \times \hat{a}_{h_1\omega_1}^\dagger \hat{a}_{h_2\omega_2}^\dagger |0\rangle, \quad (15)$$

where we have defined the frequency-entangled spectral wave function

$$\phi_{\text{f.e.}}^\varphi(\omega_1, \omega_2) = \phi_{\text{f.d.}}(\omega_1, \omega_2) + e^{i\varphi} \phi_{\text{f.d.}}(\omega_2, \omega_1). \quad (16)$$

The state (15) then passes through the 50 : 50 BS and it transforms into

$$|\psi_{\text{f.e.}}\rangle = \int d\omega_1 d\omega_2 \phi_{\text{f.e.}}^\varphi(\omega_1, \omega_2) e^{i\omega_1 \tau_1} e^{i\omega_2 \tau_2} \times (\hat{a}_{U\omega_1}^\dagger \hat{a}_{U\omega_2}^\dagger e^{i\theta} - \hat{a}_{L\omega_1}^\dagger \hat{a}_{L\omega_2}^\dagger e^{-i\theta} + \hat{a}_{U\omega_1}^\dagger \hat{a}_{L\omega_2}^\dagger - \hat{a}_{L\omega_1}^\dagger \hat{a}_{U\omega_2}^\dagger) |0\rangle. \quad (17)$$

From this we can read off the photonic wave function after the beam splitter $\Phi_{\sigma_1\sigma_2}(\omega_1, \omega_2) = \Phi_{s_1s_2}(\omega_1, \omega_2)$, which is characterized by four scalar functions in ω_1 and ω_2 (since s_1 and s_2 respectively can take two values, U and L). We can arrange the wave function in a 2×2 matrix:

$$\Phi_{s_1s_2}(\omega_1, \omega_2) = \phi_{\text{f.e.}}^\varphi(\omega_1, \omega_2) \begin{pmatrix} e^{i\theta} & +1 \\ -1 & -e^{-i\theta} \end{pmatrix}. \quad (18)$$

The row and column numbering of Eq. (18) is U, V .

We now employ Eqs. (18), (9), and (10) to compute the joint detection probabilities $P_{s_1s_2}(\tau_1, \tau_2)$, and we find

$$P_{s_1s_2}(\tau_1, \tau_2) = \frac{1}{4} [\mathbf{R} + d(\tau_1, \tau_2) \mathbf{C}], \quad (19)$$

where the matrices \mathbf{R} and \mathbf{C} are given in the (s_1, s_2) basis by

$$\mathbf{R} = \begin{pmatrix} 1 & 1 \\ 1 & 1 \end{pmatrix}, \quad \mathbf{C} = \begin{pmatrix} 1 & -1 \\ -1 & 1 \end{pmatrix}, \quad (20)$$

while the functional dependence on the delays τ_1 and τ_2 appears only in the function $d(\tau_1, \tau_2)$, which we specify immediately.

Note that we have chosen the bold font for $\mathbf{P}_{s_1s_2}(\tau_1, \tau_2)$ in Eq. (19) to emphasize the fact that it has to be read as a matrix. The different entries are equal to the probabilities of the various detection events. The row and column numbering of Eq. (19) is the same as in Eq. (18). For instance, the entry of row 2 and column 2 in Eq. (19) means that the probability of detecting both photons at detector L (see Fig. 1) is equal to $P_{LL}(\tau_1, \tau_2) = 1/4[1 + d(\tau_1, \tau_2)]$.

The probability $P^c(\tau_1, \tau_2) := P_{UL} + P_{LU}$ for a coincidence measurement (i.e., to detect one photon at one detector U or L and the other photon at the other detector L or U) is given by

$$P^c(\tau_1, \tau_2) = \frac{1}{2}[1 - d(\tau_1, \tau_2)], \quad (21)$$

with

$$d(\tau_1, \tau_2) = \frac{R_{\mu\xi}^\varphi(\tau_1, \tau_2) + S_{\mu\xi}(\tau_1, \tau_2)}{1 + \cos(\varphi) \text{sinc}(2\mu/\xi)}, \quad (22)$$

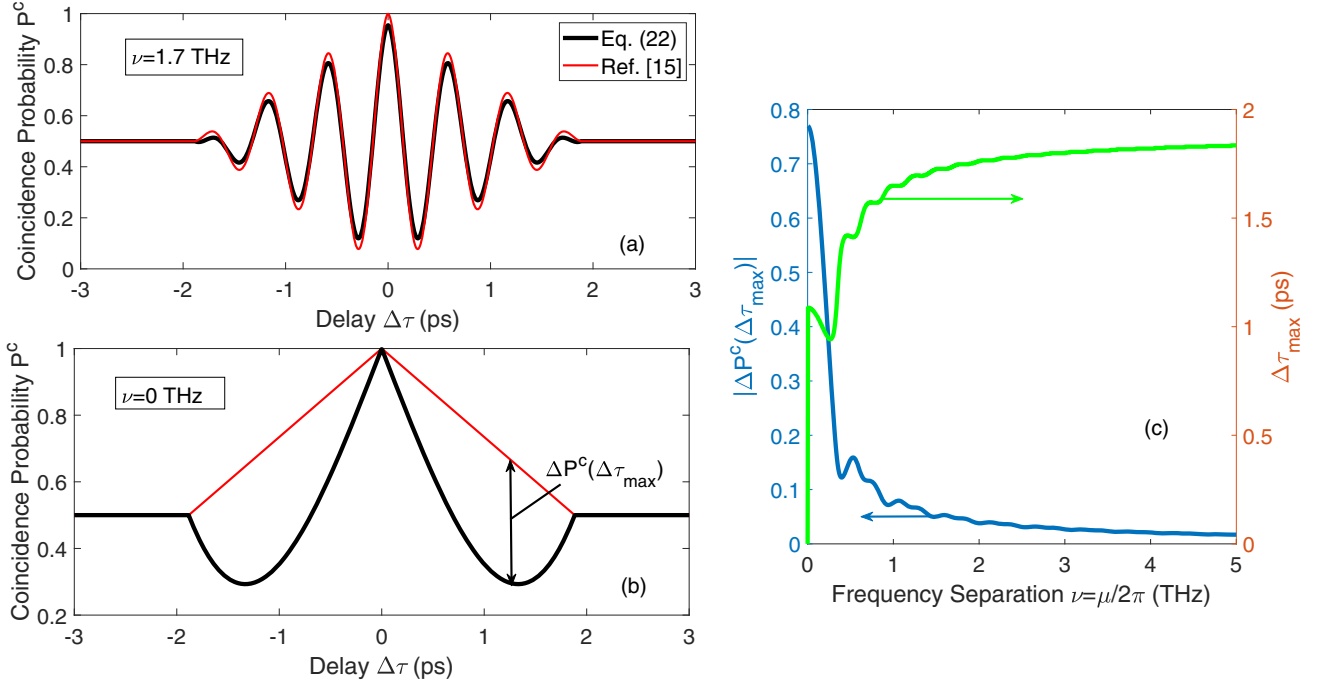


FIG. 2. Hong-Ou-Mandel interference experiment with frequency-entangled photons [see Eq. (16) for joint spectral profile]. Coincidence probability for a frequency separation of (a) $\nu = \mu/2\pi = 1.7$ THz and (b) $\nu = \mu/2\pi = 0$ THz. Note that our correction leads to a qualitative different behavior of the coincidence probability. The red curve in panel (b) predicts photon antibunching ($P^c > 0.5$) for all delays, where the black curve predicts photon bunching ($P^c < 0.5$) for some delays around $\Delta\tau \approx \pm 1.5$ ps. In panel (c) the blue curve shows the absolute value of the maximum discrepancy $|\Delta P^c(\Delta\tau_{max})|$ in the coincidence probability between our result [Eq. (22)] and the result that was obtained in Ref. [15] in dependence of the frequency separation $\nu = \mu/2\pi$. The green curve shows the delay $\Delta\tau_{max}$ at which this discrepancy is maximized. The single-photon bandwidth $\xi = 4/\tau_c = 1.356$ THz was taken from Ref. [15], where the coherence time from the mentioned reference was approximately $\tau_c \approx 0.3/0.885$ THz. The delay is $\Delta\tau = \tau_1 - \tau_2$. All computations were done for $\varphi = \pi$ in our evaluation of Eq. (22).

where we have introduced the functions

$$R_{\mu\xi}^\varphi(\tau_1, \tau_2) = \cos[\mu(\tau_1 - \tau_2) - \varphi] \text{tri}\left(\frac{\xi(\tau_1 - \tau_2)}{2}\right), \quad (23a)$$

$$S_{\mu\xi}(\tau_1, \tau_2) = \frac{\sin\left[\frac{2\mu}{\xi} \text{tri}\left(\frac{\xi(\tau_1 - \tau_2)}{2}\right)\right]}{\frac{2\mu}{\xi}}, \quad (23b)$$

and

$$\text{tri}(x) = \begin{cases} 1 - |x| & \text{if } |x| \leq 1 \\ 0 & \text{if } |x| > 1 \end{cases} \quad (24)$$

is the *triangular function*.

III. DISCUSSION

A. Relation to previous experiments

Our result (22) for the HOM effect extends the scope of application of the one obtained in previous work [15]. There, the expression $d(\tau_1, \tau_2) = R_{\mu\xi}^\varphi(\tau_1, \tau_2)$ was obtained, which coincides with our result in the limit $\mu/\xi \gg 1$ since $\lim_{\mu/\xi \rightarrow \infty} S_{\mu\xi}(\tau_1, \tau_2) = 0$. Let us call $d_0(\tau_1, \tau_2) := d(\tau_1, \tau_2)|_{\mu/\xi \rightarrow \infty}$. Since the previous experiment [15] was carried out in a parameter regime where one has $\mu/\xi > 10$, the discrepancy with our result was not measured. A qualitative difference between our result and the aforementioned result in the literature would have been revealed if the authors had driven the ppKTP crystal at lower temperatures, but they

started their measurement series from the lowest crystal temperature of $T = 33.7$ °C, which corresponds to a frequency separation of $\nu = \mu/2\pi = 1.7$ THz [see Fig. 2(a)]. Nevertheless, also at this frequency separation a slight difference between our result and the one mentioned before can be seen. Our result (22) predicts slightly lower interference fringes. This tendency was already seen in the original investigation of frequency-entangled photons by Ou and Mandel [3], where this lower fringe visibility was attributed to an imperfect alignment of the measurement apparatus. However, we suggest that this discrepancy might originate, at least in part, due to our correction term $\Delta P^c(\tau_1, \tau_2) = d_0(\tau_1, \tau_2) - d(\tau_1, \tau_2)$. In the original derivation [15] this lower fringe visibility was explained by imperfect frequency entanglement of the photons.

A clear discrepancy between the approximation formula from the result found in the literature [15] and our result for the coincidence probability (22) would have been observed if the ppKTP crystal would have been driven only 10 °C lower at a room temperature of about $T \approx 20$ °C, which would correspond to a frequency separation of $\nu = \mu/2\pi \approx 0.265$ THz. This would lead to a discrepancy of the coincidence probability to our result of $|\Delta P^c(\Delta\tau_{max})| \approx 0.2$ at a delay of $\Delta\tau_{max} \approx 1$ ps as seen in Fig. 2(c).

It is also worth noting that in the parameter regime of low-frequency separations, the additional term $S_{\mu\xi}(\tau_1, \tau_2)$ predicts physics qualitatively different than those previously obtained via the approximation formula [15], as can be seen

in Figs. 2(b) and 2(c). For a delay of $\Delta\tau_{\max} \approx \pm 1.5$ ps, our result shows the occurrence of photon bunching (i.e., $P^c < 0.5$) where the approximation formula $d_0(\tau_1, \tau_2) = R_{\mu\Delta}^\varphi(\tau_1, \tau_2)$ here predicts photon antibunching (i.e., $P^c > 0.5$).

B. Physical interpretation

The additional term $\Delta P^c(\tau_1, \tau_2) \propto S_{\mu\xi}(\tau_1, \tau_2)$, which was not yet documented in the literature [15,16], has a concrete physical meaning as it quantifies the contribution of the spectral indistinguishability related to finite-bandwidth effects to the coincidence interference pattern, which becomes more dominant for lower values of μ/ξ and, in particular, in the limit $\mu \rightarrow 0$ of vanishingly small frequency separations.

To see this, it is illusive to repeat the calculation of the coincidence detection probability with the spectrum (13) of frequency-detuned photons in place of the spectrum (16) of frequency-entangled photons. This yields

$$P^c(\tau_1, \tau_2) = \frac{1}{2}[1 - S_{\mu\xi}(\tau_1, \tau_2)], \quad (25)$$

which precisely coincides with the corresponding result of coincidence detection probability of frequency-detuned photons found in the literature [20]. Contrasting this result with the interference pattern (22) of frequency-entangled photons shows up the meaning of spectral distinguishability in HOM interference and moreover relates this to the presence of entanglement between the spectral DOF and other DOFs of the considered photons, as we explain further below.

One can regard the spectral wave function (13) of frequency-detuned photons in the $\omega_1\omega_2$ plane in the limit $\mu \gg \xi$ as a distribution peaked around the point $[(\omega_p + \mu)/2, (\omega_p - \mu)/2]$, meaning one photon is emitted at frequency $\omega_1 \approx (\omega_p + \mu)/2$ and the other at frequency $\omega_2 \approx (\omega_p - \mu)/2$. As can be seen in state (12), the photon of frequency ω_1 is emitted in mode h_1 and the photon of frequency ω_2 is emitted in mode h_2 , meaning that here we face a state in which the spatial modes of the photons are entangled with their frequencies. This is why the photons of state (12) are spectrally distinguishable from each other. The spectral distinguishability increases with increasing values of μ/ξ , i.e., with increasing entanglement between the spectral and the spatial DOF of each photon. This suppresses the tendency of frequency-detuned photons to bunch or antibunch [15], which is reflected in the vanishing of the interference term $S_{\mu\xi}(\tau_1, \tau_2)$ in Eq. (25) for increasing values of μ/ξ .

This emphasizes the role of distinguishability in the context of second quantization, in which no particle can be addressed individually by means of a “label” of the particle. This is the reason why it is often stated that in the second quantization formalism the involved particles are always considered as being indistinguishable. However, the second quantization formalism also carries a notion of distinguishability of particles, which is not encoded in the particle “labels” but in their properties (e.g., DOFs), and the interested reader is referred to Refs. [22,23] for the original and more detailed discussion on the topic, which was summarized in Ref. [24].

In the case of two completely indistinguishable photons of two frequencies, ω_1 and ω_2 , it is impossible for an

experimenter to detect (i.e., to address) a photon of a certain frequency, say ω_1 . However, because the property of the photon’s frequency (i.e., the photon’s frequency DOF) is entangled with its transmission path (i.e., its spatial DOF) in state (12), the experimenter can simply place a detector in the transmission path h_1 to detect and address the photon of frequency ω_1 with certainty (in the limit $\mu/\xi \rightarrow \infty$).

In contrast to this, the spectrum (16) of frequency-entangled photons is invariant against the exchange of the function arguments ω_1 and ω_2 for $\varphi = 0$. Operationally, this means that an experimenter is unable to detect and address a photon of a certain frequency, $\omega_1 \approx (\omega_p + \mu)/2$ or $\omega_2 \approx (\omega_p - \mu)/2$ thorough *any* measurement. This is because [in contrast to the state (12)] the frequency of the photons is not entangled with their spatial modes (or other DOFs). The only information which is known with certainty is that at whatever frequency ω_1 or ω_2 one photon of the state (15) is detected, the other photon is detected at the other frequency ω_2 or ω_1 . In other words the two frequencies at which the two photons are detected in state (15) are known, while the frequency of each individual photon is completely unknown, which is the essence of (spectral) entanglement [25].

This in turn shows up the relation between distinguishability and entanglement in second quantization. The impossibility to address a certain DOF of single particles (for instance, the frequency of a single photon) through *any* measurement corresponds to the indistinguishability of the considered particles with respect to this DOF, which is closely related to the presence of entanglement of the considered particles with respect to this DOF. However, one should note that the indistinguishability of two particles with respect to a certain property (DOF) is not equivalent but rather is a necessary condition for the presence of entanglement in the considered DOF. This means that two photons can be completely indistinguishable in their frequency DOF but nevertheless frequency unentangled (like it is the case with photons from the original HOM experiment [2]). However, the amount of frequency entanglement in a two-photon state is limited by the spectral indistinguishability of the considered photons.

This can be also seen as a consequence of the theorem of *entanglement monogamy*, which states that any pair of physical systems that are maximally entangled with each other cannot be entangled with any other physical system and that any entanglement with another, third, physical system comes at the cost of shrinking the amount of entanglement between the first two systems. This is why the interference term $S_{\mu\xi}(\tau_1, \tau_2)$ of the coincidence detection probability (25) of frequency-detuned photons vanishes in the limit $\mu \rightarrow \infty$, because with growing frequency separation μ the photon frequencies get stronger and stronger entangled with their spatial DOF (i.e., their transmission path), thereby becoming spectrally more and more distinguishable and thus imposing an upper limit on the exploitable frequency entanglement certified by the occurrence of photon antibunching [19].

C. Further mathematical considerations

Finally, we want to provide some mathematical arguments why the interference pattern $d_0(\tau_1, \tau_2)$, commonly used in the literature, cannot characterize the coincidence

detection statistics of frequency-entangled photons in its whole generality. This can be best seen in the limit $\mu \rightarrow 0$. In this limit the spectrum of frequency-detuned photons (13) is invariant under the exchange of the function arguments [i.e., $\phi_{\text{f.d.}}(\omega_1, \omega_2) = \phi_{\text{f.d.}}(\omega_2, \omega_1)$] and thus coincides [apart from a prefactor $(1 + e^{i\varphi})$] with the spectrum of frequency-entangled photons (16). Thus, in the limit $\mu \rightarrow 0$ also the corresponding interference patterns of frequency-detuned and frequency-entangled photons should coincide and, in particular, be independent from the phase φ (because it only enters the calculations as a prefactor of the photonic wave function). Note that $\varphi = \pi$ [the case shown in Fig. 2(b)] is a special case which we discuss further below separately; i.e., we first consider the case $\varphi \neq \pi$. Indeed our results (21) and (25) are identical for $\varphi \neq \pi$ and $\mu \rightarrow 0$, and both result in $\lim_{\mu \rightarrow 0, \varphi \neq \pi} d(\tau_1, \tau_2) = \text{tri}(\xi |\Delta\tau|/2)$, where $d_0(\tau_1, \tau_2)$ does not reproduce the interference pattern of frequency-detuned photons (25) in the limit $\mu \rightarrow 0$ (except for $\varphi = 0$). For $\varphi = \pi/2$ and $\mu \rightarrow 0$ the approximation formula even predicts the absence of interference, i.e., $d_0(\tau_1, \tau_2) = 0$. It is interesting to see that for the special case $\varphi = \pi$ our result for the interference terms in the limit $\mu \rightarrow 0$ is $\lim_{\mu \rightarrow 0, \varphi=\pi} d(\tau_1, \tau_2) = -\Theta(\xi |\Delta\tau|/2)[(\xi |\Delta\tau|)^3 - 6\xi |\Delta\tau| + 4]/4$, which is shown in Fig. 2(b), where $\Theta(x)$ is the Heaviside step function. Despite $\varphi = \pi$ being an interesting mathematical special case, in the limit $\mu \rightarrow 0$ this special case is physically unstable, since any deviation from the value $\varphi = \pi$ forces the interference term to collapse to the triangular function. Moreover, the special case $\varphi = \pi$ is unphysical in the limit $\mu \rightarrow 0$ when one considers frequency-entangled photons, since in this case the corresponding spectral wave function of frequency-entangled photons (16) vanishes. However, we wanted to show this case here [see Fig. 2(b)].

IV. OUTLOOK

There are several possible extensions to this work. First of all, we think that our formalism can be easily extended to a much broader class of multiphoton interference experiments [21] and moreover also to atom interference experiments [26]. The analysis of many-particle interference with bosons, fermions, or both would be covered by our formalism by a generalized symmetrization operator \mathcal{S} in Eq. (9), accounting for the respective parity of the wave function of the quantum system under consideration, and similar results in this direction have already been reported in combinatorial approaches in Refs. [27,28]. We think that these considerations can be translated into our formalism and vice versa. However, showing a strict mathematical analogy between these different formalisms remains a subject of future work.

Moreover, a general theoretical framework for the entanglement analysis in the second quantization formalism, which was recognized [29] early to be fundamentally different from the conventional entanglement analysis of distinguishable particles [30], would be desirable. However, despite tremendous progress [24,31,32] it is still a subject of ongoing research how to translate key concepts from standard quantum mechanics such as the execution of partial traces [33–35] and mixed states [32,36], various entanglement criteria

[18,37–39], or the separability problem in general [40,41] to second quantization.

Furthermore, we want to emphasize that HOM experiments are ruled by the spectral properties of the employed light sources which are sensitive to one of the trademark predictions from general relativity, namely, the redshift on photons propagating through curved space-time. Moreover, as constituting highly accurate entangled photonic clocks, the study of frequency-entangled photons in HOM interference in a relativistic setting is of great interest. We intend to cover these aspects in a follow-up work.

Finally, we want to point out that the considerations of the present work might be connected to recent experimental advances in the study of the relation between entanglement and indistinguishability [42–46]. For instance, the authors of Ref. [42] conducted a direct measurement of the particle exchange phase of fermions, bosons, and anyons (particles with a mixed wave function parity) and showed that this can be useful for quantum-enhanced phase estimation. As frequency-entangled photons can reveal bosonic, fermionic, or anyonic behavior represented through the occurrence of photon bunching, photon antibunching, or a mixture of both in HOM experiments, they could be interesting to be considered as resources for similar studies addressing the physics of the wave-function parity. Other experiments recently demonstrated that the indistinguishability of photons can be used as a resource for various elementary processes in quantum technological applications, such as coherence generation [43], quantum teleportation [44], and remote entanglement distribution in quantum networks [45,46]. All these works suggest that the degree of coherence and, in particular, entanglement correlations are closely related to the indistinguishability of the involved photons. The theoretical relation studied in this work, between indistinguishability and quantum entanglement via the theorem of entanglement monogamy (for photons in HOM interference), might be used as an estimator for the exploitable resources in quantum technological applications due to the indistinguishability of the involved particles and could possibly constitute a step towards a better understanding and control of these quantum qualities in future experiments.

V. CONCLUSIONS

Indistinguishability and entanglement are two of the most important genuine quantum mechanical principles without classical analogs. Both these principles play a crucial role in HOM interference experiments which cannot be explained without considering the particle character of single photons which by itself can only be explained within an entirely quantum mechanical theory of electromagnetism. Therefore, HOM experiments are ideal candidates to study the quantum nature of photons and, moreover, the relation between indistinguishability and quantum entanglement.

Using Glauber's theory of optical coherence we developed a formalism to predict the detection statistics of HOM interference experiments in a systematic way where we treated all photonic DOFs on equal footing under the inclusion of entanglement correlations. This formalism naturally extends also to more complicated experimental setups and multipartite quantum states.

We analyzed the role of indistinguishability and entanglement in HOM interference in the example of two fundamental two-photon sources: Sources which produce spectrally distinguishable frequency-detuned photons [20] and sources which produce spectrally indistinguishable frequency-entangled photons [15].

The comparison between these sources showed that the amount of entanglement which can be exploited in HOM interference through the occurrence of photon antibunching is limited by the spectral indistinguishability of the employed photons, which by itself is limited by the amount of entanglement between the spectral DOF of the photons with other DOFs, for instance, the spatial one. Therefore, we could relate the relation between indistinguishability and entanglement in HOM interference to the theorem of entanglement monogamy.

Apart from that, with our formalism we found an additional term in the interference pattern of frequency-entangled photons. Because frequency-entangled photons seem to be

one of the most promising candidates to test fundamental aspects of physics and, moreover, because they can be used as a resource in quantum technological applications related to high-precision metrology, it is important to accurately characterize their spectral properties, also in the regime of low-frequency separations.

ACKNOWLEDGMENTS

We gratefully acknowledge Dennis Rätzel, David Edward Bruschi, and Andreas Wolfgang Schell for fruitful discussions on the topic. R.B. was funded by the Deutsche Forschungsgemeinschaft (DFG, German Research Foundation) under Germany's Excellence Strategy-EXC-2123 QuantumFrontiers, Grant No. 390837967. We further gratefully acknowledge support through the TerraQ initiative from the Deutsche Forschungsgemeinschaft (DFG, German Research Foundation), Project-ID 434617780-SFB 1464, and the Research Training Group 1620 "Models of Gravity".

-
- [1] G. Czycholl, *Theoretische Festkörperphysik: Von den klassischen Modellen zu Modernen Forschungsthemen* (Springer-Verlag, Berlin, 2007).
 - [2] C. K. Hong, Z. Y. Ou, and L. Mandel, *Phys. Rev. Lett.* **59**, 2044 (1987).
 - [3] Z. Y. Ou and L. Mandel, *Phys. Rev. Lett.* **61**, 54 (1988).
 - [4] F. Bouchard, A. Sit, Y. Zhang, R. Fickler, F. M. Miatto, Y. Yao, F. Sciarrino, and E. Karimi, *Rep. Prog. Phys.* **84**, 012402 (2020).
 - [5] M. C. Tichy, *Phys. Rev. A* **91**, 022316 (2015).
 - [6] M. Tillmann, S.-H. Tan, S. E. Stoeckl, B. C. Sanders, H. de Guise, R. Heilmann, S. Nolte, A. Szameit, and P. Walther, *Phys. Rev. X* **5**, 041015 (2015).
 - [7] R. Quan, Y. Zhai, M. Wang, F. Hou, S. Wang, X. Xiang, T. Liu, S. Zhang, and R. Dong, *Sci. Rep.* **6**, 30453 (2016).
 - [8] A. Valencia and Y. Scarcelli, G. and Shih, *Appl. Phys. Lett.* **85**, 2655 (2004).
 - [9] V. Giovannetti, S. Lloyd, and L. Maccone, *Nature (London)* **412**, 417 (2001).
 - [10] M. Mohageg, L. Mazzarella, C. Anastopoulos, J. Gallicchio, B.-L. Hu, T. Jennewein, S. Johnson, S.-Y. Lin, A. Ling, C. Marquardt, M. Meister, R. Newell, A. Roura, W. P. Schleich, C. Schubert, D. V. Strekalov, G. Vallone, P. Villoresi, L. Wörner, N. Yu, A. Zhai, and P. Kwiat, *EPJ Quantum Technology* **9**, 25 (2022).
 - [11] R. Barzel, M. Gündoğan, M. Krutzik, D. Rätzel, and C. Lämmerzahl, [arXiv:2209.02099](https://arxiv.org/abs/2209.02099).
 - [12] R. Barzel, D. E. Bruschi, A. W. Schell, and C. Lämmerzahl, *Phys. Rev. D* **105**, 105016 (2022).
 - [13] R. Glauber, *Phys. Rev.* **130**, 2529 (1963).
 - [14] A. Pradana and L. Chew, *New J. Phys.* **21**, 053027 (2019).
 - [15] S. Ramelow, L. Ratschbacher, A. Fedrizzi, N. K. Langford, and A. Zeilinger, *Phys. Rev. Lett.* **103**, 253601 (2009).
 - [16] F. Kaneda, H. Suzuki, R. Shimizu, and K. Edamatsu, *Opt. Express* **27**, 1416 (2019).
 - [17] Z. Ou, *Phys. Rev. A* **74**, 063808 (2006).
 - [18] K. Eckert, J. Schliemann, D. Bruß, and M. Lewenstein, *Ann. Phys.* **299**, 88 (2002).
 - [19] K. Wang, *J. Phys. B: At., Mol. Opt. Phys.* **39**, R293(R) (2006).
 - [20] A. Fedrizzi, T. Herbst, M. Aspelmeyer, M. Barbieri, T. Jennewein, and A. Zeilinger, *New J. Phys.* **11**, 103052 (2009).
 - [21] J. W. Pan, Z. B. Chen, C. Y. Lu, H. Weinfurter, A. Zeilinger, and M. Żukowski, *Rev. Mod. Phys.* **84**, 777 (2012).
 - [22] G. Ghirardi, L. Marinatto, and T. Weber, *J. Stat. Phys.* **108**, 49 (2002).
 - [23] G. C. Ghirardi and L. Marinatto, *Opt. Spectrosc.* **99**, 386 (2005).
 - [24] L. Amico, R. Fazio, A. Osterloh, and V. Vedral, *Rev. Mod. Phys.* **80**, 517 (2008).
 - [25] E. Schrödinger, *Naturwissenschaften* **23**, 807 (1935).
 - [26] A. M. Kaufman, M. C. Tichy, F. Mintert, A. M. Rey, and C. A. Regal, in *Advances In Atomic, Molecular, and Optical Physics*, edited by E. Arimondo, L. F. DiMauro, and S. F. Yelin, Vol. 67 (Academic Press, San Diego, 2018), pp. 377–427.
 - [27] M. C. Tichy, M. Tiersch, F. Mintert, and A. Buchleitner, *New J. Phys.* **14**, 093015 (2012).
 - [28] M. C. Tichy, M. Tiersch, F. de Melo, F. Mintert, and A. Buchleitner, *Phys. Rev. Lett.* **104**, 220405 (2010).
 - [29] A. Peres, *Quantum Theory: Concepts and Methods* (Springer, Berlin, 2002).
 - [30] R. Horodecki, P. Horodecki, M. Horodecki, and K. Horodecki, *Rev. Mod. Phys.* **81**, 865 (2009).
 - [31] F. Benatti, R. Floreanini, F. Franchini, and U. Marzolino, *Phys. Rep.* **878**, 1 (2020).
 - [32] R. Lo Franco and G. Compagno, *Sci. Rep.* **6**, 20603 (2016).
 - [33] R. Lo Franco and G. Compagno, *Phys. Rev. Lett.* **120**, 240403 (2018).
 - [34] S. Chin and J. Huh, *Phys. Rev. A* **99**, 052345 (2019).
 - [35] H. S. Mani, R. N, and V. V. Sreedhar, *Phys. Rev. A* **101**, 022314 (2020).
 - [36] A. C. Lourenço, T. Debarba, and E. I. Duzzioni, *Phys. Rev. A* **99**, 012341 (2019).

- [37] G. Compagno, A. Castellini, and R. Lo Franco, *Philos. Trans. R. Soc. A* **376**, 20170317 (2018).
- [38] S. Sciara, R. Lo Franco, and G. Compagno, *Sci. Rep.* **7**, 44675 (2017).
- [39] S. Bose and D. Home, *Phys. Rev. Lett.* **110**, 140404 (2013).
- [40] A. Reusch, J. Sperling, and W. Vogel, *Phys. Rev. A* **91**, 042324 (2015).
- [41] B. Morris, B. Yadin, M. Fadel, T. Zibold, P. Treutlein, and G. Adesso, *Phys. Rev. X* **10**, 041012 (2020).
- [42] Y. Wang, M. Piccolini, Z.-Y. Hao, Z.-H. Liu, K. Sun, J.-S. Xu, C.-F. Li, G.-C. Guo, R. Morandotti, G. Compagno, and R. Lo Franco, *Phys. Rev. Appl.* **18**, 064024 (2022).
- [43] K. Sun, Z.-H. Liu, Y. Wang, Z.-Y. Hao, X.-Y. Xu, J.-S. Xu, C.-F. Li, G.-C. Guo, A. Castellini, L. Lami, A. Winter, G. Adesso, G. Compagno, and R. L. Franco, *Proc. Natl. Acad. Sci. USA* **119**, e2119765119 (2022).
- [44] K. Sun, Y. Wang, Z.-H. Liu, X.-Y. Xu, J.-S. Xu, C.-F. Li, G.-C. Guo, A. Castellini, F. Nosrati, G. Compagno, and R. L. Franco, *Opt. Lett.* **45**, 6410 (2020).
- [45] M. R. Barros, S. Chin, T. Pramanik, H.-T. Lim, Y.-W. Cho, J. Huh, and Y.-S. Kim, *Opt. Express* **28**, 38083 (2020).
- [46] Y. Wang, Z.-Y. Hao, Z.-H. Liu, K. Sun, J.-S. Xu, C.-F. Li, G.-C. Guo, A. Castellini, B. Bellomo, G. Compagno, and R. Lo Franco, *Phys. Rev. A* **106**, 032609 (2022).

Chapter 3

Observer dependance in two photon interference

3.1 Introduction

In this chapter, we consider the *observer-dependence* of the genuine quantum phenomena of photon bunching and anti-bunching in Hong-Ou-Mandel (HOM) interference experiments due to spectral shift of photons.

Our findings suggest that the redshift effects, resulting from relative velocities between the source and the observer—mainly caused by the associated Doppler shift—can alter the detection statistics to such an extent that it can be resolved in experiments under the employment of state-of-the-art optical sources for highly detuned and narrow-bandwidth frequency entangled photons [45, 46].

However, our results show, that, at least in principle, shifting the expected outcomes from ideal bunching to ideal anti-bunching or vice versa is possible, although currently limited by the capabilities of present day technology.

This observer-dependent alteration reveals the character of the photonic wave function’s spectral parity properties and the associated quantum statistics, as a notion that depends on the motional state of the photon source and measurement laboratory including all intermediate optical instruments employed, and thus provides a novel avenue to probe the fundamental aspects of quantum field theory in curved spacetime.

Furthermore, our findings are particularly significant for the field of long-distance quantum communication, as even today the spectral degree of freedom, being continuous, is the most heavily utilized for *encoding large data at low resource consumption*. This is why frequency entanglement is regarded as one of the most attractive resources for entanglement-based or assisted quantum communication. Therefore, it is crucial to study the behavior of this phenomenon in a relativistic setting, especially in the context of space-based, long-distance communications.

3.2 Observer dependence of interference

At first glance, it may seem counterintuitive that phenomena such as photon anti-bunching are observer-dependent, given their role in certifying the presence of entanglement within the resources used. However, despite these expectations, photon anti-bunching remains an optical interference phenomenon. As such, it is intrinsically linked to the spectral properties of the employed light. Spectral properties represent the principal DOF influenced by both special and general relativity, manifesting a significant dependence on the observer's frame of reference relative to possibly present senders in case of communication.

However, while the variation in measurement results depends solely on the local properties of the communicators, phenomena such as entanglement are preserved (at least in our case as seen below). They may exhibit altered behaviors under these conditions, but can typically be restored through appropriate re-adjustment of the measurement settings. This is also the case because the redshift effect altering the spectral shape of photons and photon pairs can be modeled by a *unitary dilation operation*.

3.2.1 Redshift

As HOM interference is fundamentally related to the spectral properties of the utilized resources, it is crucial to consider the spectral alternation of photons between an emitting sender and a measuring receiver. This relationship is governed by the *mutual redshift* z_{AB} between the sending party A and the receiving party B , which relates the frequency ω_A of a photon in the local rest frame of the sender to the frequency ω_B of the same photon when received in the local rest frame of the observer B through the ratio

$$\frac{\omega_A}{\omega_B} = \Theta_{AB} = 1 + z_{AB}, \quad (3.1)$$

which retains positive values ($z_{AB} > 0$) in the case of a *chromatic redshift* (i.e., an observed frequency decrease from emitter to receiver) and negative values ($z_{AB} < 0$) in the case of a *chromatic blueshift* (i.e., an observed frequency increase from emitter to receiver).

3.2.2 Redshifted photon states

In a quantum field theoretical formulation the redshift relation (3.1) is governed by the relation between the photonic creation operators $a_{A\omega_A}^\dagger$ of the spectral modes of the sender's frame A and the modes $a_{B\omega_B}^\dagger$ of the receiver's frame B , which can be identified with each other when characterizing the same photon that is exchanged between the respective frames, i.e.

$$a_{A\omega_A}^\dagger = a_{B\omega_B}^\dagger, \quad (3.2)$$

where the relation (3.1) between the respectively observed frequencies ω_A and ω_B in the corresponding frames A and B holds.

In order to express the modes in a common frequency variable—for instance the one of frame A , i.e., ω_A —one has to characterize the photon in frame B in terms of the spectral modes of frame A , which requires the choice

$$a_{B\omega_B}^\dagger = \Theta_{AB}^{-1/2} a_{B\omega_A}^\dagger, \quad (3.3)$$

where the factor $\Theta_{AB}^{-1/2}$ arises through the requirement of the canonical commutator relations (2.30b) to hold, as we have [47]

$$\left[a_{B\omega_B}, a_{B\omega'_B}^\dagger \right] = \delta(\omega_B - \omega'_B), \quad (3.4a)$$

$$\begin{aligned} \left[a_{B\Theta_{AB}\omega_A}, a_{B\Theta_{AB}\omega'_A}^\dagger \right] &= \delta(\Theta_{AB}(\omega_A - \omega'_A)) = \frac{1}{|\Theta_{AB}|} \delta(\omega_A - \omega'_A) \\ &= \left[\Theta_{AB}^{-1/2} a_{B\omega_A}, \Theta_{AB}^{-1/2} a_{B\omega'_A}^\dagger \right]. \end{aligned} \quad (3.4b)$$

When written in a common frame-independent frequency variable ω Eqs. (3.2) and (3.3) give

$$a_{A\omega}^\dagger = \sqrt{\Theta_{AB}} a_{B\Theta_{AB}^{-1}\omega}^\dagger, \quad (3.5)$$

aligning with the comutator relations (3.4), and moreover also following from exchanging the labels A with B in Eq. (3.3).

Equation (3.2) naturally generalizes to non-monochromatic photons,

$$a_{A\Phi_A}^\dagger = a_{B\Phi_B}^\dagger, \quad (3.6)$$

rendering a spectrum $\Phi_\sigma(\omega)$ when measured in frame $\sigma = A, B$ of associated modes

$$a_{\sigma\Phi_\sigma}^\dagger = \int d\omega \Phi_\sigma(\omega) a_{\sigma\omega}^\dagger, \quad (3.7)$$

which by help of (3.5) implies the function equation between the emitter's and observer's spectra of the same photon

$$\Phi_B(\omega) = \sqrt{\frac{1}{\Theta_{AB}}} \Phi_A \left(\frac{\omega}{\Theta_{AB}} \right). \quad (3.8)$$

Indeed, this transformation behavior naturally extents to multi-photon states as we want to show on the example of the two-photon pair mode

$$p_{\sigma_1\sigma_2\Phi_{\sigma_1\sigma_2}}^\dagger = \int d\omega_1 d\omega_2 \Phi_{\sigma_1\sigma_2}(\omega_1, \omega_2) a_{\sigma_1\omega_1}^\dagger a_{\sigma_2\omega_2}^\dagger, \quad (3.9)$$

with $\sigma = A, B$, which describes a pair of photons, in a pair of frames A_1 and A_2 of two senders, which then should be transmitted to a pair of receivers respectively associated to the frames B_1 and B_2 , where now the frequencies between the senders and receivers are related as $\omega_{Ai} = \Theta_{A_i B_i} \omega_{Bi}$, leading to the transformation behavior

$$\Phi_{B_1 B_2}(\omega_1, \omega_2) = \sqrt{\frac{1}{\Theta_{A_1 B_1} \Theta_{A_2 B_2}}} \Phi_{A_1 A_2} \left(\frac{\omega_1}{\Theta_{A_1 B_1}}, \frac{\omega_2}{\Theta_{A_2 B_2}} \right). \quad (3.10)$$

This is a central result of [BBSL22], from which the alternation of interferograms follows, which we stress next.

3.2.3 Redshifted Interferogram

Before discussing the relationship between interferograms recorded by two pairs of observers with a mutual redshift—specifically A_i and B_i with $i = 1, 2$ —we must first extend our notion of the

photonic wave function from the previous section. Regardless of the detection frame σ , a photon possesses additional internal degrees of freedom (DOFs), denoted by the bold font σ . Here, we treat the DOFs corresponding to the frequency ω and the detection frame σ separately, defining the complete set of DOFs as $\omega = \{\sigma, \boldsymbol{\sigma}, \omega\}$.

We consider a pair of observers, σ_1 and σ_2 , each applying a temporal optical delay τ_{σ_1} and τ_{σ_2} in their respective frames, measured in units of their proper time. This setup is illustrated in Fig. 3.1.

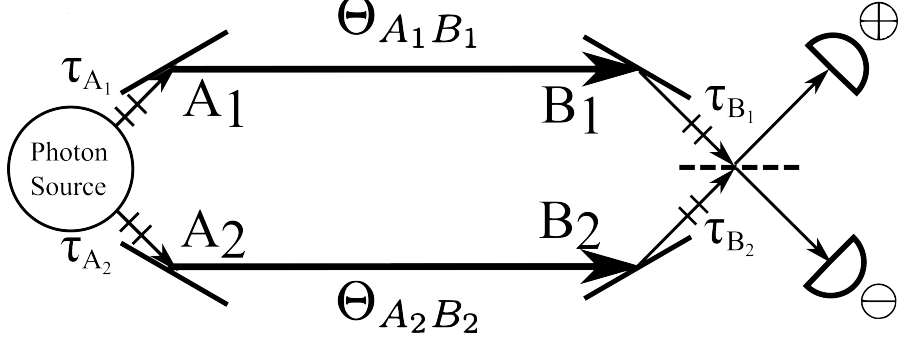


Figure 3.1: HOM experiment involving a pair of sending observers, A_1 and A_2 , and a pair of receiving/measuring observers, B_1 and B_2 , with pairwise redshift factors $\Theta_{A_1B_1}$ and $\Theta_{A_2B_2}$, respectively. Optical delays τ_{σ_i} are applied in frame σ_i , with $\sigma = A, B$ and $i = 1, 2$. The detector modes are labeled \oplus and \ominus .

The corresponding two-photon modes are expressed as

$$p_{\sigma_1\sigma_2}^\dagger(\tau_{\omega_1}, \tau_{\omega_2}) = \int d\omega_1 d\omega_2 \Phi_{\sigma_1\sigma_2}^{\sigma_1\sigma_2}(\omega_1, \omega_2) e^{i\omega_1\tau_{\omega_1}} e^{i\omega_2\tau_{\omega_2}} a_{\sigma_1\sigma_1\omega_1}^\dagger a_{\sigma_2\sigma_2\omega_2}^\dagger, \quad (3.11)$$

and the corresponding measurement statistics are given by

$$P_{\sigma_1\sigma_2}^{\sigma_1\sigma_2}(\tau_{\sigma_1}, \tau_{\sigma_2}) = \int d\omega_1 d\omega_2 |\mathcal{S}_{\omega_1\omega_2} [\Phi_{\sigma_1\sigma_2}^{\sigma_1\sigma_2}(\omega_1, \omega_2) e^{i\omega_1\tau_{\omega_1}} e^{i\omega_2\tau_{\omega_2}}]|^2. \quad (3.12)$$

From Eq. (3.10), it follows that the relationship between two interferograms recorded by two observer pairs with mutual redshift—specifically A_i and B_i with $i = 1, 2$ —is given by

$$P_{\sigma_1\sigma_2}^{B_1B_2}(\tau_{B_1}, \tau_{B_2}) = P_{\sigma_1\sigma_2}^{A_1A_2}(\tau_{A_1}, \tau_{A_2}) \quad (3.13)$$

which corresponds to a dilation, specifically the inverse of the spectral dilation described in Eq. (3.10)

$$\tau_{B_i} = \Theta_{A_1B_2}\tau_{A_i}. \quad (3.14)$$

This result is central to the findings in [BBSL22].

Before summarizing the central results of [BBSL22] and related literature [17–20], we explore an alternative approach to constructing spectral dilations using *unitary dilation operators*. Indeed, it is insightful, that the redshift effect corresponds to a unitary operation, which conserves the overall entanglement, though it may alter its nature, such as by changing the photon statistics.

3.2.4 Unitary dilation

Just as there is a *unitary translation/displacement operator* in quantum mechanics

$$\hat{T}(a) = \exp\left(-\frac{ia\hat{p}}{\hbar}\right) \quad (3.15)$$

acting on a wave function $\psi(x)$ as

$$\hat{T}(a)\psi(x) = \psi(x + a) \quad (3.16)$$

there is also a *dilation operator*

$$\hat{D}(\alpha) = \exp\left(-\frac{i \ln(\sqrt{\alpha}) \{\hat{x}, \hat{p}\}}{\hbar}\right) \quad (3.17)$$

acting on a wave function $\psi(x)$ as

$$\hat{D}(\alpha)\psi(x) = \sqrt{\frac{1}{\alpha}}\psi\left(\frac{x}{\alpha}\right), \quad (3.18)$$

which is precisely the transformation behavior of (3.8), with the anti-commutator

$$\{\hat{x}, \hat{p}\} = \hat{x}\hat{p} + \hat{p}\hat{x}, \quad (3.19)$$

where we have to set $\alpha = \Theta_{AB}$ and

$$\hat{x} = \omega, \quad \hat{p} = -i\hbar\frac{\partial}{\partial\omega}, \quad (3.20)$$

to find

$$\Phi_B(\omega) = \hat{D}(\Theta_{AB})\Phi_A(\omega). \quad (3.21)$$

This transformation can be easily derived from the dilation operator when the exponential is explicitly written in terms of differential operators –by employing (3.19) and (3.20). This representation is known as a *Lagrange-shift operator*

$$\hat{D}(\alpha) = \sqrt{\frac{1}{\alpha}} \exp\left(-\ln(\alpha)\omega\frac{\partial}{\partial\omega}\right) = \sqrt{\frac{1}{\alpha}}\alpha^{-\omega\partial_\omega}, \quad (3.22)$$

where we employed the notation $\partial_\omega := \partial/\partial\omega$.

3.2.4.1 Pair dilation operators

In case of photon pairs we have a pair dilation operator

$$\hat{D}(\alpha_1, \alpha_2) = \exp\left(-\frac{i}{\hbar}\sum_{j=1}^2 \ln(\sqrt{\alpha_j})\{\hat{x}_j, \hat{p}_j\}\right) \quad (3.23)$$

with $\alpha_j = \Theta_{A_j B_j}$ and

$$\hat{x}_j = \omega_j, \quad \hat{p}_j = -i\hbar\frac{\partial}{\partial\omega_j}, \quad (3.24)$$

where $j = 1, 2$.

Specifically, the commutator relations

$$[\hat{x}_k, \hat{p}_l] = i\hbar\delta_{kl}, \quad (3.25)$$

and particularly their vanishing for $k \neq l$, compel the pair dilation operator (3.23) to decompose into a tensor product:

$$\hat{D}(\alpha_1, \alpha_2) = \hat{D}_1(\alpha_1) \otimes \hat{D}_2(\alpha_2), \quad (3.26)$$

of unitary single-particle dilation operators associated to the j -th photon:

$$\hat{D}_j(\alpha_j) = \exp\left(-\frac{i \ln(\sqrt{\alpha_j}) \{\hat{x}_j, \hat{p}_j\}}{\hbar}\right). \quad (3.27)$$

This shows that the overall conservation of inter-particle entanglement is maintained, as *local unitary operations* preserve entanglement, even though they may alter its nature.

3.3 Summary of Central Results

This study explores the observer-dependence of Hong-Ou-Mandel (HOM) interference under the influence of relativistic redshift. By extending a quantum field theoretical framework to describe the deformation of photonic spectral profiles in curved spacetime, we address how relativistic effects alter quantum interference patterns, especially in the context of entangled photons.

- **Observer-Dependent Interference:** The symmetry or antisymmetry of the photonic spectral wave function, which dictates photon bunching or antibunching, is shown to depend on the observer's frame of reference. This reveals that fundamental quantum properties, like entanglement and indistinguishability, are observer-relative.
- **Redshift and Spectral Dilation:** The study demonstrates that a mutual redshift between sender and receiver results in a dilation of the photonic spectral wave function. This dilation is described by a unitary dilation operator, which preserves entanglement but may alter its characteristics.
- **Relativistic Effects on HOM Interference:** The impact of relativistic redshift on HOM interference patterns is quantified, showing that even small redshifts can significantly affect coincidence detection probabilities, particularly in experiments involving frequency-entangled photons.
- **Application to Quantum Technologies:** These findings have implications for quantum technologies, such as satellite-based quantum communication, by providing a method to estimate the impact of relativistic redshift on such systems.
- **General Framework:** A general framework is provided for describing the influence of relativistic effects on the spectral properties of quantum entanglement and interference, applicable to a wide range of quantum optical experiments.

In conclusion, this work advances the understanding of the interplay between quantum mechanics and general relativity, emphasizing the observer-dependence of quantum interference phenomena and laying the groundwork for future research in relativistic quantum technologies.

Observer dependence of photon bunching: The influence of the relativistic redshift on Hong-Ou-Mandel interference

Roy Barzel¹, David Edward Bruschi², Andreas W. Schell^{3,4}, and Claus Lämmerzahl^{1,5,6}

¹ZARM, University of Bremen, 28359 Bremen, Germany

²Institute for Quantum Computing Analytics (PGI-12), Forschungszentrum Jülich, 52425 Jülich, Germany

³Institut für Festkörperphysik, Leibniz Universität Hannover, Appelstr. 2, 30167 Hannover, Germany

⁴Physikalisch-Technische Bundesanstalt, Bundesallee 100, 38116 Braunschweig, Germany

⁵DLR-Institute for Satellite Geodesy and Inertial Sensing, c/o University of Bremen,
Am Fallturm 2, 28359 Bremen, Germany

⁶Institute of Physics, Carl von Ossietzky University Oldenburg, 26111 Oldenburg, Germany



(Received 22 February 2022; accepted 22 April 2022; published 20 May 2022)

We study the influence of the relativistic redshift on Hong-Ou-Mandel (HOM) interference and present a genuine quantum test of general relativity. We use Glauber's theory of quantum coherence to predict the coincidence probability of realistic broadband photons in HOM experiments in a nonrelativistic setting. We extend the quantum field theoretical framework previously developed to describe the deformation of the spectral profile of single photons in curved spacetimes to a multiphoton framework, which is exact for inertial observers in a flat spacetime and an approximation when observers are located in a curved spacetime. We find that, in case of frequency entangled photons, a mutual redshift between the sender and the receiver can change the coincidence statistics from photon bunching to photon antibunching and vice versa. This implies that the (anti)symmetry of the photonic spectral wave function is an observer dependent notion and that this can be probed via HOM experiments in a relativistic setting.

DOI: [10.1103/PhysRevD.105.105016](https://doi.org/10.1103/PhysRevD.105.105016)

I. INTRODUCTION

Exploring the interplay between general relativity and quantum mechanics is one of the major goals of modern physics [1]. A central problem in the development of a theory that describes the behavior of quantum particles in curved spacetimes is the lack of experimental evidence providing guidance. This is mostly rooted in the huge discrepancy of the parameter regimes where the two theories become relevant. While relativistic effects typically occur at macroscopic scales and large energies, quantum effects usually manifest at the microscopic scale, where few elementary objects interact. However, in quantum theory, there is no length scale that restricts its applicability. Moreover, in recent decades, fueled by advances in experimental capabilities and control, several experiments have been conducted to reveal the effects of gravity on quantum systems. For example, the nonrelativistic gravitational phase of neutrons was measured in the famous Colella, Overhauser and Werner (COW) experiment [2], and the general relativistic redshift on the frequency of single photons [3,4] or of clocks located on Earth or moving [5] was detected. These early successes indicate that it is possible to investigate the overlap of relativity and quantum mechanics within accessible energy scales and environments and that the limit is mostly technological.

The rapid technological progress experienced in the past decades offers the opportunity to propose experiments that operate in parameter regimes where both general relativity and quantum mechanics play a non-negligible role [6]. For example, the recent demonstration of entanglement distribution over more than 1200 km [7] opened the way for many long-distance quantum applications, such as the first satellite-to-ground quantum key distribution (QKD) implementation by the Micius satellite of the Chinese Academy of Sciences [8–10] and intercontinental quantum-secured data transfer [11,12]. Proposed quantum technologies often rely on the use of genuine quantum features, such as entanglement, shared between several distant systems or particles. Quantum mechanics has so far been successfully employed as the only formal framework to describe these scenarios. However, it is reasonable to assume that relativistic effects cannot be neglected anymore when correlated quantum systems are distributed over large distances through the inhomogeneous gravitational field of the Earth.

Relativistic and quantum information aims at understanding how gravity affects quantum information tasks and protocols [13]. One avenue has demonstrated that gravity affects the quantum state of realistic broadband photons propagating in curved spacetime [14–16]. It was shown that the effects can also be employed for sensing [15]. Furthermore, quantum correlations, such as squeezing

and entanglement, have been shown to potentially enhance the sensitivity of interferometers in this context [17] and to improve the accuracy in clock synchronization [18,19]. The latter is needed in the global positioning system (GPS) or high precision metrology in general. It has become evident that the development of modern technologies to be deployed in contexts where gravity plays a significant role, such as a GPS with quantum systems as atomic clocks, requires a full characterization of the properties of quantum systems in curved spacetime.

Indistinguishability of physical systems is one of the important defining features of quantum systems without classical analogue. In the case of bosons, indistinguishability leads to intriguing phenomena, such as photon bunching within interference experiments, first witnessed in the pioneering Hong-Ou-Mandel (HOM) experiment [20]. Only recently it was shown that HOM interference bears the potential to enhance the accuracy of clock synchronization [21,22], as already predicted theoretically [18]. Consequently, HOM-like schemes are candidates for space-based implementations where indistinguishable correlated photons are exchanged over intercontinental distances. Relativistic redshift, which plays a role already in ordinary GPS, is expected to play an important role in these scenarios as well. We conclude that HOM interference can constitute one of the most promising routes to design genuine quantum tests of general relativity. It is therefore important to understand the effect of relativity on HOM-interference-based implementations.

In the present paper, we investigate the influence of relativistic redshift on HOM-interference experiments. This has a fundamental and a practical aspect. On the fundamental side, it is of interest to reveal which scenarios witness signatures of general relativistic effects that can be observed in HOM experiments. On the practical side, it is important to find the regimes where relativity affects quantum technological applications and to quantify the magnitude of the effects. In particular, we want to quantify the signatures of general relativistic effects on observable HOM-interference patterns, which in turn, will inform us on potential new challenges to be faced in the development of novel quantum technological applications. We employ the quantum field theoretical framework developed to quantify the influence of the relativistic redshift on single photons [14,15] and extend this body of work to the case of two (or more) photons. This, in turn, allows us to quantify relativistic effects on two-photon HOM interference. Our approach can be applied to the case of inertial observers in a flat spacetime, as well as the case of scalar optics in (weakly) curved spacetime, which is the regime considered in our analysis. We also provide a comparison between the effects obtained when employing pairs of frequency uncorrelated photons, frequency detuned photons, and frequency-entangled photons. Finally, we derive the experimental conditions necessary to detect the effects of

relativistic redshift on the HOM-interference pattern with frequency entangled photons.

This work is organized as follows. In Sec. II, we briefly review our results on HOM interference from previous work [23]. In Sec. III, we provide the tools to compute the relativistic deformation of the spectral wave function. In Sec. IV, we compute the effects using the newly developed methods. In Secs. V and VI, we provide outlook and conclusions for our work.

II. HONG-OU-MANDEL INTERFERENCE

In this section, we briefly review a theoretical framework previously developed to predict the detection statistics of HOM experiments with realistic broadband photons. We leave details to the interested reader [23]. In this section, we work in a nonrelativistic context; i.e., all temporal quantities are functions of a universal background time and not of the proper time of the observers. The basic scheme of HOM interference is shown in Fig. 1.

A. Detection statistics

A general two-photon state $|\psi(\tau_1, \tau_2)\rangle$ in the context of HOM interference is given by

$$|\psi(\tau_1, \tau_2)\rangle = \int d\omega_1 d\omega_2 \Phi(\omega_1, \omega_2) e^{i\omega_1 \tau_1} e^{i\omega_2 \tau_2} \hat{a}_{\omega_1}^\dagger \hat{a}_{\omega_2}^\dagger |0\rangle, \quad (1)$$

where the bold font ω denotes the set of parameters that characterize all degrees of freedom (DOFs) of a single photon, and the \hat{a}_ω^\dagger are bosonic creation operators. We treat the frequency DOF ω separately from the other photonic DOF σ and write $\omega = \{\omega, \sigma\}$, thereby defining the alternative notation of the photonic wave function $\Phi(\omega_1, \omega_2) = \Phi(\omega_1, \sigma_1, \omega_2, \sigma_2) = \Phi_{\sigma_1 \sigma_2}(\omega_1, \omega_2)$.

The (unnormalized) probabilities $P_{\sigma_1 \sigma_2}(\tau_1, \tau_2)$ to detect one photon in a quantum state, which is characterized by σ_1 and another photon in a quantum state, which is characterized by σ_2 in the two-photon quantum state (1), have been obtained previously [23] and read

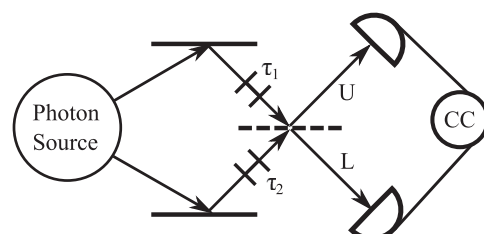


FIG. 1. Scheme of Hong-Ou-Mandel interference. Two photons are subject to optical delays $\tau_{1,2}$ and interfere on a common beam splitter to produce a joint detection statistic at the detectors U and L , which may be evaluated with a coincidence count (CC) logic.

$$\begin{aligned} P_{\sigma_1 \sigma_2}(\tau_1, \tau_2) = & \int d\omega_1 d\omega_2 [|\Phi_{\sigma_1 \sigma_2}(\omega_1, \omega_2)|^2 \\ & + |\Phi_{\sigma_2 \sigma_1}(\omega_2, \omega_1)|^2] + 2\Re \left\{ \int d\omega_1 d\omega_2 \right. \\ & \times \Phi_{\sigma_1 \sigma_2}(\omega_1, \omega_2) \Phi_{\sigma_2 \sigma_1}^*(\omega_2, \omega_1) \\ & \left. \times e^{-i(\omega_1 - \omega_2)(\tau_1 - \tau_2)} \right\}. \end{aligned} \quad (2)$$

We also call the probabilities $P_{\sigma_1 \sigma_2}(\tau_1, \tau_2)$ in (2) the *detection statistics* of a HOM experiment. Here, τ_1 and τ_2 are optical delays that can be applied independently to wave packets in HOM interferometry [24]. Note that the probabilities are always a function of the difference $\Delta\tau := \tau_1 - \tau_2$ as can be seen from (2). Nevertheless, we keep track of both delays τ_1 and τ_2 in our work since this will be necessary when considering relativistic effects on the detection statistics in Sec. IV.

B. Two-photon sources

In this section, apart from the frequency DOF, we consider the spatial DOF of the photons [i.e., $\sigma = (U, L)$] as the only left photonic DOF and do not consider, for instance, the polarization of the photons and so forth. We consider two-photon sources, which possess photonic wave functions that can be written in matrix form (see [23] for details) as

$$\Phi_{\sigma_1 \sigma_2}(\omega_1, \omega_2) = \phi(\omega_1, \omega_2) \begin{pmatrix} e^{i\theta} & +1 \\ -1 & -e^{-i\theta} \end{pmatrix}, \quad (3)$$

where θ is the phase associated with BS reflection. The row and column numbering of the matrix in (3) is U, L , and $\phi(\omega_1, \omega_2)$ is the joint photonic *spectral wave function*, for which we may impose w.l.o.g., the normalization condition $\int d\omega_1 d\omega_2 |\phi(\omega_1, \omega_2)|^2 = 1$.

Inserting (3) into (2) and computing the coincidence detection probability $P^c = P_{UL} + P_{LU}$; i.e., the probability to detect one photon at one detector U or L and the other photon at the other detector L or U yields after subsequent normalization (such that $P_{UU} + P_{LL} + P_{UL} + P_{LU} = 1$) the result

$$P^c(\tau_1, \tau_2) = \frac{1}{2} [1 - d_\phi(\tau_1, \tau_2)], \quad (4)$$

where

$$d_\phi(\tau_1, \tau_2) = 2\Re \left\{ \int d\omega_1 d\omega_2 \phi(\omega_1, \omega_2) \phi^*(\omega_2, \omega_1) e^{-i\Delta\omega\Delta\tau} \right\}, \quad (5)$$

with $\Delta\omega = \omega_1 - \omega_2$ and $\Delta\tau = \tau_1 - \tau_2$ containing the dependence on the optical delays τ_1 and τ_2 and depending on the spectral profile $\phi(\omega_1, \omega_2)$ of the two photons.

In Sec. IV, we investigate the influence of relativistic effects on HOM experiments that are operated with three different types of two-photon sources each owning a different two-photon spectral profile. We investigate a source of spectrally indistinguishable frequency uncorrelated photons (employed in the original work of Hong, Ou, and Mandel [20]) which features a spectral profile,

$$\phi_{\text{HOM}}(\omega_1, \omega_2) = f_\mu(\omega_1) f_\mu(\omega_2), \quad (6)$$

with

$$f_\mu(\omega) = \frac{1}{\sqrt{\sqrt{2\pi}\xi}} e^{-\frac{(\omega-\mu)^2}{4\xi^2}}. \quad (7)$$

Further, we investigate parametric down converting photon sources generating spectrally distinguishable frequency detuned photons with a spectral profile of

$$\phi_{\text{f.d.}}(\omega_1, \omega_2) = \sqrt{\frac{2}{\pi\xi}} \delta(\omega_p - \omega_1 - \omega_2) \text{sinc}\left(\frac{\omega_1 - \omega_2 - \mu}{\xi}\right), \quad (8)$$

where ω_p is the pump frequency of the down converting process, and μ is the frequency separation (or detuning) of the photons.

Lastly, we investigate sources of spectrally indistinguishable frequency entangled photons owning the spectral profile,

$$\phi_{\text{f.e.}}(\omega_1, \omega_2) = \mathcal{N}[\phi_{\text{f.d.}}(\omega_1, \omega_2) + e^{i\varphi} \phi_{\text{f.d.}}(\omega_2, \omega_1)], \quad (9)$$

with $\mathcal{N}^{-2} = 2\mu(1 + \cos(\varphi)\text{sinc}(2\mu/\xi))$. In all expressions (6), (8), and (9), ξ is the single-photon bandwidth. Inserting (6), (8), and (9) into (5) yields

$$d_{\phi_{\text{HOM}}}(\tau_1, \tau_2) = e^{-\xi^2 \Delta\tau^2}. \quad (10a)$$

$$d_{\phi_{\text{f.d.}}}(\tau_1, \tau_2) = S_{\mu\xi}(\tau_1, \tau_2) \quad (10b)$$

$$d_{\phi_{\text{f.e.}}}(\tau_1, \tau_2) = 2\mu\mathcal{N}^2[R_{\mu\xi}(\tau_1, \tau_2) + S_{\mu\xi}(\tau_1, \tau_2)], \quad (10c)$$

with

$$S_{\mu\xi}(\tau_1, \tau_2) = \frac{\sin\left(\frac{2\mu}{\xi} \text{tri}\left(\frac{\xi\Delta\tau}{2}\right)\right)}{\frac{2\mu}{\xi}} \quad (11a)$$

$$R_{\mu\xi}^\varphi(\tau_1, \tau_2) = \cos(\mu\Delta\tau - \varphi) \text{tri}\left(\frac{\xi\Delta\tau}{2}\right), \quad (11b)$$

where

$$\text{tri}(x) = \begin{cases} 1 - |x| & \text{if } |x| \leq 1 \\ 0 & \text{if } |x| > 1 \end{cases} \quad (12)$$

is the *triangular function*.

We want to briefly discuss some of the most important features of the interference patterns (10a)–(10c) of the three light sources. In the absence of spectral entanglement, photon antibunching (i.e., $P^c > 1/2$) cannot occur [25]. In particular, this holds true for the frequency uncorrelated photon source of the original HOM experiment [20] as seen from (10a). This contrasts with the other two interference pattern, which both show a periodic change between photon bunching and photon antibunching in the delay $\Delta\tau$ with oscillation frequency μ . This phenomenon is termed quantum beating [26] and is characteristic in the presence of spectral entanglement. Indeed both spectra (8) and (9) contain spectral entanglement as they do not factorize into single-particle spectral [27]. However, there is a striking difference between frequency detuned and frequency entangled photons, namely that the interference term (10b) of frequency detuned photons vanishes for increasing frequency separations μ where the one of frequency entangled photons (10c) does not. As extensively discussed in [23], the physical reason for this is the increasing spectral distinguishability of frequency detuned photons, which grows for larger values of μ and thus, suppresses both photon bunching and photon antibunching. Mathematically perfect spectral distinguishability is expressed through a vanishing overlap of the spectral wave function with itself under exchange of the function arguments, i.e., $\lim_{\mu \rightarrow \infty} \int d\omega_1 d\omega_2 \phi_{\text{f.d.}}(\omega_1, \omega_2) \phi_{\text{f.d.}}^*(\omega_2, \omega_1) = 0$, which forces the interference term (5) to vanish. This is different in the case of frequency entangled photons, which preserve their spectral indistinguishability, also for larger values of μ . Therefore, in contrast to the other two cases with frequency entangled photons, we can achieve the following: In the limit $\mu \rightarrow \infty$, the occurrence of photon bunching or photon antibunching is highly sensitive to a change in the optical delay $\Delta\tau = \tau_1 - \tau_2$. This fact will become important when we consider relativistic effects on HOM interference in Sec. IV.

III. RELATIVISTIC DEFORMATION OF SPECTRAL WAVE FUNCTION

We now include relativistic effects. More concretely, we show that different observers would assign different spectral wave functions to the same (multi)photon quantum state. A more detailed view on the topic in the single-particle sector is left to the literature [14,15,28].

A. Quantum fields in curved spacetime

The starting point is to describe the light field as an uncharged massless real scalar field ϕ for the sake of simplicity and without loss of generality. The field ϕ obeys the massless Klein-Gordon equation,

$$(\sqrt{-g})^{-1} \partial_\mu (\sqrt{-g} g^{\mu\nu} \partial_\nu \phi) = 0, \quad (13)$$

where $g_{\mu\nu}$ is the metric tensor of the underlying spacetime, and g is its determinant [28].¹ If the spacetime is stationary, it possess a timelike Killing vector field, which is ∂_ξ , and elements of the metric tensor are independent of the time ξ . In our case, we consider that the time parameter coincides with the coordinate time t , and therefore, invariance of the metric under translations induced by the Killing vector field ∂_t implies energy conservation. In turn, this allows one to decompose any solution of the Klein-Gordon equation into energy eigenstates $\phi_{\mathbf{k}}$ as $\phi = \int d^3k [\alpha_{\mathbf{k}} \phi_{\mathbf{k}} + \alpha_{\mathbf{k}}^* \phi_{\mathbf{k}}^*]$. Here, \mathbf{k} collects the relevant quantum numbers, $\{\alpha_{\mathbf{k}}\}$ are Fourier coefficients for the classical field expansion, and $i\partial_t \phi_{\mathbf{k}} = \omega_{\mathbf{k}} \phi_{\mathbf{k}}$ is the eigenvector equation for the modes $\phi_{\mathbf{k}}$, where $\omega_{\mathbf{k}}$ is the (positive) eigenvalue. Canonical quantization promotes the expansion coefficients $\alpha_{\mathbf{k}}^*$ and $\alpha_{\mathbf{k}}$ of this decomposition into creation and annihilation operators $\hat{a}_{\mathbf{k}}^\dagger$ and $\hat{a}_{\mathbf{k}}$, respectively. These operators satisfy the canonical commutation relations $[\hat{a}_{\mathbf{k}}, \hat{a}_{\mathbf{k}'}^\dagger] = \delta^3(\mathbf{k} - \mathbf{k}')$.

B. Single-photon wave packet deformation

Full characterization of a realistic photon would require the use of electrodynamics in curved spacetime, which can be extremely cumbersome and might obfuscate the final results. Here, we choose to follow another route.

In the past decade, a new body of work has developed the theory of photons propagating in (weakly) curved spacetime from different perspectives [14,15,29,30]. We assume that a photon can be indeed modeled by using a massless scalar field, and that it is effectively strongly confined to the direction of propagation in a (weakly curved) static spacetime. In this way, we can effectively assume that the photon is localized along a lightlike path, and therefore, we can ignore the deformation effects that occur in the perpendicular directions [29,30]. Nevertheless, we expect that the gravitational redshift will still affect the photon, and this effect in the context of a localized wavepacket has been pioneered in the literature [14,15].

We therefore characterize a single photon generated by a photon source through the spectral emission profile $\Phi(\omega)$ by the creation operator,

$$\hat{A}^\dagger(t) = \mathcal{N}_{\psi_1} \int d\omega \Phi(\omega) e^{i\omega t} \hat{a}_\omega^\dagger, \quad (14)$$

where t is the coordinate time, and \mathcal{N}_{ψ_1} is a normalization constant specified further below. The corresponding single-photon quantum state is

$$|\psi_1(t)\rangle = \hat{A}^\dagger(t)|0\rangle. \quad (15)$$

¹We employ Einstein summation convention. The metric has signature $(-, +, +, +)$.

The same photon as seen from a moving observer K exploring the proper time τ_K would be described by the creation operator $\hat{A}_K^\dagger(\tau_K)$, which has been computed in the literature [14,15], and reads

$$\hat{A}_K^\dagger(\tau_K) = \int_0^\infty d\omega_K \Phi^K(\omega_K) e^{i\omega_K \tau_K} \hat{a}_{\omega_K}^\dagger. \quad (16)$$

Thus, different observers K will assign different spectral distributions $\Phi^K(\omega_K)$ to the very same photon. In particular, they will define the single photon quantum states $|\psi_1(\tau_K)\rangle$ as

$$|\psi_1(\tau_K)\rangle = \hat{A}_K^\dagger(\tau_K)|0\rangle, \quad (17)$$

where the relation between the spectra $\Phi^K(\omega_K)$ of two observers Alice and Bob, with $K = A, B$ respectively, has been computed in the literature [14], and is given by

$$\phi^B(\omega_B) = \sqrt{\frac{1}{1 + z_{AB}}} \Phi^A(\omega_A). \quad (18)$$

Here, we have used the defining relation between the frequencies as measured locally by Alice and Bob, which reads

$$\omega_A = \frac{\omega_B}{1 + z_{AB}}, \quad (19)$$

where z_{AB} is the mutual redshift between observer A and B as defined in [31]. The relations (18) and (19) follow from requiring Eq. (17) to yield proportional results for $K = A$ and $K = B$ [i.e., $|\psi_1(\tau_B)\rangle \propto |\psi_1(\tau_A(\tau_B))\rangle$] together with the normalization condition,

$$(\mathcal{N}_{\psi_1})^{-2} = \int d\omega_K |\Phi^K(\omega_K)|^2, \quad (20)$$

which ensures $\langle\psi_1(\tau_K)|\psi_1(\tau_K)\rangle = 1$ in all frames. Note that Eqs. (16)–(19) are only valid approximations in a weakly curved spacetime [14,15]. They become exact in the case that $K = A, B$ are inertial observers in flat a spacetime [32].

As mentioned above, we here only consider the spectral aspects of the light field since we use the Klein-Gordon equation, which is a good approximation to the longitudinal (or transverse) modes of the electromagnetic field in scalar optics. A description of the observer dependent transformation properties of other DOFs of the light field, such as the helicity or the light's orbital momentum, would amount for a more elaborated treatment of the electromagnetic field. For this, one would have to quantize Maxwell's equations on a curved spacetime background.

However, we proceed with a description within scalar optics and (artificially) incorporate the other photonic DOFs by describing single photon states using a generalized version of the creation operator (16), which reads

$$\hat{A}_K^\dagger(\tau_K) = \int_0^\infty d\omega_K \Phi^K(\omega_K) e^{i\omega_K \tau_K} \hat{a}_{\omega_K}^\dagger, \quad (21)$$

where we defined the entire set of photonic DOFs as $\omega_K := \{\omega_K, \sigma\}$, and σ is the set of photonic DOFs excluding for the photons frequency ω_K . Clearly, these DOFs are those potentially measured by from an observer K. The observer dependent photonic wave function is $\Phi^K(\omega_K)$, which we alternatively write as $\Phi_\sigma^K(\omega_K) = \Phi^K(\omega_K)$.

C. Two-photon wave packet deformation

We now turn to the description of two photons. In analogy to (15), we can write a general two-photon state, which is a solution of the Klein-Gordon equation (with a stationary metric), as

$$|\psi_2(t)\rangle = \mathcal{N}_{\psi_2} \int d\omega_1 d\omega_2 \Phi(\omega_1, \omega_2) e^{i\omega_1 t} e^{i\omega_2 t} |1_{\omega_1} 1_{\omega_2}\rangle, \quad (22)$$

where $|1_{\omega_1} 1_{\omega_2}\rangle := \hat{a}_{\omega_1}^\dagger \hat{a}_{\omega_2}^\dagger |0\rangle$, and \mathcal{N}_{ψ_2} is a normalization constant, which we specify further below.

Now we work out how this quantum state is characterized by two observers K_1 and K_2 both moving in a curved spacetime. Our aim is to find a generalization of the transformation (18) and (19) for the two-photon spectral wave function $\Phi^{K_1 K_2}(\omega_{K_1}, \omega_{K_2})$ as seen by the observer pair K_1, K_2 . However, a straightforward generalization to the single particle case here is not possible as quantum fields (and, in particular, those of several distant particles) in quantum field theory are inherently nonlocal objects where the notion of an observer from general relativity is strictly local [14].

In a first attempt, we follow a simplified approach and consider inertial observers moving in a flat spacetime geometry, which is the extreme case of considering a weakly curved spacetime and small accelerations. This has the advantage that all observers in this scenario share a common vacuum state, and therefore, a common notion of particles, and thus circumvents the conceptional problems related to nonlocality in curved spacetimes. Nevertheless, also in this simplified approach, the mutual redshift between all considered observers among each other and with respect to the photon source enters in a nontrivial way, such that one can study the most basic spectral aspects of HOM interferometry under relativistic influences. Once we have worked out how the measurement outcome of a HOM experiment is influenced by a mutual redshift between the

observers among each other and with respect to the photon source, we can replace the redshift in the resulting formulas by the gravitational redshift to get an estimate of general relativistic influences on the measurement outcome of HOM experiments under the assumption of weakly curved spacetimes and small accelerations. It is crucial to note that from now on, since we consider two photons, all measurements have to be considered with respect to two observers or an *observer pair*. This also includes the special case where the two considered observers in a pair coincide.

In analogy to (21), we make the ansatz to characterize two-photon states as seen from two observers K_1 and K_2 (the corresponding observer pair is denoted as K_1, K_2) as

$$|\psi_2(\tau_{K_1}, \tau_{K_2})\rangle = \mathcal{N}_{\psi_2} \int_0^\infty d\omega_{K_1} d\omega_{K_2} \Phi^{K_1 K_2}(\omega_{K_1}, \omega_{K_2}) \\ \times e^{i\omega_{K_1}\tau_{K_1}} e^{i\omega_{K_2}\tau_{K_2}} a_{\omega_{K_1}}^\dagger a_{\omega_{K_2}}^\dagger |0\rangle, \quad (23)$$

where now $\Phi^{K_1 K_2}(\omega_{K_1}, \omega_{K_2}) \equiv \Phi_{\sigma_1 \sigma_2}^{K_1 K_2}(\omega_{K_1}, \omega_{K_2}) = \Phi^{K_1 K_2}(\omega_{K_1}, \omega_{K_2})$ is the joint two-photon wave function as seen from the observers K_1 and K_2 , and \mathcal{N}_{ψ_2} is a normalization constant in order to fulfill $\langle \psi_2 | \psi_2 \rangle = 1$ in all frames, which is determined by

$$(\mathcal{N}_{\psi_2}^2)^{-2} = \int d\omega_{K_1} d\omega_{K_2} |\Phi_S^{K_1 K_2}(\omega_{K_1}, \omega_{K_2})|^2, \quad (24)$$

where we defined the symmetrized two-photon wave function $\Phi_S^{K_1 K_2}(\omega_{K_1}, \omega_{K_2}) = (\Phi^{K_1 K_2}(\omega_{K_1}, \omega_{K_2}) + \Phi^{K_1 K_2}(\omega_{K_2}, \omega_{K_1}))/\sqrt{2}$. The normalization constant (24) reflects the fact that only the symmetric part of the photonic wave function is of physical relevance as photons are bosons. Indeed, one can use the canonical commutator relations to rewrite the two-photon state (23) solely in terms of the symmetrized wave function $\Phi_S^{K_1 K_2}(\omega_{K_1}, \omega_{K_2})$. Also, if one does not use symmetrized photonic wave functions, the second quantization formalism automatically accounts only for the symmetric part of the photonic wave function.

In Eq. (23), the parameters τ_{K_1} and τ_{K_2} are the lapse that the respective observers associate to the separate phase in their local time. The ansatz (23) is exact in case of inertial observers K_1 and K_2 in a flat spacetime [32]. Now we want to analyze how the joint spectral profile of two photons as seen from a given pair of inertial observers, say $K_1 = A_1$ and $K_2 = A_2$, changes when seen from a different pair of inertial observers, say $K_1 = B_1$ and $K_2 = B_2$. In analogy to the single photon case, we require

$$|\psi_2(\tau_{B_1}, \tau_{B_2})\rangle \propto |\psi_2(\tau_{A_1}(\tau_{B_1}), \tau_{A_2}(\tau_{B_2}))\rangle, \quad (25)$$

under the normalization condition (24). This yields the relation,

$$\Phi_{\sigma_1 \sigma_2}^{B_1 B_2}(\omega_{B_1}, \omega_{B_2}) = \sqrt{\frac{1}{(1+z_{A_1 B_1})(1+z_{A_2 B_2})}} \\ \times \Phi_{\sigma_1 \sigma_2}^{A_1 A_2}(\omega_{A_1}, \omega_{A_2}), \quad (26)$$

where we have

$$\omega_{A_i} = \frac{\omega_{B_j}}{1+z_{A_i B_j}}, \quad i, j = 1, 2, \quad (27)$$

and $z_{A_i B_j}$ as before being the mutual redshift between the two observers A_i and B_j . One can check that photonic wave functions obeying the transformation behavior of Eqs. (26) and (27) fulfill the requirements defined by (24) and (25).

Note that Eq. (26) only depends on the mutual redshifts $z_{A_1 B_1}$ and $z_{A_2 B_2}$ of the first and second observer in an observer pair respectively but not on the redshifts $z_{A_1 B_2}$ and $z_{A_2 B_1}$. It might therefore appear that our formalism is able to extract the which-path information and that our results may vary if one exchanges the two observers of an observer pair. However, this is not the case. To see this, we first note that the prefactor of (26) is invariant under the exchange of the observers of one observer pair, because $(1+z_{A_1 B_1})(1+z_{A_2 B_2}) = (1+z_{A_1 B_2})(1+z_{A_2 B_1}) = (1+z_{A_1 B_1})(1+z_{A_2 B_1})$, which follows from the transitivity property of the redshift [33] and can be inferred from (27). Secondly, as only the symmetrized (transformed) photonic wave function $(\Phi_{\sigma_1 \sigma_2}^{B_1 B_2}(\omega_{B_1}, \omega_{B_2}) + \Phi_{\sigma_1 \sigma_2}^{B_1 B_2}(\omega_{B_2}, \omega_{B_1}))\sqrt{2}$ enters the calculations, it follows that the expression (26) is fully invariant under the exchange of A_1 with A_2 and B_1 with B_2 .

The relations (26) and (27) quantify the deformation of the joint spectral distribution of the two-photon state (23) when seen from different pairs of inertial observers in a flat spacetime. Note that the here presented framework is also capable to describe the spectral aspects of moving interference experiments like the Sagnac-interferometer [34,35]. Also simple phenomena like the change in frequency of a light beam when it is reflected on a moving mirror can be described with this framework. Moreover, the generalization to three, four, and more photons is straightforward.

IV. RELATIVISTIC INFLUENCE ON HOM INTERFERENCE

We are now equipped with the tools necessary to quantify the changes of the interference pattern of a HOM experiment subject to the relativistic frequency shift. The validity of Eq. (2) in a local inertial frame is well confirmed by many experiments [20,26,36–38]. Thus, we assume that Eq. (2) locally holds true; that is, we replace the optical delays τ_1 and τ_2 in (2) by optical delays τ_{K_1} and τ_{K_2} as measured in the proper time of the respective observer K_1 and K_2 , applying the respective optical delay. Furthermore, we replace the two-photon wave function $\Phi_{\sigma_1 \sigma_2}(\omega_1, \omega_2)$, which enters Eq. (2) by the corresponding

two-photon wave function $\Phi_{\sigma_1 \sigma_2}^{K_1 K_2}(\omega_1, \omega_2)$ as seen by the observer pair K_1, K_2 . Accordingly, we can write the relativistic version of (2) as

$$\begin{aligned} \tilde{P}_{\sigma_1 \sigma_2}^{K_1 K_2}(\tau_{K_1}, \tau_{K_2}) &= \int d\omega_1 d\omega_2 [|\Phi_{\sigma_1 \sigma_2}^{K_1 K_2}(\omega_1, \omega_2)|^2 \\ &\quad + |\Phi_{\sigma_2 \sigma_1}^{K_1 K_2}(\omega_2, \omega_1)|^2] \\ &\quad + 2\Re \left\{ \int d\omega_1 d\omega_2 \Phi_{\sigma_1 \sigma_2}^{K_1 K_2}(\omega_1, \omega_2) \right. \\ &\quad \times \left. \Phi_{\sigma_2 \sigma_1}^{K_1 K_2*}(\omega_2, \omega_1) e^{-i(\omega_1 - \omega_2)(\tau_{K_1} - \tau_{K_2})} \right\}. \end{aligned} \quad (28)$$

To obtain the normalized probabilities of a certain detection event, which is characterized by σ_1 and σ_2 , one has to compute

$$P_{\sigma_1 \sigma_2}^{K_1 K_2}(\tau_{K_1}, \tau_{K_2}) = \frac{\tilde{P}_{\sigma_1 \sigma_2}^{K_1 K_2}(\tau_{K_1}, \tau_{K_2})}{\int d\sigma_1 d\sigma_2 \tilde{P}_{\sigma_1 \sigma_2}^{K_1 K_2}(\tau_{K_1}, \tau_{K_2})}. \quad (29)$$

Note that Eq. (28) is invariant under the exchange of τ_{K_1} and τ_{K_2} . This means that our formalism does not depend on the information of which observer of an observer pair applies which optical delay.

Equations (28) and (29) are central results of the present paper as they capture the observer dependence of the spectral aspects of HOM interference. The dependence of the proper times τ_{K_1} and τ_{K_2} describes how the interference pattern changes when recorded by different observer pairs, and the dependence on the wave function $\Phi_{\sigma_1 \sigma_2}^{K_1 K_2}(\omega_1, \omega_2)$ as seen by the respective observer pair reflects the influence of a redshift between the light source and the observers on the interference pattern.

We employ Eqs. (26), (28), and (29) to obtain the relation between the interference patterns obtained by two distinct observer pairs,

$$P_{\sigma_1 \sigma_2}^{B_1 B_2}(\tau_{B_1}, \tau_{B_2}) = P_{\sigma_1 \sigma_2}^{A_1 A_2}(\tau_{A_1}, \tau_{A_2}), \quad (30)$$

where the relation between the delays τ_{A_i} and τ_{B_i} reads

$$\tau_{A_i} = (1 + z_{A_i B_i}) \tau_{B_i}, \quad i = 1, 2. \quad (31)$$

Note that Eq. (31) is precisely the relation that tells how much the (proper) time τ_{A_i} has evolved on the world line of observer A_i , when a (proper) time of τ_{B_i} has evolved on the world line of observer B_i [39]. Equations (30) and (31) relate the interference patterns of two HOM experiments, which are done by two different observer pairs A_1, A_2 and B_1, B_2 featuring a mutual redshift to each other.

In the following, we always assume that Alice operates the two-photon source and distributes the photons.

However, also Alice can measure the HOM-interference pattern of the photon source. If the photon source, all reflecting elements and detectors rest in the local inertial frame of Alice, she defines an observer pair A_1, A_2 . Therefore $P_{\sigma_1 \sigma_2}^{A_1 A_2}(\tau_{A_1}, \tau_{A_2})$ is the corresponding interference pattern of the photon source in the local rest frame of the same, i.e., the source specific interference pattern of the considered photon source without relativistic effects. However, Alice can also send the photons to another observer pair B_1, B_2 (Bob), who, in this case, would record the interference pattern $P_{\sigma_1 \sigma_2}^{B_1 B_2}(\tau_{B_1}, \tau_{B_2})$, which is related to interference pattern $P_{\sigma_1 \sigma_2}^{A_1 A_2}(\tau_{A_1}, \tau_{A_2})$ via Eqs. (30) and (31). Alice might provide the photons to yet another observer pair C_1, C_2 (Charlie), who would record the interference pattern $P_{\sigma_1 \sigma_2}^{C_1 C_2}(\tau_{C_1}, \tau_{C_2})$, which is related to interference pattern $P_{\sigma_1 \sigma_2}^{A_1 A_2}(\tau_{A_1}, \tau_{A_2})$ by replacing B_1 and B_2 in Eqs. (30) and (31) by C_1 and C_2 . From the transitivity property of the redshift [which we discussed below Eq. (27)], we can obtain the relations between the interference pattern recorded by Bob's and Charlie's observer pairs, and they are given by simply replacing A_1 and A_2 in Eqs. (30) and (31) by C_1 and C_2 . Interestingly, this implies that the relation between the interference patterns respectively recorded by Bob's and Charlie's observer pair does not depend on the mutual redshift w.r.t. the photon source (i.e., to Alice' observer pair) but only on the mutual redshift between Bob's and Charlie's observer pairs. This might be interesting for Geodesy, where Bob and Charlie are provided with photons from a common light source and can infer information about the geometry of spacetime, solely by comparing their HOM-interference patterns with each other, without knowledge about the actual state of motion and the position of the light source. However, each of the interference pattern recorded by Bob and Charlie depend on the mutual redshift with respect to the photon source, which can be quantified by considering the observer pairs B_1, B_2 or C_1, C_2 on one side and the pair A_1, A_2 on the other side of Eqs. (30) and (31).

Note that Eq. (30) also accounts for the situation in which the two photons explore different redshifts (i.e., $z_{A_1 B_1} \neq z_{A_2 B_2}$) when propagating between the photon source and the two different receivers. Such scenario would be of interest for the study of the spectral aspects of the Sagnac-effect in HOM interference [34], where the emission direction of the two photons from the photon source can have different angles with respect to the velocity vector of the photon source, thereby leading to different Doppler shifts between the photons.

For the rest of this work, we consider a simplified situation, in which the two photons are received by the receiving observers with the same total redshift with respect to the emitter. This would occur, for instance, in the case when the two photons are generated by a source that rests on Earth and are sent to a moving satellite where they are

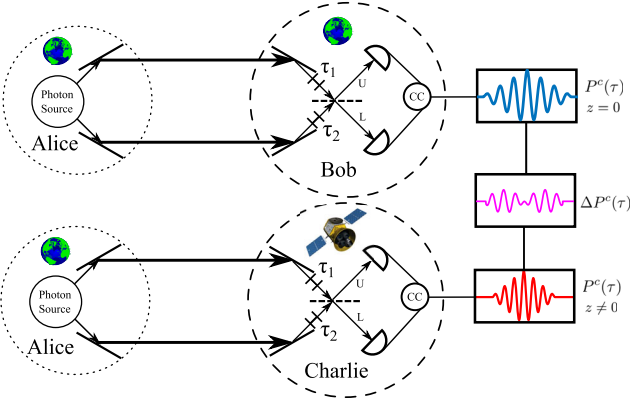


FIG. 2. Top: HOM experiment without relativistic influence (i.e., vanishing redshift $z = 0$). Bottom: HOM experiment with relativistic influence (i.e., nonvanishing redshift $z \neq 0$). The dotted circles indicate the location, where the photons are generated (in both cases by Alice on Earth). The location where the coincidence statistics are recorded (by Bob on Earth in the upper plot and on a moving satellite by Charlie in the lower plot) are indicated by dashed circles, which we term detection instance. The graphs on the right side represent the coincidence interference pattern, which is recorded at the respective detection instance Bob and Charlie. Bob on Earth records the blue curve and Charlie on a satellite records the red one. Both Bob and Charlie apply optical delays τ_1 and τ_2 in units of their local proper times respectively. Due to the different redshifts between the photon source and the respective detection instance, slightly different coincidence interference patterns are recorded, and their difference is displayed by the purple curve.

received from a similar direction (to avoid additional Doppler shifts between the photons). Onboard the satellite, optical delays are employed (in units of the proper time of the satellite). This situation is illustrated in Fig. 2. There it is seen that we consider a photon source held by Alice who is situated on Earth and who sends photon pairs to Bob, who is situated on Earth as well. The mutual redshift between Alice and Bob is zero, i.e., $z_{A_1B_1} = z_{A_2B_2} = 0$. In other words, Bob is located in the same local rest frame as the photon source. In a second scenario, Alice sends the photon pair to Charlie, who is situated on a satellite and has a nonvanishing redshift with respect to Alice, i.e., $z_{A_1C_1} = z_{A_2C_2} =: z$. Both Bob and Charlie make a coincidence measurement and record the interference profile by tuning their optical delays (in units of their own proper times). The effects of the redshift between the photon source (dotted circle) and Charlie's detection instance (dashed circle) will lead to a difference (purple curve in Fig. 2) of his interference pattern (red curve) with respect to the one recorded by Bob (blue curve). We now quantify this difference.

We are interested in the difference $\Delta P_{\sigma_1\sigma_2}(\tau_1, \tau_2)$ between the interference patterns of Bob and Charlie defined by

$$\Delta P_{\sigma_1\sigma_2}(\tau_1, \tau_2) = P_{\sigma_1\sigma_2}^{C_1C_2}(\tau_1, \tau_2) - P_{\sigma_1\sigma_2}^{B_1B_2}(\tau_1, \tau_2). \quad (32)$$

Notice that, as we have mentioned before, this difference is obtained operationally by recording the interference pattern *with respect to the proper time* and then exchanging the pattern to be compared.

Bob is located at the same height as Alice in the gravitational potential, and therefore has a vanishing redshift with respect to the photon source; i.e., we have $P_{\sigma_1\sigma_2}^{B_1B_2}(\tau_1, \tau_2) = P_{\sigma_1\sigma_2}^{A_1A_2}(\tau_1, \tau_2)$. Assuming a common mutual redshift between the input ports of Charlie's measurement apparatus with respect to the photon source, i.e., $z_{A_1C_1} = z_{A_2C_2} = z$, we know that $P_{\sigma_1\sigma_2}^{C_1C_2}(\tau_1, \tau_2) = P_{\sigma_1\sigma_2}^{A_1A_2}((1+z)\tau_1, (1+z)\tau_2)$, and Eq. (32) simplifies to

$$\Delta P_{\sigma_1\sigma_2}(\tau_1, \tau_2) = P_{\sigma_1\sigma_2}^{A_1A_2}((1+z)\tau_1, (1+z)\tau_2) - P_{\sigma_1\sigma_2}^{A_1A_2}(\tau_1, \tau_2). \quad (33)$$

It is clear from (33) that Bob's results act as a reference, and therefore, $\Delta P_{\sigma_1\sigma_2}(\tau_1, \tau_2) = 0$ when $z = 0$.

We then let $P^c(\tau_1, \tau_2)$ be the coincidence detection probability of the two-photon source in the local inertial frame of the photon source. From Eq. (33), we can compute the difference $\Delta P^c(\tau_1, \tau_2)$ between the coincidence probabilities of two HOM experiments with and without relativistic influence, which reads

$$\Delta P^c(\tau_1, \tau_2) = P^c((1+z)\tau_1, (1+z)\tau_2) - P^c(\tau_1, \tau_2). \quad (34)$$

To see this, note that the coincidence probability $P^c(\tau_1, \tau_2)$ is just a linear combination of the probabilities $P_{\sigma_1\sigma_2}(\tau_1, \tau_2)$ of specific detection events (with respect to any observer pair).

In case of all three light source types, which were considered in Sec. II, the coincidence probabilities were always functions of the delay $\Delta\tau = \tau_1 - \tau_2$, and they were all of the form,

$$P^c(\Delta\tau) = \frac{1}{2}(1 - d(\Delta\tau)), \quad (35)$$

where $d(\Delta\tau)$ depends on the joint spectral distribution of the respectively employed light source [cf. Eqs (5)]. Then, the difference between the coincidence detection probabilities as a function of the redshift and the delay reads

$$\Delta P^c(\Delta\tau) = \frac{1}{2}(d((1+z)\Delta\tau) - d(\Delta\tau)). \quad (36)$$

In case of the traditional HOM experiment employing polarization entangled photons with the joint spectral distribution (6), the difference of the coincidence detection probability reads

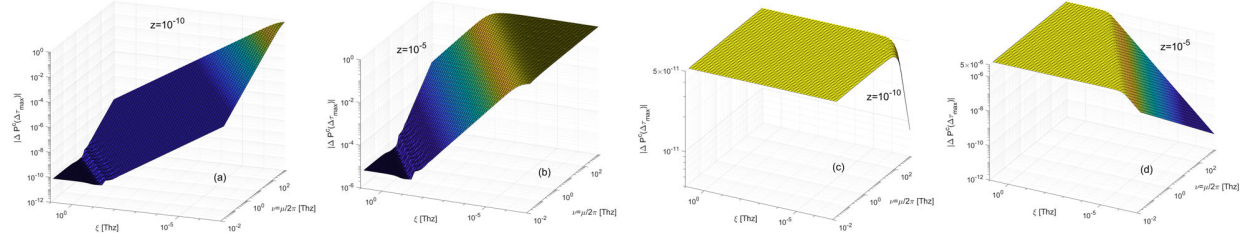


FIG. 3. All plots show the absolute value of the maximum discrepancy $|P^c(\Delta\tau_{\max})|$ (i.e., the impact of the relativistic redshift on HOM interference) as a function of the frequency separation ν and the single photon band width ξ . The upper plots show the influence of a redshift of (a) $z = 10^{-10}$ and (b) $z = 10^{-5}$ on a HOM experiment employing frequency entangled photons. The lower plots show the influence of a redshift of (c) $z = 10^{-10}$ and (d) $z = 10^{-5}$ on a HOM experiment employing frequency-detuned polarization-entangled photons. It can be seen that in the case of frequency entangled photons adjusting the experimental parameters ν to higher values and ξ to lower values amplifies the relativistic influence on the HOM-interference pattern. In case of frequency-detuned polarization-entangled photons, the maximum discrepancy of $|P^c(\Delta\tau_{\max})| \approx z/2$ cannot be exceeded by a parameter adjustment. The plots (a) and (b) are computed with Eq. (10c) for $\varphi = 0$ and the plots (c) and (d) are computed with Eq. (10b).

$$\Delta P^c(\Delta\tau) = \frac{1}{2} (e^{-\xi^2(1+z)^2\Delta\tau^2} - e^{-\xi^2\Delta\tau^2}), \quad (37)$$

which reaches its maximum at a delay of

$$\Delta\tau_{\max} = \frac{1}{\xi} \sqrt{2 \frac{\ln(1+z)}{z(2+z)}}. \quad (38)$$

The maximum value of the difference is independent of the bandwidth ξ of the photon source, since there is only one timescale $1/\xi$ that can be absorbed in the definition of time, and it reads

$$\Delta P^c(\Delta\tau_{\max}) = \frac{1}{2} \left[(1+z)^{-\frac{2(1+z)^2}{z(2+z)}} - (1+z)^{-\frac{2}{z(2+z)}} \right]. \quad (39)$$

This result shows that it would be extremely difficult to measure the influence of the redshift using the scheme described here in a practical scenario. In fact, a discrepancy of only 1% (i.e., $\Delta P^c(\Delta\tau_{\max}) = 0.01$) would require the experimenter to achieve a redshift of the order of $z \approx 0.01$, which is about three orders of magnitude higher than the strongest redshifts (mainly caused by the Doppler-effect) between two satellites counter orbiting around the Earth ($z \approx 10^{-5}$). Since Eq. (39) is independent of the bandwidth ξ , achieving lower bandwidths will not amplify the influence of relativistic effects.

This is however different if one employs a source of frequency entangled photons with a joint frequency profile of (9), which leads to the difference of the coincidence probability (36), where one has to use the function $d(\Delta\tau)$ from Eq. (10c). Figure 4 shows the difference between the coincidence detection probabilities of two HOM experiments with and without the influence of a redshift of $z = 10^{-10}$ for different frequency separations $\nu = \mu/2\pi$ as a function of the delay $\Delta\tau = \tau_1 - \tau_2$. It can be seen that the maximum discrepancy is achieved for a delay,

$$\Delta\tau_{\max} \approx \frac{1}{\xi}. \quad (40)$$

The reason therefore is explained below. Furthermore, it can be seen that the absolute value of the maximum discrepancy $|\Delta P^c(\Delta\tau_{\max})|$ increases with increasing frequency separation $\nu = \mu/2\pi$ (also explained below).

Figures 3(a) and 3(b) show the result of the absolute value of the maximum (maximized over the delay $\Delta\tau$) difference $|\Delta P^c(\Delta\tau_{\max})|$ as a function of the experimental parameters ξ and μ under the influence of a redshift $z = 10^{-10}$ [Fig. 3(a)] and $z = 10^{-5}$ [Fig. 3(b)]. It can be seen that the influence of the relativistic redshift on the coincidence probability increases for higher frequency separations μ and for lower single photon bandwidths ξ and for larger redshifts z . Therefore, the most interesting parameter regime is the limit $\mu/\xi \rightarrow \infty$, where the function (10c) is well approximated by $d(\Delta\tau) \approx R_{\mu\xi}^\varphi(\Delta\tau)$ with $R_{\mu\xi}^\varphi(\Delta\tau)$ taken from (11b). Thus, the difference of the joint detection probabilities is approximately

$$\Delta P^c(\Delta\tau) \approx \frac{1}{2} (R_{\mu\xi}^\varphi((1+z)\Delta\tau) - R_{\mu\xi}^\varphi(\Delta\tau)). \quad (41)$$

Our numeric calculations yield that there is no qualitative difference between the results shown in Fig. 3 for different values of φ in the parameter region of interest $\mu \gg \xi$. This is why from here on we proceed our discussion for $\varphi = 0$.

We see from (41) for $\varphi = 0$ that the (absolute value of the) difference of the cosine functions $\cos(\mu(1+z)\Delta\tau) - \cos(\mu\Delta\tau)$ increases for larger delays $\Delta\tau$, but the increase of this difference is suppressed due to the triangular function appearing in (11b) such that Eq. (40) is a good approximation for the delay time at which the discrepancy (41) is maximized. Inserting (40) in (41) and making a power series expansion around $z = 0$ yields to first order in z

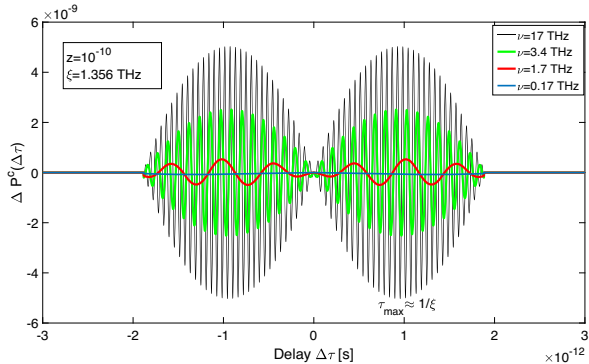


FIG. 4. Difference $\Delta P^c(\Delta\tau)$ [see Eq. (36)] between the coincidence detection probabilities of two HOM experiments with frequency entangled photons [see Eq. (9) for spectral profile] under the influence of a redshift $z = 10^{-10}$ for different frequency separations ν . The plot is shown for $\varphi = \pi$.

$$\Delta P^c(\Delta\tau_{\max}) = \frac{\mu}{4\xi} \sin\left(\frac{\mu}{2\xi}\right) z + \mathcal{O}(z^2). \quad (42)$$

The occurrence of the sine function in (42) is rooted in the oscillating behavior of $\Delta P^c(\Delta\tau)$ as seen in Fig. 4. We are only interested in the envelope of the difference $\Delta P^c(\Delta\tau)$ in Fig. 4 and therefore set the value of the sine-function in (42) equal to one; i.e., we get

$$\Delta P^c(\Delta\tau_{\max}) \approx \frac{\mu}{4\xi} z. \quad (43)$$

We confirmed the validity of the approximation (43) numerically within an accuracy of less than 1% for the parameter values for μ and ξ shown in Figs. 3(a) and 3(b) under the condition $\mu/\xi > 1$ and $\Delta P^c(\Delta\tau_{\max}) < 0.9$.

Equation (43) is a rough error estimation for technologies based on HOM interference with frequency entangled photons, such as remote clock synchronization [21], since it quantifies the influence of the redshift between the photon source and the measurement laboratory on the coincidence statistics.

From (43), we obtain an estimate for the ratio of the frequency separation to the single photon bandwidth μ/ξ , which must be achieved in an experiment with a given detector resolution ΔP_{res}^c in order to resolve the influence of a given redshift z . We find

$$\frac{\mu}{\xi} = \frac{4\Delta P_{\text{res}}^c}{z}. \quad (44)$$

Equation (44) is a benchmark for future experiments, which intend to reveal the influence of the relativistic redshift on the coincidence probability of a HOM experiment employing frequency entangled photons. For instance, assuming a quite moderate detector resolution of $\Delta P_{\text{res}}^c = 0.1$ and a redshift between two counter rotating Earth satellites of

$z = 10^{-5}$ would amount for a frequency separation to single photon bandwidth ratio of $\mu/\xi = 4 \times 10^4$. To our knowledge, the highest frequency separation $\mu \approx 100$ THz of frequency entangled photons has been already demonstrated [40]. There, a single photon bandwidth of $\xi \approx 0.253$ THz was achieved leading to a value $\mu/\xi \approx 4 \times 10^2$, which could reveal the influence of the relativistic Doppler-shift between counter propagating satellites provided by a detector resolution of 1%, i.e., $\Delta P_{\text{res}}^c = 0.01$. No sub-GHz narrow band generation of frequency entangled photon pairs has been reported to date. In the case of cavity enhanced spontaneous parametric down conversion of frequency degenerated photons, ultra-narrow-band emission with $\xi \approx 265$ kHz has also already been demonstrated [38]. In combination with a frequency separation $\mu \approx 100$ THz, this would suffice to even resolve the influence of the general relativistic redshift of z^{-10} between a geostation on Earth and a satellite since these parameters satisfy Eq. (44) to a good approximation for a detector resolution of $\Delta P_{\text{res}}^c = 0.01$.

We want to place particular emphasis on the fact that the maximum difference between two HOM-interference experiments employing frequency entangled photons with and without relativistic aspects can reach unity in the limit $\mu/\xi \rightarrow \infty$ as can be seen in Figs. 3(a) and 3(b). This means that, in the case of identical locally adjusted optical delays, the outcome of a coincidence measurement of frequency entangled photons can change between ideal photon bunching ($P^c = 0$) to ideal photon antibunching ($P^c = 1$) and vice versa as a function of relativistic redshift. It has been shown that the necessary and sufficient criterion for the occurrence of ideal photon bunching of two photons is that their joint spectral wave function is symmetric, i.e., $\phi(\omega_1, \omega_2) = \phi(\omega_2, \omega_1)$, see [25]. In that case, it was also shown that the necessary and sufficient criterion for the occurrence of ideal photon antibunching of two photons is that their joint spectral wave function is antisymmetric, i.e., $\phi(\omega_1, \omega_2) = -\phi(\omega_2, \omega_1)$. In the case of quantum beating, i.e., a periodic change between photon bunching and antibunching in the delay, the authors made the interesting argument that due to the adjustment of different optical delays, the parity of the spectral wave function changes from being symmetric to antisymmetric and vice versa. This means that one observer might observe photon bunching thereby exploring a symmetric spectral wave function with a certain adjustment of the local optical delays, while another observer with mutual redshift with respect to the first one might explore an antisymmetric wave function through the measurement of photon antibunching with the same setting of the (local) optical delays in his local laboratory. From this, we infer that the parity of the joint spectral wave function is observer dependent. The peculiarity of our results is that, the parity of the joint spectral wave function does not only depend on the observer's delay settings but also on his state of motion.

This is a central result of our paper. This observer dependence becomes especially important in the case of spectrally indistinguishable frequency entangled photons in the limit of large frequency separations. However, according to Eq. (30), the coincidence detection probability at the zero delay setting (i.e., $\Delta\tau = \tau_1 - \tau_2 = 0$) is independent of the redshift between the photon source and the measurement laboratory and thus, can yield some information about the optical paths through which the photons propagated before they interfere at the common BS of the detection instance (see Fig. 2).

Finally, we discuss the behavior of frequency-detuned quantum states [see Eq. (8) for spectral profile]. This case is less interesting than the one of frequency entangled photons. Here, the discrepancy between the coincidence detection probabilities reads

$$\Delta P^c(\Delta\tau) = \frac{1}{2}(S_{\mu\xi}((1+z)\Delta\tau) - S_{\mu\xi}(\Delta\tau)), \quad (45)$$

with $S_{\mu\xi}(\tau)$ from (11a). Figures 3(c) and 3(d) show the absolute value of the maximum discrepancy of a HOM experiment, which uses frequency detuned photons under the influence of a redshift of $z = 10^{-10}$ and $z = 10^{-5}$ with respect to a HOM experiment without relativistic influence. It can be seen that in the limit $\mu/\xi \rightarrow 0$ the maximum discrepancy is $|\Delta P^c(\Delta\tau_{\max})| \approx z/2$, which cannot be resolved in a HOM experiment for realistic redshifts $z \lesssim 10^{-5}$. Taking the limit $\mu/\xi \rightarrow \infty$ even suppresses the effect further. This is originated in the fact that in this limit $S_{\mu\xi}(\tau)$, and thus, $\Delta P^c(\Delta\tau)$ approaches zero, which by itself is rooted in the increasing spectral distinguishability of the frequency detuned photons. Since spectrally indistinguishable frequency entangled photons do not suffer from this effect, it makes them more attractive to study the impact of general relativity on quantum mechanics.

V. OUTLOOK

There are several possible extensions to this work. The presented framework can be used to study the spectral aspects of Sagnac-interferometry [35], where photons impact from different directions on moving BSs to interfere. While the present work is concerned with theoretical and fundamental aspects of relativistic and quantum photonic science, it is also of great interest to study relativistic effects in HOM-interference-based quantum technologies. For example, one can quantify the change in accuracy within HOM-based space-based clock synchronization [18]. Furthermore, a greater understanding of the effects described here and in previous work [14–16,41] would be achieved by considering different initial states, such as coherent states, squeezed states, cat states and, more realistically, mixed states. Mixed states in particular are expected to provide a benchmark for the effects witnessed by pure states as it was already shown in the context of

gravitational redshift effects on quantum states [41]. Particular attention can also be given to optimizing spectral wave functions and the initial quantum states to obtain to greatest (or the least) gravitational effects on HOM interference.

Another aspect to be investigated is gravity-induced entanglement dynamics of photons that propagate through different (possibly correlated) paths in spacetime. Intriguingly, recent works showed that gravitational effects give rise to change the entanglement between different light field modes, which can be envisaged in two-photon interference experiments such as the HOM experiment [16]. Other work claims that gravitational time dilation induces entanglement between external and internal DOFs of quantum particles [42]. We think that HOM experiments can be interpreted precisely in this way. The occurrence of quantum beating would correspond to a periodic creation and depletion of entanglement between the internal and external DOFs, complementary to the depletion and creation of frequency entanglement among the photons. We believe that our formalism can be extended to study both of these aspects and yield a more comprehensive understanding on the influence of general relativity on genuine quantum features of physical systems.

VI. CONCLUSIONS

We have employed Glauber's theory of optical coherence, together with a quantum field theoretical framework previously developed to describe the deformation of the frequency profile of photons propagating through curved spacetime [14,15], to develop a formalism that describes large-scale HOM experiments where quantum and relativistic effects are both non-negligible.

In HOM experiments, the particle nature of photons plays a special role. Such experiments can only be explained by means of quantum mechanical principles such as the indistinguishability and quantum entanglement of the involved systems. These lead to phenomena like photon bunching and photon antibunching, both without classical analog. Therefore, our predictions of the effects of the gravitational frequency shift on these inherently quantum mechanical experiments can be interpreted as a genuine quantum test of gravity. Apart from the fundamental aspects of our work, the results presented here are also of practical relevance since they provide methods to estimate how strongly quantum technological applications based on HOM interference might be distorted from an ideal operation [see Eq. (44)].

We focused our methods on three cases with different photon sources, each one generating photons with a different spectral profile: the case analogous to the one found in the original HOM experiment [20], which employs spectrally indistinguishable frequency uncorrelated photons; the case of spectrally distinguishable frequency detuned photons [37]; and the case of spectrally

indistinguishable frequency entangled photons [36]. We found that in the original HOM experiment, no adjustment of the experimental parameters (which consisted in the photon's bandwidth alone) yields an amplification of the relativistic impact on HOM interferometry. This has the interesting implication that in case of frequency uncorrelated photons, the impact of the redshift in HOM interference is universal. Concretely, this means that it depends only on the redshift between the photon source and the detectors, and not on the photon's bandwidth [as can be seen from Eq. (39)]. This contrasts with the case of frequency entangled photons. In this case, we have shown that, due to the increase of the photon frequency separation μ and decrease of the single photon bandwidth ξ , the effect of the relativistic frequency shift becomes more important since higher frequency separations lead to an increasing sensitivity of the occurrence of photon bunching or antibunching on the delay. A particularly interesting property of frequency entangled photons is that the relativistic frequency shift between the photon source and the detectors can change the detection statistics from ideal photon bunching to ideal photon antibunching, and vice versa. This is reflected in the fact that Eq. (41) can reach unity. Since photon bunching in quantum mechanics is equivalent to the symmetry of the joint spectral wave function, and photon antibunching is equivalent to the antisymmetry of the joint spectral wave function [25], this leads to conclude that the parity of the joint photonic spectral wave function is an observer dependent quantity, which is one of the central results of this work. We conclude from this that the

outcomes of HOM experiments rely not only on the optical path difference between the measured photons before detection, but also on the state of motion of the photon source and the observers.

The main contribution of the present work consists in a formalism that can be used to describe the impact of the relativistic redshift on the spectral aspects of quantum entanglement and quantum indistinguishability of photons within the context of HOM interference. Our work, therefore, adds to the ongoing effort of understanding the interplay between gravity and quantum coherence and entanglement [1,41], and constitutes another step toward the development of relativistic and quantum technologies. Experimental verification of the effects presented here, as well as in this body of work more broadly, can serve as a demonstration of quantum field theory in (weakly) curved spacetime, and provide new insights in the quest for a unified theory of Nature.

ACKNOWLEDGMENTS

R. B. and A. W. S. were funded by the Deutsche Forschungsgemeinschaft (DFG, German Research Foundation) under Germany's Excellence Strategy—EXC-2123 QuantumFrontiers—390837967. We further gratefully acknowledge support through the TerraQ initiative from the Deutsche Forschungsgemeinschaft (DFG, German Research Foundation)—Project-ID 434617780—SFB 1464 and the Research Training Group 1620 “Models of Gravity.”

-
- [1] R. Feynman, F. Morinigo, W. Wagner, B. Hatfield, J. Preskill, and K. Thorne, *Feynman Lectures on Gravitation* (CRC Press, Boca Raton, USA, Florida, 2018).
 - [2] R. Colella, A. W. Overhauser, and S. A. Werner, *Phys. Rev. Lett.* **34**, 1472 (1975).
 - [3] R. Pound and G. Rebka, *Phys. Rev. Lett.* **4**, 337 (1960).
 - [4] R. Pound and J. Snider, *Phys. Rev. Lett.* **13**, 539 (1964).
 - [5] H. Müller, A. Peters, and S. Chu, *Nature (London)* **463**, 926 (2010).
 - [6] J. Dowling and G. J. Milburn, *Phil. Trans. R. Soc. A* **361**, 1655 (2003).
 - [7] J. Yin, Y. Cao, Y.-H. Li, S.-K. Liao, L. Zhang, J.-G. Ren, W.-Q. Cai, W.-Y. Liu, B. Li, H. Dai *et al.*, *Science* **356**, 1140 (2017).
 - [8] S. Liao, W. Cai, W. Liu, L. Zhang, Y. Li, J. Ren, J. Yin, Q. Shen, Y. Cao, Z. Li *et al.*, *Nature (London)* **549**, 43 (2017).
 - [9] J. Ren, P. Xu, H. Yong, L. Zhang, S. Liao, J. Yin, W. Liu, W. Cai, M. Yang, and t. L. Li, *Nature (London)* **549**, 70 (2017).
 - [10] J. Yin, Y. Cao, Y. H. Li, J. G. Ren, S. K. Liao, L. Zhang, W. Q. Cai, W. Y. Liu, B. Li, H. Dai, M. Li, Y. M. Huang, L. Deng, L. Li, Q. Zhang, N. L. Liu, Y. A. Chen, C. Y. Lu, R. Shu, C. Z. Peng, J. Y. Wang, and J. W. Pan, *Phys. Rev. Lett.* **119**, 200501 (2017).
 - [11] S. Liao, J. Lin, J. Ren, W. Liu, J. Qiang, J. Yin, Y. Li, Q. Shen, and L. Zhang, *Chin. Phys. Lett.* **34**, 090302 (2017).
 - [12] S. K. Liao *et al.*, *Phys. Rev. Lett.* **120**, 030501 (2018).
 - [13] R. B. Mann and T. C. Ralph, *Classical Quantum Gravity* **29**, 220301 (2012).
 - [14] D. E. Bruschi, T. C. Ralph, I. Fuentes, T. Jennewein, and M. Razavi, *Phys. Rev. D* **90**, 045041 (2014).
 - [15] D. E. Bruschi, A. Datta, R. Ursin, T. C. Ralph, and I. Fuentes, *Phys. Rev. D* **90**, 124001 (2014).
 - [16] D. E. Bruschi and A. W. Schell, arXiv:2109.00728.
 - [17] R. Schnabel, *Phys. Rep.* **684**, 1 (2017).
 - [18] V. Giovannetti, S. Lloyd, and L. Maccone, *Nature (London)* **412**, 417 (2001).
 - [19] V. Giovannetti, S. Lloyd, and L. Maccone, *Science* **306**, 1330 (2004).
 - [20] C. K. Hong, Z. Y. Ou, and L. Mandel, *Phys. Rev. Lett.* **59**, 2044 (1987).
 - [21] R. Quan, Y. Zhai, M. Wang, F. Hou, S. Wang, X. Xiang, T. Liu, S. Zhang, and R. Dong, *Sci. Rep.* **6**, 1 (2016).

- [22] A. Valencia, G. Scarcelli, and Y. Shih, *Appl. Phys. Lett.* **85**, 2655 (2004).
- [23] R. Barzel and C. Laemmerzahl, arXiv:2202.07522.
- [24] A. Pradana and L. Chew, *New J. Phys.* **21**, 053027 (2019).
- [25] K. Wang, *J. Phys. B* **39**, R293 (2006).
- [26] Z. Y. Ou and L. Mandel, *Phys. Rev. Lett.* **61**, 54 (1988).
- [27] K. Eckert, J. Schliemann, D. Bruß, and M. Lewenstein, *Ann. Phys. (Amsterdam)* **299**, 88 (2002).
- [28] N. Birrell and P. C. Davies, *Quantum Fields in Curved Space*, Cambridge Monographs on Mathematical Physics (Cambridge University Press, Cambridge, England, 1982).
- [29] Q. Exirifard, E. Culf, and E. Karimi, *Commun. Phys.* **4**, 171 (2021).
- [30] Q. Exirifard and E. Karimi, arXiv:2110.13990.
- [31] D. Philipp, V. Perlick, D. Puetzfeld, E. Hackmann, and C. Lämmerzahl, *Phys. Rev. D* **95**, 104037 (2017).
- [32] S. M. Carroll, *Spacetime and Geometry: An Introduction to General Relativity* (Cambridge University Press, Cambridge, England, 2005).
- [33] R. Wald, *General Relativity* (University of Chicago Press, Chicago, 2010).
- [34] S. Restuccia, M. Toroš, G. M. Gibson, H. Ulbricht, D. Faccio, and M. J. Padgett, *Phys. Rev. Lett.* **123**, 110401 (2019).
- [35] A. J. Brady and S. Haldar, *Phys. Rev. Research* **3**, 023024 (2021).
- [36] S. Ramelow, L. Ratschbacher, A. Fedrizzi, N. K. Langford, and A. Zeilinger, *Phys. Rev. Lett.* **103**, 253601 (2009).
- [37] A. Fedrizzi, T. Herbst, M. Aspelmeyer, M. Barbieri, T. Jennewein, and A. Zeilinger, *New J. Phys.* **11**, 103052 (2009).
- [38] J. Liu, J. Liu, P. Yu, and G. Zhang, *APL Photonics* **5**, 066105 (2020).
- [39] D. Philipp, V. Perlick, D. Puetzfeld, E. Hackmann, and C. Lämmerzahl, *Phys. Rev. D* **95**, 104037 (2017).
- [40] Y. Chen, M. Fink, F. Steinlechner, J. P. Torres, and R. Ursin, *npj Quantum Inf.* **5**, 1 (2019).
- [41] D. E. Bruschi, S. Chatzinotas, F. K. Wilhelm, and A. W. Schell, *Phys. Rev. D* **104**, 085015 (2021).
- [42] M. Zych, F. Costa, I. Pikovski, and C. Brukner, *Nat. Commun.* **2**, 505 (2011).

Chapter 4

Gravitationally driven entanglement dynamics

4.1 Introduction

In this chapter, we explore the *entanglement dynamics of photon pairs and quantum memories* in a gravitational field, with particular emphasis on the Earth’s gravitational field as a possible experimental setting to probe our predictions in a *terrestrial* environment (see Ref. [BGK⁺24]), making the conduction of these or similar experiments increasingly attractive from a financial point of view.

The contrast to our previous work [BL23, BBSL22] is threefold:

1. First, as just stated, we specify the influence of an abstract redshift—investigated in chapter 3—to the specific case of the *Earth’s gravitational field* acting on photon pairs *before* interfering at a common beam splitter.
2. Second, besides photonic excitations (the sole scope of application of Refs. [BL23, BBSL22]), we also consider excitations that are coherently stored, processed/manipulated, and released within *massive material systems*, so-called *quantum memories*. This is necessary in order to reach parameter regimes, more concretely, coherent storage/interrogation times at low gravitational redshift factors, which the Earth features in the order of $z \approx 10^{-14}$. Therefore, storage times on the *order of seconds* are required, which is due to the fundamental light attenuation of fiber cables, making coherent exchange possible only up to 400 km—one of the major challenges in quantum communication.
3. Lastly, but all the more important from a theoretical perspective, we quantify with the help of *entanglement measures* the intra- and inter-particle entanglement contained in the considered resources (which we only mention in this work and derive in detail in [BGK⁺24]).

Additionally, in our work (Ref. [BGK⁺24]), we examined not only Hong-Ou-Mandel (HOM) interference but also *Mach-Zehnder (MZ) interference* (which we do not intend to revise in detail here).

Our findings suggest that the parameters required to observe the predicted effects scale inversely with the number of entangled particles, a characteristic common to multiparticle effects. Specif-

ically, the required propagation time is *halved* for HOM interference with (spectrally) entangled photons compared to single-particle MZ experiments.

Moreover, we contrast quantum states that are sensitive to relativistic effects related to time dilation against others that are resilient (see Appendix A of [BGK⁺24]).

4.2 Theory model for relativistic effects on quantum resources

In the following, we show how our simple theory-model from [BGK⁺24] can be derived. This incorporates *both*, on the one hand the *gravitational redshift on photons* altering their frequencies conditioned on their spatial mode in the gravitational field, and on the other hand the *local position-invariance* of massive¹ quantum clocks like atoms or in our case *quantum memories*, thereby justifying their theoretical interpretation as "proper clocks", that irrespectively of their position, locally oscillate with the same frequency (at least up to the in this work and Ref. [BGK⁺24] considered level of approximation).

4.2.1 Existing literature's approaches

As our ultimate goal is the draw-back of the gravitational impact on genuine quantum properties, we must model all resources in a quantum mechanical framework. The investigation of gravitationally induced entanglement dynamics of photons and quantum clocks is by no means a new idea, but attracted already a decade ago remarkable scientific attention, and up to day remains a field of vast exploration [29–36].

4.2.1.1 Heuristic models

Usually simple semi-heuristic or entirely heuristic theory models are employed to give rise to a mathematical construction of well tested relativistic phenomenology, which usually is indeed experimentally investigated by quantum systems due to their accuracy or rather precision, like atomic hyper transitions in the Pound and Rebka experiment [1] or atomic clocks either utilizing hyperfinestructure transitions in the experimental series of Hafele and Keating [3] to resolve gravitational and motional time dilation, i.e. first-order effects.

4.2.1.2 Models from first principles

Therefore, there is a well justified and widely consensual criticism [48–51], to the common approaches[29–36]. This is accompanied *with the desire* that demands for a theoretically clean and systematic treatment.

4.2.2 Outline of possible approach

Thus, there is a vast facility of approaches to model quanta in the presence of relativistic effects, and in particular a curved spacetime background. Of course, a derivation from first principles is desired from a theoretic standpoint. However, there are also good reasons for heuristic ansatzes, that effectively distillate –*with high computational efficiency*– the leading order terms *steering the physical realm*.

¹All "quantum clocks" measuring propertime are massive, as massless particles do not account for a "local" time.

In question, the low-cost computation and the unsystematic –although conventional– approximations made here, are indicators that our ansatz is certainly closer to heuristic approaches than a mathematically rigorous trace-tracking of neglected terms or effects.

We will start with the *Klein-Gordon equation (KGE) on curved spacetimes*. This enables us to conveniently describe with one single equation on *equal footing* both photonic excitations under redshift and local position-invariant *Compton clocks*, for which in the following we use the term "*massive quantum clock*" as synonym.

As characterizing bosons, the KGE is particularly suited to model photons –although being spin-1 bosons instead of spin-2² particles– and also *quantum memories*. This is because their excitations –the *spin-waves*– are, despite, being implemented by means of fermionic electrons, feature the effective nature of *bosonic quasi-particles*, the so-called *magnons*, as we explain later in Sec. 4.3.

4.2.3 Relativistic description of spacetime

In the framework of General Relativity, spacetime is described by the metric tensor $g_{\mu\nu}$, which encodes the gravitational field and defines the line element

$$ds^2 = g_{\mu\nu} dx^\mu dx^\nu. \quad (4.1)$$

The dynamics of the metric are governed by Einstein's field equations (EFEs), which relate the curvature of spacetime to the energy-momentum tensor of matter and radiation. Truly rendering the worst case scenario of differential equations, that are, non-linear multivariate and coupled systems of partial differential equations, it is not surprising that over the decades the offer of simplified versions of the EFEs has grown immense.

One of the most foundational approaches with direct *operational meaning* are the so-called *post-Newtonian approximations*, which are particularly attractive for investigations targeting the quantification of the most important contributions of relativistic effects, which –as the name already suggests– go beyond the Newtonian theory of gravity.

We are interested in the leading relativistic effects on the considered quanta. Therefore, we will not consider the entire metric, but only its first and second order *parametrized post-Newtonian approximation*.

4.2.3.1 First and second order ppN-metric

The *parametrized post-Newtonian* (ppN) approximation is a calculational tool to expand the solution to Einstein's field equations –the metric tensor around the weak-field, slow-motion limit. The ppN metric to first and second order can be written respectively as

$$ds^2 = - \left(1 - 2 \frac{U}{c^2} \right) c^2 dt^2 + \delta_{ij} dx^i dx^j, \quad (4.2a)$$

$$ds^2 = - \left(1 - 2 \frac{U}{c^2} + 2\beta \frac{U^2}{c^4} \right) c^2 dt^2 + \left(1 + 2\gamma \frac{U}{c^2} \right) \delta_{ij} dx^i dx^j, \quad (4.2b)$$

²solely the case for the Higgs boson

where in the following, as usual, Greek indices run from $\mu, \nu = 0, 1, 2, 3$, Latin indices run from $i, j = 1, 2, 3$, and

$$U(t, x^i) = G \int \frac{\rho(t, x')}{|x^i - x'|} d^3 x' \quad (4.3)$$

is the Newtonian gravitational potential. Note that we consciously avoided off-diagonal terms in the metric, i.e., for instance velocity terms as $g_{i0} = 0$. The spatial coordinates x^i in (4.2) are Cartesian coordinates, and t is a *common global* time coordinate.

Furthermore, β and γ are ppN parameters that characterize the strength of the gravitational field, where $\beta = \gamma = 1$ align with Einsteins theory of general relativity (GR), and it is still a field of highly active research to find any deviations from the case of GR.

4.2.4 Quantum description

In the quantum description of fields and particles, the effects of spacetime curvature can be included by modifying the standard quantum field equations to account for the curved spacetime background. This leads to modifications of the Klein-Gordon equation, in turn giving rise for instance to modified Wave and Schrödinger equations [48–50].

4.2.4.1 Klein-Gordon equation in ppN approximation

The Klein-Gordon equation in curved spacetime is given by:

$$\left(\frac{1}{\sqrt{-g}} \partial_\mu (\sqrt{-g} g^{\mu\nu} \partial_\nu) - \frac{m^2 c^2}{\hbar^2} \right) \phi(t, x) = 0, \quad (4.4)$$

where in the following, as usual, Greek indices run from $\mu, \nu = 0, 1, 2, 3$, and as common, Latin indices run from $i, j = 1, 2, 3$.

We use the exponential anstaz to solve the KGE

$$\phi(t, x) = \phi_0 e^{ix^\mu k_\mu} = \phi_0 e^{i\omega t - k_i x^i} \quad (4.5)$$

to derive the dispersion relation in second order ppN

$$\begin{aligned} & -\frac{\mathbf{k}^2}{\frac{2\gamma U}{c^2} + 1} + \frac{c^2 m^2}{\hbar^2} - \frac{ic^2(\mathbf{F} \cdot \mathbf{k})((\gamma - 1)c^4 + 2c^2U(\beta - 2\gamma) + 6\beta\gamma U^2)}{(c^4 - 2c^2U + 2\beta U^2)(c^2 + 2\gamma U)^2} \\ & - \omega \frac{ic^4(\mathbf{F} \cdot \mathbf{V})((3\gamma + 1)c^4 - 2c^2U(\beta + 2\gamma) + 2\beta\gamma U^2)}{(c^4 - 2c^2U + 2\beta U^2)^2(c^2 + 2\gamma U)} + \frac{c^2 \omega^2}{c^2 (1 - 2\frac{U}{c^2} + 2\beta \frac{U^2}{c^4})} = 0, \end{aligned} \quad (4.6)$$

which is an interesting result, by itself, because—as a complex equation— it opens up the investigation of the gravitational influence on quantum coherent phases.

In Eq. (4.6) we have set

$$k_i = \mathbf{k}, \quad (4.7a)$$

$$-\partial_i U = -\nabla U = \mathbf{F} \quad (4.7b)$$

$$\partial_t U = (-\partial_i U) \left(-\frac{dx^i}{dt} \right) = \mathbf{F} \cdot \mathbf{V}, \quad (4.7c)$$

where \mathbf{k} , \mathbf{F} and $(-\mathbf{V})$ have the physical interpretation of the wave-number vector, the gravitational force, and the relative velocity w.r.t. the gravitating object in second order ppN coordinates (4.2b).

Taking the real part of the dispersion relation (4.6)

$$\frac{c^2\omega^2}{c^2(1 - 2\frac{U}{c^2} + 2\beta\frac{U^2}{c^4})} - \frac{\mathbf{k}^2}{1 + \frac{2\gamma U}{c^2}} + \frac{c^2m^2}{\hbar^2} = 0. \quad (4.8)$$

is the basis on which we want to discuss the differences between the gravitational redshift effect shifting the oscillation frequency of photons, and the gravitational influence on the oscillation frequency of the wave function of massive particles, which in this context could be regarded as *Compton clocks*.

Photons $m = 0$

In case of photons, from Eq. (4.14) one recovers the well-known rescaling of the frequency and the wave number vector –and thus the wavelength– of locally measured photons ($m = 0$) due to relativistic time dilation and length contraction, where the locally measured frequency ω_{loc} and wave-number vector \mathbf{k}_{loc} at the gravitational potential level U would correspond in second order ppN approximation to

$$\omega_{loc}(U) = \frac{\omega}{\sqrt{(1 - 2\frac{U}{c^2} + 2\beta\frac{U^2}{c^4})}}, \quad (4.9a)$$

$$\mathbf{k}_{loc}(U) = \frac{\mathbf{k}}{\sqrt{(1 + 2\gamma\frac{U}{c^2})}}. \quad (4.9b)$$

These equations have to be understood in a *common global* coordinate frame in the coordinates x^μ from (4.2), where both, the accounted frequency and wave-number vectors feature spatial dependence. This is precisely what in the end leads to a spatially conditioned and coherent phase evolution of the considered quantum resources, altering their entanglement.

In first order ppN the result corresponding to the real part of the first order ppN approximation to the KGE dispersion relation

$$\frac{c^2\omega^2}{c^2(1 - 2\frac{U}{c^2})} - \mathbf{k}^2 + \frac{c^2m^2}{\hbar^2} = 0, \quad (4.10)$$

results in

$$\omega_{loc}(U) = \frac{\omega}{\sqrt{(1 - 2\frac{U}{c^2})}}, \quad (4.11a)$$

$$\mathbf{k}_{loc}(U) = \mathbf{k}. \quad (4.11b)$$

which interestingly characterizes a sole rescaling of the spectral part.

Regarding Eq. (4.11a), the ratio between two locally measured frequencies $\Theta_{U_1U_2} = \omega_{loc}(U_1)/\omega_{loc}(U_2)$ at distinct gravitational potentials U_1 and U_2 when expanded to first order in these potentials, correspond to the gravitational part of the redshift relation in Ref. [21], which we employ in Equation (1) of Ref. [BGK⁺24] and reads

$$\frac{\omega_{loc}(U_1)}{\omega_{loc}(U_2)} = \Theta_{U_1U_2} = 1 + z_{U_1U_2} \quad (4.12)$$

where

$$z_{U_1 U_2} = \frac{U_2 - U_1}{c^2} \quad (4.13)$$

is called the gravitational redshift between the oscillation frequencies of the same photon as measured at distinct gravitational potential levels U_1 and U_2 . Now, we want to delve into massive clocks.

Massive quantum clocks $m > 0$

In each of the first and second order ppN-expansion, we can write the dispersion relation in the intuitive way of the *free-particle dispersion relation*

$$c^2 \omega_{loc}^2 - \mathbf{k}_{loc}^2 + \frac{c^2 m^2}{\hbar^2} = 0, \quad (4.14)$$

which when solved for the positive³ local frequency in the frame –of the quatum clock–

$$\omega_{loc}(U) = \sqrt{\frac{\mathbf{k}_{loc}^2(U)}{c^2} - \frac{m^2}{\hbar^2}} \quad (4.15)$$

shows that in this frame the local oscillation frequency is independent from the gravitational potential in first order ppN approximation –due to Eq. (4.11b)– and corrections just arise from second order ppN terms, as Eq. (4.9b) depends on the gravitational potential.

This is indeed senseful, as the second order ppN-expansion gives rise to spatial curvature terms –by contrast to the first order expansion, which does not. Spatial curvature is well known to modulate the *effective potential* to which the massive quantum particle is exposed, thereby influencing the eigenenergies –and therefore the frequencies– at which the particle’s wave function oscillates.

Note that since it does not make sense to evaluate frequencies in the "frame" of photons, the consideration of Eq. (4.15) is not possible in this line of thought. This can be also understood formally by considering the ppN metric instead of (4.2), but as

$$ds^2 = -c^2 d\tau^2 + \delta_{ij} dx^i dx^j, \quad (4.16a)$$

$$ds^2 = -c^2 d\tau^2 + \left(1 + 2\gamma \frac{U}{c^2}\right) \delta_{ij} dx^i dx^j, \quad (4.16b)$$

in terms of the propertime coordinate

$$\tau = \sqrt{g^{00}} t \quad (4.17)$$

which leads to results as (4.15) for massive quantum clocks, but does not apply for photons, as these do not feature in a senseful way the concept of propertime. Then from Eq (4.16) it is seen that the gravitational influence on the ticking rate of quantum clocks just enters from the second order ppN approximation.

4.3 Modeling quantum memories

Having elaborated several times in this work on the description of photons, we now want to show a possible theoretic modeling of quantum memories (QMem) leading to the intermediate

³we do not consider pair-creation in the weak-relativistic regime

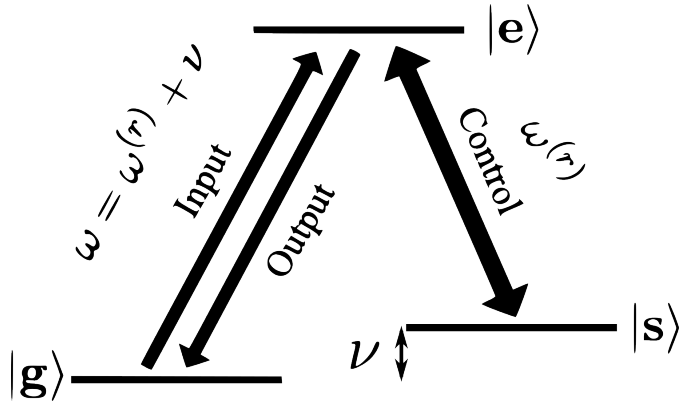


Figure 4.1: Energy scheme for ground state QMems denoted as Λ -system. The two lower states are usually hyperfine sublevels of the same electronic state. The coherent storage of (in our case photonic) quantum information takes place in the ground state transition between states $|g\rangle$ and $|s\rangle$. The local oscillation frequencies ν usually take place in the GHz regime. The storage (input) and release (output) of quantum information is steered by a control laser of frequency $\omega^{(r)}$ fulfilling the resonance condition $\omega = \omega^{(r)} + \nu$ to the signal of frequency ω . The particular property of quantum memories is that the effective decay rate of the gs -transition is macroscopically large, corresponding to coherence times up to seconds (see for instance [52])

result of the mode-swapper model we employ in [BGK⁺24]. We consider so-called Lambda-type QMems rendering an energy scheme as shown in Fig. 4.2.

Firstly, the coherence stored by QMems are of bosonic nature. Despite there are more elaborated models on long-lived QMems considering quadrupolar moments of nuclear transitions [52], we want to illustrate QMems for the sake of transparency in a much more simple way, that however should be capable to effectively capture their essential properties.

The simplest model of fully quantum mechanical light-matter interaction is the *Jaynes-Cummings model*. The coherent storage –as explained in the caption of Fig. 4.2– of photonic quantum information occurs in the gs -transition, and its excitation. This is why we effectively want to describe the level scheme of the Λ -QMem as a two-level system interacting with the signal field; the photons to be stored.

The associated light-matter interaction Hamiltonian of 3 electronic levels interacting with a signal light field mode characterized by creators a_ω^\dagger which are stored and released by a control laser –a coherent state oscillator– reads

$$H_{int}^\Lambda = i\hbar(g_{ge} a_\omega S_{ge}^\dagger - g_{ge}^* a_\omega^\dagger S_{ge}) + i\hbar\Omega_R (S_{es}^\dagger e^{-i\omega^{(r)}\tau} - S_{es} e^{i\omega^{(r)}\tau}), \quad (4.18)$$

where $S_{ij}^\dagger = f_i^\dagger f_j$ creates an electronic transition from electronic level state j to i , being by themselves composed of fermionic creation and annihilation operators $f_j^{(\dagger)}$ of particles in nuclear state j , with their usual anti-commutator relations $f_i f_j^\dagger + f_j^\dagger f_i = \delta_{ij}$.

Furthermore, the light-matter interaction constant associated to the electronic transition between states $|g\rangle$ and $|e\rangle$ interacting with the signal-field is denoted by g_{ge} . This first term of (4.18) is the fully quantum mechanical part of the light matter interaction, followed by the second term,

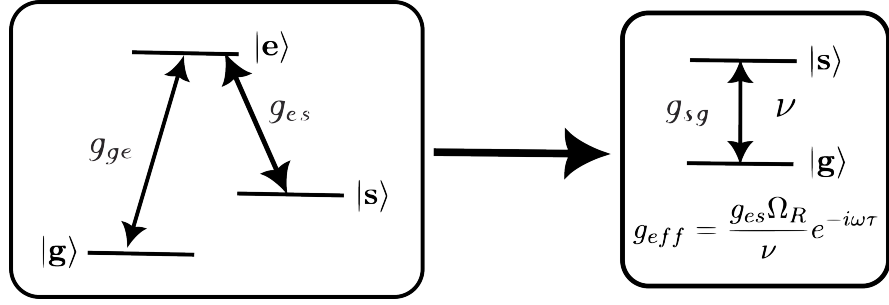


Figure 4.2: Second order perturbation theoretic mapping of a Λ -type QMem to an *effective model* of a two-level atom interacting with the *signal mode* a_ω^\dagger . The light-matter interaction constant associated to the electronic transition between states $|a\rangle$ and $|b\rangle$ is denoted by g_{ab} . The effective two-level light-matter coupling constant $g_{eff} = g_{sg}$ can be computed as from the coupling constants of the intermediate transitions as $g_{sg} = g_{es}\Omega_R/\nu$.

that obeys a semi-classical description, where the control laser is assumed to be a classical light field, and Ω_R is the Rabi-frequency of es -transition interacting with the control laser, a classical oscillator of frequency $\omega^{(r)}$.

It is to mention that in contrast to the nuclear quadrupole model, the (semiclassical) Jaynes-Cumming model arises from the *electric dipole approximation* and thus the light matter interaction and Rabi-frequency have rather to be understood as fitting parameters of a theoretical model rather than of being physical entities.

The mapping of light-matter interaction to effective "low-level number models" is a well known process and common practice, and leads to the effective two-level light-matter interaction Hamiltonian of a Λ -type QMem. From second order standard perturbation theory it follows that the effective light-matter interaction can be written as

$$H_{eff}^\Lambda = \frac{H_{int}^\Lambda H_{int}^\Lambda}{\hbar\nu} = i\hbar(g_{eff} a_\omega S_\nu^\dagger - g_{eff}^* a_\omega^\dagger S_\nu), \quad (4.19)$$

where, the effective light-matter interaction coupling constant associated to the gs -transition results in

$$g_{eff} = \frac{g_{es}\Omega_R}{\nu} e^{-i\omega\tau}. \quad (4.20)$$

4.3.1 Mode swapper

Then we follow a very simple approach to describe the storage and release of photonic coherence in QMems as a unitary mode-swapping operation

$$U_{s/r} = \exp(\pi/2(e^{i\phi_{s/r}} a_\omega S_\nu^\dagger - e^{-i\phi_{s/r}} a_\omega^\dagger S_\nu)), \quad (4.21)$$

which can be deduced from the effective light-mater interaction (4.19) by

$$U_{s/r} = e^{-iH_{eff}^\Lambda \tau_{int}}, \quad (4.22)$$

when requiring the condition of a $\pi/2$ -Rabi flop within an interaction duration τ_{int} of

$$g_{eff}\tau_{int} = e^{i\phi_{s/r}} \frac{\pi}{2}, \quad (4.23)$$

where the storage/release phases ("s" for storage and "r" for release) are equal to

$$\phi_s = -\omega^{(r)}(\tau_s^0 + \tau_{int}) \quad (4.24a)$$

$$\phi_r = \phi_s - \omega^{(r)}(\tau_s + \tau_{int}), \quad (4.24b)$$

where τ_s^0 is the temporal instance when the storage process starts, and $(\tau_s^0 + \tau_{int})$, when it finalized.

Furthermore, in the following the storage duration τ_s is assumed to largely exceed the interaction time, i.e., we assume

$$\tau_s \gg \tau_{int}. \quad (4.25)$$

In particular, we have (when neglecting the interaction time)

$$\phi_s - \phi_r = \omega^{(r)}\tau_s \quad (4.26)$$

Here, it is left to be said, that with a_ω^\dagger we not only consider monochromatic photons, but also extended spectra of single photons, which might be entirely stored in the spin-wave excitation S_ν^\dagger provided that the QMem-bandwidths largely exceeds the bandwidth of the respectively stored photonic spectrum centered around a carrier frequency of ω (see Eq. (46) of [BGK⁺24]).

Additionally, we equipped the QMem-excitation operators $S_{i\sigma}^\dagger$ ⁽⁴⁾ in Ref. [BGK⁺24] with indices i -labeling the respective frequency peak of a photonic spectrum (as for instance the two peaks in case of frequency entangled photons with a spectrum (2.70)) and indices $\sigma = U, L$ depending on at which potential level the respective QMem is installed.

4.4 Quantum memory assisted HOM-interference in a gravitational field

We have now all theoretic components to compose them in an entire model for HOM-interference in the vicinity of gravity that is –apart from the standardly employed optical temporal delays in HOM-interference– furthermore supplied by quantum memories.

Figure 4.3 shows the experimental setup under investigation targeting to highlight the difference between optical delays and QMems, that is, that optical delay process photons subject to the relativistic redshift, where QMems –as optical clocks– operate locally at a fixed oscillation frequency (see caption of Fig. 4.3). The scheme is drawn suggestively in such a way that all shown quantities –those of delay and storage duration together with the oscillation frequencies– are respectively given at the local point of processing. This is beneficial, as the outcome of interference experiments solely depends on the *local* manipulation of the resources in the intermediate steps.

4.4.1 Single particle evolution

We want to consider first how single particles propagate through the HOM-interferometer shown in Fig. 4.3. This leads –although the HOM-experiment is a multi particle interference experiment– to fairly out-reaching results through quite simple and transparent considerations.

⁴ ν is suppressed in the notation of [BGK⁺24]

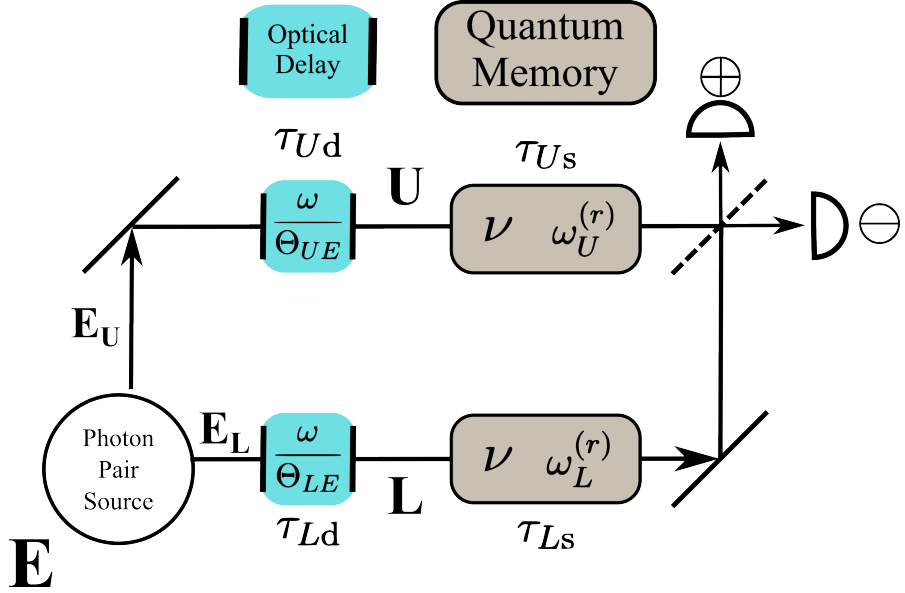


Figure 4.3: Quantum memory-assisted HOM-interference in an inhomogeneous gravitational field with interferometer arms placed at distinct gravitational potential levels U and L . The common global reference frame E is set to the photon source. We further distinguish between the distinct emission modes E_U and E_L , which are *both* associated with the same gravitational potential level E , and transmit into the modes U and L . All quantities are given as locally measured at the respective arm, i.e. for instance the optical delay τ_{Ud} is given in units of the local propertime at site U , where the redshifted optical frequency $\omega_U = \omega/\Theta_{UE}$ is received and processed. In contrast, the QMem –as a proper clock– fretures an oscillation frequency ν that remains locally invariant. The control laser’s frequency, however, needs to be adjusted conditioned on the site $\sigma = U, L$ in order to fulfil the resonance condition $\omega_\sigma^{(r)} = \omega/\Theta_{\sigma E} - \nu$ to allow for optimal storage, i.e. minimal signal loss.

This, by itself, is possible due to the fact that in HOM interference solely linear optical instruments are used, that act independently on the photons. Indeed, it is one of the remarkable points about HOM-interference that in the end the fundamental multi-particle effects of photon (anti-)bunching take place in a linear optical setting.

Starting from a photon emission mode $a_{E_\sigma\omega}^\dagger$ of frequency ω generated in the photon source’s reference frame E and subsequently transmitted to the frame $\sigma = U, L$ the very same photon is seen there as the mode $a_{\sigma\omega_\sigma}^\dagger$, with the redshifted frequency

$$\omega_\sigma = \frac{\omega}{\Theta_{\sigma E}}, \quad (4.27)$$

to which, first, an optical delay of local duration $\tau_{\sigma d}$ is applied (we neglect the temporal evolution of the intermediate propagation) rendering a field mode in arm σ of $a_{\sigma\omega_\sigma}^\dagger e^{i\varphi_{\sigma d}}$ with a *delayed phase* of

$$\varphi_{\sigma s} = \frac{\omega}{\Theta_{\sigma E}} \tau_{\sigma d}. \quad (4.28)$$

Then the mode swapping of the QMem takes place transforming the state into the –already delayed– storage spin-wave mode

$$S_{\sigma\nu}^\dagger e^{i\varphi_{\sigma d}} e^{i\phi_{\sigma s}} = U_s a_{\sigma\omega_\sigma}^\dagger U_s^\dagger e^{i\varphi_{\sigma d}} \quad (4.29)$$

with the storage phase imprinted by the control laser (we keep neglecting the interaction time of the mode-swapper)

$$\phi_{\sigma s} = -\omega_\sigma^{(r)} \tau_{\sigma d}, \quad (4.30)$$

initialized after the delay duration $\tau_{\sigma d}$, where the control laser's frequency is adjusted to *locally* fulfil the resonance condition, i.e.,

$$\omega_\sigma^{(r)} = \frac{\omega}{\Theta_{\sigma E}} - \nu. \quad (4.31)$$

The spin-wave then during the local storage time $\tau_{\sigma s}$ accumulates a *storage-phase*,

$$\varphi_{\sigma s} = \nu \tau_{\sigma s}. \quad (4.32)$$

rendering a resulting mode

$$S_{\sigma\nu}^\dagger e^{i\varphi_{\sigma d}} e^{i\phi_{\sigma s}} e^{i\chi\varphi_{\sigma s}} \quad (4.33)$$

immediately before the release, where we additionally –by incorporation of the parameter χ – accounted for the option that the internal phase evolution of the spin-wave *is not* imprinted on the output state ($\chi = 0$), or alternatively, *it is* imprinted on the output state ($\chi = 1$).

Then, the release-transformation steered by the control laser transforms the spin-wave back into a photon according to

$$a_{\sigma\omega_\sigma}^\dagger e^{-i\phi_{\sigma r}} = U_r S_{\sigma\nu}^\dagger U_r^\dagger \quad (4.34)$$

with the release-phase imprinted by the control laser (we keep neglecting the interaction time of the mode-swapper)

$$\phi_{\sigma r} = \phi_{\sigma s} - \omega_\sigma^{(r)} \tau_{\sigma s}, \quad (4.35)$$

such that the mode after the optical delay and QMem action Fig. 4.3 in arm σ results in

$$a_{\sigma\omega_\sigma}^\dagger e^{i\Psi_\sigma} = a_{\sigma\omega_\sigma}^\dagger e^{i\varphi_{\sigma d}} e^{i(\phi_{\sigma s} - \phi_{\sigma r})} e^{i\chi\varphi_{\sigma s}}, \quad (4.36)$$

where we defined the entire phase accumulated through all processes⁵ that –after some minor algebraic simplifications– reads

$$\Psi_\sigma = \frac{\omega}{\Theta_{\sigma E}} (\tau_{\sigma d} + \tau_{\sigma s}) + (\chi - 1) \nu \tau_{\sigma s}. \quad (4.37)$$

These two terms are of very distinct nature in regard of the deviation from the corresponding HOM-experiment in the *absence of gravity*, in which case $\Theta_{\sigma E} = 1$ holds. In other words, if the corresponding term does not depend on the site, σ then the associated phase evolution is not conditioned on relativistic effects.

⁵i.e., optical delays, internal QMem phase evolution and control laser phases

Regarding the first term in (4.37), $\omega/\Theta_{\sigma E}(\tau_{\sigma d} + \tau_{\sigma s})$, it can be seen that *locally equivalent* delay and storage times, i.e., the *synchronization*,

$$\tau_{Ud} = \tau_{Ld} = \tau_d \quad (4.38a)$$

$$\tau_{Us} = \tau_{Ls} = \tau_s \quad (4.38b)$$

suffice to make this term conditioned on σ as $\Theta_{\sigma E}$ appears in this term.

This is a contrast to the second term, $(\chi - 1)\nu\tau_{\sigma s}$, that is independent of σ for the synchronization choice (4.38).

However, the situation changes to the opposite⁶ in case of equivalent delay and storage durations w.r.t. to the *common global* reference frame E of the photon source, in which case the *synchronization* requirement

$$\Theta_{UE}\tau_{Ud} = \Theta_{LE}\tau_{Ld}, \quad (4.39a)$$

$$\Theta_{UE}\tau_{Us} = \Theta_{LE}\tau_{Ls} \quad (4.39b)$$

holds.

In the following, we however consider the case of locally equivalent storage durations and furthermore do not consider optical delays, i.e., $\varphi_{\sigma d} = 0$.

Indeed, locally equivalent storage durations are closer to the fundamental character of the here discussed experimental proposal, as an effect that is conditioned on the mutual synchronization of the control laser⁷ –an instrument of mere assistance to the scheme– seems not to give rise to effects that are fundamental to physics between quantum mechanics and general relativity.

Furthermore, in the following, we neglect the second term in Eq. (4.37), i.e. we consider

$$\Psi_\sigma = \frac{\omega}{\Theta_{\sigma E}}\tau_s = \omega_\sigma\tau_s \quad (4.40)$$

as typically for Λ -type QMems

$$\omega \gg \nu \quad (4.41)$$

holds (cf. Fig. 4.2), and we consider the weak field limit $\Theta_{\sigma E} = 1 + z_{\sigma E}$ with the redshift being assumed to render $z_{\sigma E} \ll 1$.

To summarize, the propagation and manipulation through the optical delays and quantum memories leads to the replacement from the initial modes to the final output modes interfering on the beam splitter of

$$a_{E_\sigma\omega}^\dagger \rightarrow a_{\sigma\omega_\sigma}^\dagger e^{i\Psi_\sigma}, \quad (4.42)$$

which we specialized to

$$a_{E_\sigma\omega}^\dagger \rightarrow a_{\sigma\omega_\sigma}^\dagger e^{i\omega_\sigma\tau_s}, \quad (4.43)$$

which is of very similar form as the standard replacement in ordinary HOM-interference in a non-relativistic setting (cf. Eq. (1) in Ref. [BL23]), that is in particular included as a special case in (4.42) for $\tau_s = 0$ and $\Theta_{\sigma E} = 1$.

⁶i.e., the first term becomes independent, and the second term becomes dependent on σ in Eq. (4.37)

⁷Note that the synchronization of the QMem storage occurs via the control laser.

4.4.2 Two-particle considerations

Having worked out the details on single particle manipulation by optical delays and QMems in the former section, it is now convinient to set up the corresponding two-particle considerations.

We consider an initial pair-mode of two photons

$$p^\dagger := \int d\omega_1 d\omega_2 \Phi_E(\omega_1, \omega_2) a_{E_1 \omega_1}^\dagger a_{E_2 \omega_2}^\dagger, \quad (4.44)$$

in the Earth frame, E , with emission modes E_1 and E_2 (cf. Fig. 4.3) obeying a joint spectrum of $\Phi_E(\omega_1, \omega_2)$, when measured in frame E .

Applying the replacement (4.43) this mode is rewritten as

$$p^\dagger = \int d\omega_1 d\omega_2 \Phi_E(\omega_1, \omega_2) e^{i\omega_{1U}\tau_s} e^{i\omega_{2L}\tau_s} a_{U\omega_{1U}}^\dagger a_{L\omega_{2L}}^\dagger, \quad (4.45)$$

and is now expressed by means of single particle modes

$$a_{\sigma\omega_{i\sigma}}^\dagger \quad \sigma = U, L, \quad i = 1, 2 \quad (4.46)$$

with

$$\omega_{i\sigma} = \frac{\omega_i}{\Theta_{\sigma E}} \quad \sigma = U, L, \quad i = 1, 2 \quad (4.47)$$

being the redshifted single photon frequencies. Then inserting (4.47) into (4.45) and using (3.5) yields after some substitution of the integral variables

$$p^\dagger = \int d\omega_1 d\omega_2 \Phi_E(\omega_1, \omega_2) e^{i\omega_1\tau_1} e^{i\omega_2\tau_2} a_{U\omega_1}^\dagger a_{L\omega_2}^\dagger. \quad (4.48)$$

This is a familiar result in HOM-interference, as it is the general initial state that enters the standard HOM-calculation beginning from Eq. (1) of Ref. [BL23]. U and L are now the interfering beam splitters input modes and \oplus and \ominus (see Fig. 4.3) are it's output modes.

However, now the quantities τ_1 and τ_2 (corresponding to the delays in ordinary HOM-interference) are not allowed to be freely chosen, but depend on the redshift factor

$$\tau_1 = \tau_s / \Theta_{UE} \quad (4.49a)$$

$$\tau_2 = \tau_s / \Theta_{LE}. \quad (4.49b)$$

4.5 HOM-interferogram

We first want to state what we mean with interferogram, i.e. with the interference pattern. Abstractly we mean with this any outcome of a linear measurement of photons, which is technically speaking any result of the trace of the photon-pair's density operator with some linear hermitian operator, so to say an observable.

In standard HOM-interferernce, where the detectors are solely sensitive against the spatial DOF this would correspond to any linear combination of probabilities how the photons exit the interfereing beam splitter, throgh the exit ports $\{\oplus\oplus, \oplus\ominus, \ominus\oplus, \ominus\ominus\}$ (cf. Fig. 4.3), i.e.,

$$P(\tau_1, \tau_2) = aP_{\oplus\oplus} + bP_{\oplus\ominus} + cP_{\ominus\oplus} + dP_{\ominus\ominus} \quad (4.50)$$

with $a, b, c, d \in \mathbb{R}$

It is well known (and shown in Eq. (8) of Ref. [BL23]) that the interference pattern in standard HOM-interference is a function $P(\tau_1, \tau_2) = P(\tau)$ that solely depends on the difference $\tau = \tau_2 - \tau_1$ of the delays, which according to Eq. (4.49) in our consideration equals

$$\tau = \Delta_{\Theta^{-1}} \tau_s$$

with the *differential redshift factor*

$$\Delta_{\Theta^{-1}} = \frac{1}{\Theta_{LE}} - \frac{1}{\Theta_{UE}}. \quad (4.51)$$

This is a very convenient result, as it allows for computing for each known interference pattern $P(\tau_1, \tau_2)$ the associated HOM-interference pattern in the vicinity of gravity as

$$P(\tau_1, \tau_2) = P(\Delta_{\Theta^{-1}} \tau_s). \quad (4.52)$$

In particular, the associated interferogram in the absence of relativistic effects (in which case we have $\Delta_{\Theta^{-1}} \tau_s = 0$) constantly measures the zero-delay setting $P(0)$. This means, in turn, that the slope of the HOM-interference pattern w.r.t. the storage time (and the same would hold for optical delays)

$$\frac{\partial P(\Delta_{\Theta^{-1}} \tau_s)}{\partial \tau_s} = \Delta_{\Theta^{-1}} \frac{\partial P(\tau)}{\partial \tau} \quad (4.53)$$

is proportional to the differential redshift (we used the chain rule in Eq. (4.53)), and thus could be used to measure deviations from the non-relativistic case (certainly owing highest sensitivity at zero-crossings of the interferogram).

4.5.1 Interpretation in terms of entanglement

One interferogram that admits for zero-crossings is the one in which we are particularly interested in, that is, the interferogram of the difference between the photon bunching and the photon anti-bunching probability

$$P_c = (P_{\oplus\oplus} + P_{\ominus\ominus}) - (P_{\oplus\ominus} + P_{\ominus\oplus}) \quad (4.54)$$

This interferogram has certain association to entanglement measures that capture the mutual entanglement between the photons, for which (4.54) is indeed a measure, as it is equal to the photon pair's *negativity*

$$\mathcal{N}_{\text{HOM}} = -\frac{|P_c|}{2}, \quad (4.55)$$

see Eq. (33) of Ref. [BGK⁺24].

The entanglement between distinct DOFs of the respectively same photon in the photon pairs, which we capture by the linear entropy

$$\mathcal{S}_{\text{HOM}} = 1 - P_c, \quad (4.56)$$

(see Eq. (32) of Ref. [BGK⁺24]) in turn, is limited by our *correlation measure* (4.54).

We do not want to delve into the detailed derivation of these measures as these are given in detail in [BGK⁺24] and are mostly technical, but only want to mention the trade-off between the "inter particle entanglement" \mathcal{N}_{HOM} and "intra-particle entanglement" \mathcal{S}_{HOM} , for which we show for the special case of our consideration of the HOM-experiment operated with frequency entangled photons in [BGK⁺24] (Eqs. (32,33)) the relation

$$\mathcal{S}_{\text{HOM}} = \frac{1}{2}(1 - 4\mathcal{N}_{\text{HOM}}^2). \quad (4.57)$$

In the following we want to examine the experimental observability and the interpretation of the predicted effects.

4.6 Experimental observability and interpretation

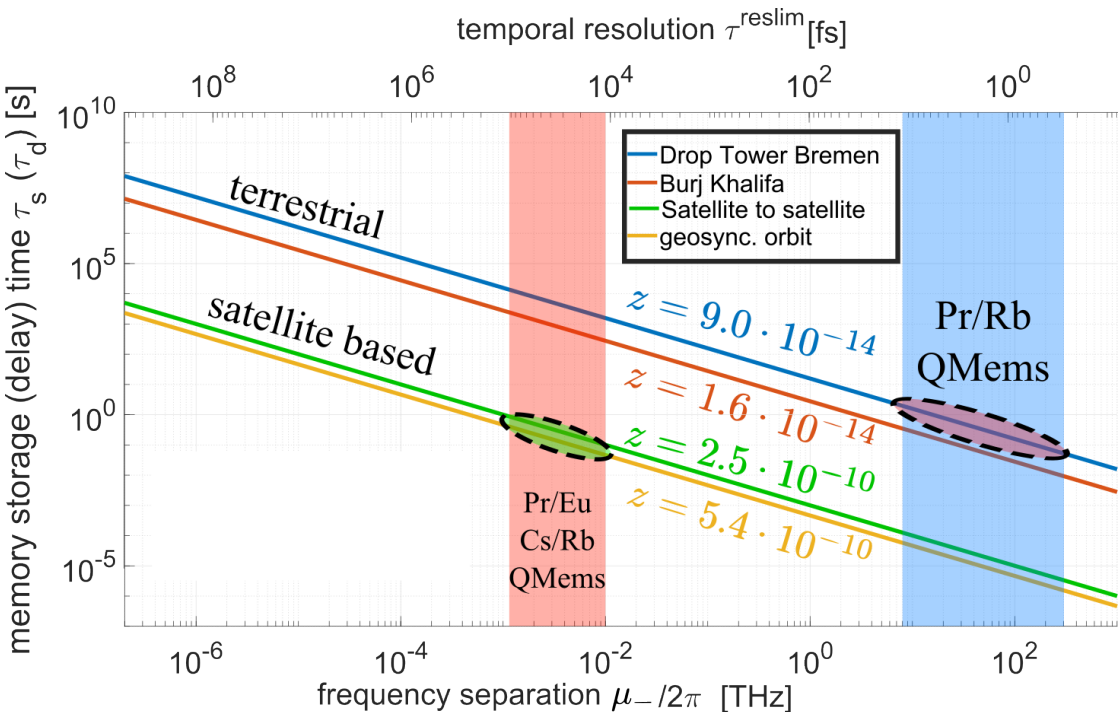


Figure 4.4: Required storage (or delay time) to cross the value $P_c(\tau_s) = 0$ depending on from the frequency separation $\mu_-/(2\pi)$. The red and blue shaded areas correspond to the spectral operation-regimes of Pr/Eu, Cs and Rb QMems-combinations, that were already investigated experimentally with acceptance-frequencies in the range of (1–10) GHz [10–14] (red) and (10–100) THz [15, 16] (blue). The most remarkable point about these results are captures in the green and red shaded ellipses, that mark the parameter regimes, where present QMem-technology renders promising chances to observe the predicted alternation of the detection statistics in HOM-interference due to relativistic effects. Particularly, the red ellipse marks a possible parameter regime for a *terrestrial* genuine quantum test of metric gravity within the *Drop Tower of the University of Bremen*.

Certainly, also plenty of further approaches to operationally quantify the presence of relativistic effects could be thought of from this starting point. We, however, want to simply read off from

the interferogram (4.54) where it crosses the value of zero, for mainly two reasons.

On the one hand, it marks the border from where photon anti-bunching –a genuine non-classical effect– occurs, whose experimental observation is a sufficient indicator for the presence of quantum entanglement shared between the photons. In other words, it is a *Bell-observable*.

On the other hand it is the point where the spatial correlation between the photons –their mutual entanglement– is forfeited as a consequence of the generation of entanglement between the internal DOFs of the photons –i.e. their frequency with their spatial DOF– which can be easily understood from the redshift effect as it conditions the frequency of photons on their spatial position, or propagation path.

Then, due to the theorem of *entanglement monogamy* this internal entanglement can only come at the cost of lowering the mutual entanglement shared between the photons, for instance in their spatial (but also in their spectral) DOF.

For these considerations, it is necessary to operate the HOM-interferometer with resources that a priory contain entanglement. Frequency entangled photon sources are resources, which meanwhile are characterized theoretically to a large extent and are nowadays routinely employed by a variety of working groups all over the world. In other words, they are cheap, robust and well understood. Moreover, they certainly bare the potential to encode quantum information entanglement-based in is most desired in the DOF that is most desired

Employing the interference pattern of frequency entangled photons (2.72) to (4.52) one obtains the HOM-interferogram under relativistic influence in dependance from the QMem storage time

$$P_c(\tau_s) = \frac{R_{\mu\xi}^{\varphi z \tau_s} + S_{\mu\xi}^{\varphi z \tau_s}}{1 + R_{\mu\xi}^{\varphi 0} S_{\mu\xi}^{\varphi 0}} \quad (4.58)$$

with

$$R_{\mu\xi}^{\varphi z \tau_s} = \cos(\mu z \tau_s - \varphi) \operatorname{tri}\left(\frac{\xi z \tau_s}{2}\right), \quad (4.59a)$$

$$S_{\mu\xi}^{\varphi z \tau_s} = \operatorname{sinc}\left(\frac{\mu}{2\xi} \operatorname{tri}\left(\frac{\xi z \tau_s}{2}\right)\right) \operatorname{tri}\left(\frac{\xi z \tau_s}{2}\right), \quad (4.59b)$$

where –as before– $\operatorname{tri}(x)$ being the triangular function, and we have set $\Delta_{\Theta^{-1}} = z$ with $z = z_{UL}$, which is the result of the linear expansion of the differential redshift factor (4.51) for $E = L$ in the redshift z_{UL} .

Equation (4.58) refines our result for the interferogram from Ref. [BGK⁺24], which was only given in the small-bandwidth limit $\xi \rightarrow 0$, which is possible through our simpler (but not approximated) result (4.48), that arises from our single-particle considerations. From this, one can study finite-bandwidths effects, which are however, for the parameter regime in which we are interested not interesting, but more important for quantum communication issues related to our considerations.

We here want to solely mention our main result from Ref. [BGK⁺24] that is captured in Fig. 4.4 and shows that the chances are good to observe the predicted gravitationally induced erasure of the correlation interferogram (4.54) in a terrestrial experimental setting within the University of Bremen's Drop Tower by employing state-of-the-art Praseodymium and Rubidium quantum memories.

Entanglement dynamics of photon pairs and quantum memories in the gravitational field of the earth

Roy Barzel¹, Mustafa Gündoğan^{2,3}, Markus Krutzik^{2,3,4}, Dennis Rätzel^{1,2}, and Claus Lämmerzahl^{1,5}

¹ZARM, University of Bremen, Am Fallturm 2, 28359 Bremen, Germany

²Institut für Physik, Humboldt-Universität zu Berlin, Newtonstraße 15, 12489 Berlin, Germany

³IRIS Adlershof, Humboldt-Universität zu Berlin, Zum Großen Windkanal 2, 12489 Berlin, Germany

⁴Ferdinand-Braun-Institut (FBH), Gustav-Kirchoff-Str.4, 12489 Berlin, Germany

⁵Institute of Physics, Carl von Ossietzky University Oldenburg, Ammerländer Heerstr. 114-118, 26129 Oldenburg, Germany

We investigate the effect of entanglement dynamics due to gravity – the basis of a mechanism of universal decoherence – for photonic states and quantum memories in Mach-Zehnder and Hong-Ou-Mandel interferometry setups in the gravitational field of the earth. We show that chances are good to witness the effect with near-future technology in Hong-Ou-Mandel interferometry. This would represent an experimental test of theoretical modeling combining a multi-particle effect predicted by the quantum theory of light and an effect predicted by general relativity. Our article represents the first analysis of relativistic gravitational effects on space-based quantum memories which are expected to be an important ingredient for global quantum communication networks.

1 Introduction

It has become one of the major problems of theoretical physics to understand the interplay between our most successful theories, quantum mechanics (QM) and general relativity (GR) [1]. A resolution of this problem can only be driven by experiments or observations at the interface of the two theories. In addition, the race in the development of space-based quantum technologies, where quantum resources are generated and probed locally [2, 3] or are exchanged over thousands of kilometers through the inhomogeneous gravitational field of Earth [4, 5, 6, 7, 8], fuels the need to understand the influence of general relativistic effects on quantum resources also from a practical point of view.

A particular example of an interesting fundamental effect at the interface of quantum mechanics and general relativity is the generation of entanglement between the internal energy structure of a quantum system and its external (motional) degrees of freedom (DOFs) due to gravitational time dilation or redshift.

Roy Barzel: roy.barzel@zarm.uni-bremen.de

Dennis Rätzel: dennis.raetzel@zarm.uni-bremen.de

These entanglement dynamics (EDs) due gravity have been proposed to be witnessed in atom interferometry [9], with single photons in Mach-Zehnder (MZ) interference [10], photon pairs in Hong-Ou-Mandel (HOM) interference [11] and phonons in Bose-Einstein condensates [12]. For the case of massive quantum systems that are in superposition states of their center of mass degree of freedom, EDs due to gravity were found to induce decoherence [13, 14], underlining their fundamental significance.

In this article, we investigate the case of EDs of photons and Quantum Memories (QMem) [15, 16] due to gravity in MZ and HOM interferometry setups as shown in Fig. 1. Furthermore, we provide an experimental proposal and a feasibility study to witness the effect in HOM experiments whose necessary spatial extensions are dramatically smaller than those of proposed experiments that only employ photons [10, 17, 11]. Furthermore, we want to emphasize that the associated non-locality in the presence of entanglement between photons in different arms of a HOM interferometer extends the quality of the conceptional discussion from previous works considering MZ-interference of photons (see e.g. [18, 19, 20, 11] for other investigations of gravitational effects in interference of several particles). Due to the close relation of EDs due to gravity to decoherence, our results are also of practical relevance as they inform us about potential new challenges to be faced in the development of novel space-based quantum technological applications. Before we derive the appearance of EDs of photons and QMem due to gravity in MZ- and HOM-interferometry setups, we first consider a simple example. In the following, we will set $\hbar = 1$.

2 Qubit in spatial superposition

The simplest system in which EDs due to gravity take place is a single two-level system, with internal energy states $|\mu_{1,2}\rangle$ of corresponding energies $\mu_{1,2}$ which is allowed to be situated at two different gravitational potential levels U and L . In the following, we assume a stationary situation, where U and L correspond to

two local laboratories that are at rest in Earth's gravitational field, where "at rest" means that they are located at a fixed position in the co-rotating reference system of Earth, that is, geosynchronous and a fixed radial distance from Earth's center, i.e. they are assumed to move on timelike Killing trajectories through spacetime. For simplicity, we describe the dynamics of the considered system from the perspective of a third resting but not further specified reference observer, o , evolving w.r.t. to proper time τ_o . Then, the considered two-level system evolves w.r.t. the proper time $\tau_\sigma = \Theta_\sigma \tau_o$ depending on the site $\sigma = U, L$, where $\Theta_\sigma = 1 + z_{o\sigma}$ is related to the redshift $z_{o\sigma}$ between the resting reference observer o and the observers at $\sigma = U, L$, as defined in [21]. To leading order, we can describe the redshift with the approximated formula [22]

$$\begin{aligned} z_{o\sigma} &= (W_\sigma - W_o)/c^2, \quad \text{where} \\ W_\alpha &= -GM/R_\alpha - v_{\text{orb},\alpha}^2/2, \end{aligned} \quad (1)$$

for $\alpha = \sigma, o$, and R_α and $v_{\text{orb},\alpha}$ are the corresponding radial distance from the center of Earth and the orbital velocity, respectively, and G is Newton's gravitational constant and M is Earth's mass.

The single particle of our example can effectively be regarded as a two-qubit system, where one qubit is encoded in the particle's internal DOF $\mu_{1,2}$ and the other qubit is encoded in its external DOF σ . The associated Hilbert space is of dimension four and is spanned by the basis $\{|\mu_1\rangle \otimes |U\rangle, |\mu_2\rangle \otimes |U\rangle, |\mu_1\rangle \otimes |L\rangle, |\mu_2\rangle \otimes |L\rangle\}$. To be subject to EDs due to gravity, the internal sub-state of the particle needs to describe a coherent superposition of energy eigenstates

$$|\psi_{\text{int}}(\tau_o)\rangle = (|\mu_1\rangle + e^{i\varphi(\tau_o)}|\mu_2\rangle)/\sqrt{2}, \quad (2)$$

usually denoted as clock state because during its time evolution it precesses like a clock around the equator of its associated Bloch-sphere. The relative phase $\varphi(\tau_o)$ can then be identified as the time which the clock "shows". The single-particle Hamiltonian \hat{H}_1 which generates the time evolution of the particle is diagonal in the previously mentioned basis and reads

$$\hat{H}_1 = \text{diag}(\Theta_U \mu_1, \Theta_U \mu_2, \Theta_L \mu_1, \Theta_L \mu_2). \quad (3)$$

It can be deduced from a phenomenologically motivated ansatz, that is, effectively the coordinate time in the Schrödinger equation is replaced by the proper time [13]. However, it reproduces the experimental results of the Hafele Keating experiment [23] correct, in other words, one recovers the well known redshift relation of clock frequencies at different gravitational potential levels. EDs due to gravity take place for a clock-state in a coherent superposition of both sites

$$|\phi(0)\rangle = (|\mu_1\rangle + |\mu_2\rangle)/\sqrt{2} \otimes (|U\rangle + |L\rangle)/\sqrt{2}. \quad (4)$$

This can be easily shown by first evolving the state with the single-particle Hamiltonian to $|\phi(\tau_o)\rangle =$

$e^{-i\hat{H}_1\tau_o}|\phi(0)\rangle$, computing the corresponding density matrix $\hat{\rho}(\tau_o) = |\phi(\tau_o)\rangle\langle\phi(\tau_o)|$ and subsequently tracing out the internal (energy) DOFs of the particle, which results in the reduced 2×2 density matrix $\hat{\rho}_{\text{red}}(\tau_o) = \sum_{i=1,2} \langle \mu_i | \hat{\rho}(\tau_o) | \mu_i \rangle$. The *purity* of the reduced density matrix

$$\mathcal{P}(\tau_o) = \sum_{\sigma=U,L} \langle \sigma | \hat{\rho}_{\text{red}}(\tau_o) | \sigma \rangle = 1 - \frac{\sin^2(\Delta_\Theta \mu_- \tau_o / 2)}{2}, \quad (5)$$

with $\mu_- = \mu_1 - \mu_2$ and $\Delta_\Theta := \Theta_L - \Theta_U = z_{oL} - z_{oU}$ indicates that the initially pure spatial sub-state of the particle decohered into the maximally mixed state

$$\hat{\rho}_{\text{red}}(\tau_{o,\text{ent}}^{(1)}) = (|U\rangle\langle U| + |L\rangle\langle L|)/2 \quad (6)$$

after the time

$$\tau_{o,\text{ent}}^{(1)} = \frac{\pi}{\Delta_\Theta \mu_-} \quad (7)$$

since $\mathcal{P}(\tau_{o,\text{ent}}^{(1)}) = 1/2$. Because the entire state $\hat{\rho}(\tau_o)$ is pure for all times, one can infer that the time evolution of \hat{H}_1 generated entanglement between the internal and positional DOFs of the considered particle.

Equivalently, one can consider the *linear entropy* of the reduced spatial sub-state

$$\mathcal{S}(\tau_o) = 1 - \mathcal{P}(\tau_o) = \frac{\sin^2(\Delta_\Theta \mu_- \tau_o / 2)}{2}, \quad (8)$$

as a measure of entanglement between the internal and external DOF of the considered particle. The maximal entanglement between external and internal DOFs at $\tau_{o,\text{ent}}^{(1)}$ does then correspond to a maximum of \mathcal{S} .

After having seen that gravitational effects can influence the entanglement between different DOFs of a single particle, it is natural to ask whether this effect might influence the mutual entanglement between different distant particles. The answer to this question is yes. In App. A, we consider the example of two particles subject to EDs due to gravity and show that some entanglement correlations between different particles feature non-trivial dynamics, where other entanglement correlations between different particles are robust against the gravitational effects.

However, one should note that entanglement dynamics is a general result of the time evolution generated by a diagonal Hamiltonian of the form \hat{H}_1 of which the present example of EDs due to gravity is only a specific example. The only relevant quantity is $\Delta_\Theta \mu_- = (d_1 - d_2) - (d_3 - d_4)$, where d_i are the diagonal entries of \hat{H}_1 . This quantity can be interpreted as the coupling between two qubits of a two-qubit system in general as it is a measure of how much the energetic distance between the two states of one qubit changes conditioned on the quantum state of the other qubit. Non-zero-values of $\Delta_\Theta \mu_-$ imply non-trivial entanglement dynamics in general. For instance, also a

Quantity	Symbol
relative redshift	$z_{o\sigma}$
local redshift factor	Θ_σ
difference frequencies	μ_-, Ω_-, ν_-
sum frequencies	μ_+, Ω_+, ν_+
differential redshift between U and L	Δ_Θ
differential inverse redshift between U and L	$\Delta_{\Theta^{-1}}$
purity of spatial substate	\mathcal{P}
linear entropy of spatial substate	\mathcal{S}
wavefunction normalization constants	$N_{\text{MZ}}, N_{\text{HOM}}$
local QMem storage times	$\tau_{\sigma,s}$
interference patterns	$P_c^{\text{MZ}}, P_c^{\text{HOM}}$
bunching anti-bunching probability difference	P_c^{HOM}

Table 1: Table of the most important recurring quantities and the corresponding symbols.

spin-1/2 particle which is exposed to magnetic fields of different magnitude at two different lattice sites $\sigma = U, L$ would experience the same effect, in complete absence of relativistic effects [24].

3 EDs due to gravity in interference experiments

Now, we draw our attention towards effects of EDs due to gravity in interference experiments with quantum states of photons involving quantum memories (QMems). We describe pure single- and two-photon states as

$$|\psi_1\rangle = \sum_{\sigma} \int d\omega \psi_{\sigma}(\omega) \hat{a}_{\sigma\omega}^\dagger |0\rangle, \quad (9a)$$

$$|\psi_2\rangle = \frac{1}{\sqrt{2}} \sum_{\sigma_1, \sigma_2} \int d\omega_1 d\omega_2 \psi_{\sigma_1 \sigma_2}(\omega_1, \omega_2) \hat{a}_{\sigma_1 \omega_1}^\dagger \hat{a}_{\sigma_2 \omega_2}^\dagger |0\rangle, \quad (9b)$$

where ω is the internal frequency/energy DOF and σ is the spatial DOF of the considered photon. The operators $\hat{a}_{\sigma\omega}^\dagger$ create a photon of frequency ω in spatial mode σ without knowledge of polarization, $|0\rangle$ is the corresponding vacuum state of the electromagnetic field and $\psi_{\sigma}(\omega)$ and $\psi_{\sigma_1 \sigma_2}(\omega_1, \omega_2)$ are the *photonic wave functions*.

Typically MZ-interferometers are operated with initial photonic wave function

$$\psi_{\sigma}(\omega) = \psi(\omega) \delta_{\sigma A}, \quad (10)$$

where δ is the Kronecker delta and A is one of the two input ports (A,B) of the first beam splitter of the MZI (see Fig. 1 a)). We consider the HOM-interferometer to be operated with initial two-photon wave function

$$\begin{aligned} \psi_{\sigma_1 \sigma_2}(\omega_1, \omega_2) = & \left(\psi(\omega_1, \omega_2) \delta_{\sigma_1 U} \delta_{\sigma_2 L} \right. \\ & \left. + \psi(\omega_2, \omega_1) \delta_{\sigma_2 U} \delta_{\sigma_1 L} \right) / \sqrt{2} \end{aligned} \quad (11)$$

as displayed in Fig. 1 b). Note the symmetry of the two-particle photonic wave function under simultaneous exchange of ω and σ , that is, $\psi_{\sigma_1 \sigma_2}(\omega_1, \omega_2) = \psi_{\sigma_2 \sigma_1}(\omega_2, \omega_1)$, which incorporates the indistinguishability of the two particles. We are interested in single-photon coherent superposition states of two angular frequencies Ω_1 and Ω_2 (the formal analog to the single-qubit clock-states of our example above)

$$\psi(\omega) = N_{\text{MZ}}[g_{\Omega_1 \xi}(\omega) + e^{i\varphi} g_{\Omega_2 \xi}(\omega)] \quad (12)$$

and frequency entangled two-photon states (the formal analog to the entangled two-qubit clock-states from Appendix A)

$$\begin{aligned} \psi(\omega_1, \omega_2) = & N_{\text{HOM}}[g_{\Omega_1 \xi}(\omega_1) g_{\Omega_2 \xi}(\omega_2) \\ & + e^{i\varphi} g_{\Omega_2 \xi}(\omega_1) g_{\Omega_1 \xi}(\omega_2)], \end{aligned} \quad (13)$$

where $g_{\Omega \xi}(\omega) = (2\pi\xi^2)^{-1/4} e^{-(\omega-\Omega)^2/(4\xi^2)}$ is a Gaussian distribution, ξ is the single-photon bandwidth and N_{MZ} and N_{HOM} are normalization constants. We assume the wave functions to be normalized as $\int d\omega |\psi(\omega)|^2 = 1$ and $\int d\omega_1 d\omega_2 |\psi(\omega_1, \omega_2)|^2 = 1$. This determines the normalization constants to be

$$N_{\text{MZ}} = (2[1 + \cos(\varphi)e^{\Omega^2/(8\xi^2)}])^{-1/2} \quad (14a)$$

$$N_{\text{HOM}} = (2[1 + \cos(\varphi)e^{\Omega^2/(4\xi^2)}])^{-1/2}, \quad (14b)$$

where $\Omega_- = \Omega_2 - \Omega_1$. The spectra and all frequencies Ω_i are measured in the local reference frame o which we associate with the photon (pair) source.

The initial photon states are injected into the interferometers as displayed in Fig. 1. In case of the MZ-interferometer, a first beam splitter is applied which transforms the photonic creation operators as $\hat{a}_{A\omega} \rightarrow (\hat{a}_{U\omega} - \hat{a}_{L\omega})/\sqrt{2}$ and $\hat{a}_{B\omega} \rightarrow (\hat{a}_{U\omega} + \hat{a}_{L\omega})/\sqrt{2}$. In both, the MZ- and HOM-interferometer, frequency-dependent phases $\varphi_{\sigma}(\omega)$ are added due to storage process and propagation. Then, 50 : 50 beam splitters are applied, which transform the photonic creation operators as $\hat{a}_{U\omega} \rightarrow (\hat{a}_{\oplus\omega} - \hat{a}_{\ominus\omega})/\sqrt{2}$ and $\hat{a}_{L\omega} \rightarrow$

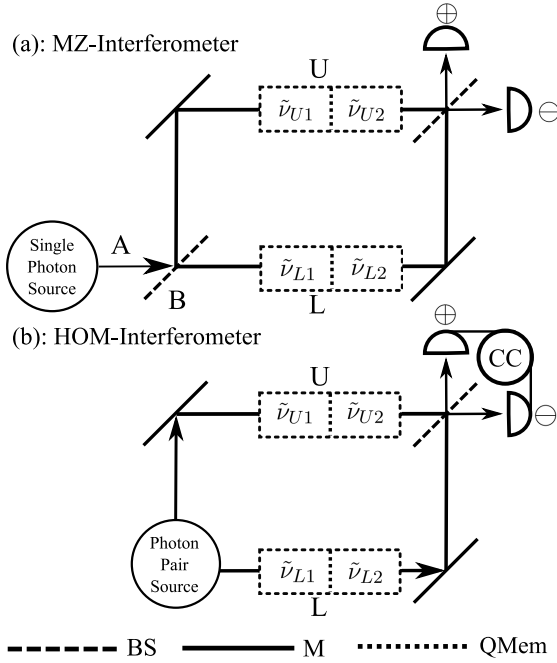


Figure 1: Interference in gravitational field. (a): MZ-Interferometer. (b): HOM-Interferometer. BS: Beam splitter. M: Mirror. CC: Coincident count logic. QMem: Quantum memory. Each transition path is respectively equipped with two QMems with internal states, which *locally* oscillate at discrete angular frequencies $\tilde{\nu}_{\sigma_i}$ and $\tilde{\nu}_{\sigma_i}$, i.e. the frequencies are measured locally in the rest frame of the respective QMem. They are tuned, together with the frequencies of corresponding control lasers, such that storage and readout process are optimized.

$(\hat{a}_{\oplus\omega} + \hat{a}_{\ominus\omega})/\sqrt{2}$. These transformations lead to the final photonic wave functions $\psi_\sigma^f(\omega)$ and $\psi_{\sigma_1\sigma_2}^f(\omega_1, \omega_2)$.

In conventional MZ- and HOM-interferometry, the detectors are frequency/energy-insensitive. Thus we are only interested in the spatial sub state of the final state, i.e. in the reduced single- and two-photon density matrices

$$\rho_{\sigma\bar{\sigma}} = \int d\omega \psi_\sigma^f(\omega) \psi_{\bar{\sigma}}^f(\omega)^*, \quad (15a)$$

$$\rho_{\sigma_1\sigma_2\bar{\sigma}_1\bar{\sigma}_2} = \int d\omega_1 d\omega_2 \psi_{\sigma_1\sigma_2}^f(\omega_1, \omega_2) \psi_{\bar{\sigma}_1\bar{\sigma}_2}^f(\omega_1, \omega_2)^*, \quad (15b)$$

The detection statistics of MZ- and HOM-experiments is encoded in the diagonal entries of the reduced density matrices (15) as we have

$$P_{\sigma'}^{\text{MZ}} = \int d\omega \langle \hat{a}_{\sigma'\omega}^\dagger \hat{a}_{\sigma'\omega} \rangle = \rho_{\sigma'\sigma'} \quad \text{and} \quad (16a)$$

$$\begin{aligned} P_{\sigma'_1\sigma'_2}^{\text{HOM}} &= \int d\omega_1 d\omega_2 \langle \hat{a}_{\sigma'_1\omega_1}^\dagger \hat{a}_{\sigma'_2\omega_2}^\dagger \hat{a}_{\sigma'_2\omega_2} \hat{a}_{\sigma'_1\omega_1} \rangle / 2 \\ &= \rho_{\sigma'_1\sigma'_2\sigma'_1\sigma'_2}, \end{aligned} \quad (16b)$$

where $\sigma', \sigma'_1, \sigma'_2 = \oplus, \ominus$. In MZ-interference, coherence can be studied by analyzing the difference be-

tween the detector intensities

$$P_c^{\text{MZ}} = P_\ominus^{\text{MZ}} - P_\oplus^{\text{MZ}}. \quad (17)$$

In HOM-interference a measure of spatial correlation between the two involved photons is the difference between the photon bunching and photon anti-bunching probability

$$P_c^{\text{HOM}} = (P_{\oplus\oplus}^{\text{HOM}} + P_{\ominus\ominus}^{\text{HOM}}) - (P_{\oplus\ominus}^{\text{HOM}} + P_{\ominus\oplus}^{\text{HOM}}). \quad (18)$$

As explained in the qubit model above, the size of the gravitational effect will depend on the time the photons spend on the different potential levels U and L. In this article, we investigate two options for the maximization of this time: QMems and optical delay lines. As our focus lies on the former, we discuss it first to compare the results to the latter case later.

3.1 EDs due to gravity in quantum memories

In this section, we discuss the application of QMems to store the photons in the interferometer arms as shown in Fig. 1. The storage process consists in a transfer of the photonic state to a matter system which we model as a mode swapping operation (details can be found in the experimental part of this paper and in App. B). This process generically alters the energies of the spectral components of the quantum state according to the given energy level structure of the QMem. We assume that each peak of the spectral wave function is mapped to a quantum memory according to the mapping $\tilde{\Omega}_{\sigma i} \rightarrow \tilde{\nu}_{\sigma i}$, where $\tilde{\nu}_{\sigma i}$ is the oscillation frequency of the i -th QMem at the potential level $\sigma = U, L$ and $\tilde{\Omega}_{\sigma i}$ is the frequency of the i -th peak of the spectral wave function as measured from the perspective of an observer at the potential level $\sigma = U, L$. Here, as in the following, we will denote frequencies in the local frames with a tilde and frequencies defined from the perspective of the global reference fixed to the frame of the photon source without a tilde. We assume that the time evolution of the state inside each QMem is governed by the simple unitary $\hat{U}_{\sigma i} = e^{-i\tilde{\nu}_{\sigma i}\tau_{\sigma s}}$, where $\tau_{\sigma s}$ is the local proper storage time at the potential level $\sigma = U, L$.

After the storage time $\tau_{\sigma s}$, the quantum state is read out from the memory and imprinted on a photonic state that is propagating to the beam splitter. The storage and read-out processes add additional phases due to the interaction with the external control lasers. These operate at the (typical optical) frequencies $\tilde{\Omega}_{\sigma i}^{(r)}$ in the local reference frames corresponding to U and L. For the storage process to be effective, one generally has to assume a fixed relation between the local frequencies $\tilde{\nu}_{\sigma i}$, $\tilde{\Omega}_{\sigma i}^{(r)}$ and $\tilde{\Omega}_{\sigma i} = \Omega_i/\Theta_\sigma$, where $\Theta_\sigma = 1+z_{o\sigma}$ and $z_{o\sigma}$ is the redshift with respect to the photon source. In the following, we consider the case of a specific type of QMem called Lambda system (see Fig. 2, details can be found in Section 4), where we

set $\tilde{\nu}_{\sigma i} + \tilde{\Omega}_{\sigma i}^{(r)} = \tilde{\Omega}_{\sigma i}$. Performing a straightforward calculation (whose details we outline in App. B), the resulting state after the storage becomes

$$|\psi'_{\text{MZ}}\rangle = \sum_{\sigma} \int d\omega \psi'_{\sigma}(\omega) \hat{a}_{\sigma\omega}^{\dagger} |0\rangle, \quad (19a)$$

$$|\psi'_{\text{HOM}}\rangle = \int d\omega_1 d\omega_2 \psi'(\omega_1, \omega_2) a_{U\omega_1}^{\dagger} a_{L\omega_2}^{\dagger} |0\rangle, \quad (19b)$$

where the photonic wave functions altered by the QMems are

$$\begin{aligned} \psi'_{\sigma}(\omega) &= (-1)^{\tilde{n}(\sigma)} N_{\text{MZ}}[g_{\Omega_1\xi}(\omega)e^{i\tilde{\Omega}_{\sigma 1}\tau_{\sigma s}} \\ &\quad + e^{i\varphi} g_{\Omega_2\xi}(\omega)e^{i\tilde{\Omega}_{\sigma 2}\tau_{\sigma s}}]/\sqrt{2} \end{aligned} \quad (20a)$$

$$\begin{aligned} \psi'(\omega_1, \omega_2) &= N_{\text{HOM}}[g_{\Omega_1\xi}(\omega_1)g_{\Omega_2\xi}(\omega_2) \\ &\quad + e^{i\varphi'_{\text{HOM}}} g_{\Omega_2\xi}(\omega_1)g_{\Omega_1\xi}(\omega_2)], \end{aligned} \quad (20b)$$

$\tilde{n}(U) = 0$, $\tilde{n}(L) = 1$ and

$$\varphi'_{\text{HOM}} = \varphi + \tilde{\Omega}_{U-\tau_{Us}} - \tilde{\Omega}_{L-\tau_{Ls}} \quad (21)$$

where $\tilde{\Omega}_{\sigma-} = \tilde{\Omega}_{\sigma 2} - \tilde{\Omega}_{\sigma 1} = (\Omega_2 - \Omega_1)/\Theta_{\sigma}$. Note that neither $\tilde{\nu}_{\sigma i}$ nor $\tilde{\Omega}_{\sigma i}^{(r)}$ appear in equations (20). This is because the internal dynamics with $\tilde{\nu}_{\sigma i}$ and the temporal phase evolution of the control laser combine to the phase evolution with $\tilde{\Omega}_{\sigma i}$. The situation would be different, for example, if the internal evolution is not imprinted on the output state. The general results can be found in App. B. It should be noted, however, that for ground state QMems, the resulting phases due to the internal evolution are very small in comparison to the much larger phases imprinted by the control lasers (see also 4).

Finally, to predict the outcome of the interference experiments shown in Fig. 1, we have to specify the relation of τ_{Us} and τ_{Ls} . There are two basic options for the synchronization of the storage processes: equivalent local storage times and synchronization in a global reference frame. In the latter case, $\tau_{Us}/\Theta_U = \tau_{Ls}/\Theta_L$ and no gravitational effect on the interference patterns can be observed.

The first case comprises to set $\tau_{Us} = \tau_{Ls} = \tau_s$. For example, this may be achieved by placing a reference clock next to each of the QMems. We obtain for the coherence measures (17) and (18) in the large bandwidth limit (where expressions simplify significantly and analytical calculations can be performed with reasonable effort) $\Omega_2 - \Omega_1 \gg \xi$ the MZ- and HOM-interference patterns

$$P_c^{\text{MZ}} = \cos(\Delta_{\Theta^{-1}}\Omega_+\tau_s/2) \cos(\Delta_{\Theta^{-1}}\Omega_-\tau_s/2), \quad (22a)$$

$$P_c^{\text{HOM}} = \cos(\Delta_{\Theta^{-1}}\Omega_-\tau_s - \varphi), \quad (22b)$$

where $\Omega_{\pm} = \Omega_2 \pm \Omega_1$ and $\Delta_{\Theta^{-1}} = 1/\Theta_L - 1/\Theta_U$. We want to emphasize the appearance of $\Delta_{\Theta^{-1}}$ in the frequencies of EDs in contrast to the qubit case discussed above, where the frequency of EDs is proportional to

Δ_{Θ} . This shows a subtle difference in the appearance of EDs due to gravity in these two cases: In the photon case, the effect is a result of gravitational redshift, and in the qubit case, it is gravitational time dilation. These effects are of course intimately related.

From Eq. (22a), one can see that the well known rapid oscillations of the MZ-interference signal are recovered in the first factor featuring the average frequency $\Omega_+/2$. The rapid oscillations are modulated on a much longer time scale by the second factor featuring the difference frequencies. This modulation of the interferometric contrast is a result of EDs due to gravity. In other words, the internal frequency degree of freedom becomes entangled with the photon path which means that a measurement of the internal degree of freedom would provide which-path information, thereby erasing the interferometric contrast. A full loss of contrast is obtained for $\Delta_{\Theta^{-1}}\Omega_-\tau_s = \pi$, which corresponds to a storage time

$$\tau_{s,\text{ent}}^{\text{MZ}} = \frac{\pi}{\Delta_{\Theta^{-1}}\Omega_-}. \quad (23)$$

Indeed, with the help of Eq. (15a), one finds the reduced density matrix of the photon's spatial DOF for this setting in a maximally mixed state of both detector modes (c.f. (82))

$$\rho_{\sigma\bar{\sigma}}(\tau_{s,\text{ent}}^{\text{MZ}}) = \frac{1}{2} \begin{pmatrix} 1 & 0 \\ 0 & 1 \end{pmatrix}, \quad (24)$$

that attains the minimum value of one half for the purity (see Appendix D for further details)

$$\mathcal{P}_{\text{MZ}} = \sum_{\sigma, \bar{\sigma}} |\rho_{\sigma\bar{\sigma}}|^2 = \frac{1}{2} (1 + \mathcal{V}^2), \quad (25)$$

where

$$\mathcal{V} = \cos(\Delta_{\Theta^{-1}}\Omega_-\tau_s/2), \quad (26)$$

is the slowly oscillating envelope of the MZ-interferogramm (22a), known as the *visibility*, the interferometric contrast. From Eq. (25) it is apparent that lower values of the interferometric contrast \mathcal{V} correspond to lower values of the purity of the reduced spatial sub-state. Therefore, the loss of the interferometric contrast, i.e. $\mathcal{V} = 0$, maximizes the linear entropy

$$\mathcal{S}_{\text{MZ}} = 1 - \mathcal{P}_{\text{MZ}} = \frac{1}{2} (1 - \mathcal{V}^2), \quad (27)$$

which also in this case serves as a measure of entanglement between the internal and external DOFs of the considered photon.

The interference pattern of the HOM-experiment (22b) vanishes for $\Delta_{\Theta^{-1}}\Omega_-\tau_s = \pi/2$, that is, $P_c^{\text{HOM}} = 0$, which means that photon bunching and photon anti-bunching are equiprobable at this setting, i.e. the photons are not correlated (entangled) in their spatial

DOF. Also, here the physical explanation is that during the propagation through the HOM-interferometer, the frequency DOF of each of the two entangled photons respectively gets entangled with the path of the respective photon. Put differently, the theorem of entanglement monogamy implies that the frequency-path entanglement can only be generated at the cost of lowering the entanglement between the photons' spatial DOFs [25], reflected by the equiprobability of photon bunching and photon anti-bunching. Indeed, with the help of Eq. (15b), one finds the spatial sub-state of the photons at the corresponding storage time

$$\tau_{s,\text{ent}}^{\text{HOM}} = \frac{\pi}{2\Delta_{\Theta^{-1}}\Omega_-} \quad (28)$$

to be (c.f. Eq. (88))

$$\rho_{\sigma_1\sigma_2\bar{\sigma}_1\bar{\sigma}_2}(\tau_{s,\text{ent}}^{\text{HOM}}) = \frac{1}{4} \begin{pmatrix} 1 & 0 & 0 & -1 \\ 0 & 1 & -1 & 0 \\ 0 & -1 & 1 & 0 \\ -1 & 0 & 0 & 1 \end{pmatrix}, \quad (29)$$

where we have chosen for the row and column numbering $\{\oplus\oplus, \oplus\ominus, \ominus\oplus, \ominus\ominus\}$. The reduced spatial density matrix (29) characterizes a mixed state as certified by the purity (see Appendix D for further details)

$$\mathcal{P}_{\text{HOM}} = \sum_{\substack{\sigma_1, \sigma_2, \\ \bar{\sigma}_1, \bar{\sigma}_2}} |\rho_{\sigma_1\sigma_2\bar{\sigma}_1\bar{\sigma}_2}|^2 = \frac{1}{2} \left(1 + (P_c^{\text{HOM}})^2 \right) \quad (30)$$

as one in particular finds

$$\mathcal{P}_{\text{HOM}}(\tau_{s,\text{ent}}^{\text{HOM}}) = \frac{1}{2}. \quad (31)$$

Also in the HOM-experiment, the linear entropy of the spatial sub-state

$$\mathcal{S}_{\text{HOM}} = 1 - \mathcal{P}_{\text{HOM}} = \frac{1}{2} \left(1 - (P_c^{\text{HOM}})^2 \right) \quad (32)$$

is a measure of entanglement between the internal and external DOFs of the photons, which is maximized at the equiprobability of photon bunching and photon anti-bunching, i.e. $P_c^{\text{HOM}} = 0$.

Not only entanglement between the internal and external DOFs of the photons is built up in HOM-interference. At the same time, the mutual entanglement shared between the spatial degrees of freedom of the photons and the spectral degrees of freedom of the photons, respectively, is depleted. We discuss the mutual entanglement between the photons only in their spatial DOF in the following, but want to emphasize that completely analogous results can be derived, in principle, for their spectral DOF (although the entanglement analysis and the associated continuous eigenvalue problem is slightly more involved). As P_c^{HOM} quantifies the spatial correlation of the photons to exit the same or distinct output ports of the beam

splitter in the HOM-experiment, this quantity is an intuitive candidate for a measure of spatial entanglement shared between the photons. This is indeed the case as the absolute value of P_c^{HOM} is proportional to the *negativity*, i.e.

$$\mathcal{N}_{\text{HOM}} = - \sum_{\lambda_{\text{PT}} < 0} \lambda_{\text{PT}} = \frac{|P_c^{\text{HOM}}|}{2}, \quad (33)$$

where λ_{PT} are the eigenvalues of the partial transpose of the reduced spatial density matrix (15b). Apart from being an entanglement monotone, the negativity unambiguously certifies by its positivity the presence of entanglement in the spatial sub-state of the two photons considered here (see Appendix D for derivation and discussion). Thus, Eq. (32) asserts that the creation of entanglement between the internal and external DOFs of the involved photons (i.e. the increase of \mathcal{S}_{HOM}) comes at the cost of depleting the mutual spatial entanglement shared between the photons (i.e. the decrease of P_c^{HOM}), and therefore in turn emphasizes the role of entanglement monogamy in HOM-interference.

Note that the mutual spatial entanglement between the two photons in the HOM-experiment is depleted twice as fast as the entanglement between the internal and external DOFs of a single photon in MZ-interference is built up. Further note that, in contrast to the MZ-interference pattern, the HOM-interference pattern is not subject to high-frequency oscillations with periodicity $\Omega_+/2$ which makes the HOM-experiments more robust against finite detector resolution and noise effects. However, also in the HOM-case one has to impose temporal resolution limits on the employed optical delays and the storage times of the QMems as $\tau_s^{\text{reslim}} = \pi/4\Omega_-$ in order to resolve the oscillations of the interference patterns which would otherwise be washed out by phase fluctuations.

Note also that we want to observe at least a half cycle of the entanglement dynamics such that the spatial correlations are not just lost but a full revival is witnessed. This is because, the loss of spatial correlations could also be, for example, due to decoherence through interaction with the environment.

3.2 EDs due to gravity in delay lines

If one wants to witness EDs due to gravity just with free photons, they have to travel for distances of the order of $c\tau_{s,\text{ent}}$. It has been proposed to employ optical delay lines for this purpose (see e.g. [11]). Applying locally equivalent optical delay lines in the distinct interferometer arms with local delay time τ_d (given by the length divided by the speed of light in the fiber) leads to a time evolution of the photonic state, which is governed by the unitary evolution $\hat{a}_{\sigma\omega} \rightarrow \hat{a}_{\sigma\omega} e^{i\omega\tau_d/\Theta_\sigma}$. In this case, we obtain for the spectra (12) and (13) in the large bandwidth limit

$\Omega_2 - \Omega_1 \gg \xi$ and $\Delta_{\Theta^{-1}}\tau_d\xi \ll 1$ the MZ- and HOM-interference patterns (see App. C for the derivation)

$$P_c^{\text{MZ}} = \cos(\Delta_{\Theta^{-1}}\Omega_+\tau_d/2) \cos(\Delta_{\Theta^{-1}}\Omega_-\tau_d/2), \quad (34a)$$

$$P_c^{\text{HOM}} = \cos(\Delta_{\Theta^{-1}}\Omega_-\tau_d - \varphi), \quad (34b)$$

The equations (34) are equivalent to equations (22) up to the replacement $\tau_s \rightarrow \tau_d$. Accordingly, the discussion following equations (22) equivalently applies to the case of delay lines under the replacement of the storage time by the optical delay time.

As for the case of the QMems (with equivalent local storage times), the effect of the delay lines arises due to the gravitational redshift of the photons and the resulting shift of the frequency difference between the two components of the photons' spectral wave function. Alternatively¹, the effect of the delay lines can be interpreted in terms of the Shapiro delay [10], that is the variation of the speed of light depending on the gravitational potential as perceived from the perspective of a distant observer [26, 27].

4 Experimental implementation

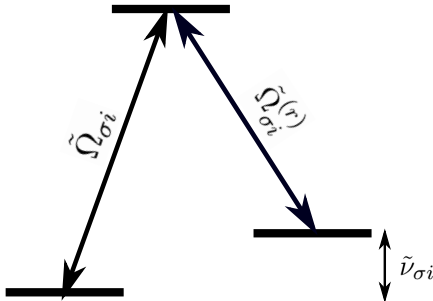


Figure 2: Energy scheme for ground state QMems denoted as Lambda system. The two lower states are usually hyperfine sublevels of the same electronic state. The frequencies of the internal dynamics $\tilde{\nu}_{\sigma i}$ are then in the GHz regime. The acceptance-frequency of the i -th QMem is denoted as $\tilde{\Omega}_{\sigma i}$ and the frequency of the i -th control laser is $\tilde{\Omega}_{\sigma i}^{(r)}$.

Now we will discuss the experimental requirements to realize EDs due to gravity in our proposal. Firstly, single-photon frequency superposition states and frequency entangled two-photon states can be created via nonlinear optical methods such as spontaneous parametric down conversion [28], sum/difference frequency generation [29] and Bragg scattering four wave mixing [30]. The central element of our proposal are QMems with sufficiently long storage times that are

¹By performing the temporal Fourier transform of the spectral wave function after applying the frequency dependent phase shift operation corresponding to the optical delay line, one obtains photon wave packets that are temporally translated by $\Theta_\sigma\tau_d$.

capable of storing photonic states in the forms of Eqs. (12) and (13). Here one crucial requirement is that each QMem in Fig. 1 should be able to store different frequency components, ($\tilde{\Omega}_{\sigma 1}$ and $\tilde{\Omega}_{\sigma 2}$) of the frequency superposition states. In Fig. 3 we plot the required memory time, τ_s as a function of Ω_- for different arrangements of the levels U and L .

Two different QMems operating at frequencies $\tilde{\Omega}_{\sigma 1}$ and $\tilde{\Omega}_{\sigma 2}$ can be combined together in each arm of the interferometer to ensure the efficient storage of both frequency components. We identified two different domains for such combinations: i) $\Omega_- \sim 1 - 10$ GHz (red shaded area in Fig. 3) and ii) $\Omega_- \sim 10 - 200$ THz (blue shaded area). The first domain requires $\tau_s > 1$ h (0.1 – 1 s) for terrestrial (space-borne) implementations, whereas the second domain requires $\tau_s < 1$ s (10^{-5} s) for terrestrial (space-borne) experiments. Storage times of up to hours [31, 32] is within reach with rare-earth ion doped (REID) QMems [33, 34, 35]. REID systems owe such long storage times to their electronic structure: their optically active electronic orbitals lie within the filled outer electronic shells that create a shielding effect that results in long optical and spin coherence lifetimes [36]. Furthermore, these system exhibit large inhomogeneous broadening which can be up to 20 GHz. This would allow storing different $\tilde{\Omega}_{\sigma 1}$ and $\tilde{\Omega}_{\sigma 2}$ components with equally long storage times within the same material through frequency multiplexing [37, 38]. For this scenario the required temporal resolution, τ^{reslim} , is around 10 – 100 ps which can be achieved with today's electronics. Furthermore, synchronization between remote clocks that are separated farther than our proposal requires for terrestrial experiments have been achieved with near-femtosecond precision [39, 40]. Picosecond precision of synchronization has been achieved in quantum optics experiments [41, 42]. Thus, the first domain is fully compatible with the state-of-the-art in REID QMems.

$\Omega_- \sim 10 - 100$ THz of the second domain can be achieved by combining different types of QMems while satisfying the requirements on τ_s . For instance, Pr ($\tilde{\Omega}_{\sigma 1} = 606$ nm) [33, 37] and Eu ($\tilde{\Omega}_{\sigma 2} = 580$ nm) [34, 32, 35] based REID QMems would yield $\Omega_- = 22$ THz. Cold and warm alkali gases can also be considered for our scheme: optical memories with lifetimes beyond 1 s have been demonstrated with Rb [43, 44] ($\tilde{\Omega}_{\sigma 1} = 795$ nm) and Cs [45] ($\tilde{\Omega}_{\sigma 2} = 894$ nm) gases. This combination would result in $\Omega_- = 42$ THz. The different frequency separations, which can be attained, are summarized in Tab. 1 in the Appendix G. The achieved storage times with these systems would enable a terrestrial test of our scheme. Combining a REID and an alkali gas QMem would result in $\Omega_- > 100$ THz, for example by combining a Pr and Rb QMem. In this case τ^{reslim} is around a few fs which, as has been stressed above, recently been achieved in [39, 40]. Therefore, timing

resolution requirements for terrestrial experiments in both domains are within today's technological reach.

A great advantage of terrestrial experiments based on QMems would be that, in addition to the HOM experiment, a MZ experiment would also be possible as the vertical scale of the required interferometers is orders of magnitude smaller than for the previous photonic proposals that do not employ QMems [10, 17, 11] and thus is already within the experimental realm [46, 47, 48, 49].

Finally, we discuss the prospects of using simple delay lines for the demonstration of EDs due to gravity. Note that similar considerations can be found in [17, 11]. From Fig. 3, one finds that, for an ambitious synchronization resolution of $\tau_{\text{res}} \sim 1$ ps across GEO and Earth's surface (limited due to the effect of Earth's atmosphere), one needs a fibre delay line with a length of around 750 km (assuming a minimal attenuation factor ~ 0.2 dB/m and a refractive index ~ 1.47). The associated loss of ~ 150 dB would render any detection impossible. One would be bound to perform the experiment outside Earth's atmosphere to have the chance to obtain τ_{res} of the order of 1 fs. Then, a delay line of ~ 6 km (corresponding to a loss of $\sim 40\%$ of the signal) would enable the detection of EDs due to gravity for frequency entangled photons at the two telecom wavelength 1550 nm and 1310 nm (maximal attenuation factor of ~ 0.36 dB/m and refractive index ~ 1.47) and a setup of two satellites where one is located at a geosynchronous orbit and the other at 10,000 km above Earth's surface. Of course, the latter is not fulfilling our condition of stationarity with respect to the Earth's surface, however, for the duration of the experiment τ_d this is still a good approximation (see App. E).

5 Conclusions

To conclude, we have investigated EDs due to gravity in MZ interferometry of two-frequency superposition states of single photons and HOM interferometry of frequency entangled two-photon states involving QMems. EDs due to gravity arise because of the geometry of the considered setup, where the arms of the interferometer correspond to different paths through spacetime. More specifically, in each arm, the photons pass through QMems that store the photonic correlations in localized memory excitations for an equivalent local storage time τ_s . The QMems in different interferometer arms are located at different potential levels in the gravitational field of the earth. Redshift (or equivalently gravitational and relativistic time dilation) then implies that the states of the localized storage excitations evolve differently (as seen from a global coordinate-dependent perspective). This difference in evolution leads to entanglement between the spatial and frequency degrees of freedom of the restored photons in the readout process. We want to

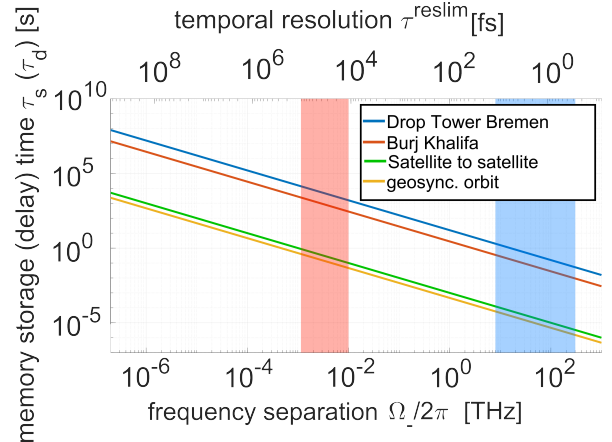


Figure 3: Experimental requirements to witness EDs due to gravity in HOM-interference. The diagonal lines correspond to the required storage (delay) time $\tau_{s(d)} = \pi/(2\Delta_{\theta-1}\Omega_-)$ in the HOM-experiment to observe EDs due to gravity for four different redshift factors: Drop Tower Bremen ($\Delta_{\theta-1} \approx 1.6 \cdot 10^{-14}$), Burj Khalifa ($\Delta_{\theta-1} \approx 9.0 \cdot 10^{-14}$), satellite-to-satellite scenario ($\Delta_{\theta-1} \approx 2.5 \cdot 10^{-10}$) and the redshift between a geostation and a geosynchronous orbit ($\Delta_{\theta-1} \approx 5.4 \cdot 10^{-10}$). The red (blue) shaded area indicates the regime of frequency separation $\Omega_- = 1 - 10$ GHz ($\Omega_- = 10 - 100$ THz) at which combinations of RIED QMems discussed in the main text operate. The upper horizontal axis indicates the required temporal resolution of the memory time (optical delay time) at a given frequency separation Ω_- . See App. F for further details on the calculation of the required temporal resolution τ^{reslim} .

emphasize that EDs through localized excitation as an intermediate state is fundamentally different from EDs in previous proposals where only photons were considered and EDs arise due to their propagation through space (e.g. [10, 17, 11, 20]). Accordingly, EDs due to gravity of photons and QMems necessitates a different description as we have developed it for this article.

We have derived the detection statistics of photons behind the interfering beam splitter, i.e. the interference patterns, as a function of the storage time τ_s . In the case of MZ interferometry of two-frequency superposition states of single photons, the interferogram shows two oscillations with τ_s , a fast oscillation proportional to the average frequency and a beating proportional to the difference frequency. For HOM interferometry of frequency entangled two-photon states, only one oscillation appears, which is twice as fast as the beating oscillation of MZ interferometry. This feature is indicative of quantum-enhanced phase estimation, a phenomenon where the accumulated phase in an interference experiment scales with the number of particles involved. Quantum-enhanced phase estimation can also be achieved with particles in a NOON state [50, 20], wherein all photons co-propagate through an unknown but common path in

the interferometer, usually of the MZ type. In stark contrast, the HOM setup ensures that each photon in the pair propagates through a separate arm of the interferometer, as indicated by Eq. (19b).

We also gave a detailed analysis of the involved EDs due to gravity in terms of entanglement measures, the linear entropy and the negativity of the reduced density matrix of the spatial sub-state. In particular, the entanglement measures show oscillations with the difference frequency and the storage time that can be directly related to the oscillations of the interference patterns. Additionally, we compared our results to the similar case where optical delay lines instead of QMems are employed to realize long evolution times of photons at different gravitational potential levels.

We have discussed the prospects of experimental realization of EDs due to gravity with implementations employing QMems and optical delay lines. We have found that HOM interferometry of frequency entangled two-photon states has the clear advantage that the absence of high-frequency oscillations (that appear in the MZ case) implies that phase stability is not necessary and allows for a much smaller timing precision of storage and free-space propagation. Furthermore, we have found that the necessary storage times to perform the proposed tests of EDs due to gravity with QMems have already been realized in the lab. We conclude that chances are good that corresponding experiments can be conducted with near future technology in satellite-based implementations and even in terrestrial implementations when QMems are employed. Such experimental verification of EDs due to gravity would constitute an experimental test of theoretical modeling combining a multi-particle effect predicted by the quantum theory of light and an effect predicted by general relativity.

It should be noted, however, that this effect already occurs in flat spacetime geometries, for example, Rindler space (corresponding to a uniformly accelerated frame that can be associated with a uniform gravitational field via the equivalence principle), since relativistic time dilation as a first order effect does not presuppose a non-trivial spacetime curvature. From a theoretical view point it would be interesting to investigate the contributions of curvature and higher order expansions of the metric tensor in a Post-Newtonian framework to the EDs and examine the experimental prerequisites to detect these contributions like the required storage time and temporal resolution on the QMems. Also the investigation of non-locality on EDs due to gravity in Fermi normal coordinates appears as an interesting outlook for future considerations, as this would also address the question of how gravity influences quantum coherences and in particular genuine quantum properties like entanglement and indistinguishability of particles with a wave function of finite spatial extension, i.e. spatial wave packets, where the work on hand is rather concerned with the gravita-

tional influences in the spectral and temporal domain.

Our analysis is based on second quantization, which serves as a convenient tool for the analysis of interferometry of several indistinguishable particles and the development of theoretical methods to explicitly characterize multi-particle quantum phenomena under gravitational influences. Furthermore, our formal treatment explores a practical path that may be used to describe spacetime curvature related effects on quantum resources in a full quantum field theoretical description.

We have discussed in the main text and shown in the appendix that some entanglement correlations between different particles are robust against non-trivial EDs in the gravitational field of the earth. This is an important result for the design of entanglement based quantum technological applications employing non-local entanglement shared between possibly distant particles as, presently, one of the major challenges in entanglement based quantum technologies is the avoidance of decoherence of entanglement correlations.

Acknowledgements

The authors thank Daniel Oi, Igor Pikovski, Albert Roura, Ernst M. Rasel, Rainer Dumke, Waldemar Herr, Arash Ahmadi, Erhan Sağlamyürek, Patrick Ledingham, Andreas W. Schell and David Edward Bruschi for useful discussions and comments about the topic of the article. R.B. acknowledges funding by the Deutsche Forschungsgemeinschaft (DFG, German Research Foundation) under Germany’s Excellence Strategy – EXC-2123 QuantumFrontiers – 390837967 and support by the Research Training Group 1620 “Models of Gravity”. D.R. acknowledges funding by the Federal Ministry of Education and Research of Germany in the project “Open6GHub” (grant number: 16KISK016) and support through the Deutsche Forschungsgemeinschaft (DFG, German Research Foundation) under Germany’s Excellence Strategy – EXC-2123 QuantumFrontiers – 390837967, the Research Training Group 1620 “Models of Gravity” and the TerraQ initiative from the Deutsche Forschungsgemeinschaft (DFG, German Research Foundation) – Project-ID 434617780 – SFB 1464. M. G. and M. K. acknowledge the support from DLR through funds provided by BMWi (OPTIMO, No. 50WM1958 and OPTIMO-II, No. 50WM2055). M. G. further acknowledges funding from the European Union’s Horizon 2020 research and innovation programme under the Marie Skłodowska-Curie grant agreement No. 894590.

References

- [1] Richard Feynman. “Feynman lectures on gravitation”. CRC Press. (2018).
- [2] David C. Aveline, Jason R. Williams, Ethan R. Elliott, Chelsea Dutenhoffer, James R. Kellogg, James M. Kohel, Norman E. Lay, Kamal Oudrhiri, Robert F. Shotwell, Nan Yu, and Robert J. Thompson. “Observation of bose-einstein condensates in an earth-orbiting research lab”. *Nature* **582**, 193–197 (2020).
- [3] Maike D. Lachmann, Holger Ahlers, Dennis Becker, Aline N. Dinkelaker, Jens Grosse, Or-twin Hellmig, Hauke Müntinga, Vladimir Schkolnik, Stephan T. Seidel, Thijs Wendrich, André Wenzlawski, Benjamin Carrick, Naceur Gaaloul, Daniel Lüdtke, Claus Braxmaier, Wolfgang Ertmer, Markus Krutzik, Claus Lämmerzahl, Achim Peters, Wolfgang P. Schleich, Klaus Sengstock, Andreas Wicht, Patrick Windpassinger, and Ernst M. Rasel. “Ultracold atom interferometry in space”. *Nature Communications* **12**, 1317 (2021).
- [4] Juan Yin, Yuan Cao, Yu-Huai Li, Sheng-Kai Liao, Liang Zhang, Ji-Gang Ren, Wen-Qi Cai, Wei-Yue Liu, Bo Li, and Hui Dai *et al.* “Satellite-based entanglement distribution over 1200 kilometers”. *Science* **356**, 1140–1144 (2017).
- [5] Ping Xu, Yiqiu Ma, Ji-Gang Ren, Hai-Lin Yong, Timothy C. Ralph, Sheng-Kai Liao, Juan Yin, Wei-Yue Liu, Wen-Qi Cai, Xuan Han, Hui-Nan Wu, Wei-Yang Wang, Feng-Zhi Li, Meng Yang, Feng-Li Lin, Li Li, Nai-Le Liu, Yu-Ao Chen, Chao-Yang Lu, Yanbei Chen, Jingyun Fan, Cheng-Zhi Peng, and Jian-Wei Pan. “Satellite testing of a gravitationally induced quantum decoherence model”. *Science* **366**, 132–135 (2019).
- [6] Mustafa Gündoğan, Jasminder S. Sidhu, Victoria Henderson, Luca Mazzarella, Janik Wolters, Daniel K. L. Oi, and Markus Krutzik. “Proposal for space-borne quantum memories for global quantum networking”. *npj Quant. Inf.* **7**, 128 (2021).
- [7] Jasminder S. Sidhu, Siddarth K. Joshi, Mustafa Gündoğan, Thomas Brougham, David Lowndes, Luca Mazzarella, Markus Krutzik, Sonali Mohapatra, Daniele Dequal, Giuseppe Vallone, Paolo Villoresi, Alexander Ling, Thomas Jennewein, Makan Mohageg, John Rarity, Ivette Fuentes, Stefano Pirandola, and Daniel K. L. Oi. “Advances in space quantum communications”. *IET Quant. Comm.* **2**, 182–217 (2021).
- [8] Chao-Yang Lu, Yuan Cao, Cheng-Zhi Peng, and Jian-Wei Pan. “Micius quantum experiments in space”. *Rev. Mod. Phys.* **94**, 035001 (2022).
- [9] Magdalena Zych, Fabio Costa, Igor Pikovski, and Časlav Brukner. “Quantum interferometric visibility as a witness of general relativistic proper time”. *Nature Communications* **2**, 505 (2011).
- [10] Magdalena Zych, Fabio Costa, Igor Pikovski, Timothy C Ralph, and Časlav Brukner. “General relativistic effects in quantum interference of photons”. *Classical and Quantum Gravity* **29**, 224010 (2012).
- [11] Makan Mohageg, Luca Mazzarella, Charis Anastopoulos, Jason Gallicchio, Bei-Lok Hu, Thomas Jennewein, Spencer Johnson, Shih-Yuin Lin, Alexander Ling, Christoph Marquardt, Matthias Meister, Raymond Newell, Albert Roura, Wolfgang P. Schleich, Christian Schubert, Dmitry V. Strekalov, Giuseppe Vallone, Paolo Villoresi, Lisa Wörner, Nan Yu, Aileen Zhai, and Paul Kwiat. “The deep space quantum link: prospective fundamental physics experiments using long-baseline quantum optics”. *EPJ Quantum Technology* **9** (2022).
- [12] David Edward Bruschi, Carlos Sabín, Angela White, Valentina Baccetti, Daniel K L Oi, and Ivette Fuentes. “Testing the effects of gravity and motion on quantum entanglement in space-based experiments”. *New Journal of Physics* **16**, 053041 (2014).
- [13] Igor Pikovski, Magdalena Zych, Fabio Costa, and Časlav Brukner. “Universal decoherence due to gravitational time dilation”. *Nature Physics* **11**, 668–672 (2015).
- [14] Igor Pikovski, Magdalena Zych, Fabio Costa, and Časlav Brukner. “Time dilation in quantum systems and decoherence”. *New Journal of Physics* **19**, 025011 (2017).
- [15] Mikael Afzelius, Nicolas Gisin, and Hugues de Riedmatten. “Quantum memory for photons”. *Physics Today* **68**, 42–47 (2015).
- [16] Khabat Heshami, Duncan G. England, Peter C. Humphreys, Philip J. Bustard, Victor M. Acosta, Joshua Nunn, and Benjamin J. Sussman. “Quantum memories: emerging applications and recent advances”. *Journal of Modern Optics* **63**, 2005–2028 (2016).
- [17] Sam Pallister, Simon Coop, Valerio Formichella, Nicolas Gampierakis, Virginia Notaro, Paul Knott, Rui Azevedo, Nikolaus Buchheim, Silvio De Carvalho, Emilia Järvelä, et al. “A blueprint for a simultaneous test of quantum mechanics and general relativity in a space-based quantum optics experiment”. *EPJ Quantum Technology* **4**, 1–23 (2017).
- [18] Roy Barzel, David Edward Bruschi, Andreas W. Schell, and Claus Lämmerzahl. “Observer dependence of photon bunching: The influence of the relativistic redshift on hong-ou-mandel interference”. *Phys. Rev. D* **105**, 105016 (2022).
- [19] David Edward Bruschi and Andreas Wolfgang Schell. “Gravitational redshift induces quan-

- tum interference". *Annalen der Physik* **535**, 2200468 (2023).
- [20] Thomas B. Mieling, Christopher Hilweg, and Philip Walther. "Measuring space-time curvature using maximally path-entangled quantum states". *Phys. Rev. A* **106**, L031701 (2022).
- [21] Dennis Philipp, Volker Perlick, Dirk Puetzfeld, Eva Hackmann, and Claus Lämmerzahl. "Definition of the relativistic geoid in terms of isochronometric surfaces". *Phys. Rev. D* **95**, 104037 (2017).
- [22] Dennis Philipp, Eva Hackmann, Claus Lämmerzahl, and Jürgen Müller. "Relativistic geoid: gravity potential and relativistic effects". *Phys. Rev. D* **101**, 064032 (2020).
- [23] J. C. Hafele and Richard E. Keating. "Around-the-world atomic clocks: Observed relativistic time gains". *Science* **177**, 168–170 (1972).
- [24] Yair Margalit, Zhifan Zhou, Shimon Machluf, Daniel Rohrlich, Yonathan Japha, and Ron Folman. "A self-interfering clock as a "which path" witness". *Science* **349**, 1205–1208 (2015).
- [25] Roy Barzel and Claus Lämmerzahl. "Role of indistinguishability and entanglement in hong-ou-mandel interference and finite-bandwidth effects of frequency-entangled photons". *Phys. Rev. A* **107**, 032205 (2023).
- [26] Irwin I. Shapiro. "Fourth test of general relativity". *Phys. Rev. Lett.* **13**, 789–791 (1964).
- [27] Irwin I. Shapiro, Michael E. Ash, Richard P. Ingalls, William B. Smith, Donald B. Campbell, Rolf B. Dyce, Raymond F. Jurgens, and Gordon H. Pettengill. "Fourth test of general relativity: New radar result". *Phys. Rev. Lett.* **26**, 1132–1135 (1971).
- [28] Daniel Rieländer, Andreas Lenhard, Osvaldo Jiménez Farias, Alejandro Máttar, Daniel Cavalcanti, Margherita Mazzera, Antonio Acín, and Hugues de Riedmatten. "Frequency-bin entanglement of ultra-narrow band non-degenerate photon pairs". *Quantum Science and Technology* **3**, 014007 (2017).
- [29] Nicolas Maring, Pau Farrera, Kutlu Kutluer, Margherita Mazzera, Georg Heinze, and Hugues de Riedmatten. "Photonic quantum state transfer between a cold atomic gas and a crystal". *Nature* **551**, 485–488 (2017).
- [30] Stéphane Clemmen, Alessandro Farsi, Sven Ramelow, and Alexander L. Gaeta. "Ramsey interference with single photons". *Phys. Rev. Lett.* **117**, 223601 (2016).
- [31] Manjin Zhong, Morgan P. Hedges, Rose L. Ahlefeldt, John G. Bartholomew, Sarah E. Beavan, Sven M. Wittig, Jevon J. Longdell, and Matthew J. Sellars. "Optically addressable nuclear spins in a solid with a six-hour coherence time". *Nature* **517**, 177–180 (2015).
- [32] Yu Ma, You-Zhi Ma, Zong-Quan Zhou, Chuan-Feng Li, and Guang-Can Guo. "One-hour coherent optical storage in an atomic frequency comb memory". *Nat. Commun.* **12**, 2381 (2021).
- [33] Mustafa Gündoğan, Patrick M. Ledingham, Kutlu Kutluer, Margherita Mazzera, and Hugues de Riedmatten. "Solid state spin-wave quantum memory for time-bin qubits". *Phys. Rev. Lett.* **114**, 230501 (2015).
- [34] Pierre Jobez, Cyril Laplane, Nuala Timoney, Nicolas Gisin, Alban Ferrier, Philippe Goldner, and Mikael Afzelius. "Coherent spin control at the quantum level in an ensemble-based optical memory". *Phys. Rev. Lett.* **114**, 230502 (2015).
- [35] Antonio Ortú, Adrian Holzapfel, Jean Etesse, and Mikael Afzelius. "Storage of photonic time-bin qubits for up to 20 ms in a rare-earth doped crystal". *npj Quantum Information* **8**, 29 (2022).
- [36] Philippe Goldner, Alban Ferrier, and Olivier Guillot-Noël. "Chapter 267 - rare earth-doped crystals for quantum information processing". In Jean-Claude G. Bünzli and Vitalij K. Pecharsky, editors, *Handbook on the Physics and Chemistry of Rare Earths*. Volume 46, pages 1–78. Elsevier (2015).
- [37] Alessandro Seri, Dario Lago-Rivera, Andreas Lenhard, Giacomo Corrielli, Roberto Osellame, Margherita Mazzera, and Hugues de Riedmatten. "Quantum storage of frequency-multiplexed heralded single photons". *Phys. Rev. Lett.* **123**, 080502 (2019).
- [38] Alexandre Fossati, Shuping Liu, Jenny Karlsson, Akio Ikesue, Alexandre Tallaire, Alban Ferrier, Diana Serrano, and Philippe Goldner. "A frequency-multiplexed coherent electro-optic memory in rare earth doped nanoparticles". *Nano Letters* **20**, 7087–7093 (2020).
- [39] Jean-Daniel Deschênes, Laura C. Sinclair, Fabrizio R. Giorgetta, William C. Swann, Esther Baumann, Hugo Bergeron, Michael Cermak, Ian Coddington, and Nathan R. Newbury. "Synchronization of distant optical clocks at the femtosecond level". *Phys. Rev. X* **6**, 021016 (2016).
- [40] Hugo Bergeron, Laura C. Sinclair, William C. Swann, Isaac Khader, Kevin C. Cossel, Michael Cermak, Jean-Daniel Deschênes, and Nathan R. Newbury. "Femtosecond time synchronization of optical clocks off of a flying quadcopter". *Nature Communications* **10**, 1819 (2019).
- [41] Runai Quan, Yiwei Zhai, Mengmeng Wang, Feiyan Hou, Shaofeng Wang, Xiao Xiang, Tao Liu, Shougang Zhang, and Ruifang Dong. "Demonstration of quantum synchronization based on second-order quantum coherence of entangled photons". *Scientific Reports* **6**, 30453 (2016).
- [42] Raju Valivarthi, Lautaro Narváez, Samantha I. Davis, Nikolai Lauk, Cristián Peña, Si Xie, Ja-

- son P. Allmaras, Andrew D. Beyer, Boris Korzh, Andrew Mueller, Mandy Kiburg, Matthew D. Shaw, Emma E. Wollman, Panagiotis Spentzouris, Daniel Oblak, Neil Sinclair, and Maria Spiropulu. “Picosecond synchronization system for quantum networks”. *Journal of Lightwave Technology* **40**, 7668–7675 (2022).
- [43] Y. O. Dudin, L. Li, and A. Kuzmich. “Light storage on the time scale of a minute”. *Phys. Rev. A* **87**, 031801 (2013).
- [44] Sheng-Jun Yang, Xu-Jie Wang, Xiao-Hui Bao, and Jian-Wei Pan. “An efficient quantum light-matter interface with sub-second lifetime”. *Nature Photonics* **10**, 381–384 (2016).
- [45] Or Katz and Ofer Firstenberg. “Light storage for one second in room-temperature alkali vapor”. *Nature Communications* **9**, 2074 (2018).
- [46] Jiří Minář, Hugues de Riedmatten, Christoph Simon, Hugo Zbinden, and Nicolas Gisin. “Phase-noise measurements in long-fiber interferometers for quantum-repeater applications”. *Phys. Rev. A* **77**, 052325 (2008).
- [47] R. Stockill, M. J. Stanley, L. Huthmacher, E. Clarke, M. Hugues, A. J. Miller, C. Matthiesen, C. Le Gall, and M. Atatüre. “Phase-tuned entangled state generation between distant spin qubits”. *Phys. Rev. Lett.* **119**, 010503 (2017).
- [48] Yong Yu, Fei Ma, Xi-Yu Luo, Bo Jing, Peng-
- Fei Sun, Ren-Zhou Fang, Chao-Wei Yang, Hui Liu, Ming-Yang Zheng, Xiu-Ping Xie, Wei-Jun Zhang, Li-Xing You, Zhen Wang, Teng-Yun Chen, Qiang Zhang, Xiao-Hui Bao, and Jian-Wei Pan. “Entanglement of two quantum memories via fibres over dozens of kilometres”. *Nature* **578**, 240–245 (2020).
- [49] Dario Lago-Rivera, Samuele Grandi, Jelena V. Rakonjac, Alessandro Seri, and Hugues de Riedmatten. “Telecom-heralded entanglement between multimode solid-state quantum memories”. *Nature* **594**, 37–40 (2021).
- [50] Hwang Lee, Pieter Kok, and Jonathan P Dowling. “A quantum rosetta stone for interferometry”. *Journal of Modern Optics* **49**, 2325–2338 (2002).
- [51] Michał Horodecki, Paweł Horodecki, and Ryszard Horodecki. “Separability of mixed states: necessary and sufficient conditions”. *Physics Letters A* **223**, 1–8 (1996).
- [52] Kyung Soo Choi. “Coherent control of entanglement with atomic ensembles”. PhD thesis. California Institute of Technology. (2011).
- [53] C K Hong, Z Y Ou, and L. Mandel. “Measurement of subpicosecond time intervals between two photons by interference”. *Phys. Rev. Lett.* **59**, 2044–2046 (1987).

A Entangled clock states under EDs due to gravity

We consider two particles, which are both allowed to be situated at sites U and L and feature the same single-particle internal energy structure as in the single-particle example from the main text. The configuration space is now 16-dimensional, and we consider the two-particle system to be driven by the interaction-free two-particle Hamiltonian

$$\hat{H}_2 = \hat{H}_1 \otimes \mathbb{1}_{4 \times 4} + \mathbb{1}_{4 \times 4} \otimes \hat{H}_1 \quad (35)$$

where $\mathbb{1}_{4 \times 4}$ is the identity operator on the four-dimensional single-particle Hilbert space. Analogously to the single-particle case, we can investigate the time evolution (from the perspective of an observer evolving w.r.t. to their proper time τ_o) of some initial state $|\psi(0)\rangle$ by computing $|\psi(\tau_o)\rangle = e^{-i\hat{H}_2\tau_o} |\psi(0)\rangle$. The resulting reduced 4×4 density matrix

$$\hat{\rho}_{\text{red}}(\tau_o) = \sum_{i,j=1,2} \langle \mu_i \mu_j | \hat{\rho}(\tau_o) | \mu_i \mu_j \rangle \quad (36)$$

with $\hat{\rho}(\tau_o) = |\psi(\tau_o)\rangle \langle \psi(\tau_o)|$ describes a two-qubit system in which the presence of entanglement can be unambiguously certified by positive values of the *negativity*

$$\mathcal{N}(\tau_o) = - \sum_{\lambda_{\text{PT}} < 0} \lambda_{\text{PT}}(\tau_o), \quad (37)$$

which is the negative sum of the negative eigenvalues $\lambda_{\text{PT}}(\tau_o)$ of the partial transposed density matrix $\hat{\rho}_{\text{red}}^{\text{PT}}(\tau_o) = (\mathbb{1}_{4 \times 4} \otimes \hat{T}) \hat{\rho}_{\text{red}}(\tau_o)$, where \hat{T} is the transposition operator [51]. If we consider an initial state

$$|\psi(0)\rangle = (|\mu_1 \mu_2\rangle + |\mu_2 \mu_1\rangle) \otimes (|UL\rangle + |LU\rangle)/2 \quad (38)$$

in which both the internal and external DOFs of the two particles are entangled, the corresponding negativity

$$\mathcal{N}(\tau_o) = |\cos(\Delta_\Theta \mu_- \tau_o)|/2 \quad (39)$$

indicates that, after a time

$$\tau_{o,\text{ent}}^{(2)} = \frac{\pi}{2\Delta_\Theta\mu_-}, \quad (40)$$

the spatial entanglement between the two considered particles is depleted, where now the time to disentangle the spatial DOFs between the different particles is halved in comparison to the time needed to maximally entangle the internal and external DOF of the single-particle example from the main text, i.e. $\tau_{o,\text{ent}}^{(2)} = \tau_{o,\text{ent}}^{(1)}/2$, c.f. Eq (7) from the main text. Not only, the mutual spatial correlation between the particles gets lost. At the same time, entanglement correlations between the internal and external DOFs of the two-particle system are build up as can be seen by inspection of the linear entropy of the reduced spatial substate

$$\mathcal{S}(\tau_o) = 1 - \mathcal{P}(\tau_o) = \sin^2(\Delta_\Theta\mu_- \tau_o)/2, \quad (41)$$

where

$$\mathcal{P}(\tau_o) = \sum_{i,j=1,2} \langle \sigma_i \sigma_j | \hat{\rho}_{\text{red}}^2(\tau_o) | \sigma_i \sigma_j \rangle \quad (42)$$

is the purity of the reduced spatial substate. In particular, any coherences of the spatial sub state decohered after the time $\tau_{o,\text{ent}}^{(2)}$ since at this time, the spatial sub state

$$\hat{\rho}_{\text{red}}(\tau_{o,\text{ent}}^{(2)}) = (|UL\rangle\langle UL| + |LU\rangle\langle LU|)/2$$

only features non-vanishing diagonal elements. It is interesting to notice that quantum states where the internal sub state is in an aligned Bell state and the positional sub state is in an anti-aligned Bell state or vice versa, i.e.

$$|\bar{\psi}(0)\rangle = (|\mu_1\mu_2\rangle + |\mu_2\mu_1\rangle) \otimes (|UU\rangle + |LL\rangle)/2, \quad (43)$$

$$|\tilde{\psi}(0)\rangle = (|\mu_1\mu_1\rangle + |\mu_2\mu_2\rangle) \otimes (|UL\rangle + |LU\rangle)/2, \quad (44)$$

do not suffer from the EDs induced by \hat{H}_2 (since in this case one has $\mathcal{N}(\tau_o) = 1/2$ for all τ_o) which makes these states more attractive for quantum technological applications.

B Model for the quantum memories and imprinted phases

In this section, we present our model for the storage of the optical quantum states in QMems. Instead of focusing on a specific implementation, we assume general properties of the QMems. In particular, we assume that storage and read-out can be described by mode-swapper operations for each arm of the interferometer $\hat{U}_\sigma^{(\text{map})} = \hat{U}_{\sigma 1}^{(\text{map})}\hat{U}_{\sigma 2}^{(\text{map})}$, where (s for storage and r for readout) (see for example [52])

$$\hat{U}_{\sigma i}^{\text{s/r}} = \exp\left(\pi/2\left(e^{i\phi_{\sigma i}^{\text{s/r}}} a_{\sigma i} S_{\sigma i}^\dagger - e^{-i\phi_{\sigma i}^{\text{s/r}}} a_{\sigma i}^\dagger S_{\sigma i}\right)\right), \quad (45)$$

and

$$a_{\sigma i} = \int d\omega g_{\Omega_i \xi}(\omega) a_{\sigma \omega} \quad (46)$$

is the annihilation operator for a photon at the spectral peak $g_{\Omega_i \xi}(\omega)$ and and $S_{\sigma i}^\dagger$ and $S_{\sigma i}$ are the creation and annihilation operators for excitations in the QMems. The phases $\phi_{\sigma i}^{\text{s/r}}$ are imprinted in the storage/read-out process.

The photonic input state before the storage in the QMems is

$$|\psi_{\text{MZ}}\rangle_0 = N_{\text{MZ}}[(\hat{a}_{U1}^\dagger - \hat{a}_{L1}^\dagger) + e^{i\varphi}(\hat{a}_{U2}^\dagger - \hat{a}_{L2}^\dagger)]/\sqrt{2}|0\rangle, \quad (47)$$

$$|\psi_{\text{HOM}}\rangle_0 = N_{\text{HOM}}[\hat{a}_{U1}^\dagger \hat{a}_{L2}^\dagger + e^{i\varphi} \hat{a}_{U2}^\dagger \hat{a}_{L1}^\dagger]|0\rangle. \quad (48)$$

We assume that the storage and release operations can be considered as instantaneous in comparison to the storage time. We find for the state in the QMem

$$|\psi_{\text{MZ}}\rangle_{\text{QMem},0} = N_{\text{MZ}}[(e^{i\phi_{U1}^{\text{s}}}\hat{S}_{U1}^\dagger - e^{i\phi_{L1}^{\text{s}}}\hat{S}_{L1}^\dagger) + e^{i\varphi}(e^{i\phi_{U2}^{\text{s}}}\hat{S}_{U2}^\dagger - e^{i\phi_{L2}^{\text{s}}}\hat{S}_{L2}^\dagger)]/\sqrt{2}|0\rangle, \quad (49a)$$

$$|\psi_{\text{HOM}}\rangle_{\text{QMem},0} = N_{\text{HOM}}[e^{i(\phi_{U1}^{\text{s}}+\phi_{L2}^{\text{s}})}\hat{S}_{U1}^\dagger \hat{S}_{L2}^\dagger + e^{i(\phi_{U2}^{\text{s}}+\phi_{L1}^{\text{s}})}e^{i\varphi}\hat{S}_{U2}^\dagger \hat{S}_{L1}^\dagger]|0\rangle. \quad (49b)$$

When stored in the QMems, the time evolution of the excitations is defined by their respective energy $\tilde{\nu}_{\sigma 1}$ and $\tilde{\nu}_{\sigma 2}$ and the local proper storage times $\tau_{\sigma s}$. We introduce a parameter χ that is 1 if the internal phase evolution is imprinted on the output state of the QMem and 0 otherwise, and we find

$$|\psi_{\text{MZ}}\rangle_{\text{QMem,f}} = N_{\text{MZ}} [(\hat{S}_{U1}^\dagger e^{i(\chi\tilde{\nu}_{U1}\tau_{Us} + \phi_{U1}^s)} - \hat{S}_{L1}^\dagger e^{i(\chi\tilde{\nu}_{L1}\tau_{Ls} + \phi_{L1}^s)}) \\ + e^{i\varphi} (\hat{S}_{U2}^\dagger e^{i(\chi\tilde{\nu}_{U2}\tau_{Us} + \phi_{U2}^s)} - \hat{S}_{L2}^\dagger e^{i(\chi\tilde{\nu}_{L2}\tau_{Ls} + \phi_{L2}^s)})] / \sqrt{2} |0\rangle, \quad (50\text{a})$$

$$|\psi_{\text{HOM}}\rangle_{\text{QMem,f}} = N_{\text{HOM}} [S_{U1}^\dagger S_{L2}^\dagger e^{i(\chi\tilde{\nu}_{U1}\tau_{Us} + \chi\tilde{\nu}_{L2}\tau_{Ls} + \phi_{U1}^s + \phi_{L2}^s)} + e^{i\varphi} S_{U2}^\dagger S_{L1}^\dagger e^{i(\chi\tilde{\nu}_{U2}\tau_{Us} + \chi\tilde{\nu}_{L1}\tau_{Ls} + \phi_{U2}^s + \phi_{L1}^s)}] |0\rangle. \quad (50\text{b})$$

Up to a global phase, the resulting state after the storage becomes

$$|\psi'_{\text{MZ}}\rangle = \sum_{\sigma} \int d\omega \psi'_{\sigma}(\omega) \hat{a}_{\sigma\omega}^\dagger |0\rangle, \quad (51\text{a})$$

$$|\psi'_{\text{HOM}}\rangle = \int d\omega_1 d\omega_2 \psi'(\omega_1, \omega_2) a_{U\omega_1}^\dagger a_{L\omega_2}^\dagger |0\rangle, \quad (51\text{b})$$

$$\psi'_{\sigma}(\omega) = (-1)^{\tilde{n}(\sigma)} N_{\text{MZ}} [g_{\Omega_1\xi}(\omega) e^{i(\chi\tilde{\nu}_{\sigma 1}\tau_{\sigma s} + \phi_{\sigma 1}^s - \phi_{\sigma 1}^r)} + e^{i\varphi} g_{\Omega_2\xi}(\omega) e^{i(\chi\tilde{\nu}_{\sigma 2}\tau_{\sigma s} + \phi_{\sigma 2}^s - \phi_{\sigma 2}^r)}] / \sqrt{2} \quad (52\text{a})$$

$$\psi'(\omega_1, \omega_2) = N_{\text{HOM}} [g_{\Omega_1\xi}(\omega_1) g_{\Omega_2\xi}(\omega_2) + e^{i\varphi'_{\text{HOM}}} g_{\Omega_2\xi}(\omega_1) g_{\Omega_1\xi}(\omega_2)], \quad (52\text{b})$$

where $\tilde{n}(U) = 0$, $\tilde{n}(L) = 1$ and

$$\varphi'_{\text{HOM}} = \varphi + \chi(\tilde{\nu}_{U-}\tau_{Us} - \tilde{\nu}_{L-}\tau_{Ls}) + ((\phi_{U2}^s - \phi_{U1}^s) - (\phi_{L2}^s - \phi_{L1}^s)) - ((\phi_{U2}^r - \phi_{U1}^r) - (\phi_{L2}^r - \phi_{L1}^r)) \quad (53)$$

and $\tilde{\nu}_{\sigma-} = \tilde{\nu}_{\sigma 2} - \tilde{\nu}_{\sigma 1}$.

We assume that an independent external phase reference (e.g. a laser serving as a local local oscillator) is provided for U and L each which operate at the frequencies $\tilde{\Omega}_{\sigma i}^{(r)}$, for $i = 1, 2$ and $\sigma = U, L$, which are measured in the common time frame of the photon source. The additional phase difference which arises due to the usage of independent local phase references is $\phi_{\sigma i}^s - \phi_{\sigma i}^r = \tilde{\Omega}_{\sigma i}^{(r)} \tau_{\sigma s}$. In this case, we find

$$\psi'_{\sigma}(\omega) = (-1)^{\tilde{n}(\sigma)} N_{\text{MZ}} [g_{\Omega_1\xi}(\omega) e^{i(\chi\tilde{\nu}_{\sigma 1} + \tilde{\Omega}_{\sigma 1}^{(r)})\tau_{\sigma s}} + e^{i\varphi} g_{\Omega_2\xi}(\omega) e^{i(\chi\tilde{\nu}_{\sigma 2} + \tilde{\Omega}_{\sigma 2}^{(r)})\tau_{\sigma s}}] / \sqrt{2} \quad (54)$$

and

$$\varphi'_{\text{HOM}} = (\chi\tilde{\nu}_{U-} + \tilde{\Omega}_{U-}^{(r)})\tau_{Us} - (\chi\tilde{\nu}_{L-} + \tilde{\Omega}_{L-}^{(r)})\tau_{Ls} + \varphi, \quad (55)$$

where $\tilde{\Omega}_{\sigma-}^{(r)} = \tilde{\Omega}_{\sigma 2}^{(r)} - \tilde{\Omega}_{\sigma 1}^{(r)}$. Taking into account that $\tilde{\nu}_{\sigma i} + \tilde{\Omega}_{\sigma i}^{(r)} = \tilde{\Omega}_{\sigma i}$, we find

$$\psi'_{\sigma}(\omega) = (-1)^{\tilde{n}(\sigma)} N_{\text{MZ}} [g_{\Omega_1\xi}(\omega) e^{i(\tilde{\Omega}_{\sigma 1} + (\chi-1)\tilde{\nu}_{\sigma 1})\tau_{\sigma s}} + e^{i\varphi} g_{\Omega_2\xi}(\omega) e^{i(\tilde{\Omega}_{\sigma 2} + (\chi-1)\tilde{\nu}_{\sigma 2})\tau_{\sigma s}}] / \sqrt{2} \quad (56)$$

and

$$\varphi'_{\text{HOM}} = ((\chi-1)\tilde{\nu}_{U-} + \tilde{\Omega}_{U-})\tau_{Us} - ((\chi-1)\tilde{\nu}_{L-} + \tilde{\Omega}_{L-})\tau_{Ls} + \varphi \\ = \Omega_- (\tau_{Us}/\Theta_U - \tau_{Ls}/\Theta_L) + (\chi-1)(\tilde{\nu}_{U-}\tau_{Us} - \tilde{\nu}_{L-}\tau_{Ls}) + \varphi. \quad (57)$$

with $\tilde{\Omega}_{\sigma\pm} = \tilde{\Omega}_{\sigma 2} \pm \tilde{\Omega}_{\sigma 1}$, $\tilde{\nu}_{\sigma\pm} = \tilde{\nu}_{\sigma 2} \pm \tilde{\nu}_{\sigma 1}$ and $\Omega_{\pm} = \Omega_2 \pm \Omega_1$, where the relation between the i -th spectral peak frequency $\tilde{\Omega}_{\sigma i}$ as perceived from the local rest frame of the QMems at $\sigma = U, L$ to the respective frequency peak Ω_i as perceived from the rest frame of the photon source is given by $\tilde{\Omega}_{\sigma i} = \Omega_i/\Theta_{\sigma}$.

Next, we derive the MZ- and HOM-interference patterns. First, we apply a 50 : 50 beam splitter to Eq. (51) which transforms the photonic creation operators as $\hat{a}_{U\omega} \rightarrow (\hat{a}_{\oplus\omega} - \hat{a}_{\ominus\omega})/\sqrt{2}$ and $\hat{a}_{L\omega} \rightarrow (\hat{a}_{\oplus\omega} + \hat{a}_{\ominus\omega})/\sqrt{2}$. After the beam splitter, we have

$$|\psi''_{\text{MZ}}\rangle = \int d\omega (\hat{a}_{\oplus\omega}^\dagger (\psi'_U(\omega) + \psi'_L(\omega)) - \hat{a}_{\ominus\omega}^\dagger (\psi'_U(\omega) - \psi'_L(\omega))) / \sqrt{2} |0\rangle, \quad (58\text{a})$$

$$|\psi''_{\text{HOM}}\rangle = \int d\omega_1 d\omega_2 \psi'(\omega_1, \omega_2) (\hat{a}_{\oplus\omega_1}^\dagger - \hat{a}_{\ominus\omega_1}^\dagger) (\hat{a}_{\oplus\omega_2}^\dagger + \hat{a}_{\ominus\omega_2}^\dagger) / 2 |0\rangle, \quad (58\text{b})$$

which both can be represented in the form of (9), that is

$$|\psi''_{\text{MZ}}\rangle = \sum_{\sigma} \int d\omega \psi_{\sigma}^{\text{f}}(\omega) \hat{a}_{\sigma\omega}^{\dagger} |0\rangle, \quad (59\text{a})$$

$$|\psi''_{\text{HOM}}\rangle = \frac{1}{\sqrt{2}} \sum_{\sigma_1, \sigma_2} \int d\omega_1 d\omega_2 \psi_{\sigma_1 \sigma_2}^{\text{f}}(\omega_1, \omega_2) \hat{a}_{\sigma_1 \omega_1}^{\dagger} \hat{a}_{\sigma_2 \omega_2}^{\dagger} |0\rangle, \quad (59\text{b})$$

where one has

$$\psi_{\sigma}^{\text{f}}(\omega) = \frac{1}{\sqrt{2}} [\delta_{\sigma \oplus} (\psi'_U(\omega) + \psi'_L(\omega)) - \delta_{\sigma \ominus} (\psi'_U(\omega) - \psi'_L(\omega))], \quad (60\text{a})$$

$$\begin{aligned} \psi_{\sigma_1 \sigma_2}^{\text{f}}(\omega_1, \omega_2) &= \frac{1}{2\sqrt{2}} \left[\psi'(\omega_1, \omega_2) (\delta_{\sigma_1 \oplus} \delta_{\sigma_2 \oplus} - \delta_{\sigma_1 \ominus} \delta_{\sigma_2 \ominus} + \delta_{\sigma_1 \oplus} \delta_{\sigma_2 \ominus} - \delta_{\sigma_1 \ominus} \delta_{\sigma_2 \oplus}) + ((\sigma_1, \omega_1) \longleftrightarrow (\sigma_2, \omega_2)) \right] \\ &= \frac{1}{2\sqrt{2}} \left[(\psi'(\omega_1, \omega_2) + \psi'(\omega_2, \omega_1)) (\delta_{\sigma_1 \oplus} \delta_{\sigma_2 \oplus} - \delta_{\sigma_1 \ominus} \delta_{\sigma_2 \ominus}) \right. \\ &\quad \left. + (\psi'(\omega_1, \omega_2) - \psi'(\omega_2, \omega_1)) (\delta_{\sigma_1 \oplus} \delta_{\sigma_2 \ominus} - \delta_{\sigma_1 \ominus} \delta_{\sigma_2 \oplus}) \right] \\ &= \frac{N_{\text{HOM}}}{2\sqrt{2}} \left[(1 + e^{i\varphi'_{\text{HOM}}}) (g_{\Omega_1 \xi}(\omega_1) g_{\Omega_2 \xi}(\omega_2) + g_{\Omega_2 \xi}(\omega_1) g_{\Omega_1 \xi}(\omega_2)) (\delta_{\sigma_1 \oplus} \delta_{\sigma_2 \oplus} - \delta_{\sigma_1 \ominus} \delta_{\sigma_2 \ominus}) \right. \\ &\quad \left. + (1 - e^{i\varphi'_{\text{HOM}}}) (g_{\Omega_1 \xi}(\omega_1) g_{\Omega_2 \xi}(\omega_2) - g_{\Omega_2 \xi}(\omega_1) g_{\Omega_1 \xi}(\omega_2)) (\delta_{\sigma_1 \oplus} \delta_{\sigma_2 \ominus} - \delta_{\sigma_1 \ominus} \delta_{\sigma_2 \oplus}) \right] \\ &= \frac{N_{\text{HOM}}}{\sqrt{2}} e^{i\varphi'_{\text{HOM}}/2} \left[\cos(\varphi'_{\text{HOM}}/2) (g_{\Omega_1 \xi}(\omega_1) g_{\Omega_2 \xi}(\omega_2) + g_{\Omega_2 \xi}(\omega_1) g_{\Omega_1 \xi}(\omega_2)) (\delta_{\sigma_1 \oplus} \delta_{\sigma_2 \oplus} - \delta_{\sigma_1 \ominus} \delta_{\sigma_2 \ominus}) \right. \\ &\quad \left. - i \sin(\varphi'_{\text{HOM}}/2) (g_{\Omega_1 \xi}(\omega_1) g_{\Omega_2 \xi}(\omega_2) - g_{\Omega_2 \xi}(\omega_1) g_{\Omega_1 \xi}(\omega_2)) (\delta_{\sigma_1 \oplus} \delta_{\sigma_2 \ominus} - \delta_{\sigma_1 \ominus} \delta_{\sigma_2 \oplus}) \right], \end{aligned} \quad (60\text{b})$$

where $\sigma = \oplus, \ominus$. From Eqs. (16) from the main text, i.e.

$$P_{\sigma'}^{\text{MZ}} = \int d\omega \langle \hat{a}_{\sigma' \omega}^{\dagger} \hat{a}_{\sigma' \omega} \rangle = \rho_{\sigma' \sigma'} \quad \text{and} \quad (61\text{a})$$

$$\begin{aligned} P_{\sigma'_1 \sigma'_2}^{\text{HOM}} &= \int d\omega_1 d\omega_2 \langle \hat{a}_{\sigma'_1 \omega_1}^{\dagger} \hat{a}_{\sigma'_2 \omega_2}^{\dagger} \hat{a}_{\sigma'_2 \omega_2} \hat{a}_{\sigma'_1 \omega_1} \rangle / 2 \\ &= \rho_{\sigma'_1 \sigma'_2 \sigma'_1 \sigma'_2}, \end{aligned} \quad (61\text{b})$$

with $\sigma = \oplus, \ominus$, we obtain the probabilities of the various detection events and combine them according to Eq. (17) and (18), that is, and $P_c^{\text{MZ}} = P_{\ominus}^{\text{MZ}} - P_{\oplus}^{\text{MZ}}$ as well as $P_c^{\text{HOM}} = (P_{\oplus \oplus}^{\text{HOM}} + P_{\ominus \ominus}^{\text{HOM}}) - (P_{\oplus \ominus}^{\text{HOM}} + P_{\ominus \oplus}^{\text{HOM}})$.

Inserting (56) into Eq. (20) with (57) and taking the corresponding diagonal elements of the resulting reduced density matrices yields

$$\begin{aligned} P_c^{\text{MZ}} &= - \int d\omega (\psi'_U(\omega) (\psi'_L(\omega))^* + \psi'_L(\omega) (\psi'_U(\omega))^*) \\ &= \sum_i \cos((\tilde{\Omega}_{Ui} + (\chi - 1)\tilde{\nu}_{Ui})\tau_{Us} - (\tilde{\Omega}_{Li} + (\chi - 1)\tilde{\nu}_{Li})\tau_{Ls}) N_{\text{MZ}}^2 \int d\omega g_{\Omega_i \xi}(\omega)^2 \\ &\quad + \left(\cos((\tilde{\Omega}_{U1} + (\chi - 1)\tilde{\nu}_{U1})\tau_{Us} - (\tilde{\Omega}_{L2} + (\chi - 1)\tilde{\nu}_{L2})\tau_{Ls} - \varphi) \right. \\ &\quad \left. + \cos((\tilde{\Omega}_{L1} + (\chi - 1)\tilde{\nu}_{L1})\tau_{Ls} - (\tilde{\Omega}_{U2} + (\chi - 1)\tilde{\nu}_{U2})\tau_{Us} - \varphi) \right) N_{\text{MZ}}^2 \int d\omega g_{\Omega_1 \xi}(\omega) g_{\Omega_2 \xi}(\omega) \\ &= 2N_{\text{MZ}}^2 \cos((\tilde{\Omega}_{U+} + (\chi - 1)\tilde{\nu}_{U+})\tau_{Us}/2 - (\tilde{\Omega}_{L+} + (\chi - 1)\tilde{\nu}_{L+})\tau_{Ls}/2) \times \\ &\quad \times \cos((\tilde{\Omega}_{U-} + (\chi - 1)\tilde{\nu}_{U-})\tau_{Us}/2 - (\tilde{\Omega}_{L-} + (\chi - 1)\tilde{\nu}_{L-})\tau_{Ls}/2) \\ &\quad + 2N_{\text{MZ}}^2 e^{-\Omega_-^2/8\xi^2} \cos((\tilde{\Omega}_{U+} + (\chi - 1)\tilde{\nu}_{U+})\tau_{Us}/2 - (\tilde{\Omega}_{L+} + (\chi - 1)\tilde{\nu}_{L+})\tau_{Ls}/2) \times \\ &\quad \times \cos((\tilde{\Omega}_{U-} + (\chi - 1)\tilde{\nu}_{U-})\tau_{Us}/2 + (\tilde{\Omega}_{L-} + (\chi - 1)\tilde{\nu}_{L-})\tau_{Ls}/2 + \varphi) \\ &= 2N_{\text{MZ}}^2 \cos(\Omega_+ \tau_{Us}/2\Theta_U - \Omega_+ \tau_{Ls}/2\Theta_L + (\chi - 1)(\tilde{\nu}_{U+} \tau_{Us} - \tilde{\nu}_{L+} \tau_{Ls})/2) \times \\ &\quad \times \cos(\Omega_- \tau_{Us}/2\Theta_U - \Omega_- \tau_{Ls}/2\Theta_L + (\chi - 1)(\tilde{\nu}_{U-} \tau_{Us} - \tilde{\nu}_{L-} \tau_{Ls})/2) \\ &\quad + 2N_{\text{MZ}}^2 e^{-\Omega_-^2/8\xi^2} \cos(\Omega_+ \tau_{Us}/2\Theta_U - \Omega_+ \tau_{Ls}/2\Theta_L + (\chi - 1)(\tilde{\nu}_{U+} \tau_{Us} - \tilde{\nu}_{L+} \tau_{Ls})/2) \times \\ &\quad \times \cos(\Omega_- \tau_{Us}/2\Theta_U + \Omega_- \tau_{Ls}/2\Theta_L + (\chi - 1)(\tilde{\nu}_{U-} \tau_{Us} + \tilde{\nu}_{L-} \tau_{Ls})/2 + \varphi), \end{aligned} \quad (62)$$

where $\Omega_{\pm} = \Omega_2 \pm \Omega_1$. For HOM interference, we find

$$\begin{aligned}\rho_{\sigma_1\sigma_2\bar{\sigma}_1\bar{\sigma}_2} &= \int d\omega_1 d\omega_2 \psi_{\sigma_1\sigma_2}^f(\omega_1, \omega_2) \psi_{\bar{\sigma}_1\bar{\sigma}_2}^f(\omega_1, \omega_2)^* \\ &= \frac{1}{8} \int d\omega_1 d\omega_2 |\psi'(\omega_1, \omega_2) + \psi'(\omega_2, \omega_1)|^2 (\delta_{\sigma_1\oplus} \delta_{\sigma_2\oplus} - \delta_{\sigma_1\ominus} \delta_{\sigma_2\ominus}) (\delta_{\bar{\sigma}_1\oplus} \delta_{\bar{\sigma}_2\oplus} - \delta_{\bar{\sigma}_1\ominus} \delta_{\bar{\sigma}_2\ominus}) \\ &\quad + \frac{1}{8} \int d\omega_1 d\omega_2 |\psi'(\omega_1, \omega_2) - \psi'(\omega_2, \omega_1)|^2 (\delta_{\sigma_1\oplus} \delta_{\sigma_2\ominus} - \delta_{\sigma_1\ominus} \delta_{\sigma_2\oplus}) (\delta_{\bar{\sigma}_1\oplus} \delta_{\bar{\sigma}_2\ominus} - \delta_{\bar{\sigma}_1\ominus} \delta_{\bar{\sigma}_2\oplus}).\end{aligned}\quad (63)$$

Accordingly, we obtain

$$\begin{aligned}P_c^{\text{HOM}} &= (P_{\oplus\oplus}^{\text{HOM}} + P_{\ominus\ominus}^{\text{HOM}}) - (P_{\oplus\ominus}^{\text{HOM}} + P_{\ominus\oplus}^{\text{HOM}}) \\ &= \frac{1}{4} \int d\omega_1 d\omega_2 \left(|\psi'(\omega_1, \omega_2) + \psi'(\omega_2, \omega_1)|^2 - |\psi'(\omega_1, \omega_2) - \psi'(\omega_2, \omega_1)|^2 \right) \\ &= \frac{1}{2} \int d\omega_1 d\omega_2 (\psi'(\omega_1, \omega_2) \psi'(\omega_2, \omega_1)^* + \psi'(\omega_1, \omega_2)^* \psi'(\omega_2, \omega_1)) \\ &= \Re \left\{ \int d\omega_1 d\omega_2 \psi'(\omega_1, \omega_2) \psi'(\omega_2, \omega_1)^* \right\} \\ &= N_{\text{HOM}}^2 \Re \left\{ \int d\omega_1 d\omega_2 [g_{\Omega_1\xi}(\omega_1) g_{\Omega_2\xi}(\omega_2) + e^{i\varphi'_{\text{HOM}}} g_{\Omega_2\xi}(\omega_1) g_{\Omega_1\xi}(\omega_2)] \times \right. \\ &\quad \times [g_{\Omega_1\xi}(\omega_2) g_{\Omega_2\xi}(\omega_1) + e^{-i\varphi'_{\text{HOM}}} g_{\Omega_2\xi}(\omega_2) g_{\Omega_1\xi}(\omega_1)] \left. \right\} \\ &= 2N_{\text{HOM}}^2 \left[\cos(\varphi'_{\text{HOM}}) + \left(\int d\omega g_{\Omega_1\xi}(\omega) g_{\Omega_2\xi}(\omega) \right)^2 \right] \\ &= 2N_{\text{HOM}}^2 \left[\cos(\varphi'_{\text{HOM}}) + e^{-\Omega_-^2/4\xi^2} \right] \\ &= \frac{\cos(\varphi'_{\text{HOM}}) + e^{-\Omega_-^2/4\xi^2}}{1 + \cos(\varphi)} e^{-\Omega_-^2/4\xi^2}.\end{aligned}\quad (64)$$

In the limit $\Omega_- \gg \xi$, the interference patterns simplify to

$$P_c^{\text{MZ}} = \cos(\Omega_+(\tau_{U_s}/\Theta_U - \tau_{L_s}/\Theta_L)/2 + (\chi - 1)(\tilde{\nu}_{U+} \tau_{U_s} - \tilde{\nu}_{L+} \tau_{L_s})/2) \times \cos(\Omega_-(\tau_{U_s}/\Theta_U - \tau_{L_s}/\Theta_L)/2 + (\chi - 1)(\tilde{\nu}_{U-} \tau_{U_s} - \tilde{\nu}_{L-} \tau_{L_s})/2) \quad (65a)$$

$$P_c^{\text{HOM}} = \cos(\varphi'_{\text{HOM}}) = \cos(\Omega_-(\tau_{U_s}/\Theta_U - \tau_{L_s}/\Theta_L) + (\chi - 1)(\tilde{\nu}_{U-} \tau_{U_s} - \tilde{\nu}_{L-} \tau_{L_s}) + \varphi), \quad (65b)$$

and if $\chi = 1$

$$P_c^{\text{MZ}} = \cos(\Omega_+(\tau_{U_s}/\Theta_U - \tau_{L_s}/\Theta_L)/2) \cos(\Omega_-(\tau_{U_s}/\Theta_U - \tau_{L_s}/\Theta_L)/2) \quad (66a)$$

$$P_c^{\text{HOM}} = \cos(\varphi'_{\text{HOM}}) = \cos(\Omega_-(\tau_{U_s}/\Theta_U - \tau_{L_s}/\Theta_L) + \varphi). \quad (66b)$$

C Derivation of the MZ- and HOM-interference patterns for delay lines

Here we derive the MZ- and HOM-interference patterns for the case that optical delays are applied in the transmission paths from Fig. 1 from the main text instead of QMems. We start from the initial states

$$|\psi_{\text{MZ}}\rangle = \int d\omega \psi(\omega) a_{A\omega}^\dagger |0\rangle, \quad (67a)$$

$$|\psi_{\text{HOM}}\rangle = \int d\omega_1 d\omega_2 \psi(\omega_1, \omega_2) a_{U\omega_1}^\dagger a_{L\omega_2}^\dagger |0\rangle, \quad (67b)$$

which are injected into the respective interferometer in Fig. 1 from the main text. In case of the MZ-interferometer, we have a first beam splitter which transforms the photonic creation operators as $\hat{a}_{A\omega} \rightarrow (\hat{a}_{U\omega} - \hat{a}_{L\omega})/\sqrt{2}$ and $\hat{a}_{B\omega} \rightarrow (\hat{a}_{U\omega} + \hat{a}_{L\omega})/\sqrt{2}$. Both, the MZ- and HOM-interferometer employ optical delays, which transform the photonic creation operators as $\hat{a}_{\sigma\omega} \rightarrow \hat{a}_{\sigma\omega} e^{i\omega\tau_d/\Theta_\sigma}$ with $\sigma = U, L$ (c.f. Fig. 1 from the main text). Then, a 50:50 beam splitter is applied, which transforms the photonic creation operators as $\hat{a}_{U\omega} \rightarrow (\hat{a}_{\oplus\omega} - \hat{a}_{\ominus\omega})/\sqrt{2}$ and $\hat{a}_{L\omega} \rightarrow (\hat{a}_{\oplus\omega} + \hat{a}_{\ominus\omega})/\sqrt{2}$.

Passing the respective sequence of beam splitters and optical delays, the quantum states (67) transform into

$$|\psi'_{\text{MZ}}\rangle = \int d\omega \psi(\omega) \left[a_{\oplus\omega}^\dagger (e^{i\omega\tau_d/\Theta_U} - e^{i\omega\tau_d/\Theta_L}) - a_{\ominus\omega}^\dagger (e^{i\omega\tau_d/\Theta_U} + e^{i\omega\tau_d/\Theta_L}) \right] / 2 |0\rangle \quad (68\text{a})$$

$$|\psi'_{\text{HOM}}\rangle = \int d\omega_1 d\omega_2 \psi(\omega_1, \omega_2) e^{i\omega_1\tau_d/\Theta_U} e^{i\omega_2\tau_d/\Theta_L} (\hat{a}_{\oplus\omega_1}^\dagger - \hat{a}_{\ominus\omega_1}^\dagger)(\hat{a}_{\oplus\omega_2}^\dagger + \hat{a}_{\ominus\omega_2}^\dagger) / 2 |0\rangle, \quad (68\text{b})$$

which both can be represented in the form of (9), where one has

$$\psi_\sigma(\omega) = \frac{1}{2} \psi(\omega) [\delta_{\sigma\oplus}(e^{i\omega\tau_d/\Theta_U} - e^{i\omega\tau_d/\Theta_L}) - \delta_{\sigma\ominus}(e^{i\omega\tau_d/\Theta_U} + e^{i\omega\tau_d/\Theta_L})], \quad (69\text{a})$$

$$\begin{aligned} \psi_{\sigma_1\sigma_2}(\omega_1, \omega_2) &= \frac{1}{2\sqrt{2}} \left[\psi(\omega_1, \omega_2) e^{i\omega_1\tau_d/\Theta_U} e^{i\omega_2\tau_d/\Theta_L} (\delta_{\sigma_1\oplus} - \delta_{\sigma_1\ominus})(\delta_{\sigma_2\oplus} + \delta_{\sigma_2\ominus}) + ((\sigma_1, \omega_1) \longleftrightarrow (\sigma_2, \omega_2)) \right] \\ &= \frac{1}{2\sqrt{2}} \left[\left(\psi(\omega_1, \omega_2) e^{i\omega_1\tau_d/\Theta_U} e^{i\omega_2\tau_d/\Theta_L} + \psi(\omega_2, \omega_1) e^{i\omega_2\tau_d/\Theta_U} e^{i\omega_1\tau_d/\Theta_L} \right) (\delta_{\sigma_1\oplus}\delta_{\sigma_2\oplus} + \delta_{\sigma_1\ominus}\delta_{\sigma_2\ominus}) \right. \\ &\quad \left. \left(\psi(\omega_1, \omega_2) e^{i\omega_1\tau_d/\Theta_U} e^{i\omega_2\tau_d/\Theta_L} - \psi(\omega_2, \omega_1) e^{i\omega_2\tau_d/\Theta_U} e^{i\omega_1\tau_d/\Theta_L} \right) (\delta_{\sigma_1\oplus}\delta_{\sigma_2\ominus} - \delta_{\sigma_1\ominus}\delta_{\sigma_2\oplus}) \right], \end{aligned} \quad (69\text{b})$$

where $\sigma = \oplus, \ominus$. Inserting (69) into Eq. (15) from the main text and taking the corresponding diagonal elements of the resulting reduced density matrices yields

$$P_c^{\text{MZ}} = \int d\omega |\psi(\omega)|^2 \cos(\omega\Delta_{\Theta^{-1}}\tau_d), \quad (70\text{a})$$

$$P_c^{\text{HOM}} = \Re \left\{ \int d\omega_1 d\omega_2 \psi(\omega_1, \omega_2) \psi^*(\omega_2, \omega_1) e^{i\Delta\omega\Delta_{\Theta^{-1}}\tau_d} \right\}, \quad (70\text{b})$$

where $\Delta\omega = \omega_2 - \omega_1$ and $\Delta_{\Theta^{-1}} = 1/\Theta_L - 1/\Theta_U$.

Inserting the spectra (12) and (13) from the main text into (70) results in

$$P_c^X = 2N_X^2 [R_X + S_X], \quad (71\text{a})$$

$$R_{\text{MZ}} = e^{-\frac{1}{2}(\Delta_{\Theta^{-1}}\tau_d\xi)^2} \cos(\Omega_+\Delta_{\Theta^{-1}}\tau_d/2) \cos(\Omega_-\Delta_{\Theta^{-1}}\tau_d/2) \quad (71\text{b})$$

$$R_{\text{HOM}} = e^{-(\Delta_{\Theta^{-1}}\tau_d\xi)^2} \cos(\Omega_-\Delta_{\Theta^{-1}}\tau_d - \varphi) \quad (71\text{c})$$

$$S_{\text{MZ}} = e^{-\Omega_-^2/(8\xi^2)} e^{-\frac{1}{2}(\Delta_{\Theta^{-1}}\tau_d\xi)^2} \cos(\varphi) \cos(\Omega_+\Delta_{\Theta^{-1}}\tau_d/2) \quad (71\text{d})$$

$$S_{\text{HOM}} = e^{-\Omega_-^2/(4\xi^2)} e^{-(\Delta_{\Theta^{-1}}\tau_d\xi)^2} \quad (71\text{e})$$

with $X = \text{MZ, HOM}$ where $\Omega_\pm = \Omega_2 \pm \Omega_1$. In the limit $\Omega_- \gg \xi$ we have $\lim_{\Omega_-/\xi \rightarrow \infty} S_X = 0$, and the interference patterns (71a) simplify to

$$P_c^{\text{MZ}} = e^{-\frac{1}{2}(\Delta_{\Theta^{-1}}\tau_d\xi)^2} \cos(\Omega_+\Delta_{\Theta^{-1}}\tau_d/2) \cos(\Omega_-\Delta_{\Theta^{-1}}\tau_d/2), \quad (72\text{a})$$

$$P_c^{\text{HOM}} = e^{-(\Delta_{\Theta^{-1}}\tau_d\xi)^2} \cos(\Omega_-\Delta_{\Theta^{-1}}\tau_d - \varphi), \quad (72\text{b})$$

which in the limit of vanishing frequency separation, i.e. $\Omega_1 = \Omega_2 = \Omega$, reproduce the well known textbook result of the MZ-interference pattern $P_c^{\text{MZ}} = \cos(\Omega\Delta\tau)$ (for a monochromatic wave, i.e. $\xi = 0$) and the seminal result $P_c^{\text{HOM}} = e^{-(\Delta_{\Theta^{-1}}\tau_d\xi)^2}$ known as the *HOM-Dip* [53], when $\Delta\tau$ is identified with $\Delta_{\Theta^{-1}}\tau_d$. In the narrow bandwidth limit $\Delta_{\Theta^{-1}}\tau_d\xi \ll 1$, the interference patterns simplify to

$$P_c^{\text{MZ}} = \cos(\Omega_+\Delta_{\Theta^{-1}}\tau_d/2) \cos(\Omega_-\Delta_{\Theta^{-1}}\tau_d/2), \quad (73\text{a})$$

$$P_c^{\text{HOM}} = \cos(\Omega_-\Delta_{\Theta^{-1}}\tau_d - \varphi). \quad (73\text{b})$$

D Mixed states, partial traces and identification of entanglement in second quantisation

After having derived the measurement statistics of the considered MZ- and HOM-experiments employing QMems and optical delay lines in the two previous appendix sections, this chapter is dedicated to take a closer look at the

physical interpretation of these measurement statistics, where we put particular emphasis on the decoherence of the spatial correlation that arises as a consequence of EDs due to gravity. Note that the measurement statistics in any case solely depend on the diagonal elements of the reduced density matrices, as seen in Eq. (16) from the main text. However, in order to characterize the degree of coherence of a quantum (sub) state, it is essential to study the off-diagonal elements of the considered density matrices, the elements carrying information about the quantum phases.

Therefore, we first characterize mixed states quantitatively and derive the partial trace in second quantization. Concrete examples are provided by specializing our results to the here discussed MZ- and HOM-experiments, for which we show how the coherence of the spatial substate of the considered photons is lost.

In analogy to our definition of pure single- and two-photon states (9a) and (9b) that are

$$|\psi_1\rangle = \sum_{\sigma} \int d\omega \psi_{\sigma}(\omega) \hat{a}_{\sigma\omega}^{\dagger} |0\rangle, \quad (74a)$$

$$|\psi_2\rangle = \frac{1}{\sqrt{2}} \sum_{\sigma_1, \sigma_2} \int d\omega_1 d\omega_2 \psi_{\sigma_1 \sigma_2}(\omega_1, \omega_2) \hat{a}_{\sigma_1 \omega_1}^{\dagger} \hat{a}_{\sigma_2 \omega_2}^{\dagger} |0\rangle, \quad (74b)$$

we define mixed single- and two-photon states as

$$\hat{\rho}_1 = \sum_{\sigma, \bar{\sigma}} \int d\omega d\bar{\omega} \rho_{\sigma \bar{\sigma}}(\omega, \bar{\omega}) \hat{a}_{\sigma\omega}^{\dagger} |0\rangle \langle 0| \hat{a}_{\bar{\sigma}\bar{\omega}}, \quad (75a)$$

$$\hat{\rho}_2 = \frac{1}{2} \sum_{\sigma_1, \sigma_2, \bar{\sigma}_1, \bar{\sigma}_2} \int d\omega_1 d\omega_2 d\bar{\omega}_1 d\bar{\omega}_2 \rho_{\sigma_1 \sigma_2 \bar{\sigma}_1 \bar{\sigma}_2}(\omega_1, \omega_2, \bar{\omega}_1, \bar{\omega}_2) \hat{a}_{\sigma_1 \omega_1}^{\dagger} \hat{a}_{\sigma_2 \omega_2}^{\dagger} |0\rangle \langle 0| \hat{a}_{\bar{\sigma}_1 \bar{\omega}_1} \hat{a}_{\bar{\sigma}_2 \bar{\omega}_2}, \quad (75b)$$

which are characterized through the corresponding density matrices $\rho_{\sigma \bar{\sigma}}(\omega, \bar{\omega})$ and $\rho_{\sigma_1 \sigma_2 \bar{\sigma}_1 \bar{\sigma}_2}(\omega_1, \omega_2, \bar{\omega}_1, \bar{\omega}_2)$ rendering the following symmetries

$$\rho_{\sigma \bar{\sigma}}(\omega, \bar{\omega}) = \rho_{\bar{\sigma} \sigma}^{*}(\bar{\omega}, \omega) \quad (76a)$$

$$\rho_{\sigma_1 \sigma_2 \bar{\sigma}_1 \bar{\sigma}_2}(\omega_1, \omega_2, \bar{\omega}_1, \bar{\omega}_2) = \rho_{\sigma_2 \sigma_1 \bar{\sigma}_1 \bar{\sigma}_2}(\omega_2, \omega_1, \bar{\omega}_1, \bar{\omega}_2) = \rho_{\sigma_1 \sigma_2 \bar{\sigma}_2 \bar{\sigma}_1}(\omega_1, \omega_2, \bar{\omega}_2, \bar{\omega}_1) = \rho_{\bar{\sigma}_1 \bar{\sigma}_2 \sigma_1 \sigma_2}^{*}(\bar{\omega}_1, \bar{\omega}_2, \omega_1, \omega_2), \quad (76b)$$

which can be inferred by use of the canonical commutation relations. Physically, the first two equal signs of Eq. (76b) are a consequence of the requirement for a bosonic two-particle density function to be symmetric under particle exchange, and the last equal signs from Eqs. (76a) and (76b) reflect the hermiticity of the density operators. For pure states, the density matrices take the form of dyadic products

$$\rho_{\sigma \bar{\sigma}}(\omega, \bar{\omega}) = \psi_{\sigma}(\omega) \psi_{\bar{\sigma}}^{*}(\bar{\omega}) \quad (77a)$$

$$\rho_{\sigma_1 \sigma_2 \bar{\sigma}_1 \bar{\sigma}_2}(\omega_1, \omega_2, \bar{\omega}_1, \bar{\omega}_2) = \psi_{\sigma_1 \sigma_2}(\omega_1, \omega_2) \psi_{\bar{\sigma}_1 \bar{\sigma}_2}^{*}(\bar{\omega}_1, \bar{\omega}_2). \quad (77b)$$

To consider substates of a quantum system, basically any DOFs can be traced out by the *partial trace*. In this article, we trace out certain DOFs of a quantum system shared by all particles, thereby leaving the particle number of the system unchanged. In MZ- and HOM-interference, one is usually interested in the spatial substate of the photons (i.e. at which detector a photon is detected) for the case of frequency insensitive photo detectors.

To consistently define the partial trace, we have to define a tensor product structure first. To this end, we assume that the single particle Hilbert space \mathcal{H} can be written consistently as the tensor product of a spatial Hilbert space \mathcal{H}_s and a frequency Hilbert space \mathcal{H}_f , i.e. $\mathcal{H} = \mathcal{H}_s \otimes \mathcal{H}_f$, which implies that there must exist an abstract basis of \mathcal{H} of single particle wave functions that can be written as $\{|\sigma\rangle \otimes |\omega\rangle\}_{\sigma, \omega}$, where $\{|\sigma\rangle\}_{\sigma}$ is a basis of \mathcal{H}_s and $\{|\omega\rangle\}_{\omega}$ is a basis of \mathcal{H}_f , i.e. spatial degree of freedom and frequency completely decouple.

From the single particle Hilbert space, we construct the 2-particle Hilbert space as the tensor product, $\mathcal{H} \otimes \mathcal{H}$ which we can identify with $\mathcal{H}_s \otimes \mathcal{H}_f \otimes \mathcal{H}_s \otimes \mathcal{H}_f$ via the basis $\{|\sigma\rangle \otimes |\omega\rangle \otimes |\bar{\sigma}\rangle \otimes |\bar{\omega}\rangle\}_{\sigma, \bar{\sigma}, \omega, \bar{\omega}}$, where $\bar{\sigma} = (\sigma, \bar{\sigma})$ and $\bar{\omega} = (\omega, \bar{\omega})$. A simple rearrangement enables the identification with $\mathcal{H}_s^{\otimes 2} \otimes \mathcal{H}_f^{\otimes 2}$ with basis states $\{|\sigma, \bar{\sigma}\rangle \otimes |\omega, \bar{\omega}\rangle\}_{\sigma, \bar{\sigma}, \omega, \bar{\omega}}$, where $|\sigma, \bar{\sigma}\rangle = |\sigma\rangle \otimes |\bar{\sigma}\rangle$ and $|\omega, \bar{\omega}\rangle = |\omega\rangle \otimes |\bar{\omega}\rangle$. Note that this structure implicitly requires a labelling of the photons with the position in the state vector $|\sigma, \bar{\sigma}\rangle$ and $|\omega, \bar{\omega}\rangle$. Since photons are indistinguishable the symmetrization has to be subsequent. Explicitly, we obtain

$$\hat{a}_{\sigma\omega}^{\dagger} \hat{a}_{\bar{\sigma}\bar{\omega}}^{\dagger} |0\rangle = \frac{1}{\sqrt{2}} (|\sigma, \bar{\sigma}\rangle \otimes |\omega, \bar{\omega}\rangle + |\bar{\sigma}, \sigma\rangle \otimes |\bar{\omega}, \omega\rangle). \quad (78)$$

Therefore, we can write the partial trace of the two-particle density matrix over the frequency sub-space as

$$\begin{aligned}
\text{Tr}_f[\hat{\rho}_2] &= \frac{1}{2} \sum_{\substack{\sigma_1, \sigma_2, \\ \bar{\sigma}_1, \bar{\sigma}_2}} \int d\omega'_1 d\omega'_2 d\omega_1 d\omega_2 d\bar{\omega}_1 d\bar{\omega}_2 \rho_{\sigma_1 \sigma_2 \bar{\sigma}_1 \bar{\sigma}_2}(\omega_1, \omega_2, \bar{\omega}_1, \bar{\omega}_2) \langle \omega'_1, \omega'_2 | \hat{a}_{\sigma_1 \omega_1}^\dagger \hat{a}_{\sigma_2 \omega_2}^\dagger | 0 \rangle \langle 0 | \hat{a}_{\bar{\sigma}_1 \bar{\omega}_1} \hat{a}_{\bar{\sigma}_2 \bar{\omega}_2} | \omega'_1, \omega'_2 \rangle \\
&= \frac{1}{4} \sum_{\substack{\sigma_1, \sigma_2, \\ \bar{\sigma}_1, \bar{\sigma}_2}} \int d\omega'_1 d\omega'_2 d\omega_1 d\omega_2 d\bar{\omega}_1 d\bar{\omega}_2 \rho_{\sigma_1 \sigma_2 \bar{\sigma}_1 \bar{\sigma}_2}(\omega_1, \omega_2, \bar{\omega}_1, \bar{\omega}_2) \times \\
&\quad \times (|\sigma_1, \sigma_2\rangle \delta(\omega'_1 - \omega_1) \delta(\omega'_2 - \omega_2) + |\sigma_2, \sigma_1\rangle \delta(\omega'_1 - \omega_2) \delta(\omega'_2 - \omega_1)) \times \\
&\quad \times (\langle \bar{\sigma}_1, \bar{\sigma}_2 | \delta(\omega'_1 - \bar{\omega}_1) \delta(\omega'_2 - \bar{\omega}_2) + \langle \bar{\sigma}_2, \bar{\sigma}_1 | \delta(\omega'_1 - \bar{\omega}_2) \delta(\omega'_2 - \bar{\omega}_1)) \\
&= \sum_{\substack{\sigma_1, \sigma_2, \\ \bar{\sigma}_1, \bar{\sigma}_2}} \int d\omega'_1 d\omega'_2 \rho_{\sigma_1 \sigma_2 \bar{\sigma}_1 \bar{\sigma}_2}(\omega'_1, \omega'_2, \omega'_1, \omega'_2) |\sigma_1, \sigma_2\rangle \langle \bar{\sigma}_1, \bar{\sigma}_2| \\
&=: \sum_{\substack{\sigma_1, \sigma_2, \\ \bar{\sigma}_1, \bar{\sigma}_2}} \rho_{\sigma_1 \sigma_2 \bar{\sigma}_1 \bar{\sigma}_2} |\sigma_1, \sigma_2\rangle \langle \bar{\sigma}_1, \bar{\sigma}_2|,
\end{aligned} \tag{79}$$

where we used the symmetries in equation (76b). Note that the spatial states $|\sigma_1, \sigma_2\rangle\langle$ inherit the implicit labeling of particles with the position in the state vector. Therefore in general, $|\sigma_1, \sigma_2\rangle$ is not the same state as $|\sigma_2, \sigma_1\rangle$ for $\sigma_1 \neq \sigma_2$. This is only the case if the two involved photons are completely indistinguishable, that is, are in the same frequency state. Then, $\hat{\rho}_2$ is separable in spatial and frequency degrees of freedom and the reduced density matrix is that of a pure state. Accordingly, the reduced density matrix $\rho_{\sigma_1 \sigma_2 \bar{\sigma}_1 \bar{\sigma}_2}$ is not generically symmetric under the exchange of indices within the pairs (σ_1, σ_2) and $(\bar{\sigma}_1, \bar{\sigma}_2)$.

For the n-particle sector, the reduced density matrix is simply defined as

$$\rho_{\sigma_1 \dots \sigma_n \bar{\sigma}_1 \dots \bar{\sigma}_n} = \int d\omega_1 \dots d\omega_n \rho_{\sigma_1 \dots \sigma_n \bar{\sigma}_1 \dots \bar{\sigma}_n}(\omega_1, \dots, \omega_n, \omega_1, \dots, \omega_n) \dots \tag{80}$$

A measure of the entanglement between the spatial and frequency degrees of freedom can then be defined through the purity of the reduced density matrix

$$\mathcal{P}(\rho^E) = \sum_{\substack{\sigma_1, \dots, \sigma_n, \\ \bar{\sigma}_1, \dots, \bar{\sigma}_n}} |\rho_{\sigma_1 \dots \sigma_n \bar{\sigma}_1 \dots \bar{\sigma}_n}^E|^2, \tag{81}$$

where values below one indicate the presence of entanglement between the internal and external DOFs in case that the original state is pure.

Next we compute the reduced spatial density matrices at the detectors of the MZ- and HOM-experiments which employ QMems, and similar considerations hold for the case of delay lines.

For the MZ- experiment that employs QMems the density matrix at the detectors is equal to

$$\rho_{\sigma \bar{\sigma}}(\omega, \bar{\omega}) = \psi_\sigma^f(\omega) \psi_{\bar{\sigma}}^f(\bar{\omega}), \quad \sigma, \bar{\sigma} = \oplus, \ominus \tag{82}$$

where $\psi_\sigma^f(\omega)$ has to be taken from (60a), and can be given in vectorial notation as. Then the computation of the reduced spatial density matrix results in

$$\rho_{\sigma \bar{\sigma}} = \int d\omega \rho_{\sigma \bar{\sigma}}(\omega, \bar{\omega}) = \frac{1}{2} \begin{pmatrix} 1 - \cos(\Omega_+ \Delta_{\Theta^{-1}} \tau_s / 2) \cos(\Omega_- \Delta_{\Theta^{-1}} \tau_s / 2) & -i \sin(\Omega_+ \Delta_{\Theta^{-1}} \tau_s / 2) \cos(\Omega_- \Delta_{\Theta^{-1}} \tau_s / 2) \\ i \sin(\Omega_+ \Delta_{\Theta^{-1}} \tau_s / 2) \cos(\Omega_- \Delta_{\Theta^{-1}} \tau_s / 2) & 1 + \cos(\Omega_+ \Delta_{\Theta^{-1}} \tau_s / 2) \cos(\Omega_- \Delta_{\Theta^{-1}} \tau_s / 2) \end{pmatrix}, \tag{83}$$

where we have directly taken the large bandwidth limit $\Omega_- \gg \xi$, and have set

$$\int d\omega g_{\Omega_i \xi}(\omega) g_{\Omega_j \xi}(\omega) = \delta_{ij}, \quad N_{\text{MZ}} = 1/\sqrt{2} \tag{84}$$

for better readability of Eq. (83). It follows immediately that the purity of the reduced density matrix of the spatial substate (83) in the considered MZ-experiment equals

$$\mathcal{P}_{\text{MZ}}(\tau_s) = \sum_{\sigma, \bar{\sigma} = \oplus, \ominus} |\rho_{\sigma \bar{\sigma}}|^2 = \frac{1}{4} (3 + \cos(\Omega_- \Delta_{\Theta^{-1}} \tau_s)), \tag{85}$$

which reaches its minimum value of $\mathcal{P}(\tau_{s,\text{ent}}^{\text{MZ}}) = 1/2$ at

$$\tau_{s,\text{ent}}^{\text{MZ}} = \frac{\pi}{\Omega_- \Delta_{\Theta^{-1}}}, \quad (86)$$

which we call *entangling time* since at this time the spatial substate (83) is apparently mixed, although the entire photonic state (82) is obviously pure, i.e. that the external DOF of the considered photon must be entangled with its internal DOF, the frequency.

For the HOM- experiments that employ QMems the density matrix at the detectors is equal to

$$\rho_{\sigma_1 \sigma_2 \bar{\sigma}_1 \bar{\sigma}_2}(\omega_1, \omega_2, \bar{\omega}_1, \bar{\omega}_2) = \psi_{\sigma_1 \sigma_2}^f(\omega_1, \omega_2) \psi_{\bar{\sigma}_1 \bar{\sigma}_2}^f(\bar{\omega}_1, \bar{\omega}_2), \quad (87)$$

where $\psi_{\sigma_1 \sigma_2}^f(\omega_1, \omega_2)$ has to be taken from (60b). Then the computation of the reduced spatial density matrix results in

$$\rho_{\sigma_1 \sigma_2 \bar{\sigma}_1 \bar{\sigma}_2} = \frac{1}{4} \begin{pmatrix} 1 + \cos(p) & 0 & 0 & -1 - \cos(p) \\ 0 & 1 - \cos(p) & -1 + \cos(p) & 0 \\ 0 & -1 + \cos(p) & 1 - \cos(p) & 0 \\ -1 - \cos(p) & 0 & 0 & 1 + \cos(p) \end{pmatrix}, \quad (88)$$

where $p = \Omega_- \Delta_{\Theta^{-1}} \tau_s - \varphi$. In Eq. (88) the row and column numbering corresponds to $\{\oplus\oplus, \oplus\ominus, \ominus\oplus, \ominus\ominus\}$, and we again employed the large bandwidth limit for better readability. The purity of the spatial substate in this case results in

$$\mathcal{P}_{\text{HOM}}(\tau_s) = \sum_{\sigma_1, \bar{\sigma}_1, \sigma_2, \bar{\sigma}_2 = \oplus, \ominus} |\rho_{\sigma_1 \sigma_2 \bar{\sigma}_1 \bar{\sigma}_2}|^2 = \frac{1}{4}(3 + \cos(2\Omega_- \Delta_{\Theta^{-1}} \tau_s - 2\varphi)) \quad (89)$$

which for $\varphi = 0$ reaches its minimum value of $\mathcal{P}(\tau_{s,\text{ent}}^{\text{HOM}}) = 1/2$ at

$$\tau_{s,\text{ent}}^{(2)} = \frac{\pi}{2\Omega_- \Delta_{\Theta^{-1}}}. \quad (90)$$

We want to add that, from an information theoretic perspective, it is more conventional to quantify the mixedness of a quantum state by the linear entropy $\mathcal{S} = 1 - \mathcal{P}$ instead of the purity \mathcal{P} , where now $\mathcal{S} = 0$ corresponds to pure states, i.e. values $\mathcal{S} > 0$ of reduced substates of a pure quantum state indicate the presence of entanglement. For the here discussed MZ- and HOM-experiments, the linear entropy results in

$$\mathcal{S}_{\text{MZ}}(\tau_s) = 1 - \mathcal{P}_{\text{MZ}}(\tau_s) = \frac{1}{2} \sin^2(\Omega_- \Delta_{\Theta^{-1}} \tau_s / 2) \quad (91a)$$

$$\mathcal{S}_{\text{HOM}}(\tau_s) = 1 - \mathcal{P}_{\text{HOM}}(\tau_s) = \frac{1}{2} \sin^2(\Omega_- \Delta_{\Theta^{-1}} \tau_s - \varphi), \quad (91b)$$

which stands in perfect analogy to the corresponding results (5) and (41), which describe the gravitationally induced dynamics of entanglement between the internal and external DOFs of qubit clock states.

Finally, we want to investigate the entanglement contained in the spatial sub-state (88), i.e. the mutual spatial entanglement shared among the two photons, which can be explored by frequency insensitive detectors in the considered HOM-experiment. The density matrix (88) characterizes a two-qubit state, where one qubit is encoded in the spatial DOF of one photon and the other qubit is encoded in the spatial DOF of the other photon. In such a system the presence of entanglement can be unambiguously certified by positive values of the negativity, which is equal to the negative sum of the negative eigenvalues of the partially transposed density matrix of (88), which is

$$\rho_{\sigma_1 \sigma_2 \bar{\sigma}_1 \bar{\sigma}_2}^{\text{PT}} = \frac{1}{4} \begin{pmatrix} 1 + \cos(p) & 0 & 0 & -1 + \cos(p) \\ 0 & 1 - \cos(p) & -1 - \cos(p) & 0 \\ 0 & -1 - \cos(p) & 1 - \cos(p) & 0 \\ -1 + \cos(p) & 0 & 0 & 1 + \cos(p) \end{pmatrix}, \quad (92)$$

and featuring the eigenvalues $\lambda_{\text{PT}} = 1/2(1, 1, \cos(p), -\cos(p))$. Thus, the associated negativity results in

$$\mathcal{N}_{\text{HOM}} = - \sum_{\lambda_{\text{PT}} < 0} \lambda_{\text{PT}} = |\cos(\Omega_- \Delta_{\Theta^{-1}} \tau_s - \varphi)|/2, \quad (93)$$

thereby establishing the analogy to the result (37), which characterizes the mutual spatial entanglement of two particles subject to EDs due to gravity from Appendix A.

In conclusion, we can simplify the expressions for the linear entropy and negativity by expressing them in terms of the quantities $P_c^{\text{HOM}} = \cos(\Omega_- \Delta_{\Theta^{-1}} \tau_s - \varphi)$ and $\mathcal{V} = \cos(\Omega_- \Delta_{\Theta^{-1}} \tau_s / 2)$. We obtain

$$\mathcal{S}_{\text{MZ}} = \frac{1}{2} (1 - \mathcal{V}^2) \quad (94\text{a})$$

$$\mathcal{S}_{\text{HOM}} = \frac{1}{2} \left(1 - (P_c^{\text{HOM}})^2 \right), \quad (94\text{b})$$

$$\mathcal{N}_{\text{HOM}} = \frac{|P_c^{\text{HOM}}|}{2}. \quad (94\text{c})$$

E Effect of longitudinal Doppler shift

In this appendix, we estimate the effect of the longitudinal Doppler shift between two satellites that are moving on circular orbits. The expression for the Doppler shift to leading order (Newtonian) is $\Delta v/c$, where Δv_{long} is the relative velocity of the two satellites. In the following, we assume that both orbits lie in the equatorial plane, and at $t = 0$, the positions of the two satellites are aligned with the center of Earth which implies that $\Delta v(t = 0) = 0$. We find for the distance between the two satellites at $t > 0$

$$\Delta R(t) = \sqrt{r_1^2 + r_2^2 - 2r_1 r_2 \cos(\omega_1 - \omega_2)t} \quad (95)$$

and for the relative velocity

$$\Delta v_{\text{long}}(t) = \frac{r_1 r_2 (\omega_1 - \omega_2) \sin(\omega_1 - \omega_2)t}{\sqrt{r_1^2 + r_2^2 - 2r_1 r_2 \cos(\omega_1 - \omega_2)t}}, \quad (96)$$

where $\omega_{1/2} = \sqrt{GM/r_{1/2}^3}$ and $r_{1/2}$ are the orbital angular frequencies and radii of the two satellites, respectively.

Let us assume that we have two circular orbits, one at 10000 km above the Earth's surface (16371 km from the center) and one at a geosynchronous orbit. Let us further assume that the pulse from the upper arm arrives at U at $t = 0$. Then, at $t = \tau_d = 8.5 \text{ km}/c \sim 3 \times 10^{-5} \text{ s}$ when the pulse from the lower arm arrives at the beam splitter, there will be a red-shift of $z_{\text{Doppler}}(\tau_d) = \Delta v_{\text{long}}(\tau_d)/c \sim 1 \times 10^{-13}$ and a phase difference due to the difference in travel distance of the photons of $\Delta R(\tau_d)/\lambda \sim 4 \times 10^{-4}$. So it seems that the longitudinal Doppler effect can indeed be neglected if the timing of the experiment is precise enough.

F Estimation of the required temporal resolution

In the following we estimate the resolution of the optical delays and the storage time of the QMems, which is required in order to infer that the relativistic redshift is the origin of the loss of spatial correlation between the photons in the HOM-experiment considered in Fig. 3 from the main text, and not just appropriate (noisy) delay settings as discussed in the main text. In Eq. (22b) the argument of the cosine function is

$$C(\tau_s) := \Delta_{\Theta^{-1}} \Omega_- \tau_s, \quad (97)$$

where here and in the following the subscript "s" for storage time can be replaced the subscript "d" for delay in order to obtain the corresponding analysis for optical delays. Note that the result (97) is based on the assumption that both storage times of the QMems in the two distinct arms of the interferometer $\tau_{U,s}$ and $\tau_{L,s}$ are locally adjusted to precisely the same value $\tau_{U,s} = \tau_{L,s} = \tau_s$ with infinite precision. However, in practice the storage time in each arm can only be adjusted to a finite precision, the absolute resolution error τ_s^{res} . In the general case, that is, $\tau_{U,s} \neq \tau_{L,s}$ Eq. (97) generalizes to

$$C(\tau_{U,s}, \tau_{L,s}) = \Omega_- (\tau_{U,s}/\Theta_U - \tau_{L,s}/\Theta_L), \quad (98)$$

We are interested in the error of C (which we call ΔC), which is caused by the uncertainties of the storage times of the QMems τ_s^{res} and find from the standard error estimation

$$\Delta C = \left(\left| \frac{\partial C}{\partial \tau_{U,s}} \right| + \left| \frac{\partial C}{\partial \tau_{L,s}} \right| \right) \tau_s^{\text{res}} = \Omega_- (1/\Theta_U + 1/\Theta_L) \tau_s^{\text{res}} = \Omega_- \left(\frac{1}{1+z_{sU}} + \frac{1}{1+z_{sL}} \right) \tau_s^{\text{res}} \approx 2\Omega_- \tau_s^{\text{res}}. \quad (99)$$

In order to exclude the possibility that the finite resolution effects are the reason for the loss of spatial correlation in the considered HOM-experiment (and not relativistic effects) one has to require $\Delta C \ll \pi/2$ (since we are

interested in the parameters, which render $C = \pi/2$). A necessary condition for this are the restrictions on the resolution of the optical delays and QMems

$$\tau_s^{\text{res}} \ll \tau_s^{\text{reslim}} = \frac{\pi}{4\Omega_-}. \quad (100\text{a})$$

which we displayed as the top axis in Fig. 3 of the main text. The superscript "reslim" stands for resolution limit.

Vice versa Eq. (100) yields the maximum frequency separations for a given temporal resolution and τ_s^{res} , that is

$$\Omega_- \ll \Omega_-^{\text{lim}} = \frac{\pi}{4\tau_s^{\text{res}}}. \quad (101\text{a})$$

Finally, we want to remark that the above requirement on the temporal resolution is identical to the following condition on the relative temporal accuracy at the entanglement time

$$\frac{\tau_s^{\text{res}}}{\tau_{s,\text{ent}}^{\text{HOM}}} \ll \frac{\tau_s^{\text{reslim}}}{\tau_{s,\text{ent}}^{\text{HOM}}} = \frac{\Delta_{\Theta^{-1}}}{2}, \quad (102)$$

for the case of HOM interference, and an analogous expression is obtained for MZ interference.

G Different QMem combinations

Below, the differences between the acceptance frequencies of the various QMem combinations which are discussed in chapter 4 in the main text are seen. As discussed in the main text, inhomogenous broadening of the REID materials would enable frequency multiplexing with $\Omega_- \sim 1 - 10$ GHz. And in fact, storing frequency superposition states with Ω_- as small as ~ 10 MHz is possible with these system but then the required storage time will be out of reach with such QMems.

	Rb (377.1 THz) (795 nm) [43])	Cs (335.3 THz) (894 nm) [45])	Pr (494.7 THz) (606 nm) [33])	Eu (517.9 THz) (579 nm) [35])
Rb		41.8	117.6	140.9
Cs			159.6	182.6
Pr			$10^{-3} - 10^{-2}$	23.2
Eu				$10^{-3} - 10^{-2}$

Table 1: The achievable Ω_- for different QMem combinations. If not stated differently, all quantities in the table are given in units of THz.

Chapter 5

Conclusion

5.1 Summary of the methodological approach

In summary, this thesis delves into the impact of relativistic effects on quantum entanglement and indistinguishability within the framework of Hong-Ou-Mandel (HOM) interference experiments. By developing new theoretical approaches, extending existing frameworks, and proposing experimental setups, this work aims to test these theoretical predictions with minimal resource requirements.

The initial phase of this research focused on understanding the interplay between quantum entanglement and indistinguishability, the core quantum resources in HOM interferometry [BL23]. This understanding was crucial for extending the theory to relativistic contexts in curved space-times. [BBSL22, BGK⁺24]

To simplify the mathematical framework for describing multi-particle interference, the research employed *Glauber's theory of optical coherence* [39]. This approach showed that the detection statistics—essentially the outcomes of multi-particle detection events—align with the squared modulus of the multi-particle wave function. This wave function encapsulates the full generality of the particle ensemble's degrees of freedom (DOFs) [BL23].

A significant finding was that quantum entanglement and indistinguishability are intrinsically linked, connected through the concept of entanglement monogamy [BL23]. The research then abstractly extended this description to include the redshift effect on photons [BBSL22], by adopting considerations from older works—as for instance [20]—deducing this effect from the commutation relations. In this work, we extended this theoretical consideration through modeling the redshift effect by a unitary dilation operation on the photonic creation and annihilation operators, which relates distinct observer frames through mutual redshift and determines the transformation of the photonic wave function between these frames—either through a unitary dilation operation.

Further, the study on hand incorporated the Klein-Gordon equation on curved spacetime backgrounds, informing the transformation of bosonic modes under reference frame changes. This also allowed for considering the effects of time dilation and spatial curvature on massive quantum clocks—Compton clocks—and their ticking rates under relativistic gravity.

The thesis also modeled quantum memories characterized by bosonic excitations, specifically magnons, and their interactions with photons within HOM interference experiments through a

Jaynes-Cumming model. This led to theoretical predictions about the evolution of the combined photon and quantum memory system in gravitational fields with distinct redshift levels. The effective light-matter interaction was modeled using a simple mode swapper model as in [BGK⁺24], capturing the essential features of quantum coherence transfer between photons and quantum memories.

Special attention was given to *frequency-entangled photons* (FEP) due to their pronounced *quantum beating* phenomenon —the periodic transition between photon bunching and anti-bunching in the temporal delay. In this context, the redshift and time dilation induced by gravitational fields were shown to modulate this quantum beating. The final part of the thesis interprets the alteration of detection statistics due to redshift in light of previous findings and draws conclusions about the gravitational impact on non-local quantum entanglement between photons.

Chapter 6

Outlook

This work paves the way for a wide range of potential future research, encompassing both thematic exploration and methodological advancements.

We divide the outlook into two parts, namely into

- I. the direct extensions of the topics addressed in this work, particularly about the modelling of *quantum memories in a relativistic setting* in Sec. 6.1, and
- II. the fairly more foundational considerations concerned with the *mathematical characterization of the quantum mechanical state space* leading to implications for various areas of physics and science in Sec. 6.2.

6.1 Quantum Memories in Space

6.1.1 Introduction

Quantum memories are of crucial importance in current quantum science, addressing one of the most critical challenges in quantum technologies: the preservation of coherence. Maintaining quantum coherence is essential for extending the coherence times and lengths of resources such as light and matter. This extension could render quantum systems scalable to macroscopic levels, thereby facilitating robust quantum applications. By stabilizing coherent correlations, quantum memories form the foundation of reliable quantum technologies, opening the door to new applications and significant performance enhancements; endowed by *quantum supremacy*.

6.1.2 Incorporating Relativistic Effects

In our previous study [BGK⁺24], we established the basics for describing quantum memories within a relativistic framework—a domain that—to the best of our knowledge—had not been explored before. Given that existing technological applications like GPS rely on relativistic effects for high performance and accuracy, it is natural to consider such effects in quantum applications as well. For instance, a quantum version of GPS based on entangled encryption would inherently require relativistic considerations.

6.1.3 Developing Advanced Theoretical Models

Developing more accurate and realistic theoretical models for quantum memory networks interacting with light signals over intercontinental distances is of high interest and constitutes one of the central intentions for future work in this thesis. In our publication [BGK⁺24], we employed an elementary model—a mode swapper model—for quantum memory pairs interacting with light in the vicinity of post-Newtonian gravity. In the current work, we extend this description through the use of unitary dilation in Section 3.2.4, an approach not yet reported or developed in the literature.

6.1.4 Spatio-Temporal Continuum Description

This extended description allows us to model light and matter as spatio-temporally extended continua—that is, as quantum systems with spatially extended wave functions that experience differential temporal evolution depending on the local spacetime geometry. This approach goes beyond the characterization in [BGK⁺24], which considered solely two discrete potential levels with distinct temporal evolution related to the redshift.

6.1.5 Including Decoherence and Environmental Effects

Our future vision includes incorporating dissipation and environmental effects leading to decoherence. In a unitary model, this would involve accounting for the entire physical environment in which quantum information processing with light and quantum memories occurs. Decoherence would emerge from partially tracing out environmental degrees of freedom, such as atmospheric effects.

However, this unitary approach involves extremely large Hilbert space dimensions, making practical calculations computationally infeasible due to complexity. To achieve feasible calculation times, reducing computational complexity is necessary. Instead of evolving the entire density operator of the system and environment, we propose using a reduced model that employs *Heisenberg equations of motion for expectation values*. This involves describing light-matter interactions between optical signals and quantum memories via *Liouville-von Neumann equations* derived from a Jaynes-Cummings model. Our current work paves the way for this target through contributions in Section 4.3.

6.1.6 Matter-Assisted Quantum Optics on Curved Spacetime

Ultimately, our goal is to describe matter-assisted quantum optics on curved spacetime. From a methodological perspective, it would be interesting to investigate relativistic corrections on quantum evolution approaches such as Heisenberg’s equations of motion and the unitary Schrödinger evolution. Our unitary description in Section 3.2.4 also paves the way for a path-integral formulation of these systems, whose specialization to the restriction of two discrete paths U and L was treated in Ref. [BGK⁺24].

6.1.7 Investigating Relativistic Effects and Decoherence

From a fundamental standpoint, this description provides a rich opportunity to investigate the influence of relativistic effects in conjunction with off-resonant interactions between light and matter. These include inhomogeneous and homogeneous broadening due to thermodynamic or motional effects, environmental influences, optical effects such as geometric loss and noise, and other distortion effects that lead to decoherence. A central quest is to precisely quantify

the limits of decoherence avoidance within such systems. Understanding these limitations and quantifying their impacts is essential for determining the operational bounds and potential future achievements for quantum memory applications.

6.1.8 Balancing Accuracy and Computational Efficiency

In this context, designing theoretical descriptions that balance quantitative accuracy and computational cost is desirable. Ideally, this would enable the simulation of quantum communication tasks in real-time operation, parallel to their execution—such as the proposed Heisenberg model quantum networks in space.

6.1.9 Future Collaborations and Applications

These numerical implementations constitute the objective of future applications we aim to pursue collaboratively as scientists at the Center of Applied Space Technology and Microgravity (ZARM) in Bremen, in partnership with the German Aerospace Center (DLR). This joint endeavor seeks to explore and develop the potential of relativistic quantum memory descriptions for next-generation space-based quantum technologies.

6.2 Mathematical Characterization of Quantum Mechanics

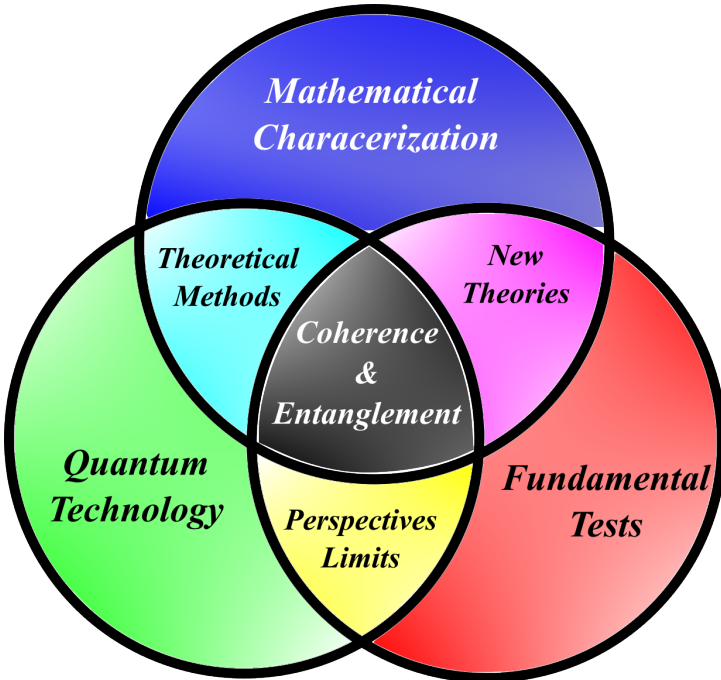


Figure 6.1: Author's scope of research during promotion.

In addition, beyond to the results documented here, this work represents a significant step towards a deeper mathematical understanding of quantum entanglement, with a particular focus on the implications of entanglement from a theoretical and foundational perspective. The insights developed here will serve as a foundation for future research on entanglement and related phenomena.

Despite being displayed already in Sec. 1.3, for convenience we show here once again in Fig. 6.1 the entire scope of the author's research.

Where the thesis on hand mainly focuses on *Fundamental Test* (red area in Fig. 6.1), the considerations sketched in this section are of relevance for the development of *Theoretical Methods* (cyan area in Fig. 6.1) for quantum technologies, the development of *New Theories* (purple area in Fig. 6.1) incorporating gravity and quantum mechanics, and –all above– the *Mathematical Characterization* of quantum coherence and quantum entanglement (blue area in Fig. 6.1) on which the other topics are built up on.

6.2.1 The Separability Problem in Quantum Mechanics

The central question underlying the presence, classification, and quantification of entanglement is known as the *Separability Problem* (SP). From the early 2000s to the end of the 2010s, this problem received substantial attention within the scientific community. However, its relevance has diminished as research interest, and –due to political will– increasingly shifted towards concrete applications in quantum technologies – for better or *worse*.

One key insight of our investigations of quantum entanglement is that the separability problem is mathematically equivalent to non-linear, tensorial eigenvalue problems of higher-order tensors.

This equivalence has potential relevance for various areas in science, like:

1. Mathematics

- (a) **Number Theory:** The Separability Problem can be generically translated into the question of how anything –for instance numbers– decompose into a combination of a sequence of operations –multiplication and addition. Thus it can be used for the prime factor decomposition of whole numbers and much more.
- (b) **Convex Optimization**
- (c) **Game Theory**
- (d) **Computational Complexity Theory**

2. Foundations of Physics

- (a) **Quantum Entanglement:** The *Separability Eigenvalue Equations* (SEE) define the presence, type, and strength of entanglement, framing entanglement as a non-linear tensorial eigenvalue problem.

We found operational entanglement criteria, that go far beyond the hitherto in the literature documented ones, which are basically solely restricted to the bipartite qubit-qutrit case through the PPT criterion. We generalize this criterion generically by means of representation and invariant theory in its whole generality, in contrast to the present literature, which only contains partial results in this issue.

We found methods to construct the entire set of *positive maps* of quantum states on the convex cone of positive semi definite hermitian matrices—also in case for more sophisticated requirements such as separability, i.e., the absence of entanglement, or certain entanglement but also classical correlations of desire. Both the solution of the separability problem and the characterization of positive maps are long standing problems in quantum physics.

The essential "trick" we found stems from *geometric algebra*, that is to embed the density matrix into the higher dimensional space of its *symmetric tensor algebra*, in order to untangle the interference between classical incoherent and quantum coherent correlations.

Further, our formulation connects the non-linear separability problem in a unique way with a corresponding linear problem, namely the associated linear eigenvalue problem, and vice versa. This one-to-one mapping between linear and non-linear problems, offers a distinguished way for quantizing gravity. This is because the fundamental mathematical difference between quantum mechanics and general relativity is that quantum mechanics is linear, while general relativity is non-linear. Our findings suggest a potential path to bridge these two pillars of physics.

- (b) **Quantization of Gravity:** The *Einstein field equations* (EFE) can be understood as a non-linear tensorial eigenvalue problem involving differential operators, similar to how the Schrödinger equation represents a linear tensorial eigenvalue problem. Inspired by the separability problem, we show how EFE can be *linearized without*

approximations, leading to a linear theory of gravity that can be quantized and exhibits superposition principles.

We found that the standard EFE are solely the non-linear analog of the linear and quantizable EFE. Essentially it turns out that the quantizable object in general relativity is not the metric—physically the *geometric structure* of spacetime—but it is the Light cone—physically the *causal structure* of spacetime.

This is because the object in which general relativity is linear is *not*—as in the non-linear standard case of GR—the metric $g_{\mu\nu}$ giving the line element

$$ds^2 = g_{\mu\nu} dx^\mu dx^\nu, \quad (6.1)$$

but actually the area measure

$$dA^2 = G_{\mu\nu\rho\sigma} dx^\mu dx^\nu dy^\rho dy^\sigma \quad (6.2)$$

quantifying the area enclosed by the vectors $x = x^\mu \partial_\mu$ and $x = y^\nu \partial_\nu$ in the tangent space of each point on the space time manifold.

The standard EFE are then recovered through the demand that the area element mathematically arises from a line element, that is

$$G_{\mu\nu\rho\sigma} = g_{\mu\nu} g_{\rho\sigma} - g_{\mu\rho} g_{\nu\sigma}, \quad (6.3)$$

which by itself is the separability condition that renders the non-linearity of the standard EFE.

The last equation reflects that the quantizability of gravity relies on the causal structure, as $G_{\mu\nu\rho\sigma}$ represents the light cone. More concretely it projects

- (c) **Gravitization of Quantum Mechanics:** Alternatively, by enforcing separability constraints—or equivalently requiring the prohibition of entanglement, as proposed by EPR in 1935 [53]—it is possible to explore a non-linear theory of quantum mechanics that aligns conceptually with the non-linear self-influence of matter as predicted by general relativity. This exploration offers new insights into potential unifying theories between quantum mechanics and theories of gravity.

However, as the existence of entanglement is now confirmed beyond doubt, we conjecture that gravity exhibits a significantly stronger need to be quantized than quantum theory depends on being "gravitized."

3. Methods in Physics

- (a) **Quantum Technologies:** Our investigation of the separability problem using methods from representation theory leads to a characterization of *positive maps* on the quantum state space. This characterization is crucial in computing analytic metrics in quantum technologies, such as channel capacities in quantum communication and error rates in quantum computing, and more. In contrast to classical metrics, these calculations remain analytically challenging due to the complex structure of quantum state spaces and allowed transformations.
- (b) **Many-Particle Physics:** Computational efficiency is essential in many-body physics, where Hilbert space dimensions scale exponentially with the particle number. Techniques like cluster expansion reduce computational complexity by approximating large

linear problems as tractable non-linear ones. Such reductions are widely used in fields like quantum optics and semiconductor physics, where multi-particle operators are expressed as polynomials in fewer-particle terms to simplify the correlation analysis.

4. Computer Science

(a) **Computational Complexity Theory**

(b) **Semidefinite Programming**

(c) **Neural Networks in Artificial Intelligence:** Neural networks process input information through tensor operations, effectively creating a “network tensor.” The corresponding eigenvalue problem reveals information about the network’s internal character. Positive eigenvalues might confirm the consistency of output with the initial input, while negative ones indicate areas where the network challenges the input. Additionally, analyzing entangled input vectors could reveal network biases or inter-dependencies, indicating which neural “regions” are connected or independent. This understanding can inform assessments of network “intelligence,” helping identify areas well-trained, under-trained, or even misaligned with human values.

Bibliography

- [1] R. V. Pound and G. A. Rebka, “Gravitational red-shift in nuclear resonance,” *Phys. Rev. Lett.*, vol. 3, pp. 439–441, Nov 1959. [Online]. Available: <https://link.aps.org/doi/10.1103/PhysRevLett.3.439>
- [2] R. Colella, A. W. Overhauser, and S. A. Werner, “Observation of gravitationally induced quantum interference,” *Phys. Rev. Lett.*, vol. 34, pp. 1472–1474, Jun 1975. [Online]. Available: <https://link.aps.org/doi/10.1103/PhysRevLett.34.1472>
- [3] J. C. Hafele and R. E. Keating, “Around-the-World atomic clocks: Observed relativistic time gains,” *Science*, vol. 177, no. 4044, pp. 168–170, Jul. 1972.
- [4] Y. Chen, M. Fink, F. Steinlechner, J. P. Torres, and R. Ursin, “Hong-ou-mandel interferometry on a biphoton beat note,” *npj Quantum Information*, vol. 5, no. 1, p. 43, May 2019. [Online]. Available: <https://doi.org/10.1038/s41534-019-0161-z>
- [5] R. Ursin, F. Tiefenbacher, T. Schmitt-Manderbach, H. Weier, T. Scheidl, M. Lindenthal, B. Blauensteiner, T. Jennewein, J. Perdigues, P. Trojek, B. Ömer, M. Fürst, M. Meyenburg, J. Rarity, Z. Sodnik, C. Barbieri, H. Weinfurter, and A. Zeilinger, “Entanglement-based quantum communication over 144 km,” *Nature Physics*, vol. 3, no. 7, pp. 481–486, Jul 2007. [Online]. Available: <https://doi.org/10.1038/nphys629>
- [6] S. Wang, Z. Yin, D.-Y. He, W. Chen, R.-Q. Wang, P. Ye, Y. Zhou, G.-J. Fan-Yuan, F.-X. Wang, Y.-G. Zhu, P. Morozov, A. Divochiy, Z. Zhou, G.-C. Guo, and Z.-F. Han, “Twin-field quantum key distribution over 830-km fibre,” *Nature Photonics*, vol. 16, 02 2022.
- [7] C. Hilweg, F. Massa, D. Martynov, N. Mavalvala, P. T. Chruściel, and P. Walther, “Gravitationally induced phase shift on a single photon,” *New Journal of Physics*, vol. 19, no. 3, p. 033028, 2017.
- [8] A. I. Lvovsky, B. C. Sanders, and W. Tittel, “Optical quantum memory,” *Nature Photonics*, vol. 3, no. 12, pp. 706–714, Dec 2009. [Online]. Available: <https://doi.org/10.1038/nphoton.2009.231>
- [9] P. Abiuso, “Verification of continuous-variable quantum memories,” *Quantum science and technology*, vol. 9, no. 1, pp. 01LT02–01LT02, 2023.
- [10] M. Gündoğan, P. M. Ledingham, K. Kutluer, M. Mazzera, and H. de Riedmatten, “Solid state spin-wave quantum memory for time-bin qubits,” *Phys. Rev. Lett.*, vol. 114, p. 230501, Jun 2015. [Online]. Available: <https://link.aps.org/doi/10.1103/PhysRevLett.114.230501>
- [11] A. Seri, D. Lago-Rivera, A. Lenhard, G. Corrielli, R. Osellame, M. Mazzera, and H. de Riedmatten, “Quantum storage of frequency-multiplexed heralded single

- photons,” *Phys. Rev. Lett.*, vol. 123, p. 080502, Aug 2019. [Online]. Available: <https://link.aps.org/doi/10.1103/PhysRevLett.123.080502>
- [12] P. Jobez, C. Laplane, N. Timoney, N. Gisin, A. Ferrier, P. Goldner, and M. Afzelius, “Coherent spin control at the quantum level in an ensemble-based optical memory,” *Phys. Rev. Lett.*, vol. 114, p. 230502, Jun 2015. [Online]. Available: <https://link.aps.org/doi/10.1103/PhysRevLett.114.230502>
- [13] Y. Ma, Y.-Z. Ma, Z.-Q. Zhou, C.-F. Li, and G.-C. Guo, “One-hour coherent optical storage in an atomic frequency comb memory,” *Nature Communications*, vol. 12, no. 1, p. 2381, Apr 2021. [Online]. Available: <https://doi.org/10.1038/s41467-021-22706-y>
- [14] A. Ortú, A. Holzapfel, J. Etesse, and M. Afzelius, “Storage of photonic time-bin qubits for up to 20 ms in a rare-earth doped crystal,” *npj Quantum Information*, vol. 8, no. 1, p. 29, Mar 2022. [Online]. Available: <https://doi.org/10.1038/s41534-022-00541-3>
- [15] J.-D. Deschênes, L. C. Sinclair, F. R. Giorgetta, W. C. Swann, E. Baumann, H. Bergeron, M. Cermak, I. Coddington, and N. R. Newbury, “Synchronization of distant optical clocks at the femtosecond level,” *Phys. Rev. X*, vol. 6, p. 021016, May 2016. [Online]. Available: <https://link.aps.org/doi/10.1103/PhysRevX.6.021016>
- [16] H. Bergeron, L. C. Sinclair, W. C. Swann, I. Khader, K. C. Cossel, M. Cermak, J.-D. Deschênes, and N. R. Newbury, “Femtosecond time synchronization of optical clocks off of a flying quadcopter,” *Nature Communications*, vol. 10, no. 1, p. 1819, Apr 2019. [Online]. Available: <https://doi.org/10.1038/s41467-019-09768-9>
- [17] D. E. Bruschi, T. C. Ralph, I. Fuentes, T. Jennewein, and M. Razavi, “Spacetime effects on satellite-based quantum communications,” *Phys. Rev. D*, vol. 90, p. 045041, Aug 2014. [Online]. Available: <https://link.aps.org/doi/10.1103/PhysRevD.90.045041>
- [18] D. E. Bruschi, A. Datta, R. Ursin, T. C. Ralph, and I. Fuentes, “Quantum estimation of the schwarzschild spacetime parameters of the earth,” *Phys. Rev. D*, vol. 90, p. 124001, Dec 2014. [Online]. Available: <https://link.aps.org/doi/10.1103/PhysRevD.90.124001>
- [19] N. D. Birrell and P. C. W. Davies, “Quantum fields in curved space,” 1984.
- [20] D. E. Bruschi, S. Chatzinotas, F. K. Wilhelm, and A. W. Schell, “Spacetime effects on wavepackets of coherent light,” *Phys. Rev. D*, vol. 104, p. 085015, Oct 2021. [Online]. Available: <https://link.aps.org/doi/10.1103/PhysRevD.104.085015>
- [21] D. Philipp, V. Perlick, D. Puetzfeld, E. Hackmann, and C. Lämmerzahl, “Definition of the relativistic geoid in terms of isochronometric surfaces,” *Phys. Rev. D*, vol. 95, p. 104037, May 2017. [Online]. Available: <https://link.aps.org/doi/10.1103/PhysRevD.95.104037>
- [22] S. Restuccia, M. Toroš, G. M. Gibson, H. Ulbricht, D. Faccio, and M. J. Padgett, “Photon bunching in a rotating reference frame,” *Phys. Rev. Lett.*, vol. 123, p. 110401, Sep 2019. [Online]. Available: <https://link.aps.org/doi/10.1103/PhysRevLett.123.110401>
- [23] D. E. Bruschi, A. Datta, R. Ursin, T. C. Ralph, and I. Fuentes, “Quantum estimation of the schwarzschild spacetime parameters of the earth,” *Phys. Rev. D*, vol. 90, p. 124001, Dec 2014. [Online]. Available: <https://link.aps.org/doi/10.1103/PhysRevD.90.124001>
- [24] C. K. Hong, Z. Y. Ou, and L. Mandel, “Measurement of subpicosecond time intervals between two photons by interference,” *Phys. Rev. Lett.*, vol. 59, pp. 2044–2046, Nov 1987. [Online]. Available: <https://link.aps.org/doi/10.1103/PhysRevLett.59.2044>

- [25] Z. Y. Ou and L. Mandel, "Observation of spatial quantum beating with separated photodetectors," *Phys. Rev. Lett.*, vol. 61, pp. 54–57, Jul 1988. [Online]. Available: <https://link.aps.org/doi/10.1103/PhysRevLett.61.54>
- [26] K. Wang, "Quantum theory of two-photon wavepacket interference in a beamsplitter," *J. Phys. B: At. Mol. Opt. Phys.*, vol. 39, no. 18, pp. R293–R324, sep 2006. [Online]. Available: <https://doi.org/10.1088/0953-4075/39/18/r01>
- [27] J. S. Bell, "On the einstein podolsky rosen paradox," *Physics Physique Fizika*, vol. 1, no. 3, p. 195, 1964.
- [28] G. Weihs, T. Jennewein, C. Simon, H. Weinfurter, and A. Zeilinger, "Violation of bell's inequality under strict einstein locality conditions," *Phys. Rev. Lett.*, vol. 81, pp. 5039–5043, Dec 1998. [Online]. Available: <https://link.aps.org/doi/10.1103/PhysRevLett.81.5039>
- [29] I. Pikovski, M. Zych, F. Costa, and Č. Brukner, "Universal decoherence due to gravitational time dilation," *Nature Physics*, vol. 11, no. 8, pp. 668–672, 2015.
- [30] G. Rosi, G. D'Amico, L. Cacciapuoti, F. Sorrentino, M. Prevedelli, M. Zych, Č. Brukner, and G. M. Tino, "Quantum test of the equivalence principle for atoms in coherent superposition of internal energy states," *Nature communications*, vol. 8, no. 1, p. 15529, 2017.
- [31] M. Zych, F. Costa, I. Pikovski, and Č. Brukner, "Quantum interferometric visibility as a witness of general relativistic proper time," *Nature communications*, vol. 2, no. 1, p. 505, 2011.
- [32] M. Zych, F. Costa, I. Pikovski, T. C. Ralph, and Č. Brukner, "General relativistic effects in quantum interference of photons," *Classical and Quantum Gravity*, vol. 29, no. 22, p. 224010, 2012.
- [33] I. Pikovski, M. Zych, F. Costa, and Č. Brukner, "Time dilation in quantum systems and decoherence," *New Journal of Physics*, vol. 19, no. 2, p. 025011, 2017.
- [34] M. Zych, *Quantum systems under gravitational time dilation*. Springer, 2017.
- [35] M. Toroš, M. Cromb, M. Paternostro, and D. Faccio, "Generation of entanglement from mechanical rotation," *Physical Review Letters*, vol. 129, no. 26, p. 260401, 2022.
- [36] S. Chen and T. Ralph, "Estimation of gravitational acceleration with quantum optical interferometers," *Physical Review A*, vol. 99, no. 2, p. 023803, 2019.
- [37] E. Schrödinger, "Discussion of probability relations between separated systems," *Mathematical Proceedings of the Cambridge Philosophical Society*, vol. 31, no. 4, p. 555–563, 1935.
- [38] J.-W. Pan, Z.-B. Chen, C.-Y. Lu, H. Weinfurter, A. Zeilinger, and M. Żukowski, "Multiphoton entanglement and interferometry," *Rev. Mod. Phys.*, vol. 84, pp. 777–838, May 2012. [Online]. Available: <https://link.aps.org/doi/10.1103/RevModPhys.84.777>
- [39] R. J. Glauber, "The quantum theory of optical coherence," *Phys. Rev.*, vol. 130, pp. 2529–2539, Jun 1963. [Online]. Available: <https://link.aps.org/doi/10.1103/PhysRev.130.2529>
- [40] F. Kaneda, H. Suzuki, R. Shimizu, and K. Edamatsu, "Direct generation of frequency-bin entangled photons via two-period quasi-phase-matched parametric downconversion," *Opt. Express*, vol. 27, no. 2, pp. 1416–1424, Jan 2019. [Online]. Available: <http://www.osapublishing.org/oe/abstract.cfm?URI=oe-27-2-1416>

- [41] S. Ramelow, L. Ratschbacher, A. Fedrizzi, N. K. Langford, and A. Zeilinger, “Discrete tunable color entanglement,” *Phys. Rev. Lett.*, vol. 103, p. 253601, Dec 2009. [Online]. Available: <https://link.aps.org/doi/10.1103/PhysRevLett.103.253601>
- [42] Z. Y. Ou and L. Mandel, “Observation of Spatial Quantum Beating with Separated Photodetectors,” *Phys. Rev. Lett.*, vol. 61, pp. 54–57, Jul 1988. [Online]. Available: <https://link.aps.org/doi/10.1103/PhysRevLett.61.54>
- [43] C. H. Bennett and G. Brassard, “Quantum cryptography: Public key distribution and coin tossing,” *Proceedings of IEEE International Conference on Computers, Systems and Signal Processing*, vol. 175, pp. 8–12, 1984, bangalore, India, December 1984.
- [44] A. K. Ekert, “Quantum cryptography based on bell’s theorem,” *Physical Review Letters*, vol. 67, no. 6, pp. 661–663, 1991.
- [45] M. Ozawa, “Soundness and completeness of quantum root-mean-square errors,” *npj Quantum Information*, vol. 5, no. 1, p. 1, Jan 2019. [Online]. Available: <https://doi.org/10.1038/s41534-018-0113-z>
- [46] J. Liu, J. Liu, P. Yu, and G. Zhang, “Sub-megahertz narrow-band photon pairs at 606 nm for solid-state quantum memories,” *APL Photonics*, vol. 5, no. 6, 2020.
- [47] K. J. Blow, R. Loudon, S. J. D. Phoenix, and T. J. Shepherd, “Continuum fields in quantum optics,” *Phys. Rev. A*, vol. 42, pp. 4102–4114, Oct 1990. [Online]. Available: <https://link.aps.org/doi/10.1103/PhysRevA.42.4102>
- [48] C. Kiefer and T. P. Singh, “Quantum gravitational corrections to the functional schrödinger equation,” *Phys. Rev. D*, vol. 44, pp. 1067–1076, Aug 1991. [Online]. Available: <https://link.aps.org/doi/10.1103/PhysRevD.44.1067>
- [49] P. K. Schwartz and D. Giulini, “Post-newtonian corrections to schrödinger equations in gravitational fields,” *Classical and Quantum Gravity*, vol. 36, no. 9, p. 095016, 2019.
- [50] C. Lämmerzahl, “A hamilton operator for quantum optics in gravitational fields,” *Physics Letters A*, vol. 203, no. 1, pp. 12–17, 1995. [Online]. Available: <https://www.sciencedirect.com/science/article/pii/0375960195003454>
- [51] D. Giulini, “On galilei invariance in quantum mechanics and the bargmann superselection rule,” *Annals of Physics*, vol. 249, no. 1, pp. 222–235, 1996. [Online]. Available: <https://www.sciencedirect.com/science/article/pii/S000349169690069X>
- [52] A. Holzäpfel, J. Etesse, K. T. Kaczmarek, A. Tiranov, N. Gisin, and M. Afzelius, “Optical storage for 0.53 s in a solid-state atomic frequency comb memory using dynamical decoupling,” *New Journal of Physics*, vol. 22, no. 6, p. 063009, jun 2020. [Online]. Available: <https://dx.doi.org/10.1088/1367-2630/ab8aac>
- [53] A. Einstein, B. Podolsky, and N. Rosen, “Can quantum-mechanical description of physical reality be considered complete?” *Physical review*, vol. 47, no. 10, p. 777, 1935.

Additional References

- [BBSL22] Roy Barzel, David Edward Bruschi, Andreas W. Schell, and Claus Lämmerzahl. Observer dependence of photon bunching: The influence of the relativistic redshift on hong-ou-mandel interference. *Phys. Rev. D*, 105:105016, May 2022.
- [BGK⁺24] Roy Barzel, Mustafa Gündoğan, Markus Krutzik, Dennis Rätzel, and Claus Lämmerzahl. Entanglement dynamics of photon pairs and quantum memories in the gravitational field of the earth. *Quantum*, 8:1273, 2024.
- [BL23] Roy Barzel and Claus Lämmerzahl. Role of indistinguishability and entanglement in hong-ou-mandel interference and finite-bandwidth effects of frequency-entangled photons. *Phys. Rev. A*, 107:032205, Mar 2023.

Anlage 1

E r k l ä r u n g gemäß § 7 (2)

Hiermit versichere ich, dass ich

1. die Arbeit ohne unerlaubte fremde Hilfe angefertigt habe,
2. keine anderen als die von mir angegeben Quellen und Hilfsmittel benutzt habe,
3. die, den benutzten Werken wörtlich oder inhaltlich entnommenen Stellen als solche kenntlich gemacht habe.

Datum: _____

Unterschrift: _____



Anlage 2

E r k l ä r u n g gemäß § 7 (1) (2. und 5.)

§7 (1) 2.

Hiermit versichere ich, dass ich mich bisher keinem Promotionsverfahren unterzogen bzw. ein solches beantragt habe.

§7 (1) 5.

Ich bin damit einverstanden, dass eine Überprüfung der Dissertation mit qualifizierter Software im Rahmen der Untersuchung von Plagiatsvorwürfen gestattet ist.

Datum: _____

Unterschrift: _____